INVESTIGATIONS ON TIME-DEPENDENT CHARACTERISTICS OF BLACK COTTON SOIL

PhD. Thesis

by

MOIRANGTHEM JOHNSON SINGH

(Roll No. 1801204001)

DISCIPLINE OF CIVIL ENGINEERING

INDIAN INSTITUTE OF TECHNOLOGY INDORE

June 2022

INVESTIGATIONS ON TIME-DEPENDENT CHARACTERISTICS OF BLACK COTTON SOIL

A THESIS

Submitted in partial fulfillment of the requirements for the award of the degree of

DOCTOR OF PHILOSOPHY

By

MOIRANGTHEM JOHNSON SINGH

DISCIPLINE OF CIVIL ENGINEERING
INDIAN INSTITUTE OF TECHNOLOGY INDORE
June 2022

INDIAN INSTITUTE OF TECHNOLOGY INDORE

CANDIDATE'S DECLARATION

I hereby certify that the work which is being presented in the thesis entitled **INVESTIGATIONS ON TIME-DEPENDENT CHARACTERISTICS OF BLACK COTTON SOIL** in the partial fulfillment of the requirements for the award of the degree of **DOCTOR OF PHILOSOPHY** and submitted in the **DEPARTMENT OF CIVIL ENGINEERING, INDIAN INSTITUTE OF TECHNOLOGY INDORE**, is an authentic record of my own work carried out during the time period from December 2018 to June 2022 under the supervision of **Dr. Lalit Borana, Assistant Professor, Department of Civil Engineering, Indian Institute of Technology Indore**.

The matter presented in this thesis has not been submitted by me for the award of any other degree of this or any other institute.

M. Johnson Singh 9th Sept. 2022

Signature of the student with date
(Moirangthem Johnson Singh)

This is to certify that the above statement made by the candidate is correct to the best of my/our knowledge.

9 Sept. 2022

Signature of Thesis Supervisor with date
(Dr. Lalit Borana)

Moirangthem Johnson Singh has successfully given his PhD Oral Examination held on **9th September 2022**.

Signature of Chairperson (OEB) Date: 9th Sept. 2022	Signature of External Examiner Date: 9th Sept. 2022	Signature of Thesis Supervisor Date: 9th Sept. 2022
Signature of PSPC Member #1 Date: 9th Sept. 2022	Signature of PSPC Member #2 Date: 9th Sept. 2022	Signature of PSPC Member #3 Date: 9th Sept. 2022
Signature of Convener, DPGC Date: 9th Sept. 2022	Signature of Head of Department Date: 9th Sept. 2022	

ACKNOWLEDGEMENTS

First and foremost, I would like to thank God for granting me countless blessings and strength so that I can finally accomplish the thesis.

I would like to express my deepest gratitude and sincere thanks to my thesis supervisor Dr Lalit Borana, Assistant Professor, Discipline of Civil Engineering, Indian Institute of Technology Indore. Undoubtedly, I have attained this significant life milestone because of his unwavering support and sound guidance. Furthermore, his ideology and noble thoughts have tremendously influenced my PhD journey. I would like to thank him for trusting me and offering me such an intriguing and demanding thesis topic.

I would like to thank Dr Wei-Qiang Feng, Assistant Professor, The Southern University of Science and Technology, China and Prof. Dong-Sheng Xu, the Wuhan University of Technology, China, for their insightful advice and generous support during my research. Their technical advice and recommendations greatly aided me in the development of this thesis.

I want to express my gratitude to the Director of IIT Indore for providing the opportunity to explore my research capabilities at IIT Indore. Also, I would like to thank Department Head and PSPC members; Dr Abhishek Rajput, Dr Dhirendra Kumar Rai, and Dr Sanjeev Singh, for their valuable suggestions and progress evaluations during my PhD.

I would like to convey my heartfelt gratitude to my dad M. Mohendro Singh and my mom M. Jamuna Devi for their unwavering support and sacrifice. This thesis would not have materialized without their support and guidance. I would like to express my gratitude to my younger brother M. Hemanta Singh, younger sister L. Saya Devi, her kid L. Changkhonba (Thouba) Singh, and Miss L. Sunibala Devi for their support during my difficult times. They keep me away from work stress and keep me afresh. I am indebted to them for their love, trust and motivation along this demanding journey.

I want to thank Mr Amit Yadhav, Mr Ajay Malviya, Ms Rinki Kukreja and Mr Pranjal for their help and support. I am thankful to Nikhil Kumar, Anshul Kaushik, Gyanesh Patnaik, Shivam Singh, Sanchit Gupta, Subhash Yadav and Dr Nitin Tiwari for their cooperation and support. I am grateful to the entire scientific staff of the Civil Department of IIT Indore, who has always been helpful to me.

I am thankful to all members of Central Workshop, IIT Indore, especially Dr Anand Petare, and Mr Rishiraj Chouhan, for their endless support in fabricating instruments. Also, I would like to thank all members of Safew Tech for providing testing materials on time.

Finally, I want to express my gratitude to everyone who has assisted and supported me throughout my PhD journey, whether directly or indirectly.

.....M. Johnson Singh

Dedicated to

My beloved Parents and my Gurus.

ABSTRACT

Clayey soil is one of the widely available geomaterials which exhibits long-term time-dependent stress-strain behaviour. Examining time-dependent behaviour is very important for geotechnical engineers and other infrastructural development professionals. This study primarily attempts to investigate the time-dependent stress-strain characteristics, including the creep and swelling behaviour. Creep can be defined as the viscous deformation of soil under the application of constant effective stress. While, swelling is the reverse action of creep, which is defined as the viscous expansion of saturated expansive soil during the removal of applied effective stress. Several models have been developed based on isochrone, isotache, rheological, microstructure, and EOP concepts to assess the time-dependent stress-strain behaviour of soil. Elasto Viscoplastic Model considering Swelling (EVPS Model) based on the concept of delayed compression stated is employed to investigate several compressibility behaviours of Indian Black Cotton (BC) soil in this study.

Firstly, a series of 1D-MSL Oedometer tests were conducted in BC soil under various loading patterns. The experimental result illustrated that BC soil exhibits significantly more time-dependent volume change behaviour during creep than during the swelling stage. The overburdened consolidated pressure resists the entrance of pore water through their interconnected voids and reduces cation hydrations are the responsible factors. Apart from it, particle sliding is also evident during creep. Thus, the ratio of parameters during loading is observed to be higher when compared to during unloading. The strain rate is reduced non-linearly to achieve a stable stage and is observed to be independent of the different loading pattern. In each loading-unloading cycle, the creep coefficients varied non-linearly with the applied stresses. For the BC soil, a maximum range of creep coefficient is observed in the range 630 kPa-760 kPa, and beyond this range, the creep coefficient reduced continuously. Several parameters influenced the time-dependent

compressibility characteristics of the soil including the duration, loading history and the magnitude of applied stress.

Secondly, several admixtures are employed to improve the geotechnical performance of such problematic soil. Here, fly ash (FA) is blended in different compositions and performed a series of 1D MSL Oedometer tests to investigate compressibility characteristics with special attention to creep and swelling behaviour. The microstructural and mineralogical arrangement of the FA blended reconstituted BC soil is further investigated using sophisticated instruments like Scanning Electron Microscopy (SEM), X-ray powder diffraction (XRD) and Fourier Transform Infrared Spectroscopy (FT-IR). The experimental findings illustrated that the compression stiffness of the matrix increase with the addition of FA and reduces the unloading–reloading index continuously. The addition of FA reduced the time-dependent parameters like creep coefficient, creep strain limit, swell coefficient, and swell strain limit; however, the magnitude of these parameters is not minimized to zero. The creep parameters are observed to be prominent in the 2^{nd} unloading-reloading cycles of both natural and reconstituted soil; however, the parameter is observed to reduce in further cycles. In the presence of water, the FA produce calcium silicate hydrate (C-S-H) gel due to a pozzolanic reaction. The produce gel encounters the BC soil forming a dense BC-FA matrix. Further, the comparison between the experimental and predictions derived from the EVPS model illustrated the model's suitability and applicability in predicting creep and swelling behaviour in the reconstituted soil. The amplitude sweeps test of the BC soil (different percentages of FA 0%, 5%, 15%, 25% and 35%) prepared at liquid limit is performed through the Anton Paar-Modular Compact Rheometer (MCR) 102 having a parallel-plate sensor system. The yield stress, viscoelastic parameters are varied significantly with the use of different FA content.

Thirdly, time-dependent swelling behaviour in alternate wetting-drying shrinkage test was conducted on BC soil in the presence of FA at different compositions (0%, 5%, 15%, 25% and 35%) using 1D Oedometer. The prepared samples are cured for 7 days. A series of alternate wetting-drying cycles are performed in cured samples in Oedometer for different days (7 days, 14 days, 7 days and 7 days). The concept of continuous swelling under constant effective stress, as given in the EVPS Model, is employed through a non-linear function. The mineralogical characteristics of both natural and reconstituted samples were investigated using SEM and XRD spectroscopy. Further crack behaviour in the alternate wetting-drying cycle is analyzed using image processing.

The experimental result shows that the swelling-shrinkage behaviour is significantly influenced by water retention, clay content, and the number of wetting-drying cycles. The time-dependent swelling coefficient diminished with the wetting-drying cycle and increased FA composition. The swelling strain limit is observed to be related exponentially to FA content. Further, the time-dependent swelling behaviour of FA blended reconstituted BC soil is predicted using EVPS Model and presents the accuracy and suitability of the model. The addition of FA reduces the development of preferential zones for cracking in alternate wetting-drying cycles. However, primary cracks are significant and consistent with up to 15% FA blended soil even after subjected to several numbers of wetting-drying cycle.

Parameter like the coefficient of consolidation plays a vital role in determining the settlement behaviour of clay soil. Even though this parameter can determine in the laboratory, there are several limitations. Therefore, the Machine Learning (ML) is employed to overcome some of the limitations. In this study, globally distributed soil samples were examined by considering 11 independent variables to predict the coefficient of consolidation. Data dimensionality is further minimized using the feature selection technique, namely Univariate Feature Selection (UFS). Several

ML algorithms, like Random Forest (RF), Artificial Neural Networks (ANN), and Support Vector Machine (SVM), are employed in this study. Each ML algorithm possesses its own characteristics and merits, and demerits for applicability in a particular problem. Therefore, a similar problem needs to be analyzed using different algorithms to figure out the best and most accurate one. Models having the highest coefficient of determination (R^2) and minimum mean square error (MSE) were selected and compared from each algorithm. It is observed that the Random Forest model accurately depicts the coefficient of consolidation even in a small input dataset than the ANN and SVM algorithms. This model possesses an MSE of 0.00148 and an R2 value of 0.92. The coefficient of consolidation derived from numerical simulations required different assumptions, unlike ML algorithms, which are data-driven. A comparison of the coefficient of consolidation from numerical simulation and ML algorithms shows that the ML models work well in predicting the same parameter and overcoming assumptions.

An Artificial Neural Network (ANN) model is developed furthermore and predict the creep parameter of clay soil. Algorithms like Extreme Gradient Boosting, sigmoid function and Adam optimizers are employed to develop the model, and the suitability of the proposed model is further assessed with various evaluation matrices. ANN model with three layers (the input layer has four neurons, ten neurons in the hidden layer and the output layer has only one neuron and the model has a learning rate of 0.001) is observed as a suitable and accurate model to access the creep parameter, with corresponding values of MAE and RMSE being 0.0040 and 0.00496. The future aspect of ML in developing a robust model based on the concept of the equivalent timeline is presented. Training and testing of the robust model need to consider a vast dataset, newly developed algorithms, and other inherent shortcomings like transparency and knowledge extraction

LIST OF PUBLICATIONS

Published Journal Papers (from thesis)

- M.J. Singh, Feng WQ, Xu DS, Borana L. "Experimental Study of Compression Behavior of Indian Black Cotton Soil in Oedometer Condition" *International Journal of Geosynthetics and Ground Engineering, Springer*, 6, 30 (2020). https://doi.org/10.1007/-s40891-020-00207-0. (Cite Score - 2.1)

- M.J. Singh, L. Borana, F. Weiqiang, and X. Dong-Sheng, "Long-Term Swelling Characteristics of Montmorillonitic Clay with and without Fly Ash: Wetting–Drying Cycle Influence in 1D Oedometer Condition." *Journal of Testing and Evaluation, ASTM.* https://doi.org/10.1520/JTE20210248 (*Impact Factor* - 1.264)

- M.J. Singh, Feng WQ, Xu DS, M. Dubey, Borana L. "Long-term Elasto-Visco-Plastic behavior of fly ash blended Indian Montmorillonitic clay in Oedometer condition." *International Journal of Geomechanics, ASCE. https://doi.org/10.1061/(ASCE)-GM.1943-5622.0002290* (*Impact Factor* - 3.819)

- M.J. Singh, Feng WQ, Xu DS, Borana L. "Time-dependent compressibility characteristics of Montmorillonitic Clay using EVPS Model". *Geomechanics and Engineering, Techno Press. https://doi.org/10.12989/gae.2022.28.2.171* (*Impact Factor* - 3.223)

Published Journal Papers (out of thesis)

- G. Patnaik, A. Kaushik, M.J. Singh, A. Rajput, G. Prakash, L. Borana. 2022"Damage Prediction of Underground Pipelines Subjected to Blast Loading." Arabian Journal for Science and Engineering, Springer, pp 1-20. *https://doi.org/10.1007/s13369-022-06920-4* (*Impact Factor* - 2.334)

Journal papers (Under Review)

- M.J. Singh, Ansul K., G. Patnaik, Borana L., Xu DS, Feng WQ, A. Rajput, G. Prakash. "Machine Learning-based approach for predicting the consolidation characteristics of soft soil".

- M.J. Singh, M Chetia, Feng WQ, Xu DS, Borana L. "Time-dependent compressibility characteristics of reconstituted clay: Experimental and machine learning approach"

- A. Kaushik, G. Patnaik, M.J. Singh, A. Rajput, G. Prakash, L. Borana. "Evaluation of Peak Displacement of Underground RC Tunnels subjected to Internal Explosion using Artificial Intelligence"

- M.J. Singh, Feng WQ, Xu DS, Borana L. "State of Art Review on prediction of consolidation parameters: From Conventional to Artificial Intelligence Approaches".

Book chapters published

- Kumar, R., Gonawala, R.J., Bajaj, K., Yadav, N., M.J. Singh, Borana, L. and Solanki, C.H., Dadra and Nagar Haveli and Daman and Diu. In Geotechnical Characteristics of Soils and Rocks of India (pp. 145-164). CRC Press. https://doi.org/10.1201/978100-3177159-9

- M.J. Singh, Feng W., Xu DS., Borana L. (2021) "Experimental Investigation of Long-Term Behaviour of Fly Ash Blended Indian Black Cotton Soil." In: Yao K., Zhenyu M., Komba J. (eds) Developments in Sustainable Geomaterials and Environmental Geotechnics. GeoChina 2021. Sustainable Civil Infrastructures. Springer, Cham. https://doi.org/10.1007/978-3-030-79647-1_2

TABLE OF CONTENTS

ACKNOWLEDGEMENT……I

ABSTRACT……III

LIST OF PUBLICATIONS……VII

TABLE OF CONTENTS……IX

LIST OF FIGURES……XII

LIST OF TABLES……XVI

NOMENCLATURE……XVII

ACRONYMS……XVIII

CHAPTER 1: INTRODUCTION **1**

1.1. RESEARCH BACKGROUND ---------- 1

1.2. OBJECTIVE ---------- 4

1.3. THESIS ORGANIZATION ---------- 5

CHAPTER 2: LITERATURE REVIEW **7**

2.1. OVERVIEW ---------- 7

2.1.1. CONSOLIDATION BEHAVIOUR OF NATURAL SOIL ---------- 7

2.1.2. TIME-DEPENDENT BEHAVIOUR ---------- 12

2.1.2.1. Rheological Model ---------- 14

2.1.2.2. Isotache model ---------- 15

2.1.2.3. Microstructure Model ---------- 16

2.1.2.4. Unique EOP ---------- 16

2.1.2.5. Isochrone (timeline) model ---------- 17

2.1.3. TIME-DEPENDENT BEHAVIOUR OF RECONSTITUTED SOIL ---------- 18

2.1.4. WETTING-DRYING CYCLES ---------- 24

2.1.5. MACHINE LEARNING APPROACH ---------- 32

2.2. SUMMARY ---------- 37

CHAPTER 3: TIME-DEPENDENT COMPRESSIBILITY CHARACTERISTICS OF BC SOIL IN 1D CONDITION **39**

3.1. INTRODUCTION ---------- 39

3.2. MATERIALS AND SAMPLE PREPARATION ---------- 40

3.3. DESCRIPTION OF EVPS MODEL ---------- 43

3.3.1. INSTANT TIMELINE ---------- 43

3.3.2. TIMELINES ---------- 48

3.3.3. EQUIVALENT TIMELINES---- 49
3.3.4. REFERENCE TIMELINE ---- 50
3.4. THE GENERAL EQUATION FOR 1D CONSOLIDATION ---- 51
3.4.1. LINEAR CREEP PREDICTION FUNCTION---- 51
3.4.2. NON-LINEAR FUNCTION FOR CREEP PREDICTION ---- 53
3.4.3. CREEP AND SWELLING STRAIN RATE ---- 59
3.5. CONCEPTUAL ILLUSTRATION OF EVPS MODEL IN BC SOIL ---- 63
3.6. SECONDARY COMPRESSIBILITY BEHAVIOUR ---- 65
3.7. SELF-WEIGHT CONSOLIDATION ---- 72
3.7.1. TEST SET-UP AND METHODOLOGY ---- 72
3.7.2. RESULT AND DISCUSSION ---- 74
3.8. CONCLUSION ---- 77

CHAPTER 4: LONG-TERM ELASTOVISCOPLASTIC BEHAVIOR OF RECONSTITUTED SOIL IN OEDOMETER CONDITIONS 79

4.1. INTRODUCTION ---- 79
4.2. MATERIAL AND TESTING PROCEDURE ---- 80
4.3. RESULT AND DISCUSSION---- 88
4.3.1. TIME-DEPENDENT PARAMETERS USING LINEAR FUNCTIONS---- 89
4.3.2. TIME-DEPENDENT PARAMETERS USING NON-LINEAR FUNCTIONS ---- 91
4.3.3. INFLUENCE OF UNLOADING-RELOADING CYCLE ON CREEP COEFFICIENT ----- 95
4.3.4. RELATIVE SWELLING STRAIN BEHAVIOUR---- 96
4.3.5. MICRO-STRUCTURAL ANALYSIS ---- 98
4.3.5.1. Scanning Electron Microscopy (SEM)----101
4.3.5.2. Fourier Transform Infrared Spectroscopy (FT-IR) Analysis ----102
4.3.5.3. X-ray diffraction spectroscopy ----103
4.3.6. TIME-DEPENDENT PARAMETERS WITH MICROSTRUCTURE CHANGES----106
4.3.7. RHEOLOGICAL BEHAVIOUR ----108
4.4. CONCLUSION ----111

CHAPTER 5: LONG-TERM SWELLING CHARACTERISTICS OF BC SOIL UNDER ALTERNATE WETTING–DRYING CYCLE....113

5.1. INTRODUCTION ----113
5.2. MATERIAL AND TEST PROCEDURE ----113
5.3. RESULT AND DISCUSSION----115
5.3.1. TIME-DEPENDENT SWELLING BEHAVIOUR----120
5.3.2. APPLICATION OF NON-LINEAR FUNCTION OF EVPS MODEL ----121
5.3.3. INFLUENCE OF WETTING-DRYING CYCLE IN TIME-DEPENDENT PARAMETERS 123

5.3.4. Effect of FA in time-dependent swelling behaviour ----------125
5.3.5. Prediction of time-dependent swelling behaviour under the wetting-drying cycle ----------130
5.3.6. Crack behaviour under alternate wetting-drying cycle ----------131
5.4. Recommendations for FA utilization ----------136
5.5. Conclusion ----------136

CHAPTER 6: MACHINE LEARNING IN THE PREDICTION OF GEOTECHNICAL PARAMETERS.....139

6.1. Introduction ----------139
6.2. Methodology and different algorithms ----------141
6.2.1. Feature Elimination (FE) ----------141
6.2.2. Artificial Neural Networks (ANNs) ----------142
6.2.3. Random Forest (RF) ----------144
6.2.4. Support vector machine (SVM) algorithm ----------145
6.2.5. Evaluation metrics ----------146
6.3. Coefficient of consolidation parameters ----------147
6.3.1. Data collected ----------147
6.3.2. Result and discussion ----------149
6.3.2.1. ML-based models. ----------149
6.3.2.2. Numerical simulation ----------164
6.4. Creep parameter ----------170
6.4.1. Data collection ----------170
6.4.2. Feature selection using Extreme Gradient Boosting (XGBoost) ----172
6.4.3. Result and discussion ----------173
6.4.3.1. ML approach ----------173
6.4.3.2. Future aspects of ML in creep parameter. ----------177
6.5. Conclusion ----------178

CHAPTER 7: CONCLUSIONS AND RECOMMENDATION OF FUTURE WORKS.....181

7.1. Conclusions ----------181
7.2. Recommendation and future works ----------183

REFERENCES 185

LIST OF FIGURES

FIGURE 3.1: PARTICLE SIZE DISTRIBUTION OF BC SOIL. ---------- 40
FIGURE 3.2: SCHEMATIC DIAGRAM OF THE OEDOMETER APPARATUS. ---------- 41
FIGURE 3.3: CHANGE IN VERTICAL STRAIN AGAINST THE EFFECTIVE STRESS (A) E_1, (B) E_2 AND (C) E_3. ---------- 44
FIGURE 3.4: CHANGE IN VERTICAL STRAIN AGAINST TIME (LOG SCALE) IN E_1 DURING (A) NORMAL LOADING (B) UNLOADING AND (C) RELOADING. ---------- 45
FIGURE 3.5: CHANGE IN VERTICAL STRAIN AGAINST TIME (LOG SCALE) IN E_2 DURING (A) NORMAL LOADING (B) UNLOADING AND (C) RELOADING. ---------- 46
FIGURE 3.6: CHANGE IN VERTICAL STRAIN AGAINST TIME (LOG SCALE) IN E_3 DURING (A) NORMAL LOADING (B) UNLOADING AND (C) RELOADING. ---------- 47
FIGURE 3.7: FITTING CURVE FOR CREEP PARAMETERS USING LINEAR FUNCTION. --------- 52
FIGURE 3.8: FITTING CURVE FOR SWELLING PARAMETERS USING LINEAR FUNCTION. ---- 53
FIGURE 3.9: FITTING CURVE FOR CREEP PARAMETERS USING NON-LINEAR FUNCTION. --- 54
FIGURE 3.10: FITTING CURVE FOR SWELLING PARAMETERS DERIVE FROM NON-LINEAR PARAMETERS. ---------- 56
FIGURE 3.11: PREDICTION OF THE CREEP BEHAVIOUR OF BC SOIL USING THE EVPS MODEL. ---------- 58
FIGURE 3.12: PREDICTION OF SWELLING BEHAVIOUR OF BC SOIL USING EVPS MODEL. 59
FIGURE 3.13: STRAIN RATE BEHAVIOUR DURING LOADING FOR DIFFERENT LOADING PATTERNS (A) E1, (B) E2 AND (C) E3. ---------- 61
FIGURE 3.14: STRAIN RATE BEHAVIOUR DURING SWELLING FOR DIFFERENT LOADING PATTERNS (A) E1 AND (B) E2. ---------- 62
FIGURE 3.15: CONCEPTUAL ILLUSTRATION OF EVPS MODEL IN BC SOIL. ---------- 63
FIGURE 3.16: RELATIONSHIP BETWEEN C_{AE} AND APPLIED EFFECTIVE STRESS FOR EACH RELOADING CYCLE (A) E_1 AND (B) E_3. ---------- 66
FIGURE 3.17: RELATIONSHIP BETWEEN C_{AE} AND C_C DURING LOAD INCREMENTS. --------- 69
FIGURE 3.18: RELATIONSHIP BETWEEN C_{AE} AND C_S DURING UNLOADING STAGES. -------- 71
FIGURE 3.19: FLOWCHART OF THE EXPERIMENTAL PROCEDURE. ---------- 72
FIGURE 3.20: RELATIONSHIP BETWEEN SETTLEMENT BEHAVIOUR AND TIME FOR ALL SOIL CONCENTRATIONS. ---------- 73
FIGURE 3.21: VOID RATIO PROFILE WITH EFFECTIVE STRESS (KPA). ---------- 75
FIGURE 3.22: VOID RATIO AND PORE WATER PRESSURE PROFILE. ---------- 76
FIGURE 3.23: TIME-DEPENDENT PARAMETERS OF SELF-WEIGHT CONSOLIDATED SOIL USING THE EVPS MODEL. ---------- 76
FIGURE 4.1: X-RAY DIFFRACTION SPECTROSCOPY OF FA. ---------- 80

FIGURE 4.2: RELATIONSHIP BETWEEN EFFECTIVE STRESS AND VERTICAL STRAIN OF FA-BC MATRIX USING TEST-1 LOADING PATTERN (A) BC SOIL, (B) 5% FA+BC SOIL AND (C) 25% FA+BC SOIL. ---------- 84

FIGURE 4.3: RELATIONSHIP BETWEEN EFFECTIVE STRESS AND VERTICAL STRAIN OF FA-BC MATRIX USING TEST-2 LOADING PATTERN (A) BC SOIL, (B) 5% FA+BC SOIL AND (C) 25% FA+BC SOIL. ---------- 85

FIGURE 4.4: CHANGE IN VERTICAL STRAIN WITH TIME DURING APPLICATION OF (A) 100 KPA FOR TEST-1, (B) 1000 KPA FOR TEST-1 AND (C) 250 KPA FOR TEST-2. ---------- 86

FIGURE 4.5: CHANGE IN VERTICAL STRAIN WITH TIME (LOG SCALE) DURING UNLOADING (A) 250 KPA TEST-1, (B) 10 KPA TEST-1 AND (C) 50 KPA TEST-2. ---------- 87

FIGURE 4.6: FITTING CURVE FOR CREEP PARAMETERS IN BC-FA MATRIX USING LINEAR FUNCTION DURING APPLICATION OF 1000 KPA IN TEST-1.---------- 90

FIGURE 4.7: FITTING CURVE FOR SWELLING PARAMETERS IN BC-FA MATRIX USING LINEAR FUNCTION DURING APPLICATION OF 250 KPA IN TEST-1. ---------- 90

FIGURE 4.8: FITTING CURVE OF CREEP PARAMETERS IN BC-FA MATRIX USING THE NON-LINEAR FUNCTION FOR (A) 1000 KPA TEST-1 AND (B) 250 KPA FOR TEST-2.--------- 91

FIGURE 4.9: FITTING CURVE OF SWELLING PARAMETERS IN BC-FA MATRIX USING THE NON-LINEAR FUNCTION FOR 100 KPA FOR TEST-2. ---------- 92

FIGURE 4.10: COMPARISON OF THE VERTICAL STRAIN OF BC-FA MATRIX AND PREDICTION FROM LINEAR FUNCTION AND NON-LINEAR FUNCTION (A) 500 KPA DURING LOADING AND (B) 100 KPA DURING UNLOADING. ---------- 94

FIGURE 4.11: VARIATION OF CREEP COEFFICIENT WITH THE NUMBER OF UNLOADING-RELOADING CYCLES ---------- 96

FIGURE 4.12: RELATIVE SWELLING STRAIN BEHAVIOUR FROM TEST-1 FOR (A) BC SOIL, (B) 5% FA+BC SOIL (C) 25% FA+BC SOIL AND (D) COMPARISON OF UNLOADING 1 FOR ALL SAMPLES. ---------- 97

FIGURE 4.13: SCHEMATIC DIAGRAM INDICATING (A) BEFORE CEMENTITIOUS GEL FORMATION AND (B) AFTER CEMENTITIOUS GEL FORMATION. ---------- 99

FIGURE 4.14: SEM SPECTROSCOPY OF (A) FA, (B) BC SOIL, (C) 5% FA+BC SOIL AND (D) 25% FA+BC SOIL. ---------- 100

FIGURE 4.15: COMPARISON OF FTIR SPECTROSCOPY OF BC SOIL, FA, AND RECONSTITUTED SOIL.---------- 102

FIGURE 4.16: X-RAY DIFFRACTION SPECTROSCOPY OF (A) BC SOIL, FA AND (B) 25% FA+BC SOIL FROM TEST-1 AND TEST-2. ---------- 104

FIGURE 4.17: RELATIONSHIP BETWEEN CREEP COEFFICIENT, FA CONTENT AND INTENSITY OF TOBERMORITE FORMATION. ---------- 105

FIGURE 4.18: RELATIONSHIP BETWEEN SWELL STRAIN LIMIT, FA CONTENT AND INTENSITY OF TOBERMORITE.----------107
FIGURE 4.19: RELATIONSHIP BETWEEN THE STORAGE MODULUS G′, LOSS MODULUS G″, YIELD POINT T_Y AND FLOW POINT T_F. ----------109
FIGURE 4.20: AMPLITUDE SWEEP TEST DATA FOR BC SOIL AND 45% FA BLENDED SOIL. ----------110
FIGURE 5.1: INFLUENCE OF ALTERNATE WETTING-DRYING CYCLE IN VERTICAL DEFORMATION OF BC SOIL. ----------115
FIGURE 5.2: DIFFERENCE IN VERTICAL CRACK FORMATION BEHAVIOR (A) BC SOIL AND (B) 35% FA+BC SOIL. ----------116
FIGURE 5.3: INFLUENCE OF ALTERNATE WETTING-DRYING CYCLES IN FA-BC MATRIX. 116
FIGURE 5.4: RELATIVE SWELLING STRAIN BEHAVIOUR OF BC SOIL UNDER ALTERNATE WETTING-DRYING CYCLES.----------118
FIGURE 5.5: RELATIVE SWELLING STRAIN BEHAVIOUR OF FA-BC MATRIX UNDER ALTERNATE WETTING-DRYING CYCLES. ----------119
FIGURE 5.6: DIFFERENT STAGES DURING SWELLING IN BC SOIL.----------121
FIGURE 5.7: CURVE FITTING FOR SWELLING PARAMETERS IN 5% FA+BC SOIL SUBJECTED TO WETTING-DRYING CYCLE. ----------123
FIGURE 5.8: RELATIONSHIP BETWEEN NUMBERS OF WETTING-DRYING CYCLES, PERCENTAGE FA CONTENT AND TIME-DEPENDENT SWELLING COEFFICIENT. -------124
FIGURE 5.9: SEM SPECTROSCOPY OF (A) BC SOIL, (B) FA, (C) 25% FA+BC SOIL AND (D) 35% FA+BC SOIL. ----------126
FIGURE 5.10: XRD SPECTROSCOPY OF FA+BC MATRIX (WITH 35% FA) AND NATURALLY AVAILABLE BC SOIL.----------128
FIGURE 5.11: SWELLING STRAIN BEHAVIOUR OF FA+BC MATRIX SUBJECTED TO (A) FIRST CYCLE, (B) SECOND CYCLE, (C) THIRD CYCLE AND (D) FOURTH WETTING-DRYING CYCLES.----------129
FIGURE 5.12: PREDICTION OF VERTICAL STRAIN BEHAVIOUR OF 25% FA+BC MATRIX SUBJECTED TO WETTING-DRYING CYCLE USING EVPS MODEL. ----------130
FIGURE 5.13: (A) FLOWCHART OF IMAGE PROCESSING; (B) RAW IMAGE CAPTURING SETUP. ----------131
FIGURE 5.14: CRACK BEHAVIOUR OF BOTH NATURAL AND RECONSTITUTED SOIL SAMPLES UNDER DIFFERENT WETTING DRYING CYCLES. ----------133
FIGURE 5.15: REPETITIVE PRIMARY CRACK BEHAVIOUR UNDER DIFFERENT WETTING-DRYING CYCLES.----------134
FIGURE 6.1: FLOWCHART OF PROPOSED ML ALGORITHM. ----------140
FIGURE 6.2: STRUCTURE OF ANN ALGORITHM WITH DIFFERENT LAYERS.----------143

FIGURE 6.3: STRUCTURE OF RANDOM FOREST ALGORITHM.---------- 144
FIGURE 6.4: SELECTION OF THE OPTIMUM NUMBER OF NEURONS THROUGH (A) R SCORES AND (B) RMSE SCORES. ---------- 151
FIGURE 6.5: THE PERFORMANCE OF THE ANN MODEL FOR THE (A) TRAINING, (B) VALIDATION, (C) TESTING AND (D) OVERALL DATASET. ---------- 152
FIGURE 6.6: TARGET AND PREDICTED DATASET FROM ANN MODEL DURING TRAINING, VALIDATION AND TESTING.---------- 153
FIGURE 6.7: SELECTION OF AN EFFECTIVE NUMBER OF A TREE FOR THE RANDOM FOREST ALGORITHM THROUGH (A) R SCORES AND (B) RMSE SCORES.---------- 157
FIGURE 6.8: PERFORMANCE OF RANDOM FOREST DURING (I) TRAINING AND (II) TESTING THE ALGORITHM. ---------- 158
FIGURE 6.9: TARGET AND PREDICTED DATASET FROM RANDOM FOREST DURING TESTING. ---------- 159
FIGURE 6.10: PERFORMANCE OF SVM DURING (I) TRAINING AND (II) TESTING. --------- 160
FIGURE 6.11: TARGET AND PREDICTED DATASET FROM SVM DURING TESTING. -------- 161
FIGURE 6.12: SQUARE ERRORS OF TESTING DATASET (A) ANN ALGORITHM, (B) RANDOM FOREST ALGORITHM AND (C) SVM ALGORITHM.---------- 163
FIGURE 6.13: THE BOUNDARY CONDITION AND SOIL SETTLEMENT RESULT FROM ABAQUS ANALYSIS---------- 166
FIGURE 6.14: COMPARISON OF THE COMPUTED DEGREE OF CONSOLIDATION FOR DIFFERENT SOILS. ---------- 168
FIGURE 6.15: FEATURE SCORE FOR EACH INPUT FEATURE.---------- 173
FIGURE 6.16: STRUCTURE OF ANN ALGORITHM FOR INCORPORATION OF THE ACTIVATION FUNCTION.---------- 174
FIGURE 6.17: THE PERFORMANCE OF THE ANN ALGORITHM DURING (A) TRAINING AND (B) VALIDATION + TESTING. ---------- 176
FIGURE 6.18: CONCEPTUAL ILLUSTRATION OF EVPS MODEL. ---------- 177

LIST OF TABLES

TABLE 3-1: BASIC PROPERTIES OF BC SOIL. ---------- 40

TABLE 3-2: LOADING PATTERN OF THE OEDOMETER TEST WITH CORRESPONDING LOADING DURATIONS. ---------- 42

TABLE 3-3: COMPRESSIBILITY CHARACTERISTICS OF BC SOIL. ---------- 51

TABLE 3-4: TIME-DEPENDENT PARAMETERS OF BC SOIL DURING CREEP AND SWELLING. 57

TABLE 3-5: SECONDARY COMPRESSIBILITY BEHAVIOUR IS GIVEN BY MESRI (1973). ----- 69

TABLE 4-1: WEIGHT PERCENTAGE OF ELEMENTS PRESENT IN FA. ---------- 80

TABLE 4-2: BASIC PROPERTIES OF FA BLENDED BC SOIL. ---------- 81

TABLE 4-3: LOADING PATTERN FOR OEDOMETER TEST. ---------- 82

TABLE 4-4: DIFFERENT COMPRESSIBILITY PARAMETERS OF BC-FA MATRIX UNDER DIFFERENT LOADING PATTERNS. ---------- 89

TABLE 4-5: DIFFERENT TIME-DEPENDENT PARAMETERS OF BC-FA MATRIX USING EVPS MODEL. ---------- 93

TABLE 4-6: THE PARAMETERS USED IN THE RHEOMETER. ----------109

TABLE 4-7: RHEOLOGICAL PARAMETERS OF SOIL BLENDED WITH DIFFERENT COMPOSITIONS OF FLY ASH IN LL CONDITION. ----------111

TABLE 5-1: CURVE FITTING EQUATIONS OF 5% FA+BC SOIL. ----------124

TABLE 6-1: STANDARD STATISTICAL INFORMATION OF THE FEATURES IN THE DATASET. ----------148

TABLE 6-2: REPRESENTATIVE INPUT DATASET AFTER UFS FEATURE SELECTION ALONG WITH THE REFERENCES. ----------148

TABLE 6-3: EVALUATION MATRICES CALCULATED FROM ANN ALGORITHM. ----------149

TABLE 6-4: EVALUATION MATRICES CALCULATED FROM RANDOM FOREST ALGORITHM. ----------155

TABLE 6-5: PERFORMANCE OF MODEL THROUGH EVALUATION MATRICES. ----------164

TABLE 6-6: PARAMETERS USED IN ABAQUS SIMULATION (FROM LITERATURE). ----------164

TABLE 6-7: COEFFICIENT OF CONSOLIDATION FROM SEVERAL APPROACHES. ----------169

TABLE 6-8: REPRESENTATIVE INPUT DATASET COLLECTED FROM THE LITERATURE. ----171

TABLE 6-9: STANDARD STATISTICAL INFORMATION OF THE FEATURES IN THE DATASET. ----------171

TABLE 6-10: THE BEST MODELS DEVELOPED USING THE ANN ALGORITHM. ----------175

NOMENCLATURE

λ / V : Compression parameter

$\Delta \varepsilon_z$: Strain increment,

σ'_z : Vertical effective stress,

V: Specific volume

e_o : Initial void ratio

C_c / V : Compression index

k / V : Rebounding parameter

C_r / V : Rebounding index

ε_z^c : Creep strain

ψ^c / V : Linear creep coefficient

t_o^c : Time corresponding to the beginning of creep

t_{EOP} : Time corresponding to the end of primary consolidation

t : Total duration of loading

ψ^s / V : Linear swell coefficient

$\frac{\psi_0^c}{V}$: Non-linear creep coefficient

ε_z^{cl} : Creep strain limit

$\frac{\psi_0^s}{V}$: Non-linear swell coefficient

ε_z^{sl} : Swell strain limit

ε_z^s : Swelling strain

$C_{\alpha e}$: Secondary consolidation

U= Average degree of consolidation

T_v : Time factor

H_{av} : Average drainage path length.

ACRONYMS

BC: Black cotton (expansive) soil

ASTM: American Society of Testing Material

BS: British Standards

OMC: Optimum moisture content

EOP: End of the primary consolidation

EVPS: Elasto viscoplastic model considering swelling

CEL: Creep equilibrium limit

SEL: Swell equilibrium limit

RSS: Relative swelling strain

FA: Fly ash

CH: High-plastic clays

OH: Low-plastic clays

XRD: X-ray diffraction spectroscopy

SEM: Scanning Electron Microscopy

FTIR: Fourier Transform Infrared Spectroscopy

EDX: Energy-dispersive X-ray

CSH: Calcium-silicate-hydrate

RBG: Red Blue Green

ML: Machine Learning

ANN: Artificial Neural Network

RF: Random Forest

SVM: Support Vector Machine

CoC: Coefficient of consolidation

UFS: Univariate feature selection

FE: Feature Elimination

RMSE: Root mean square error

MAE: Mean absolute error

MSE: Mean square error

Chapter 1

Introduction

1.1. Research background

Soil is a naturally available geomaterial and is a very important constituent for infrastructural development. There are different types of soils and can be classified based on their physical, chemical, and mineralogical content. Generally, the loads from civil engineering building structures are mobilized by the soil/ground. Thereby it is prudent to understand the engineering characteristics of the soil precisely.

It is noted that clayey soil is naturally available complex geomaterial and is also used for infrastructural construction purposes as filling material in the embankment, construction material in lifeline structures, in-situ material in land reclamation, and deep cement mixed column for ground improvement. It contains minerals like montmorillonite, kaolinite, illite (Burland 1967; Mitchell and Soga 1993a). The clay soil exhibits substantial cracking behaviour, strength changes with variations in water content, and time-dependent behaviour; as a result, it impairs the performance and durability of the overlying superstructures. It destroys about 250,000 new structures each year, with 10% of them sustaining significant damage during their lifetime (Jones Jr and Holtz 1973). The annual monetary loss due to geotechnical structure failure is projected to be 2.3 billion US dollars worldwide, more than double the damage caused by floods, hurricanes, tornadoes, and earthquakes (Fredlund et al. 2012). Even researchers reported the necessity of awareness of expansive soils to reduce possible damage (Vorwerk et al. 2015). One of the primary causes of such damage is the continuous settlement of the foundation geomaterial. Therefore, a precise and time-based assessment of consolidation behaviour is of paramount importance for practitioners and professional engineers to assess the stability of the superstructures (Johnson Singh et al. 2022; Park and Lee

2011). The consolidation is a combined effect of stress and time-dependent soil deformation. Hydraulic conductivity, water content, void ratio, and soil particle re-arrangement are all factors that influence it (Bardhan et al. 2022). The consolidation settlement comprises initial compression, primary consolidation, and secondary/creep settlement. Initial stage of consolidation is caused by preloading. Primary consolidation is caused by the expulsion of pore water from the interconnected void of soil. During this stage the excess pore water pressure gradually transfers into effective stress (Das 2021).

Several researchers presented a different mechanism for secondary/creep consolidation. One of the most acceptable mechanisms is the viscous movement of adsorbing water around clay particles (Yin 2013). Here, clay particles possess a negative charge due to their isomorphous substitution. An electrostatic force develops between the negative charge surface of clay particles and the exchangeable cations of the pore water in the interconnected voids. The exchangeable cations begin to move toward the negatively charged surface of clay, thus, it develops a diffuse double layer between the oppositely charged surface and the region progressed. The innermost layer of the double layer is strongly held by a clay surface and is termed as adsorbed water. The adsorbed water exhibits a more significant viscous behaviour than the freely available water. Other mechanism includes internal soil interaction, viscous arrangement and distortion of the clay particle arrangement and their skeleton structures (Mitchell and Soga 1993), particle sliding, jumping of molecule bonds, delayed water that transfers and viscous soil structural adjustments (Chen et al. 2020a; Mesri 1973; Navarro 2001).

There are numerous examples of the in-situ creep behaviour of soil**.** One example is the uneven settlement of the Tower of Pisa in Italy. Continuous creep deformation in the clay strata beneath the sandy base caused the tower to settle and tilt to one side. According to several reports,

the mean settlement of the tower is almost 1.5 m, and it continues to settle. The tower is currently inclined nearly 5.5 degrees (Havel 2004). Therefore, the study of time-dependent stress-strain characteristics in the clay soil is a concern for geotechnical engineers not only because the findings may be used right away to analyze the practical problems, but also because the findings can be used to learn fundamental details about interparticle bonding, soil structure interactions, and the mechanisms governing strength and deformation behaviour. Again, the geotechnical structures constructed on reclaimed soil are only allowed to have a settlement tolerance between 25 and 150 millimeters. Therefore, there came a necessity to anticipate the long-term settlement of the reclaimed soil accurately (Chen et al. 2020b; Zhang et al. 2018; Zhu et al. 2012).

In India, an expansive soil, known as Indian Black Cotton soil, is widely available in the central region. It is derivative of trap lava and is spread mainly across interior Madhya Pradesh, Maharashtra, Gujarat, and Karnataka on the Deccan lava plateau and the Malwa Plateau. It covers almost 0.8 million square kilometres of the country's total geographical area (Gupta and Sharma n.d.; Katti 1978). The BC soil is rich in montmorillonite minerals and characterized by higher clay content (Gidigasu and Gawu 2013). It exhibits substantial swelling-shrinkage behaviour with fluctuations in water content, crack development, and time-dependent behaviour (Kalkan 2011; Singh et al. 2020). BC soil is regarded as one of the most challenging soils in terms of construction purposes. Several researchers have attempted to investigate the time-dependent behaviour of clay soil; however, a limited information about the time-dependent behaviour of clay is available due to the complexity of rock and soil behaviour, their origin and sedimentation history, variation in mineralogical and chemical compositions, and significant regional differences (Xue et al. 2020).

Meanwhile, numerous researchers employed fly ash (FA) to improve the performance of BC soils, owing to the massive increase in FA production from 6.64 million tons in 1996-97 to 226.13 million tons in 2019-20 (Thermal Civil Design Division 2020). It has been reported the strength and other basic engineering properties of the soil can be improved with the addition of FA (Edil et al. 2006a). However, there is still a lack of information on the impact of FA, particularly the creep and swelling behaviour of the reconstituted soils.

It is noted that the primary consolidation contributes a significant portion, almost 85%-90%, of the total settlement (Datta 2005). Several parameters related to primary consolidation behaviour need to be estimated precisely to ascertain the performance and stability of the superstructure. Different empirical relationships are often employed to determine these parameters. Although these parameters can be measured from laboratories or field conditions, they are time-consuming, costly, and require skilled technicians (Shukla et al. 2009). Moreover, the accuracy of the experimental data depends on various factors like the instruments used, the expertise of the experimenters the meticulous procedures (Bui et al. 2019). Therefore, there came the necessity for predicting these parameters accurately, economically and/or in the shortest path.

1.2. Objective

Globally the time-dependent behaviour of the clayey soil is a major concern. So far, different models have been developed by different researchers; however, these models have their own applicability and limitations. For the design and construction of the geotechnical structure, an accurate prediction of both long-term and short-term settlement is a very important factor. In light of the above discussion, the following crucial research objectives were identified in the current research practices:

- To investigate the time-dependent stress-strain behaviour of the naturally available BC soil and FA blended reconstituted soil during loading and unloading conditions using the EVPS Model.
- To investigate and predict the time-dependent stress-strain behaviour of naturally available BC soil and FA blended reconstituted soil during the wetting-drying cycle.
- To propose an efficient and accurate model applicable in globally available soil using Machine Learning Techniques so that the coefficient of consolidation can be computed/predicted in the shortest path and verify the accuracy.

1.3. Thesis Organization

This thesis includes seven chapters and are organized as follows.

Chapter 1: presents the significance of the study on time-dependent behaviour, research background, objective and thesis organization.

Chapter 2: a review of the previous studies and research outcomes related to the time-dependent stress-strain behaviour of clay soil, different models are also discussed concisely and their applicability and limitations.

Chapter 3: Discuss the time-dependent stress-strain behaviour of BC soil, emphasizing creep and swelling behaviour in 1D oedometer condition, Conceptual illustration and application of EVPS Model in BC soil.

Chapter 4: It investigated the time-dependent stress-strain behaviour of industrial waste blended with reconstituted BC soil. The correlation between the creep/swelling parameters with the microstructure and mineralogical changes is investigated with sophisticated instruments like SEM, XRD and FTIR spectroscopy. The suitability and applicability of the EVPS Model in reconstituted soil are also explored and discussed in detail. Furthermore, the rheological behaviour of the reconstituted soil is also presented.

Chapter 5: The time-dependent swelling behaviour of BC soil blended with FA is investigated. The applicability of the EVPS model is further extended by wetting-drying cycles. The microstructural changes in the crack development pattern are also examined.

Chapter 6: Several Machine Learning algorithms like ANN, RF and SVM are employed to predict the geotechnical parameters related to the consolidation of globally distributed soil samples. The best model is presented and compared to the strength and weaknesses with numerical simulation in Abaqus.

Chapter 7: This chapter presents the conclusion of the overall study and incorporates recommendations and future works.

Chapter 2

Literature Review

2.1. Overview

Globally, the stability analysis on problematic/expansive soils is a significant concern for geotechnical engineering. Different soil parameters need to be assessed for proper geotechnical designs; among these, settlement behaviour is one. Several researchers have employed different admixtures to stabilize the naturally available geomaterials. Further, Machine Learning (ML) concepts are being employed to determine various geotechnical parameters, which are cost-effective and timesaving. The chapter presents a literature review on the consolidation model of soils, utilization of waste materials and ML concepts to assess the settlement analysis of soil. The literature is presented in different subsections.

2.1.1. Consolidation behaviour of natural soil

The problematic soil exhibits continuous volumetric reduction under the application of a static load, which is defined as consolidation. It is a combined effect of both stress and time-dependent deformation (Chen et al. 2020c; Feng et al. 2017b). The stress deformation is due to the interaction between pore water and the soil skeleton. It is composed of hydrodynamic pore pressure dissipation and viscous deformation during effective stress application (Hawlader et al. 2003).

Leroueil (1988) states that the duration of the consolidation and evolution of excess pore pressures during this process is controlled by combined effect of both the permeability and compressibility. The remolding and clogging phenomena underestimate the real permeability of the soil. During the determination of consolidation parameters, the creep behaviour of the soil during the primary consolidation stage needs to be considered. Applying effective stresses that are 80% of the expected pre-

consolidation pressure causes an observable creep deformation. The stress-strain curves behaviour of the clay specimen during consolidation depends on the location of sub-specimens relative to the boundary condition.

Boone (2010) stated that the concept of pre-consolidation pressure is usually employed for predicting and analyzing the settlement behaviour and normalize various geotechnical parameters. However, the traditional method is often problematic and relies mainly on uncertain graphical techniques, particularly when semi-log plots are developed. Their study proposed an alternative approach to interpret the consolidation data derived from the Oedometer test. The proposed approach does not require any subjective or graphical interpretation and is based on simple slope-intercept mathematics. The proposed technique accurately estimates the settlement behaviour for field cases.

Davis and Raymond (1965) mentioned that the primarily responsible for the dissipation of pore-water pressure and settlement in Oedometer testing is the permeability of porous stones, temperature, and electrochemical differences in pore fluid and fluid in pore-pressure gauge, side friction and compressibility of pore-pressure gauge. The experimental investigation shows that Terzaghi's theory predicts the rate of settlement but not the rate of dissipation of pore pressures for Oedometer boundary conditions. During the consolidation process, compressibility, permeability, and coefficient of soil consolidation varied continuously. For normally consolidated soil, the coefficient of consolidation is the least variable factor. A consolidation theory was developed assuming a constant coefficient of consolidation while other parameters like compressibility and permeability were allowed to decrease with increasing the applied pressure.

Rowe (1959) investigated the influence of the shape of samples, length and direction of the drainage path, behaviour of the applied stress during the consolidation and scattered off the test results. For a particular sample shape, the consolidation coefficient is found to increase significantly

with the drainage path length. It is also reported that the coefficient of consolidation data derived from the triaxial cell and Oedometer test is varied significantly. The major factors responsible for significant variation include the difference in stress conditions and changes in sample geometry. It has been reported that the drainage length to sample perimeter ratio increases the coefficient of consolidation. It might be due to the formation/termination of the drain rather than the impermeable surface with a higher ratio of the drainage surface to the total perimeter. The side drain arrangement is suitable for pore pressure and initial consolidation; however, it is not recommended for accurate determination of the coefficient of consolidation.

The study conducted by Holtz et al. (1986) showed that the pre-consolidation stress can be influence by the sample disturbances and the different types of Oedometer. A significant reduction in the coefficient of consolidation is observed during the de-structuration caused by the unload-reloading cycle. During the consolidation stage, it can be observed that de-structuration led to a significant increase in the vertical strain. Apart from it, other factors like principal stress difference during failure, alteration of the shape of the yield envelope and decrease in modulus also influenced. Thus, the secondary settlement will be overestimated in de-structured specimens compared to the normal sample.

The study performed by Leroueil et al. (1983) mentioned that the pre-consolidation pressure derived from laboratory and field conditions would differ, and is influenced by the sample quality, the strain rate, and the stress path. A unique relationship exists between pre-consolidation pressure and strain rate for a given soil at a given depth independent of the tests conducted. Further, a correlation is established in between the pre-consolidation pressure derived from the different consolidation tests and the conventional test. Furthermore, the study also proposed a method for estimating in-situ pre-consolidation pressure.

Cheng and Yin (2005) investigate the rate-dependency characteristics of natural Hong Kong marine clay using the consolidated undrained test in triaxial, Oedometer test, and CRS tests at various strain rates. A significant variation of “apparent” pre-consolidation pressure is observed with the change of strain rates. After the ‘‘apparent’’ pre-consolidation pressure, the stress-strain curves are approximately parallel. Apart from the pre-consolidation pressure, strain rate affects several soil properties like one-dimensional compressibility, pore water pressure, and undrained shear strength. A lower strain rate in CRS tests results in an increase in soil compressibility and a larger reduction of apparent pre-consolidation pressure. However, the application of a higher strain rate results in the development of a higher porewater pressure.

Leroueil et al. (1985) conducted various types of Oedometer tests including the creep tests, CRS tests, CGTs, and MSL tests and a rheological clay model was established. The model was developed especially in the normally consolidated soil; thus, the model can analyze the plastic strain. However, during the relaxation period in the over-consolidated soil sample, the elastic strain becomes relatively more important. During this stage, the model could represent only part of the behaviour. The model was developed on a sample having a small thickness. However, further study is required to verify the model's applicability in field conditions, where the clay layers are much thicker, and strain rates are much lower.

Augustesen et al. (2004) extensively investigate the time-dependent behaviour of both clay and sand through triaxial and 1D oedometer conditions. The creep result obtained from triaxial is sub-divided into primary, secondary and tertiary creep characterized by decreasing, constant and increasing strain rates, respectively. Several tests were conducted in clay and soil, including rate dependency, creep, stress relaxation, and structuration. The study report pronounced time-dependent phenomena in clay soil than in sandy soil. However, under the application of high

confining pressure, the sandy soil exhibits significant deformation due to grain crushing. Further, the study also reported that the time-dependent behaviour of clay soil could be appropriately described using the isotach concept; however, the same concept cannot describe the time-dependent behaviour of sandy soil. The structuration effect plays a vital role in time-dependent deformation in the lower strain rats. The isotach concept cannot explain the structuration effect.

Conte and Troncone (2006) proposed an analytical procedure to solve one-dimensional time-dependent consolidation-related problems. The proposed analytical procedure used the Fourier series, which considered both single and cyclic loading conditions. It also can account for the compressibility behaviour of the pore fluids. The applicability of the suggested analytical solution is further evaluated by comparing the results obtained from existing theoretical methods and observing in excellent agreement. The proposed analytical approach is further employed to evaluate the coefficient of consolidation

Tavenas et al. (1978) performed an experimental investigation on the drained and undrained creep behaviour of the over-consolidated clay. The creep deformation behaviour is composed of volumetric and shear strains. It is also reported that both strain components developed in over-consolidated clay can be described properly using the phenomenological equation given by Singh and Mitchell (Singh and Mitchell 1968). The study proposed a generic description of creep behaviour based on the limit state concept qualitative model (YLIGHT) developed by Vaid and Campanella (Vaid and Campanella 1977). The phenomenological equation is further expanded by expressing the stress function independently. In terms of the limit state of the clay, the stress function of volumetric and shear strains is represented.

2.1.2. Time-dependent behaviour

Terzaghi once said, “Everything on this earth has at least one thing in common—everything changes with time”. During the reclamation design, the limiting value for settlement of the superstructure constructed on the reclaimed soil is from 25 mm to 150 mm. Thus, a thorough understanding of the time-dependent stress-strain behaviour is necessary for accurate prediction of settlement of the problematic/expansive clay soil (Singh et al. 2021, 2022).

Some of the factors responsible for time-dependent deformation are the viscous movement of adsorbing water around clay particles (Yin 2013), internal soil interaction, viscous arrangement and distortion of the clay particle arrangement and their skeleton structures (Mitchell and Soga 1993b), particle sliding, jumping of molecule bonds, delayed water that transfers and viscous soil structural adjustments (Mesri 1973; Navarro 2001). Soft soils can exhibit a variety of time-dependent behaviors, including creep, the strain rate effect, swelling, and stress relaxation.

Creep can be defined as the viscous deformation of the soft soil under the application of a constant effective stress. It occurs after the dissipation of excess pore water pressure and leads to a noticeable settlement in both lab and field, including embankments and airport foundations (Mesri 1973).

The secondary compression corresponds to the continuously developed creep deformation after the end of primary consolidation (EOP). It is often approximated by a linear relation of strain over logarithmic time (Buisman 1936). (Mesri and Castro 1987) mentioned that $C_{\alpha\varepsilon}/CR$ is nearly constant for the same type of soil, where CR is the slope of the virgin compression line (VCL) in ε-log σ' space. For instance, $C_{\alpha\varepsilon}/CR$ for silts and inorganic clay is 0.04±0.01 while for peats and organic clay is observed to be 0.05±0.01. $C_{\alpha\varepsilon}$ is the secondary compression coefficient and represents

the constant slope of the linear relation. It is interesting to note that C. does not represent the viscosity of soil but rather the "fluidity". If $C_{\alpha e}$ is infinitely large, the soil will have zero viscous resistance, and creep is unbounded, which is analogous to an ideal fluid mobilized under shear. On the other hand, soil with zero $C_{\alpha e}$ (infinite viscosity) will behave as a solid material with no time-dependent deformation. Continuous usage of $C_{\alpha e}$ in constitutive modelling implies that volumetric creep behaviour plays a fundamental role in linking to other time-dependent aspects of behaviour.

The secondary coefficient is determined using the following equations as

$$C_{\alpha e} = \frac{-\Delta e}{\Delta \log(t)},\ e = e_0 - (C_{\alpha e} \log t) \qquad 2\text{-}1$$

$$C_{\alpha \varepsilon} = \frac{-\Delta \varepsilon_z}{\Delta \log(t)} = \frac{C_{\alpha e}}{1 + e_0}$$

e is defined as the void ratio of soil at any stage of loading, e_0 denotes the initial void ratio. $C_{\alpha e}$ indicates the coefficient of secondary consolidation which defined from the void ratio and the "secondary consolidation" coefficient which defined from the vertical strain is denoted by $C_{\alpha \varepsilon}$. Here t denotes the duration of loading. But when the duration of loading tends to infinity, the void ratio e becomes negative. This concept is not acceptable and violates the physical law of mass existence (Yin 1999).

Again, in the semi-logarithmic function

$$\varepsilon_z = \varepsilon_{z0} + \left[C_c / (1 + e_0) \right] \log\left(\sigma_z^{'} / \sigma_{z0}^{'} \right) \qquad 2\text{-}2$$

where C_c = compression index; e_0 = void ratio corresponding to $\sigma_{z0}^{'}$. Another stress-strain relationship is always invoked for the determination of volumetric strain. During the calculation of volumetric strain, a constant compressibility parameter is divided by an arbitrary reference volume from which strains are supposed to determine (Butterfield 1979). Again, when

the applied stress $\sigma_z^{'}$ tends to infinity, the void ratio becomes negative. It meant that, as long as stress has been applied, the strain will continue, which is not possible again; the void ratio of soil cannot be negative. It leads to a significant error in estimating the long-term settlement behaviour of soil. This concept is incorrect (Yin 2015).

Apart from it, the function $\varepsilon_z = \varepsilon_{z0} + \frac{\psi^c}{V}\ln\left[\left(t_o^c + t_e^c\right)/t_o^c\right]$, where t_o^c is the time parameter, t_e^c is equivalent time related to creep, ψ^c/V is the creep coefficient, ε_{z0} is the strain at a time $t = t_o^c$, leads to overestimates the creep considering the long term (Feng et al. 2017a; Singh et al. 2020).

The vertical strain, ε_z, can be defined as

$$\varepsilon_z = \varepsilon_0 + \frac{C_{\alpha e}}{1+e_0}\log\left(\frac{t}{t_{eop}}\right) \qquad 2\text{-}3$$

It is widely used equation for vertical strain determination. This linear relationship valid for a certain duration of loading, however it overestimates the settlement behaviour of the soil for longer span of loading.

Different models were developed to study time effects in compression behaviour. They can be divided into the following categories:

2.1.2.1. Rheological Model

Several rheological models were proposed using empirical relations to describe the viscous behaviour of the soil (Barden 1965; Taylor 1942). The constitutive relation is a combination of different elements, including spring, slider and dashpots, which account for the elastic, plastic and viscous stages of soil. The viscoplastic rheological model used a dashpot to develop a spontaneous viscoplastic strain $\left(\Delta\varepsilon^{vp}\right)$. Parzyna (1966) first developed a viscoplastic model driven by overstress and a viscosity parameter as follows;

$$\dot{\varepsilon}^{vp} = \frac{1}{\eta}\left(\sigma - \sigma_y\right) \quad for\ \sigma > \sigma_y \qquad 2\text{-}4$$

The above equation can define a continuous creep deformation under applying a constant effective stress σ. However, applying different stress results in a different creep rate, leading to rate-dependent yielding stress. Imai points out that the arrangement of rheological elements is not unique and matching actual behaviour with model prediction is almost coincidental. The calibration of the parameters is also difficult (Imai 1995).

2.1.2.2. Isotache model

Suklje (1957) proposed the Isotache model with a series of lines possessing an equal strain rate. Under different strain rates, the model able to define a relationship between effective stress-strain behaviour. (Garlanger and Šuklje 1973). The model cannot explain the relaxation behaviour, which decreases effective stress as the strain rate remains zero (Yuan 2016). Further, Imai (1992) proposes that the total void ratio comprises recoverable and irrecoverable components,

$$\dot{e} = \dot{e}^{r} + \dot{e}^{ir} \qquad 2\text{-}5$$

$$\dot{e}^{r} = -0.434 C_r \frac{\dot{\sigma}'}{\sigma'}$$

$$\dot{e}^{ir} = -10^{\left(e + C_c \log \sigma' - b\right)/C_\alpha}$$

The irrecoverable void ratio is given by a relationship between the current effective stress and void ratio state. It is not valid at the end of the primary consolidation but after attaining an apparent yield during primary consolidation. The model needs to calibrate different input parameters like C_c and C_α. The strain rate model developed by Kabbaj et al. (1986) does not consider the viscous behaviour of clay prior to yield. Again, several constitutive models were developed by Kelln et al. (2008) and Leroueil et al. (1985) to describe the strain-rate-dependent stress-strain behaviour and the time-dependent characteristics of soft soil. But all these 1D and 3D

models cannot consider both the creep and time-dependent swelling behaviour of soft soils (Yin and Tong 2011a).

2.1.2.3. Microstructure Model

Navarro and Alonso (2001) proposed a model based on the concept of local transfer of water mass from the microstructure to the macrostructure of the clay. The creep deformation is expressed in terms of micro void ratio as;

$$\Delta e_m = \Delta V_m / V_s \qquad 2\text{-}6$$

where, V_s and V_m are defined as the volume of solid phase and micro-pore-space. Based on the local transfer stage, there came two cases.

a. Coupled case: local transfer takes place during the primary consolidation stage.
b. Uncoupled case: local transfer doesn't occur until the end of the primary consolidation.

The thin soil sample exhibits an uncoupled case, while the thick sample exhibits coupled case. Therefore, the model considered either Hypothesis A or B depending on subjective choice.

2.1.2.4. Unique EOP

Mesri and Choi (1985) proposed the Unique EOP model; it assumes that specimens with different thicknesses possess the same strain after the primary consolidation. Thus, the model supports Hypothesis A. Traditionally used concept of consolidation settlement is based on Hypothesis A, where consolidation settlement is composed of two types of settlement, one is induced by primary consolidation and another one is due to secondary consolidation. According to Hypothesis A, creep settlement doesn't take place during the primary consolidation settlement. Compared to the field / experimental result, it underestimates the consolidation settlement. Later on several researchers have realized the limitation of this

concept and agreed that the creep settlement takes place during the primary consolidation also; this concept can be explained by Hypothesis B. Complicated numerical programs are required for determining the consolidation settlement based on the concept of Hypothesis B. To overcome this limitation, Yin and Feng (2018) developed a simple approach.

2.1.2.5. Isochrone (timeline) model

Bjerrum (1967) firstly proposed the isochrone model. It consists of a series of parallel isochrone lines drawn in the effective stress-void ratio space. At any given time, the deformation of soil is represented by isochrone lines. The deformation of soil is composed of instantaneous and delayed compression. The instantaneous compression is the effect of the consolidation process, while the "delayed compression" represents the continuous reduction of the soil volume under the application of constant effective stress.

Yin and Graham (1994) introduced an equivalent time to replace the ordinary loading duration to overcome contradictions, especially for over-consolidated clays and difficulties in modelling multi-stage consolidation tests. Further, the applicability of the model is described by performing different tests like for a constant rate of stress and strain tests, and relaxation tests. Using an equivalent timeline allows one to describe the creep behaviour for normally consolidated or overconsolidated state clay. Yin (1990) and Yin and Graham (1999) expanded the concept of the 1-Dimensional EVP model for 3D by considering a simple elliptical flow surface and failure criterion. Further, Yin et al. (2002) developed a 3D EVP model that able to describe the time-dependent stress-strain behaviour of over-consolidated clays and normally. The model introduces a nonlinear creep function and a loading surface function with a smooth shape on the π plane. The study reported a new approach to the determination of model parameters. The data obtained from one conventional isotropic stress creep

test conducted on soft Hong Kong marine deposits is employed to calibrate the model. Yin 1999 (1999) proposes a nonlinear function that overcomes the logarithmic function that determines infinite strain as loading duration tends to infinity. The function can be employed to determine time-dependent settlement or in the derivation of a new elastic visco-plastic model. However, it possesses a limitation that the loading duration must be long enough to calibrate the creep function; a minimum of one-week test duration is advised. Yin and Tong (2011) expanded the 1D EVP Model by considering the time-dependent swelling behaviour of the soil, which is further regarded as the EVPS model. The model is calibrated using the data derived from MSL test and further simulate the constant rate strain (CRSN) compression tests, and relaxation behaviour in the creep or swelling region. It is found that the model able to simulates the strain (or stress) rate effects and relaxation behaviour in the creep or swelling region accurately. Fei Tong (2013) investigated the effective stress changes with time in the 1D straining relaxation test. The test was performed using Hong Kong marine clay and a sand-bentonite mixture in both the loading and unloading stages. The study employed the EVPS model to simulate the relaxation behaviour of the soil. The required parameters are derived from a conventional Oedometer test. The simulate data obtained from the EVPS model were compared with the relaxation test data. The study mentioned the suitability of the model, accuracy and efficiency in calibrating the parameters. Feng et al. (2017) employed nonlinear functions having the concept of creep and swelling strain limit to study the time-dependent stress-strain behaviour of the Hong Kong marine clay. The nonlinear creep and swelling behaviour are taken into account in a modified Elastic Visco-Plastic Model Considering Swelling (EVPS model).

2.1.3. Time-dependent behaviour of reconstituted soil

Different techniques are being used to mitigate the damages caused by expansive soil; among these, chemical stabilization techniques are

widespread and highly practised (Das 2003; Yilmaz et al. 2019). It enable to alters the gradation, and several other basic engineering properties of the naturally available soil. The technique is being used widely because of its economic advantages and lesser requirement for a skilled workforce (Alzaidy 2019; Edil et al. 2006b). In developing countries like India and China, the continuous production of Industrial waste like fly ash (FA) has been witnessed and is expected to remain in future. In India, the production of FA significantly increased in the recent years (Bachus et al. 2019). However, the ratio of its utilization is even lesser in India (Thermal Civil Design Division 2020) and global level as reported by American Coal Ash Association ACAA 2001 (Kim et al. 2005). Improper disposal and storage of FA is a major concern leading to several environmental and economic problems, including damage to the root development of plants, leaching, and pollution of cultivated areas, groundwater and other natural resources (Cokca 2001; Prasad and Mondal 2009). Soil stabilization using FA has been practised for a long time to mitigate the damage caused by soil and reduce the environmental and economic problems caused by the deposition of FA. Several researchers also recommend the same. The addition of fly ash significantly influences different properties of the clay soil, including optimum moisture content and maximum dry density (Sridharan et al. 2001), swell potentials (Erdal Cokca 2001), and consistency limit (Sivapullaiah et al. 1996a). Further researchers also reported that the addition of FA enhances the strength behaviour of the problematic soil. From this concept, FA is being employed as sub-base material stabilizers during road construction (Bin-Shafique et al. 2010; Kumar et al. 2006).

Goktepe (2008) studied the time-dependent unconfined compressive strength of FA blended reconstituted soil. The curing periods of the samples are 1, 7, 28 and 90 days with different compositions of FA, including zero, 5%, 10%, 15% and 20%. The time-dependent strength of the reconstituted soil in an unsupervised manner by considering different algorithms like fuzzy c-means, Kohonen's self-organizing map

methodologies, and hard k-means. The study concludes that the fuzzy c-means method is suitable as compared to other algorithms. The study also mentioned the responsible factors for strength gain in the reconstituted soil, including the chemical reaction between the soil and FA and the pore refinement effect of FA.

Sobhan and Mashnad (2003) experimentally investigate the mechanical behaviour like compressive, split tensile, and flexural strength characteristics of a composite containing soil-cement–FA–high-density polyethene strips. Further, the study also assessed the effectiveness of the polyethene strips in the toughness characteristics of the composite. The diametric deformation during the application of compressive load in the orthogonal direction is recorded using LVDTs. It enabled the evaluation of the post-peak toughness behaviour during loading. The tensile stress-strain behaviour exhibits that the composite reinforced with polyethylene in the presence of either cement or cement + FA exhibits significant post-peak load-carrying capacity. A dimensional toughness index which able to quantify reinforcing effects is also proposed.

Jaditager and Sivakugan (2018) study the consolidation behaviour of dredge mud blended with fly ash-based geopolymer at different compositions (6, 12, and 18% by weight) in a 1D Oedometer test. The coefficient of consolidation of the reconstituted samples was compared using Taylor's square root of time curve-fitting method. The study concludes that the addition of fly ash-based geopolymer improved several mechanical properties, including the consolidation characteristics, permeability, and compressibility behaviour of the dredged mud.

Phanikumar (2009) investigates various mechanical properties of expansive soil with the addition of different admixtures like lime and FA. Samples are prepared by adding 0%, 10% and 20% of FA and lime content was varied as 0%, 2%, 4% and 6%. Different geotechnical properties of the soil like swelling pressure, swell potential, shear strength, compression

index, coefficient of consolidation, secondary consolidation characteristics and free swell index (FSI) were investigated. The reconstituted sample possesses higher shear strength and attain its maximum dry density at 20% FA content, whereas the consolidation behaviour and swelling potential are reduced significantly. Similarly, the increase in lime content reduces the swell potential and swelling pressure.

Mir and Sridharan (2014) improve the BC soil by mixing Class C and Class F FA in different percentages (10, 20, 40, 60, and 80% by weight). Several mechanical properties of the soil, including void ratio, swelling potential, permeability, compression index, coefficient of consolidation, and pre-consolidation pressure, were investigated. The study concludes that the addition of FA reduces the swelling potential and various compressibility characteristics. Again, it is also concluded that 20% is the optimum quantity of FA content required to optimize the compressibility characteristics of reconstituted soil subjected to 7 days of curing.

Sebastian et al. (2017) state that the performance of the problematic soil can be improved with the addition of FA in small scale. Four different types of FA are blended in different proportions (0, 10, 20, 40, and 100% by volumetric fraction) and investigate the volumetric changes. The consolidation behaviour of the reconstituted soil is predicted using a bilinear function based on the mixture theory model by including the void ratios of the clay-FA mixture. The modified Duncan-Chang model, which incorporates the strength parameters from mixture theory, is used to predict the shear behaviour of the reconstituted soil. Verification analyses indicate that the consolidation and shear behaviour of the reconstituted soil can be predicted accurately using mixture theory.

Kaniraj and Gayathri (2004) assessed the physical as well as chemical properties of FA using XRD and SEM spectroscopy. Several mechanical tests like classification, consolidation, compaction, and FA permeability tests were investigated. The study concludes that the

consolidation behaviour and coefficient of permeability of compacted FA are comparable to non-plastic silts. The compacted FA possesses an almost constant coefficient of permeability under the application of varied, effective stresses. The study also suggests that $c_v = k/(m_v \gamma_w)$ can be employed for determining the coefficient of consolidation, apart from other methods like the log-time, and the square-root-time.

Phanikumar and Sharma (2007) investigate the volume change behaviour of both expansive and non-expansive clay blended with different compositions of FA (0, 5, 10, 15, and 20%). Further, the effect of FA on different mechanical behaviour of the reconstituted soil like swelling pressure, free swell index, swell potential, secondary consolidation characteristics and compression index of both soil types were also investigated. The study states that the suction of FA blended soil would be reduced; thus, the swelling would eventually be reduced. Both the soil exhibits a significant reduction of compression index with the increase of FA; also, 50% reduction of compression index is noted in the presence of 20% FA. Compared to untreated clay, the FA blended clay exhibits significant improvement in the secondary consolidation characteristics; thus, the settlement built on the FA blended soil will be reduced.

Solanki et al. (2009) investigate the effectiveness of various soil stabilizers, including FA, hydrated lime, and cement kiln dust. Several mechanical properties were evaluated, including modulus of elasticity (M_e), unconfined compressive strength (UCS), resilient modulus (M_r) and moisture susceptibility behaviour. The specimens were cured for 28 days. The study result revealed that the increase of stabilizing agents leads to an increase in USC value, M_r and M_e. The increase of these values depends on the type of stabilizing agent blended. Among these stabilizers, cement kiln dust exhibits higher Mr, ME, and UCS values than other stabilizers; however, it possesses the least moisture susceptibility to other stabilizers.

Zia and Fox (2000) studied the mechanical behaviour of the Indiana loess soil to improve with FA at different compositions (9, 11, 15, and 20 % by dry weight) and cured for 3 h and 1, 7, 14, 21, and 28 days. The reconstituted sample exhibits significant improvement in unconfined compressive strength, Atterberg limits, and swell behaviour. For quick construction of workable loess soil, a simple method to determine optimum FA content is also present. The study noticed shrinkage cracks in the higher FA content cured samples after 7 days.

Abdullah et al. (2019) investigate the geotechnical properties of two naturally available clay soil and kaolin clay in the presence of FA-cement composite, commonly called Geopolymer. Several tests, including the consolidated undrained (CU) triaxial compression and UCS tests, were performed in various compositions. The higher geopolymers contribute to the higher stiffness of the soil, thus increasing the clay's yield strength. The stress-strain behaviour exhibits a change from a ductile response to a post-peak brittle response. Even though this sample indicates a significant improvement with the addition of geopolymer, a difference in stiffness, peak stress, and contraction/dilation tendencies upon shearing is noted. This might be due to mineralogical content differences, which differed in plasticity and activity indices.

Abdullah et al. (2019) studied the geotechnical behaviour of the FA-bentonite mixture layer system in ratios 1:1 (50% FA:50% bentonite), 2:1 (67% FA:33% bentonite), 3:1 (75% FA:25% bentonite), and 4:1 (80% FA:20% bentonite). The mixtures' chemical and mineralogical composition were investigated using SEM and X-ray spectroscopy and investigated the shear characteristics using consolidated undrained (CU) triaxial tests. It is stated that a stable embankment can be constructed if the FA-bentonite ratio is 3:1 having an interface N=3. For each ratio, the cohesion value and deviator stress are observed to increase continuously as the number of interfaces increases. Under the application of lower stress, the stress-strain

behaviour of FA-bentonite is elastic; however, stress-strain behaviour is observed to be non-linear at higher stress.

2.1.4. Wetting-drying cycles

Basma et al. (1996) investigate the swelling shrinkage behaviour of four soil having different plasticity under partially saturated and fully saturated conditions and investigate the expansive characteristics. The study reported that alternate swelling and shrinkage behaviour significantly influence the expansive behaviour of the clay. The water absorption capacity greatly influences the swelling ability of the clays. The clay soil exhibits a significant swelling potential during the fully shrunk condition. The soil aggregates are destructed, and structural particles' disorientation occurs during the higher number of swelling shrinkage cycles. The scanning electron microscope analysis of the study reports the edge-to-face contact of the structural elements for partially saturated and forming a flocculated system. However, during the cyclic wetted condition, the particles are horizontally oriented.

Chen and W Ng. (2013) investigated the hydro-mechanical behaviour of the unsaturated soil subjected to alternate wetting-drying cycles. The study reports the result obtained from a suction-controlled isotropic compression test on compacted clayey soil. The study reports the irreversible swelling and shrinkage during subsequent wetting and drying cycles. The volume change behaviour and changes in hydro-mechanical behaviour of the unsaturated soil are stress-dependent. During the alternate wetting-drying cycles, the pre-consolidation stress is found to be decreases which might be due to increase in the degree of saturation or due to the irreversible swelling. The soil exhibits a softening effect because of the increase in saturation level or irreversible swelling, which increases susceptibility to yield.

Yazdandoust and Yasrobi (2010) investigate the polymer-stabilized and untreated problematic soil under an alternate wetting-drying cycle. The study employed three different types of expansive soil and two polymers, namely Urea Formaldehyde and Melamine Formaldehyde. The swelling potential of the expansive soil is significantly reduced due to the presences of polymers. The study also assessed the influence of the polymer on the particle size distribution and Atterberg limits of the treated and untreated soil. The increase in the clay content influences the Atterberg limit. However, in the polymer-stabilized specimen, the change in particle size distribution and Atterberg limit are minimal due to the stabilizing effect of polymers on cemented aggregates. The microstructural changes are investigated using a scanning electron microscopy test and report the continuous rearrangement of clay particles during wetting-drying cycles. Both the polymer treated, and natural soil achieve equilibrium after the fourth cycle. However, clay aggregation and particle distortion breakage are observed during the sixth wetting-drying cycle.

Rao et al. (2001) investigated the behaviour of the BC soil blended with wood ash and laboratory lime while subjected to alternate the wetting-drying cycle. The study reports that the ash-modified soil becomes more porous and less saturated due to the cyclic wetting-drying cycle, leading to the collapsed specimen in the experimental flooding pressure. The clay content is observed to increase with the wetting-drying cycle, especially after the fourth cycle, and it significantly influences the Atterberg limit and swell-shrink potentials. The lime-treated specimen exhibited a partial loss of inter-particle cementation, reduction in the degree of saturation and increased porosity, and reduction in dry density during the wetting-drying cycle. During the wetting-drying cycle, reduction in cementation behaviour and increase in porosity is observed and subsequently the dry density is reduced.

Rosenbalm and Zapata (2017) report that a conventional method to predict the heave and swelling pressure of both the expansive soil and remolded soil subjected to wetting cycles. However, this practice has some limitations while applying to field conditions. Therefore, there came the necessity to assess the long-term environmental effect. A series of wetting-drying cycle tests are conducted on the two types of naturally occurring expansive soil. The swell pressure and the swelling strain attain a stable condition after four alternate stages of cycles. The wetting-drying cycle reorients the soil fabrics from a compacted state to an equilibrium soil-fabric state. The horizontal and vertical cracks are developed while subjected to the drying, which leads to observing the preferred wetting path within the soil structures. Anisotropic volume change is the responsible factor for development of cracks; the development of cracks reduces the time required for primary swell or collapse conditions. Tensile stresses developed in the restrained direction because of anisotropic volume change. The applied stress significantly influences the collapse potential of the soil. It is reported that the soil undergoes swelling while subjected to a normal stress lesser than 25% of swelling pressure. However, when the applied stress exceeds the 25% of swelling pressure, the soil is observed to collapse. The initial compacted condition significantly influences the rate of variation of swelling pressure or variation of vertical deformations. The soil compacted in 90% MDD and 110% OMC significantly reduces the swell pressure even after subjected to alternate the wetting and drying cycles.

Sajad et al. (2020) investigate the wetting-drying behaviour of the nano-silica and industrial waste treated and untreated naturally available expansive soil in the Oedometer test. The soil subjected to continuous wetting-drying cycles exhibits a reduced swelling potential. The variation of water content and void ratio during the swelling-shrinkage path of soil follows an S-shaped curve. However, the curve is found to be horizontal for the treated expansive soil, indicating minimal changes in void ratio versus water content variations. It is also reported that the treated soil attained an

equilibrium condition in fewer wetting-drying cycles than naturally available expansive soil. The naturally available expansive soil possesses the highest void ratio and deformations when the degree of saturation is between 50 and 90%. However, for nano-silica and industrial waste-treated soil it can be observed in degrees of saturation between 70 and 90%. SEM and XRD test were performed before and after the wetting-drying cycle and investigated the microstructural changes. The addition of these additives enhances the durability of the treated sample under continuous wetting-drying cycles. The addition of additives leads to the formation of CSH gels which cause the aggregation of soil particles, reducing pores between the soil particles and connecting the soil particles. All this improves soil properties and reduces the swelling potential of the soil. It is reported that the decrease of clay minerals is the responsible factor which influence the reduction of the swelling potential and formation of the cracks while subjected to wetting-drying cycles.

Wang and Wei (2015) present an approach for modelling the volumetric change in the soil under the application of alternate wetting-drying cycles. The wetting-drying cycle-induced swelling shrinkage behaviour and is decomposed of two major portions, i.e., reversible and irreversible portions. The reversible section always causes contraction during drying and expansion during wetness, changing synchronously with the cycle of suction. It depends on the current suction value as, under the same suction, similar changes in swelling-shrinkage strain are observed in each cycle. The major factors responsible for reversible components is the reversible deformation of the soil particle, and it is influence by current suction or water content. At the same time, the irreversible portion is generated in the early phase of the wetting-drying cycle. The rate of the irreversible deformation is reported to be reduced with the wettings–drying cycles. it is due to irreversible macrostructural changes of the soil particle which reflects the difference in soil structures at the current and equilibrium states. The suitability of the proposed model was validated through alternate

soaked and dried test subjected to different suction values and by simulating cyclic suction-controlled tests.

Soltani et al. (2020) investigate the swelling-shrinkage behaviour of the sulphonated oil to stabilize expansive soil under alternate wetting-drying cycles. The alternate wetting-drying cycle induces clay particle aggregation. The soil exhibits lower swelling and shrinkage tendency up to the fourth cycle while applying a series of wetting-drying cycles. Beyond the fourth cycle, the swelling and shrinkage behaviour of the soil is found to be elastic equilibrium. The addition of 0.75% SO reduces the swelling and shrinkage tendency of the soil, beyond 0.75% SO, the SO molecules self-associate and acts as a lubricant instead of acting as a stabilizing agent and does not result in additional decreases in the potentials for swelling and shrinkage.

Davidson and Page (1956) developed an apparatus for measuring swelling pressure on clay soil and investigate the influence of several factors like mineralogical composition, and exchangeable ion contents on the swelling capacities and influence on soil structure. Using the apparatus, the mechanism of swelling behaviour of clay soil is investigated and its influence on plant growth. It is reported that the soil containing montmorillonite exhibits significant swelling behaviour; apart from it, other factors like organic materials, iron content and exchangeable cation also help in modifying the tendency of swelling-shrinkage behaviour of the soil. Removal of several soil compositions like iron organic matter increases the tendency of swelling behaviour of the soil. However, the adsorption of soil conditioners enhances the swelling capacity of the clay.

Ramesh and Thyagaraj (2020) investigate the swelling shrinkage behaviour of the compacted expansive soil amended with the sand under continuous wetting-drying cycles. The development and identification of the cracks during wetting-drying are investigated through image processing. The soil containing 50% sand and 50% clay exhibits a significant decrease

in vertical, lateral and volumetric deformation compared to 100% clay content soil. The presence of the sand reduces the clay content, reduction of swelling potential clay particles in inter-void space, and encapsulation offered by sand particles. The presence of sand particles reduced the development of cracks during wetting-drying cycles. It is also reported that sand-clay mixture can be used in geotechnical and geoenvironmental applications, which is exposed to the significant fluctuation of water content like base liners and covers of landfills.

Day (1994) investigates the swelling-shrinkage behaviour of the compacted soil and reports that the swelling potential of the soil increase with the wetting-drying cycles. The continuous wetting-drying cycle destroyed the initial dispersed clay structure and resulting to a higly permeable clay characterized by flocculent structural arrangement. On the contrary, the study made by Al-Homoud et al. (1995) illustrated that the swelling potential of the soil is decreased with the wetting-drying cycles. The wetting-drying cycles result in continuous rearrangement of the soil particles resulting in particle aggregation, thereby reducing the clay content and plasticity. The decreased clay content and plasticity reduce the water absorption capacity, which is the major factor responsible for the decrease in swelling potential.

Tripathy and Rao (2009) investigated compacted expansive soil under the application of a laboratory cyclic swell-shrink test. The compacted specimen exhibits a swell fatigue behaviour as the wetting-drying cycles increases. This swell fatigue behaviour can be observed from the from the first cycle. The reversible volumetric and vertical deformations are greatly influenced by the soil suction during the shrinkage cycles. At the end of shrinkage cycles, the suction has a considerable impact on the compressibility index of the microstructure.

Yesiller et al. (2000) studied large-scale samples of low plasticity with varying fine contents to investigate the cracking behaviour under the

application of wetting-drying cycles. Crack intensity factor (CIF) is used to monitor the surficial dimensions of cracks. CIF is a parameter used to express the crack area in term of total soil surface area. It is reported that the soil containing greater fine content exhibits maximum cracks, higher suctions, rapidly increase in suction behaviour. The significant increase in crack formation is due to the addition of moisture to the soil. However, the soil containing lesser fine content exhibits minimal cracking behaviour. During the wetting-drying cycle, there are irreversible fabric changes in the soil. It leads to weaking of soil and reduction of soil strength. However, in alternate cycles, the wetting heals the cracks that developed in the last cycle. In the next drying, the cracks reopened, and the crack propagated easily.

Tang et al. (2011) investigated the initiation and propagation of cracks in the expansive soil subjected to wetting-drying cycles. The samples are prepared in slurry and subjected to five alternate wetting-drying cycles. The image processing concept is used to analyze the effect of wetting-drying cycles in crack patterns. The study report that the wetting-drying cycle significantly influences desiccation and cracking behaviour. During the first three cycles of wetting-drying, surface crack ratio, the cracking water content and final thickness are found to be increased. Beyond the three cycles, these parameters tend to attain an equilibrium, and it depends on material characteristics, especially the clay content. The crack pattern observed in the second cycle is observed to be irregular compared to the first cycle, which is accompanied by a reduction of pore volume shrinkage during drying.

Kleppe and Olson (1985) investigated the mechanical behaviour of the clay soil blended with sand. It is observed that addition of sand reduced the desiccation and cracking behaviour, and subsequent increase in mechanical stability and hydraulic conductivity. While the sample having higher clay content possesses lower hydraulic conductivity and exhibits significant cracks. Omidi et al. (1996) reported that the addition of sand

reduced the shrinkage potential and increased in the hydraulic conductivity of the compacted soil. At the same time the soil exhibits resistance to desiccation.

Rao and Tripathy (2003) investigate the ageing effect on the swelling-shrinkage behaviour of soil with a 100% liquid limit. The specimens are compacted and aged for different periods, i.e., 7, 15, 30, and 90 days. It is reported that the potential swelling decreases with ageing; however, the resistance to compression increases significantly. Initial water content and degree of saturation are responsible for the ageing effect. Ageing leads to particle rearrangements and the formation of bonds, which reduces the water-absorbing capacity of the compacted specimen. The ageing effect persists with specimens' wetting-drying cycles subjected to lower shrinkage magnitudes.

HB Seed et al. (1963) developed a method which able to predict the swelling potential behaviour of clayey soil from classification test data. Their study also showed a well-defined relationship between the swelling potential, the activity of clay, and the percentage of clay content. The partially or fully shrinkage produces different structural arrangements of soil; therefore, the swelling behaviour might diminish or increase with the wetting-drying cycle (Chen 1965). However, from the literature, it is known that the swelling potential during wetting-drying cycles depend on different factors like the percentage of the stabilizer used, test methods, the curing period and conditions of curing, and the soil type (Nabil et al. 2020).

Basma et al. (1996) investigated the behaviour of untreated soil under a series of wetting-drying cycles. The study concludes that untreated soil shows the destruction of flocculated clay under a higher number of wetting-drying cycles. The soil particles move together, form aggregates and observe a reduction in free swell characteristics, as discussed by Fateme (2010) in SEM analysis. The swell potential of lime-treated clay soil was

reduced (Sharma and Sivapullaiah 2017) and attained an equilibrium after the fourth cycle of the wetting-drying cycle.

Rao A et al. (2001) investigated the swelling behaviour of FA-treated soil under an alternate wetting-drying cycle and observed a continuous decrement of swelling potential compared to lime-treated soil. The experimental study performed by Kocataskin (1957) concluded that FA-blended soil exhibits significant resistance to the wetting-drying cycle. It is also influenced by the curing period of the sample.

Hoy et al. (2017) investigate the strength and microstructural changes of FA blended mixture subjected to wetting–drying cycles. The study observes a better durability performance of an FA blended mixture with higher NaOH content.

2.1.5. Machine Learning approach

In designing various large-scale construction projects and geotechnical structures, the coefficient of consolidation becomes a crucial mechanical parameter required for analyzing the settlement behaviour of the soil (Shukla et al. 2009; Zhang et al. 2018). Although this parameter can be determined experimentally, it is time-consuming, costly, and requires skilled technicians (Mohammadzadeh S et al. 2019). Moreover, the accuracy of the experimental result depends on several factors the instruments used, the meticulous experimental procedures and way of analyzing, and the knowledge and skill of the experimenters (Bui et al. 2019). Therefore, there came the necessity for developing advanced techniques that have the ability to quickly and accurately predict the coefficient of consolidation. Several researchers have explored the correlations between the consolidation parameters and the basic engineering properties of soil using the Machine Learning technique.

Dieu et al. (2018) propose a machine-learning based model that can predict the coefficient of soil compression. In total, 154 soil samples were

obtained for investigation from Vietnam. The samples are collected through 28 numbers of boring in different depths. Several engineering properties of the soil were considered which includes the location of sample (m), percentage of sand content, percentage of loam content, percentage of clay content, water content (%), wet density (g/cm3), void ratio, dry density (g/cm3), liquid limit (%), liquidity index, plastic limit (%), and plastic index (%). The model is developed by combination of two algorithms: Particle Swarm Optimization (PSO) and Multi-Layer Perceptron Neural Network (MLP Neural Nets). The MLP Neural Nets model structures optimization was performed using the application of the PSO metaheuristic. The study concludes that the proposed PSO-MLP Neural Nets accurately predict the soil compression coefficient, and the model is more suitable and accurate than other benchmark methods. Each position of a particle in the swarm serves as a solution for the MLP Neural Nets model when the weight and bias matrices of the model are converted to the coordination of each particle of the swarm. The key drawback of the suggested model is the selection of the PSO parameters' searching space, which restricts the particle positions.

Isik (2009) developed an artificial neural network to predict the swelling index of soft soil collected from various locations in Turkey. Two soil parameters are considered as input dataset, which includes natural water content and void ratio. The collected data are rescaled between 0 and 1 and separated, assuming 85% for training and 15% for testing. The developed model has one hidden layer and eight hidden layer nodes. A total of 42 different samples were considered in this study. A backpropagation algorithm was used to develop the model, and RMSE was found to be 0.0113. Further several empirical equations were developed using a combination of different soil properties, including void ratio, dry density, and natural water content. A comparison between the models developed from ANN and empirical equations was also presented to propose a suitable and accurate model for the prediction of the swelling index

Pham et al. (2020b) presented an ANN Model for predicting the coefficient of consolidation of soft soil available on coastal roads and highways of Ninh Binh Hai Phong, Vietnam. The study considered 188 soil samples, including 13 input variable which contains depth of soil samples, clay content, moisture content, dry density, bulk density, porosity, plastic limit, liquid limit, specific gravity, degree of saturation, plastic index, liquidity index, and void ratio. The model was trained using 70% of the input dataset, and the remaining were used to test the model's suitability. To reduce numerical bias, the input and output datasets were rescaled to the range between 0 and 1. Two different ANN structures were adopted, one having 14 neurons in a single hidden layer and another having 26 neurons in a single hidden layer. A total of 600 simulations were performed (300 simulations for each). The study shows that the developed model has a higher accuracy of RMSE (root mean square error) = 0.0614, MAE (mean absolute error)= 0.0415 and R^2 (coefficient of determination)= 0.997, which concludes that the appropriate choice of the neuron is required for excellent prediction of the coefficient of consolidation.

Manh et al. (2020) present several advanced soft computing approaches to predict the coefficient of consolidation of Vietnam soil. Biogeography-Based Optimization-based Artificial Neural Networks (ANN-BBO), ANN, Adaptive Network-based Fuzzy Inference System (ANFIS), and Support Vector Machines (SVM) were used. Relevant variables are selected by reducing the dimensionality of the through pre-processing techniques, like Principal Component Analysis (PCA) and correlation matrix. Several, evaluation matrices, including R^2, RMSE and MAE, were employed to determine the efficiency of model accuracy. The robustness of the proposed model is further verified through Monte Carlo simulation method. The study uses 188 soil samples with 13 independent variables. The study concludes that every model works well in predicting the coefficient of consolidation of soil; however, the prediction derived from the ANN-BBO model exhibits higher accuracy.

Pham et al. (2019) developed several ML models, including ANN, SVM and Adaptive Network-based Fuzzy Inference Systems (ANFIS), to predict the coefficient of consolidation of coastal areas in the Eastern side of Vietnam. The study considered 189 different soft soil samples with 13 independent variables. The study concludes that all three models work well; however, the SVM model is observed to be the best in predicting the soil consolidation coefficient. The sensitivity of the parameters was analyzed using Monte Carlo method and finding show that clay content, degree of saturation, depth of the sample availability, and specific gravity, are significantly relevant for predicting the same. Removal of insignificant variables reduces the dimensionality of the input and improves the developed models' performance.

Mittal et al. (2021) developed several ML-based models, including Multiple Linear Regression (MLR), ANN, SVR and ANFIS, to predict the coefficient of consolidation of soil. The study considered 534 soil samples from highway project of Vietnam. 13 independent variables are considered in this study. The insignificant variables are removed using feature selection techniques like Random Forests - Recursive Feature Elimination (RF-RFE), Least Absolute Shrinkage and Selection Operator algorithm (LASSO), and Mutual information have also been applied. The study concludes that the model ANFIS, a fusion of ANN and fuzzy inference system with LASSO, is the best model for predicting the coefficient of consolidation of soil with the coefficient of determination of 0.81.

Afshin et al. (2015) presented a Group Method of Data Handling (GMDH) type neural network to determine the recompression index of the overconsolidated soil using independent variables including the liquid limit, initial void ratio and specific gravity. A total of 344 datasets have been collected from different locations of Iran. A comparison between the single-parameter correlation and the developed model was present to illustrate the suitability of the developed model. The sensitivity analysis illustrated that

basic engineering properties like the void ratio and liquid limit significantly influence the recompression parameter of the soil.

Kurnaz et al. (2016) developed an ANN model to predict different compressibility parameter of the soil which includes the compression index and recompression index. The study used 246 different soil samples with 4 independent variables from different locations in Turkey. The developed ANN model accurately predicts the compression index, while the predicted recompression index is not accurately match with experimental dataset. The study also explained that there is a poor relationship between the recompression index and these independent variables.

Erzin et al. (2020) figure out the uncertainties in the determination of the compression index of normally consolidated clay. To overcome the uncertainties, a novel method based on robust optimization was developed to investigate uncertainties' effects in predicting the same. The study considered 433 Oedometer samples from different locations of Iran. For many empirical models to predict the compression index value and give the optimum values, the uncertainty definition is presented and tested against the correlation coefficients based on the Frobenius norm of the data points. The variation of the compression index is assessed with different basic properties like water content, liquid limit and void ratio with different uncertainties (0, 5 and 10%). The study concluded that the void ratio significantly influences the compression index, and the workability/suitability of the developed model is mentioned.

Nguyen et al. (2019) developed different ML models, including ANN and Random Forest, to predict the coefficient of consolidation of soil. Different 8 models were developed with different combinations of the independent input parameters. All models show a better predictive performance; however, among these, the 2nd model shows higher accuracy. It is formed by a combination of soil sample depth, clay content, and liquid limit with an R-value of 0.822. The study also concludes that the RF model

with the appropriate combination of soil properties can be implemented in geotechnical engineering for a better and more accurate prediction of the coefficient of consolidation parameter.

Mohammadzadeh S et al. (2019) proposed a gene expression model that can predict the compression index of fine-grain soil. The study collected 108 soil samples from different locations in Mashhad, Iran, with three different independent variables, namely plastic limit, liquid limit and initial void ratio. Contrary to classical models like regression models, the proposed gene expression model is highly nonlinear and includes a complex combination of influential input parameters. The result obtained from several evaluation matrices like RMSE, MAE and R2 concluded that the proposed model could be used for practical applications.

2.2. Summary

Several researchers developed different models and performed an immense study to assess the time-dependent behaviour of soft soil. However, the time-dependent behaviour of soft soil exhibits significant variation based on its origin, geological formation, clay content, the activity of soil, shape and gradation, soil structural interaction, and environmental conditions of the availability of natural soil. Different aspects, including structural construction, geotechnical foundations, underground tunnels, and many others, require the time-dependent behaviour of the soil. In India, BC soil is a widely available geomaterial which is a major concern from geotechnical concern. In this study, the time-dependent behaviour, especially the creeps and swelling behaviour of the BC soil, is assessed and predicted the same.

It is also noted that rapid urbanization severely impacts the ecological environment and disturbs nature in several aspects. One example is that coal is used as a major energy source in developing countries like India and China and is expected to remain so in the future. The continuous

evolution of FA from several thermal power stations leads to tremendous growth in the overall waste material quantities (Paul et al. 2019; Singh 2013). Several researchers also mentioned the suitability of FA as an admixture to improve the performance of soil. But there is limited information about the time-dependent behaviour of such reconstituted soil. The variation of the climate, hydrology and land use in the surrounding regions, and changes in monsoon significantly influence the water quantities in the soil. It exhibits a wetting-drying cycle in the naturally available geomaterial. However, there is limited information about the time-dependent swelling behaviour of the soil in alternate wetting-drying cycles.

There is a significant limitation in performing the experimental works, including the availability of instruments, time consumption and many others. However, for construction purposes, soil's settlement behaviour must be determined accurately and quickly. From these aspects, globally applicable models need to be developed to determine parameters like the coefficient of consolidation. Therefore, Machine Learning method can be employed to develop such a model, and the difference between the numerical simulation and ML approach needs to be assessed properly.

Chapter 3

Time-dependent compressibility characteristics of BC soil in 1D condition

3.1. Introduction

The clayey soil exhibits both creep and swelling behaviour, which can be defined as the time-dependent compression and expansion. The time-dependent behaviour of soil significantly influences the compressibility characteristics of naturally available geomaterials. Since the study of delayed strain suggested by Bjerrum (1967), substantial efforts have been made to develop different models to examine the time-dependent behaviour of soft soils (Yin et al. 2002). Considering the viscous effect during the primary consolidation, several models were developed and assessed several time-dependent parameters of the soil.

Although the previous studies provide fundamental insights into the time-dependent behaviour of soil, there are specific un-researched areas, for example, whether time-dependent strain during creep and swelling are the same or different at any instant or when time tends to infinity. Apart from it, the behaviour of the creep coefficient with the applied stress is not clearly mentioned, whether linear or non-linear, increases or decreases continuously. This study aims to investigate the above-mentioned limitation and also provide a reliable solution better to understand the long-term compressibility behaviour of problematic soils. Further, the strain rate behaviour of the soil is investigated during creep and swelling. The time-dependent parameters are examined using the elasto viscoplastic model considering swelling (EVPS Model). Further, predict the time-dependent behaviour of Indian Black Cotton soil using the same model.

3.2. Materials and sample preparation

The BC soil samples used in this investigation was collected from Madhya Pradesh. The index properties of BC soil according to their corresponding ASTM (American Society of Testing Material) standards are illustrated in **Table 3-1. Figure 3.1** illustrated the particle gradation curve of BC soil.

Table 3-1: *Basic properties of BC soil.*

Lists.	Parameters	Value
1.	Specific Gravity, G	2.72
2.	Liquid Limit, w_l (%)	73.405
3.	Plastic Limit, w_p (%)	34.12
4.	Plastic index, I_p (%)	39.285
5.	Optimum moisture content (*OMC)*	27.02
6.	Maximum dry density, ρ_d (g/cm^3)	1.406
7.	Sand (%) (4.75–0.075 mm)	17%
8.	Silt (%) (0.075–0.002 mm)	51%
9.	Clay (%) (<0.002 mm)	32%

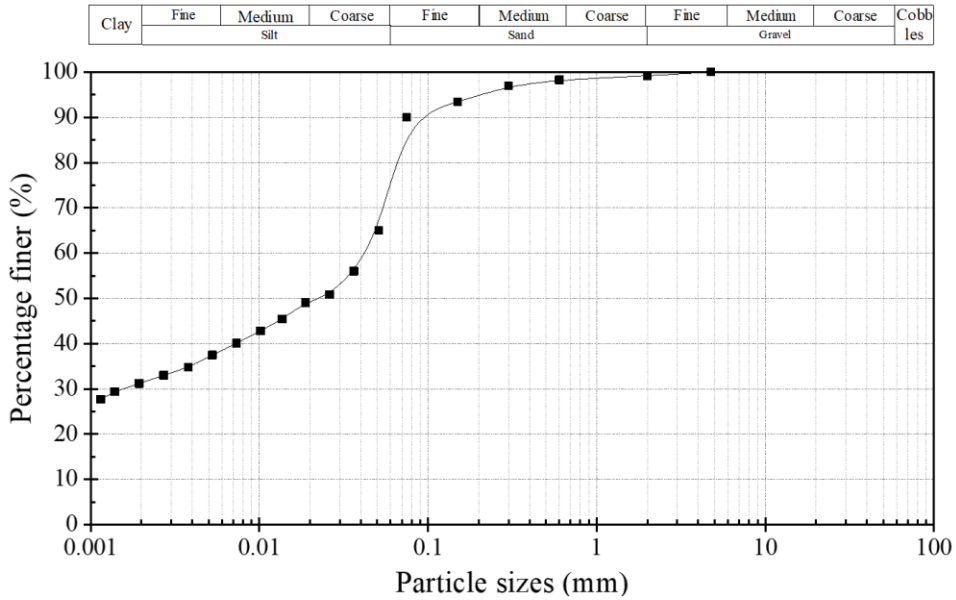

Figure 3.1: *Particle size distribution of BC soil.*

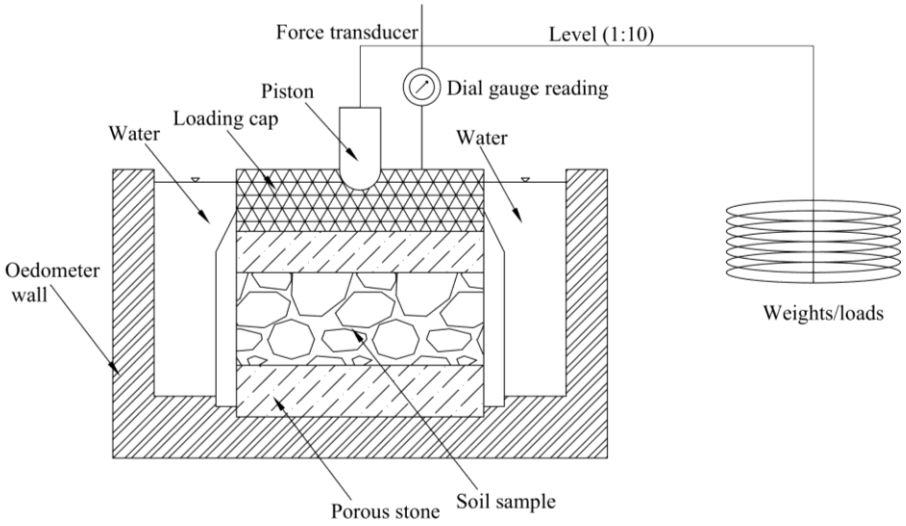

Figure 3.2: *Schematic diagram of the oedometer apparatus.*

The BC soil passing in 2mm is oven-dried at 110 ± 5°C for 24 h. After 24 h the sample is exposed to the room temperature for almost 30 minutes and allowed to attain room temperature. The BC sample is mixed with optimum moisture content and kept for 24 h in a zip polythene bag. The BC soil is compacted into three layers in maximum dry density in a known volume and extracted a sample having diameter of 60 mm and a height of 20 mm. The internal surface of the Oedometer ring is grease, so there is negligible friction between the soil and the steel surface. The extracted sample is transferred in an Oedometer ring and covered with filter paper on both soil sides. This will resist the entrance of fine particles into the porous stones. Dial gauges are clamped in their positions to record the relative movement between the loading cap and the base of the consolidation cell. A pressure of 5 kPa is applied as a seating pressure for one day (ASTM Standard 2010; BS 1377, Part 5:1990). Continuous multi-stage loading and unloading test is performed in one-dimensional Oedometer apparatus. During the whole

Table 3-2: *Loading pattern of the Oedometer test with corresponding loading durations.*

	Sl. No.	Loading (kPa)	Period (day)	Sl. No.	Loading (kPa)	Period (day)	Sl. No.	Loading (kPa)	Period (day)	Sl. No.	Loading (kPa)	Period (day)	Sl. No.	Loading (kPa)	Period (day)
	1	5	1	9	25	1	17	10	7	***25***	***250***	1	33	1000	1
	2	10	7	10	50	1	18	50	1	26	100	1	34	500	1
	3	25	1	11	100	1	19	250	1	27	10	7	35	250	1
E_1^*	4	50	1	12	500	1	20	500	1	28	100	1	36	100	1
	5	100	7	***13***	***1000***	7	21	1000	1	29	250	1	37	50	1
	6	50	1	14	500	1	22	1250	7	30	500	1	38	10	7
	7	25	1	15	250	1	23	1000	1	31	1000	1			
	8	10	7	16	50	1	24	500	1	32	1250	7	***29***	***500***	7
	1	5	7	8	10	1	15	100	1	22	1000	1	30	1000	1
	2	10	1	9	25	1	16	50	7	23	1250	7	31	100	1
	3	25	1	10	50	7	17	500	1	24	1000	1	32	50	1
E_2^{**}	4	50	7	11	100	1	18	1000	1	25	500	7	33	10	7
	5	25	1	12	250	1	19	1250	7	26	1000	1			
	6	10	1	13	500	7	20	1000	1	27	100	1			
	7	5	7	14	250	1	21	500	7	28	1000	1			
	1	5	7	5	100	7	***9***	***100***	7	13	100	7	17	1250	7
E_3^{***}	2	10	7	6	250	7	10	50	7	14	250	7			
	3	25	7	***7***	***500***	7	11	10	7	15	500	7			
	4	50	7	8	250	7	12	50	7	16	1000	7			

Symbol indicates the total duration of loading, *** denotes 119 days, ** denotes 95 days and * denotes 92 days.

In result and discussion section, bold and italic stresses are presented.

testing period, the soil samples are kept saturated, and the test is conducted at a normal room temperature of 25±2°C. A schematic diagram of the oedometer apparatus is illustrated in **Figure 3.2**. Two different loading pattern is used and renamed as E_1, E_2 and E_3. The applied stress and corresponding duration of loading and unloading are illustrated in **Table 3-2.**

In E_1 the loading and unloading occurred for every 24 h to reach limiting stress which is applied for seven continuous days. The significance of E_1 is to investigate the influence of the unloading-reloading cycle on the swelling behaviour. However, in the case of E_2 there is no trend, here continuous loading and unloading are performed till to reach a limiting stress in alternate manner. It aims to examine the effect of applied stress on swelling behaviour. In the case of E_3, all stress is applied for seven continuous days. E_3 is conducted to study the impact of loading time on swelling behaviour. Providing a longer duration of loading and unloading arrangement allows the soil to achieve an equilibrium condition (Powell *et al.* 2012), and allows to investigate the long-term time-dependent behaviour of the soil (Yin 1999, Feng *et al.* 2017a).

3.3. Description of EVPS Model

The change in the vertical strains against effective stress obtained from the Oedometer under different loading patterns is illustrated in **Figure 3.3**. The one-dimensional Oedometer test results are employed to interpret various compressibility parameters using EVPS Model. Some terminologies of the EVPS Model are defined as follows.

3.3.1. Instant timeline

It is defined by the soil skeleton's elastic-plastic deformations and instant response due to sudden changes in applied effective stress. Strains along the instant timeline are considered to be recoverable and hence elastic.

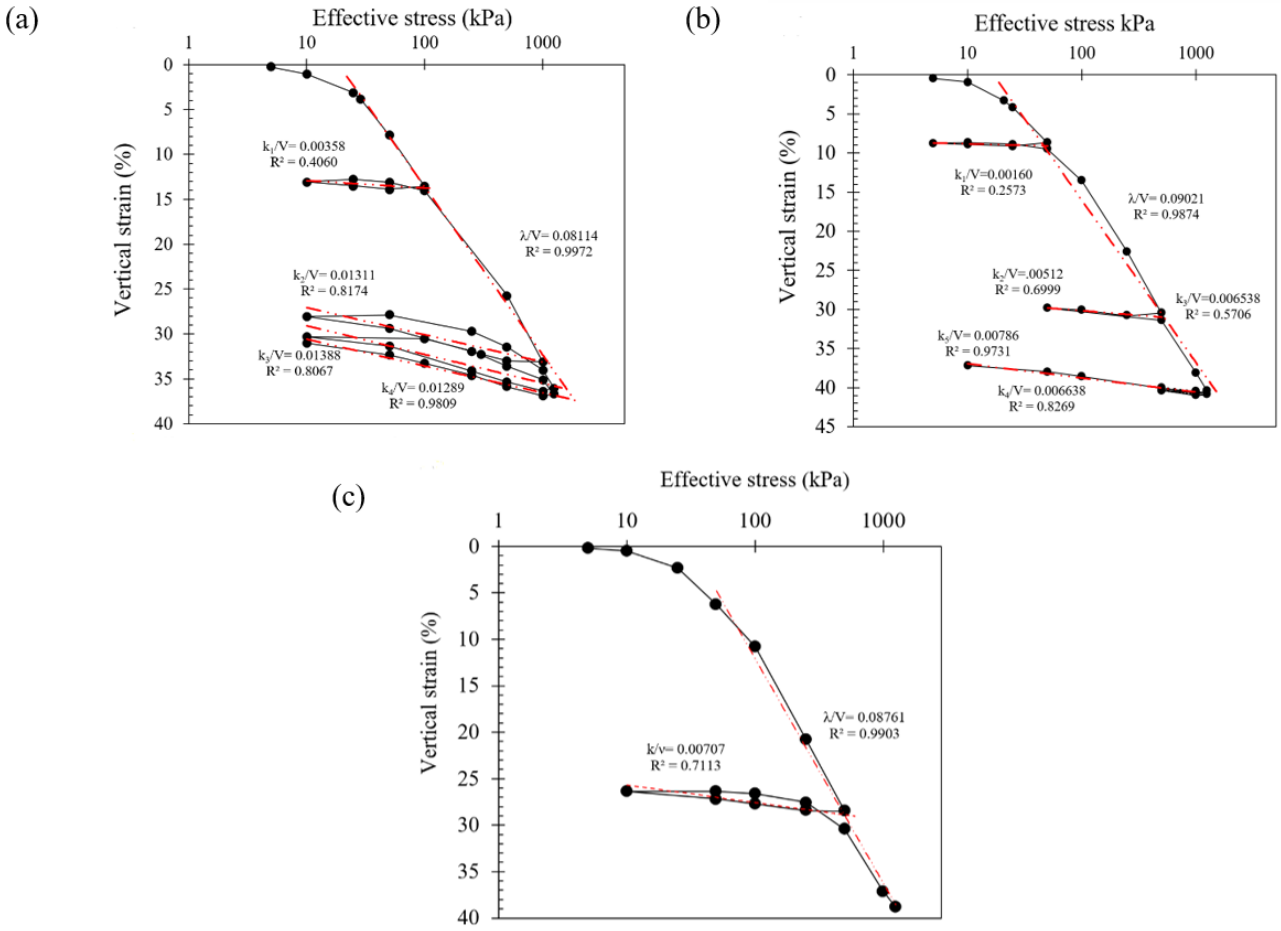

Figure 3.3: *Change in vertical strain against the effective stress (a) E_1, (b) E_2 and (c) E_3.*

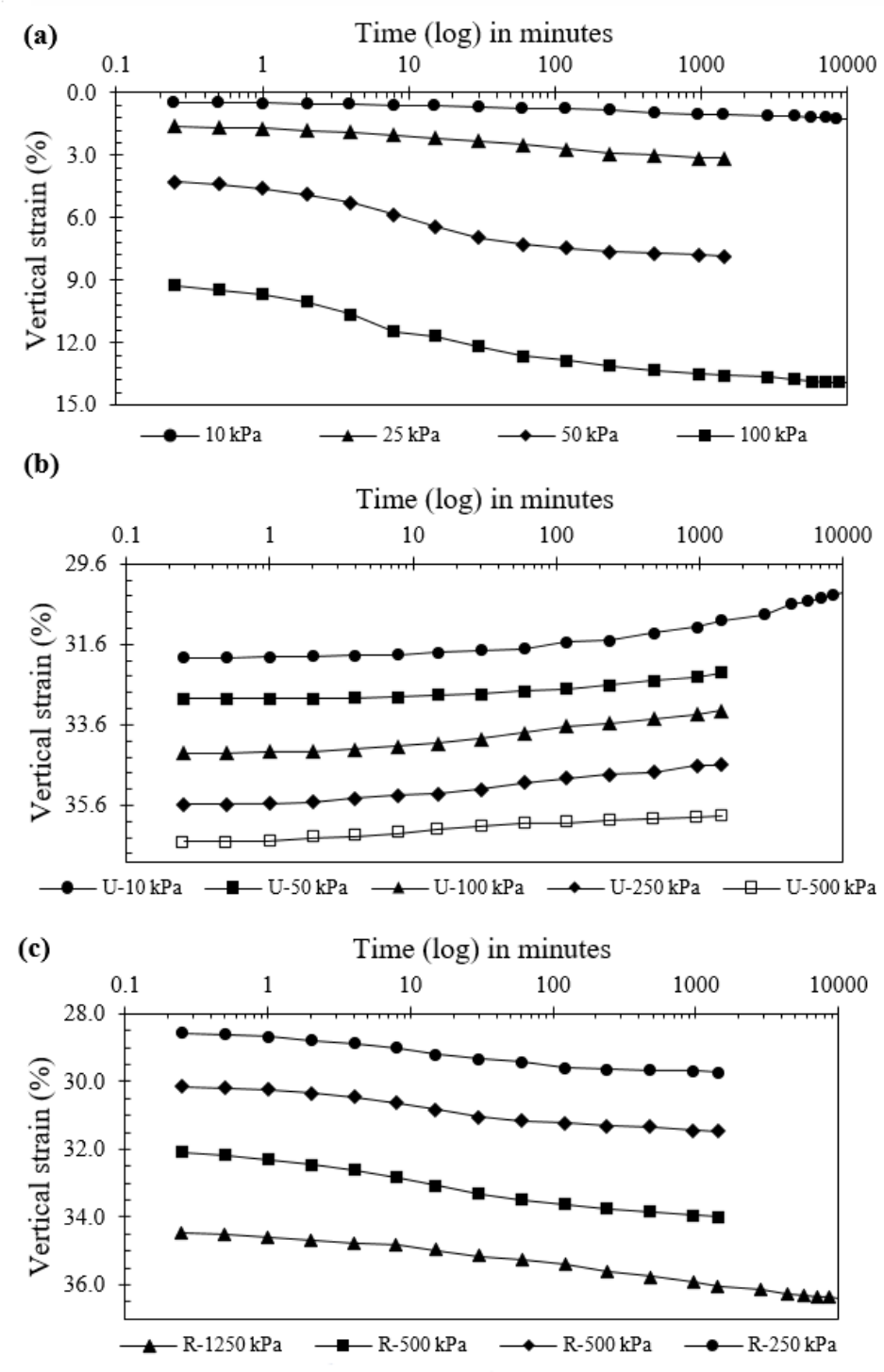

Figure 3.4: *Change in vertical strain against time (log scale) in E_1 during (a) normal loading (b) unloading and (c) reloading.*

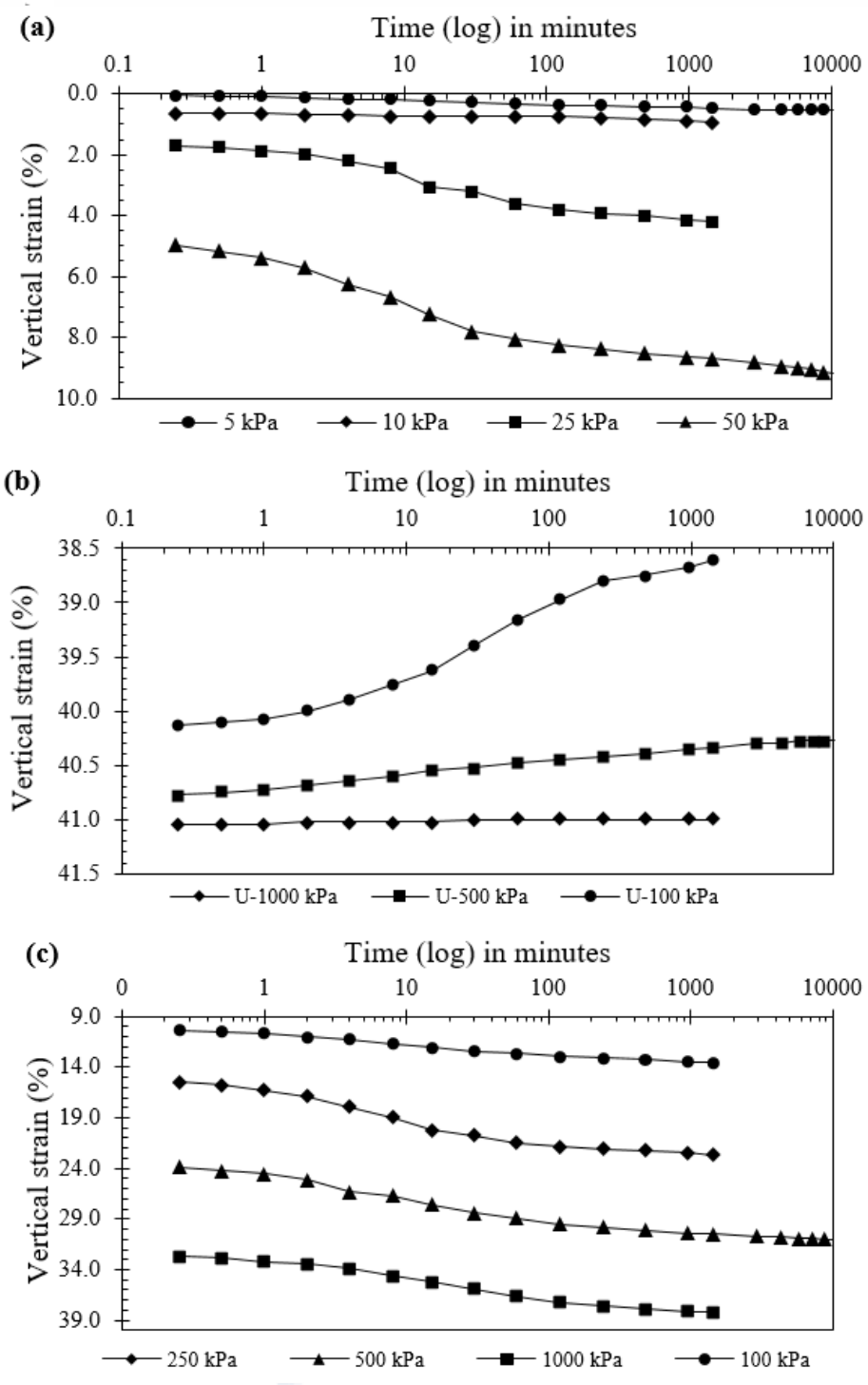

Figure 3.5: *Change in vertical strain against time (log scale) in E_2 during (a) normal loading (b) unloading and (c) reloading.*

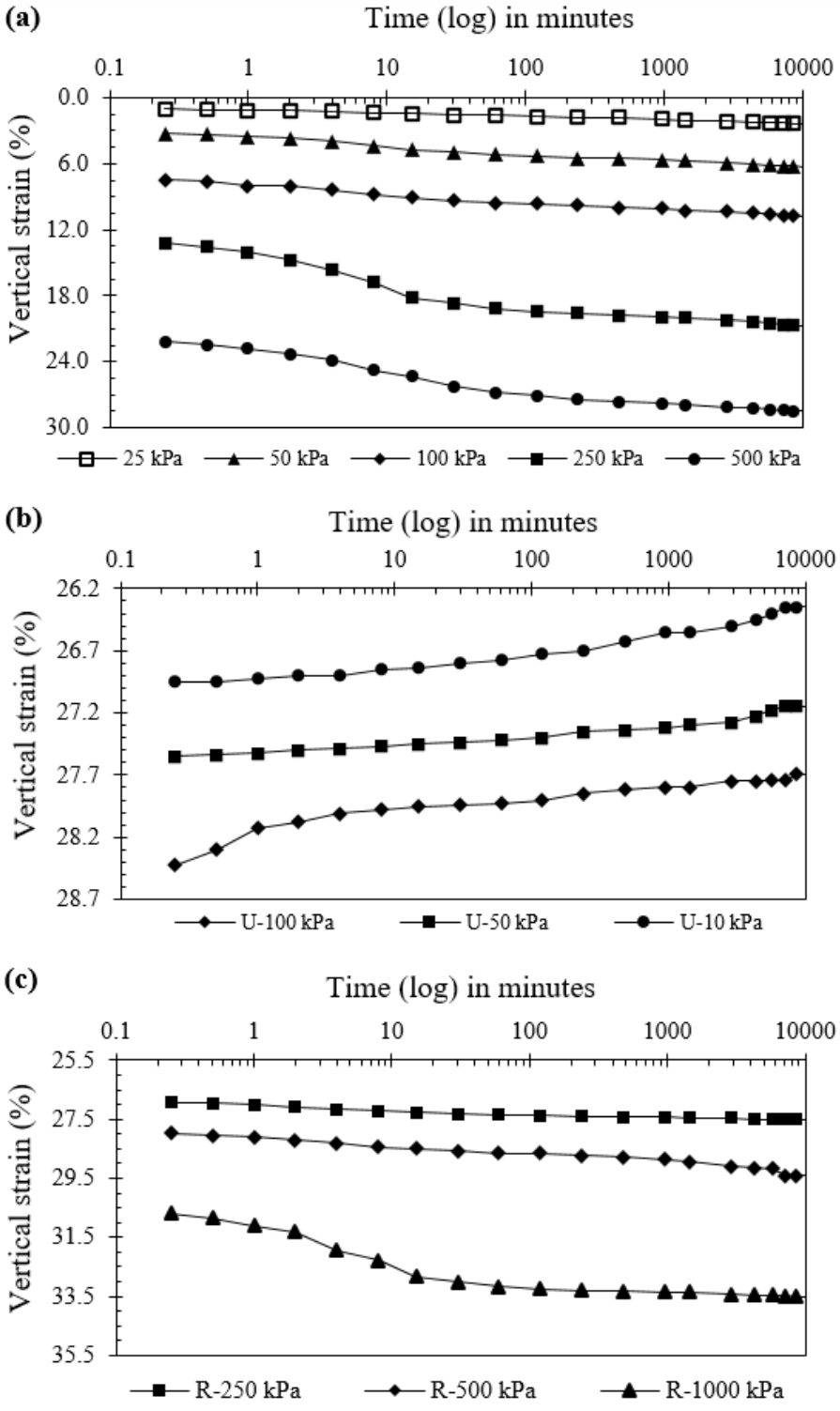

Figure 3.6: *Change in vertical strain against time (log scale) in E_3 during (a) normal loading (b) unloading and (c) reloading.*

The rebounding parameter *k/V* is analyzed using The Oedometer results, it is defined as the slope of an over-consolidated soil.

According to the EVPS Model, the elastic strain during the reloading phase signifies the rebounding parameter (Yin 1990b) and is given by the **Eqn. 3-1.** Further, the relationship between the rebounding index C_r and rebounding parameter *k/V* is also defined below

$$\varepsilon_z^e = \varepsilon_{z,i}^e + \frac{k}{V}\ln\left(\frac{\sigma_z^{/}}{\sigma_{z,i}^{/}}\right) \qquad 3\text{-}1$$

$$\frac{C_r}{V} = \ln(10)\frac{k}{V} = 2.3\frac{k}{V} \qquad 3\text{-}2$$

where $\left(\varepsilon_{z,i}^e, \sigma_{z,i}^{/}\right)$ are points in *k/V* line which is the material parameter. V denotes the specific volume of the material and is defined as 1+ e_o and e_o signifies the initial void ratio. The parameter *k* can be expressed as $\Delta e / \left[\ln\left(\sigma_z^{/} / \sigma_{z,i}^{/}\right)\right]$, *k* lines signifying the instant timeline. The superscript "*e*" is used to denote the elastic phase. In the loading pattern E_1, there is a higher number of unloading-reloading cycles. During the first unloading-reloading cycle, k/V is observed to be 0.0036 and 0.0131 during the second unloading-reloading cycle and further increases to 0.0139 during the third unloading-reloading cycle. The continuous unloading-reloading cycle leads to higher compactness of soil rearrangement of soil particles. To regain the equilibrium state of the soil particles, the soil particles exhibit a higher rebounding tendency. Thus, the material parameter *k/V* increases with a higher unloading-reloading cycle.

3.3.2. Timelines

According to the concept of the EVPS model, the timelines are defined as the lines having equal values of equivalent time. However, it is

different from the duration of the loading or unloading. The timelines are assumed to be parallel to each other, either in creep or swelling.

3.3.3. Equivalent timelines

It is the time taken by sample to exhibit creep or swell from a reference timeline under the application of constant stress. For the normally consolidated MSL test, with the application of a constant loading or unloading duration and load increment ratio (Yin and Graham 1994), the equivalent time is close to the duration of load increment or decrement. The larger equivalent time is associated with a lower creep rate.

The relationship between the change of vertical strain against time for different loading patterns is illustrated in **Figure 3.4**, **Figure 3.5** and **Figure 3.6** during loading, unloading and reloading cycles. The vertical deformation under the application of constant stress is composed of both primary and secondary consolidation. The excess pore water pressure dissipated from the interconnected voids of clayey soil coupled with the compression in primary consolidation. The stage having insignificant/negligible excess pore water pressure is called the end of the primary consolidation, EOP. The time corresponding to EOP is denoted as t_{eop} (Fatahi et al. 2013). The EOP in the BC soil is in the range of 31.75-113 mins. It is calculated by the tangent line's graphical intersection drawn from the primary consolidation phase and the secondary consolidation phase. In this study, t_{eop} is assumed as t_0^c and the reference timeline of creep and swelling are denoted by the t_0^c and t_0^s , which is the EOP during compression and swelling, respectively. Using the defined value of reference time, the equivalent time during any constant stress can be calculated as $t_e^c = t - t_0^c$, where t is the total duration of loading (Yin and Tong 2011a).

3.3.4. Reference timeline

According to the concept of the EVPS model, the reference timeline is defined as equivalent time having zero values. With respect to the reference timelines, the creep or swelling behaviour of the soil is determined. The equivalent time below the reference timeline has a value in the range of 0<equivalent time<∞. Above the reference timeline, the equivalent time is negative. As given by Yin and Graham (1994), the reference timeline can be derived from **Eqn. 3-3,** as follows;

$$\varepsilon_z^{rc} = \varepsilon_{z0}^{rc} + \frac{\lambda}{V}\ln\left(\frac{\sigma_z^{/}}{\sigma_{z0}^{/rc}}\right) \qquad 3\text{-}3$$

$$\frac{C_c}{V} = \ln(10)\frac{\lambda}{V} = 2.3\frac{\lambda}{V} \qquad 3\text{-}4$$

where $\left(\varepsilon_{z0}^{rc}, \sigma_{z0}^{/rc}\right)$ are points in on the λ/V lines. ε_z^{rc} signifies the reference strain and λ/V is a material parameter and denotes the slope of the reference line where $\lambda = \Delta e \Big/ \left[\ln\left(\sigma_z^{/}, \sigma_{z0}^{/rc}\right)\right]$. The superscript "*rc*" is used for the indication of the reference timeline. The parameter λ/V for BC soil is observed to be 0.0803 in E_1, 0.0902 in E_2 and 0.0876 in E_3. The parameter λ/V exhibits a minor change in all the tests. However, a small variation of the parameter is due to differences in loading pattern and duration of loading. Various compressibility characteristics of BC soil derived from the EVPS Model are given in **Table 3-3.**

Table 3-3: Compressibility characteristics of BC soil.

	k/V	λ/V	C_r/V	C_c/V	$C_{\alpha e}/V$	$C_{\alpha e}/C_c$
E_1	0.00358	0.08114	0.008234	0.18662	0.00555	0.02973
	0.01311		0.030153			
	0.01388		0.031924			
	0.01289		0.029647			
E_2	0.00160	0.09021	0.003681	0.20748	0.00729	0.03513
	0.00512		0.011776			
	0.00653		0.015019			
	0.00663		0.015249			
	0.00786		0.018078			
E_3	0.00707	0.08761	0.016261	0.20150	0.00544	0.02699

3.4. The general equation for 1D consolidation

The clay soil exhibits time-dependent behaviour, which is determined using the EVPS model in this study. According to the concept of the EVPS model, the total strain is defined as any point in the creep region or swelling region with respect to the reference timeline under particular stress. It is calculated as follows.

$$\varepsilon_z = \varepsilon_z^{rc} + \varepsilon_z^c = \varepsilon_{z0}^{rc} + \frac{\lambda}{V}\ln\left(\frac{\sigma_z^{/}}{\sigma_{z0}^{/rc}}\right) + \varepsilon_z^c \qquad 3\text{-}5$$

where ε_z^c denotes the creep settlement.

3.4.1. Linear creep prediction function

Two different concepts are used to determine time-dependent settlement in this study. The first one is the linear concept; here, a linear relationship between the vertical strain changes and loading period is employed to derive the creep coefficient as follows.

$$\varepsilon_z^c = \varepsilon_{z0}^c + \frac{\psi^c}{V}\ln\left(\frac{t_0^c + t_e^c}{t_0^c}\right) \qquad 3\text{-}6$$

where t_e^c denotes the equivalent time, it is defined as the time taken by constant effective stress for creep to reach the current strain with respect to the reference timeline. t_0^c signifies the time parameter, which corresponds to the beginning of showing creep strain, ε_{z0}^c signifies the strain at the time $t_0^c = t_e^c$. $\left(\psi^c / V\right)$ is the creep parameter. For the denotation of the creep stage, a superscript "*c*" is used. The best fitting curve for determination of the creep parameter is produced at $t_{eop} = t_0^c$. The fitting curve is drawn between the change in vertical strain *(*$\Delta\varepsilon$*)* and "log t" is used to derive the creep coefficient. A representative data (from E_3) is shown in **Figure 3.7**, in which

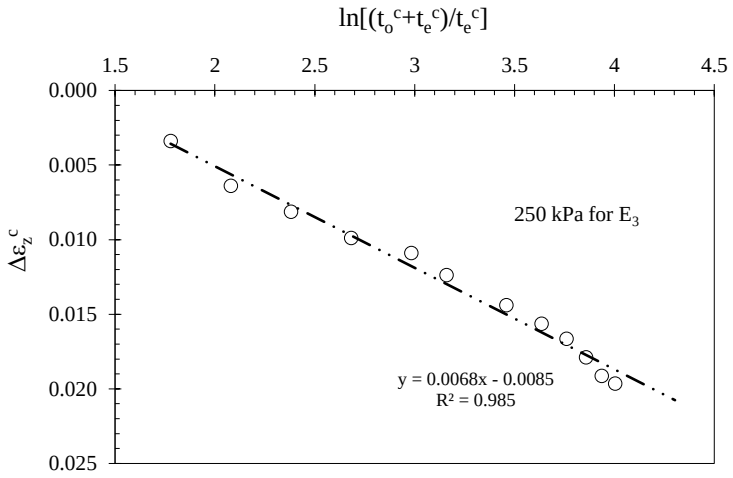

Figure 3.7: *Fitting curve for creep parameters using linear function.*

the creep coefficient $\left(\psi^c / V\right)$ is observed to be 0.0068 during the application of 250 kPa. Using a similar concept, the swelling behaviour of the clayey soil is predicted using the linear function as follows.

$$\varepsilon_z^s = \varepsilon_{z0}^s - \frac{\psi^s}{V} \ln\left(\frac{t_0^s + t_e^s}{t_0^s}\right) \qquad 3\text{-}7$$

where t_e^s denotes the equivalent time taken by soil for swelling. It is defined as the time taken by constant effective stress for swelling to reach the current strain with respect to the reference timeline. t_0^s denotes the time parameter, which corresponds to the beginning of swelling strain, ε_{z0}^s signifies the strain at $t_0^s = t_e^s$, ψ^s/V is the swelling parameter. For an indication of the swelling stage, the superscript "*s*" is used. The best fitting curve for the determination of swelling parameter is produced at $t_{eop} = t_0^s$. The swelling is the reverse action of the creep; therefore, the swelling coefficient is determined from the slope of the fitting curve plotted between the change in vertical strain *(Δε)* and "log t". A representative data (from E_1) is shown in **Figure 3.8** where the swell parameter $\left(\psi^s/V\right)$ is observed as 0.0027 under effective stress of 250 kPa unloading.

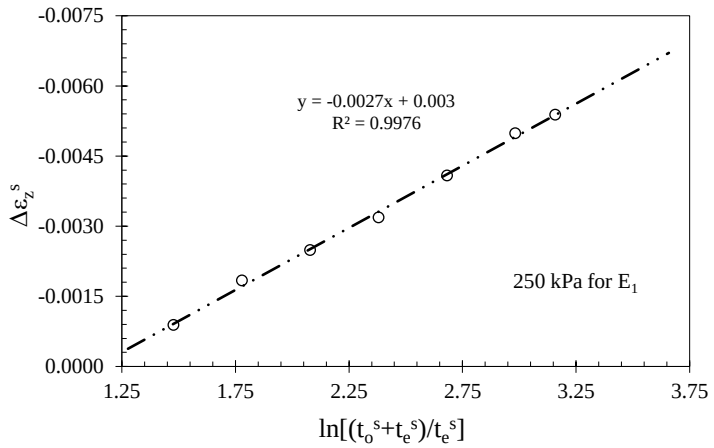

Figure 3.8: *Fitting curve for swelling parameters using linear function.*

3.4.2. Non-linear function for creep prediction

During the application of linear function, there is an overestimation of the creep behaviour of BC soil. However, better and more reliable creep prediction is of great importance for practising engineers and academicians worldwide. To overcome the overestimation or underestimation of the creep

settlement, a non-linear function proposed by Yin is used for further investigation (Yin 1999). The creep strain, excluding the initial strain, is given by

$$\varepsilon_z^c = \frac{\frac{\psi_0^c}{V}\ln\left(\frac{t_0^c + t_e^c}{t_0^c}\right)}{1+\frac{\psi_0^c}{V\varepsilon_z^{cl}}\ln\left(\frac{t_0^c + t_e^c}{t_0^c}\right)} \qquad 3\text{-}8$$

where ψ_0^c/V , ε_z^{cl} and t_0^c are the constant parameters for particular stress. ψ_0^c/V signifies the creep coefficient, ε_z^{cl} denotes the creep strain limit. It denotes the strain the soil can attain when the loading time tends to infinity

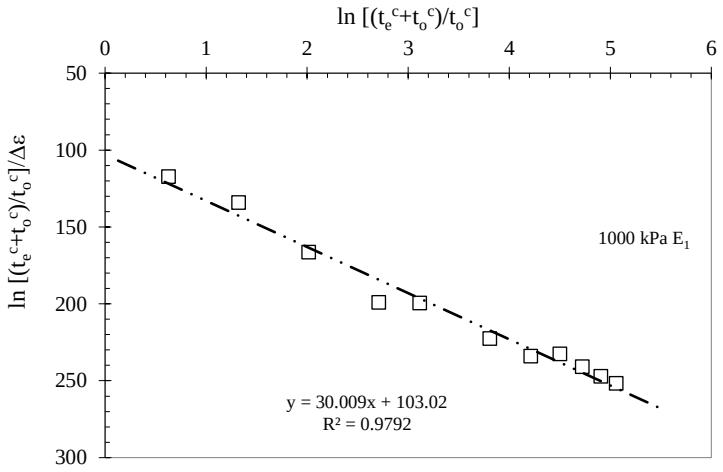

***Figure 3.9**: Fitting curve for creep parameters using non-linear function.*

and is measured as the distance between the reference timeline and the creep equivalent limit (CEL) line (Yin and Tong 2011a). When the time tends to infinity, $\varepsilon_z^c = \varepsilon_z^{cl}$ (Feng et al. 2017a; Yin 2015b). The above equation can be further simplified as follows to determine the corresponding parameters using the data obtained from Oedometer.

$$\frac{1}{\varepsilon_z^c}\ln\left(\frac{t_0^c+t_e^c}{t_0^c}\right)=\frac{1}{\varepsilon_z^{cl}}\ln\left(\frac{t_0^c+t_e^c}{t_0^c}\right)+\frac{V}{\psi_0^c} \qquad \textit{3-9}$$

If $\ln\left[\left(t_0^c+t_e^c\right)/t_0^c\right]$ is treated as *x*, the creep coefficient ψ_0^c/V as the *a* and the reciprocal of creep strain limit $1/\varepsilon_z^{cl}$ as *b*, then the **Eqn. 3-9** can be expressed in the form of a straight line "*y=bx+a*" putting $\frac{1}{\varepsilon_z^c}\ln\left(\frac{t_0^c+t_e^c}{t_0^c}\right)=y$. The Oedometer data are used to fit a straight line between the $\ln\left[\left(t_0^c+t_e^c\right)/t_0^c\right]$ against the $\ln\left[\left(t_0^c+t_e^c\right)/t_0^c\right]/\Delta\varepsilon_z^c$ to determine the corresponding slope and intercept. The intercept and slope are employed to determine the creep coefficient and creep strain limit, respectively. A fitting curve is plotted in between the $\ln\left[\left(t_0^c+t_e^c\right)/t_0^c\right]/\Delta\varepsilon_z^c$ against $\ln\left[\left(t_0^c+t_e^c\right)/t_0^c\right]$ during the application of 1000 kPa in E_1 as shown in **Figure 3.9**. The slope and intercept in the straight line obtained from the trend line are converted to corresponding parameters. The curve fitting parameter (R^2) is observed to be more significant than 0.98, which means a good fitting curve is obtained. Thus, the creep coefficient ψ_0^c/V for the BC soil is observed to be 0.00781, and the corresponding ε_z^{cl} is 0.0371. It meant that during the applied effective stress, the creep strain limit would be 0.0371 when the same stress is applied for an infinite period of time.

Further, the concept of non-linear function is studied and extended to study the time-dependent swelling behaviour of the clayey soil. Thus, the swelling strain of the clayey soil can be determined using a non-linear function as follows.

$$\varepsilon_z^s=-\frac{\frac{\psi_0^s}{V}\ln\left(\frac{t_0^s+t_e^s}{t_0^s}\right)}{1+\frac{\psi_0^s}{V\varepsilon_z^{sl}}\ln\left(\frac{t_0^s+t_e^s}{t_0^s}\right)} \qquad \textit{3-10}$$

where ψ_0^s/V , ε_z^{sl} and t_0^s are the constant parameters for particular stress. ψ_0^s/V signifies the swelling coefficient, ε_z^{sl} denotes the swell strain limit. It denotes the strain the soil can attain when the time of loading tends to infinity and is measured as the distance between the reference timeline and swell equivalent limit (SEL) line (Yin and Tong 2011a). When the time tends to infinity, $\varepsilon_z^s = \varepsilon_z^{sl}$ (Feng et al. 2017a; Yin 2015b). The above equation can be further simplified as follows to determine the corresponding parameters using the data obtained from Oedometer.

$$\frac{1}{\varepsilon_z^s}\ln\left(\frac{t_0^s+t_e^s}{t_0^s}\right) = -\frac{1}{\varepsilon_z^{sl}}\ln\left(\frac{t_0^s+t_e^s}{t_0^s}\right) + \frac{V}{\psi_0^s} \qquad 3\text{-}11$$

If $\ln\left[\left(t_0^s+t_e^s\right)/t_0^s\right]$ is treated as *x*, the swell coefficient ψ_0^s/V as the *a* and the reciprocal of creep strain limit $1/\varepsilon_z^{sl}$ as *b*, then the **Eqn. 3-11** can be

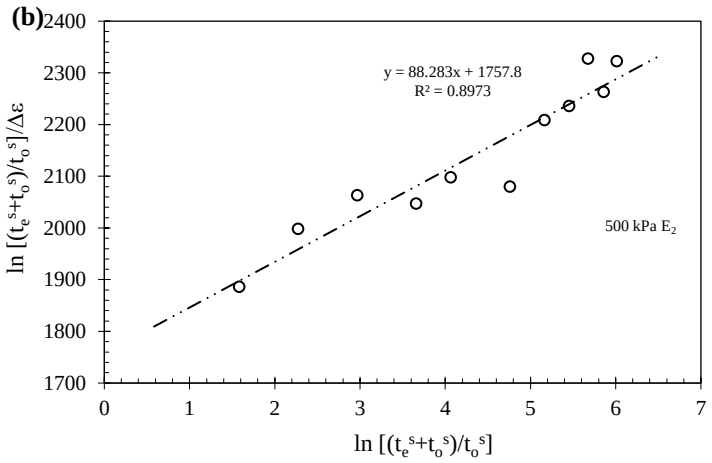

Figure 3.10: *Fitting curve for swelling parameters derive from non-linear parameters.*

***Table 3-4**: Time-dependent parameters of BC soil during creep and swelling.*

Soil Samples	**Loading (kPa)**	$\frac{\psi_0^c}{V}$	ε_z^{cl}	**Unloading (kPa)**	$\frac{\psi_0^s}{V}$	ε_z^{sl}
E_1	50	0.00514	0.00992	10	0.00018	-0.00144
	500	0.01801	0.02917	250	0.00142	-0.03191
	250	0.00337	0.00266	500	0.00085	-0.03050
	1000	0.00161	0.02555			
E_2	50	0.00350	0.03031	500	0.00051	-0.02217
	250	0.01257	0.02625	100	0.00211	-0.07895
	1000	0.01311	0.05798	10	0.00084	-0.01035
E_3	250	0.00804	0.03676	100	0.0003	0.03130
	500	0.00602	0.03421	50	0.00029	-0.00342
	1000	0.00296	0.00709	10	0.00048	-0.00587

expressed in the form of a straight line "$y=—bx+a$" putting $\frac{1}{\varepsilon_z^s}\ln\left(\frac{t_0^s+t_e^s}{t_0^s}\right)=y$ The Oedometer data are used to fit a straight line between the $\ln\left[\left(t_0^s+t_e^s\right)/t_0^s\right]$ against the $\ln\left[\left(t_0^s+t_e^s\right)/t_0^s\right]/\Delta\varepsilon_z^s$ to determine the corresponding slope and intercept. The slope and intercept are employed to determine the swell strain limit and swell coefficient, respectively.

A fitting curve is plotted in between the $\ln\left[\left(t_0^s+t_e^s\right)/t_0^s\right]/\Delta\varepsilon_z^s$ against $\ln\left[\left(t_0^s+t_e^s\right)/t_0^s\right]$ during the application of 500 kPa in E_2 as shown in **Figure 3.10**. The slope and intercept in the straight line obtained from the trend line are converted to corresponding parameters. The curve fitting parameter (R^2) is observed to be more significant than 0.89, which means a good fitting curve is obtained. Thus, the swell coefficient ψ_0^s/V for the BC soil is observed to be 0.00056, and the corresponding ε_z^{sl} is 0.0113. It meant that during the application of 500 kPa, the creep strain limit would be 0.0113 when the same stress is applied for an infinite period of time.

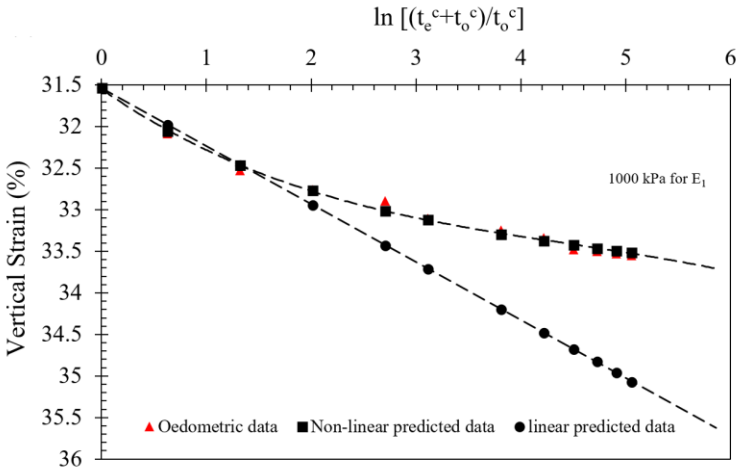

***Figure 3.11**: Prediction of the creep behaviour of BC soil using the EVPS Model.*

Using the concept of both linear and non-linear function, various parameters during creep is determined as illustrated in **Table 3-4**. The axial deformation of BC soil during the application of 1000 kPa ***(13)*** in the

loading pattern E_1 is predicted using both function as shown in **Figure 3.11**. It is observed that the axial prediction of BC soil can be predicted accurately using the non-linear function of the EVPS Model.

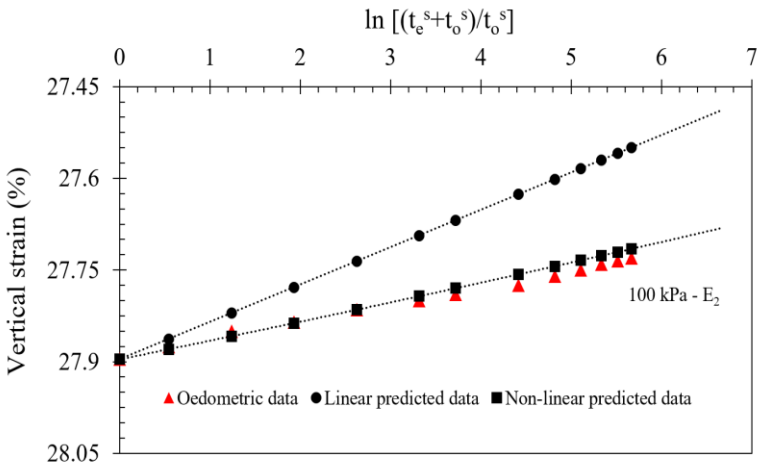

Figure 3.12: *Prediction of swelling behaviour of BC soil using EVPS Model.*

During the application of 100 kPa (9) from the loading pattern E_3, the time-dependent swelling deformation of BC soil is predicted using both linear and non-linear functions. **Figure 3.12** illustrates the accuracy of the functions against the actual Oedometric data. It is observed that BC soil can be predicted accurately using the non-linear function. In both the creep and swelling, the prediction obtained from the linear function overestimates the axial deformation, which is unacceptable.

3.4.3. Creep and swelling strain rate

During the application of a constant load, the creep or swelling will continue till to Creep Equilibrium Line (CEL) or Swell Equilibrium Line (SEL), respectively. However, the strain rate is an important factor that influences to achieve the CEL or SEL. The strain rate change during creep is determined using the non-linear function. The strain rate can be derived from **Eqn. 3-8** as follows;

$$\dot{\varepsilon}_z^c = \frac{d\varepsilon_z^c}{dt_e} = \frac{d}{dt_e}\left\{ \varepsilon_{z0}^c + \frac{\frac{\psi_0^c}{V}\ln\left(\frac{t_0+t_e}{t_0}\right)}{1+\frac{\psi_0^c}{V\varepsilon_z^{cl}}\ln\left(\frac{t_0+t_e}{t_0}\right)} \right\}$$

$$\dot{\varepsilon}_z^c = \frac{\psi_0^c / V}{t_0+t_e} \frac{1}{\left\{1+\frac{\psi_0^c}{V\varepsilon_z^{cl}}\ln\left(\frac{t_0+t_e}{t_0}\right)\right\}^2} \qquad \textit{3-12}$$

where the symbols have the usual meaning. The strain rate variation in BC soil during creep is illustrated in **Figure 3.13**. Similarly, during the swelling, the strain rate is derived from **Eqn. 3-10** and expressed as follows

$$\dot{\varepsilon}_z^s = \frac{d\varepsilon_z^s}{dt_e} = \frac{d}{dt_e}\left\{ \varepsilon_{z0}^s + \frac{\frac{\psi_0^s}{V}\ln\left(\frac{t_0+t_e}{t_0}\right)}{1-\frac{\psi_0^s}{V\varepsilon_z^{sl}}\ln\left(\frac{t_0+t_e}{t_0}\right)} \right\}$$

$$\dot{\varepsilon}_z^s = \frac{d\varepsilon_z^s}{dt_e} = -\frac{\psi_0^s / V}{t_0+t_e} \frac{1}{\left\{\left(\frac{\psi_0^s}{V\varepsilon_z^{sl}}\ln\left(\frac{t_0+t_e}{t_0}\right)\right)-1\right\}^2} \qquad \textit{3-13}$$

The changes in strain rate in BC soil with respect to time during swelling are illustrated in **Figure 3.14**. During the initial stage, the strain rate is observed to be changing fastly from t_0, afterward it is almost consistent for each loading. Under particular effective stress, either decreasing or increasing, the soil tried to achieve an equilibrium condition. The time-independent volumetric change occurs in the initial phase due to the sudden application/removal of load, leading to an equilibrium condition.

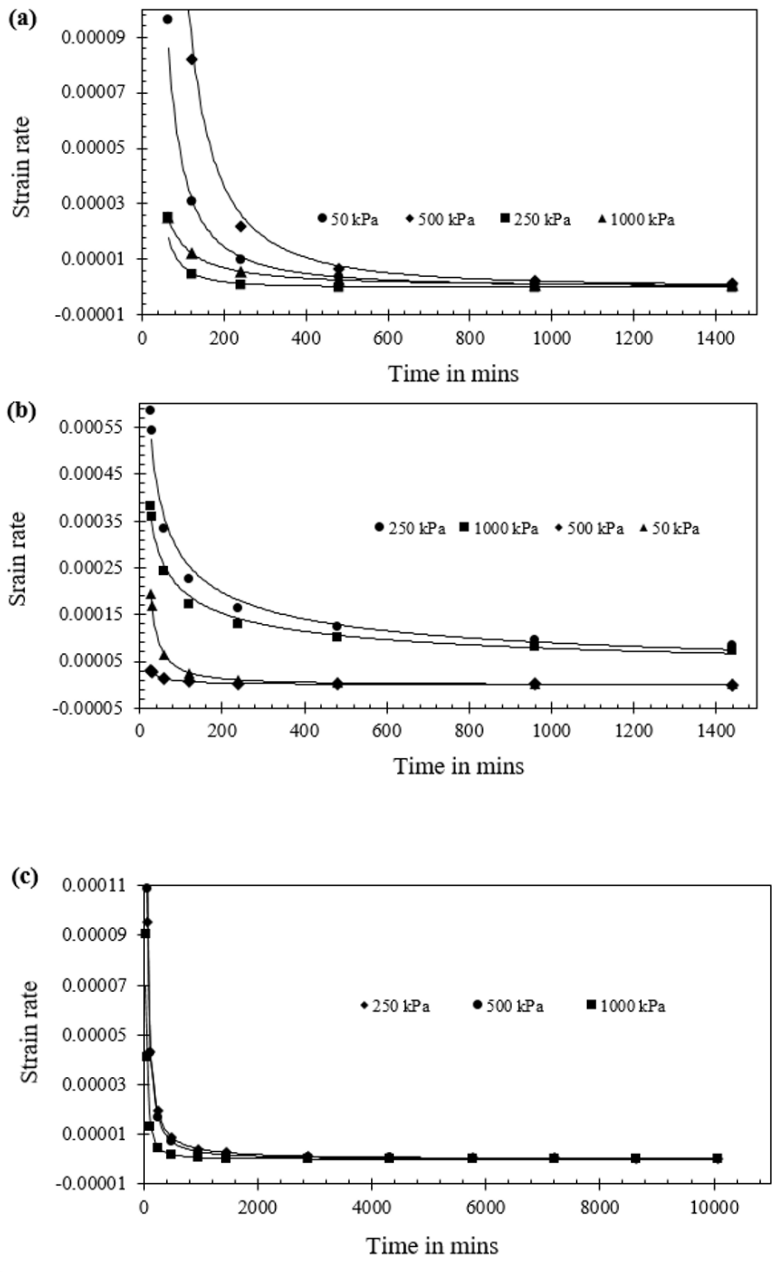

Figure 3.13: *Strain rate behaviour during loading for different loading patterns (a) E1, (b) E2 and (c) E3.*

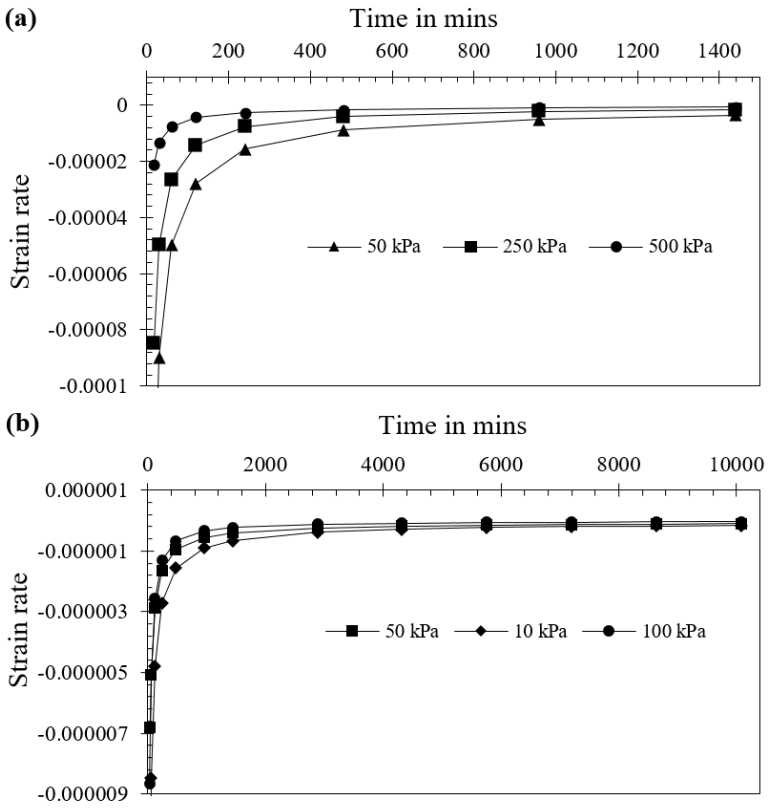

Figure 3.14: *Strain rate behaviour during swelling for different loading patterns (a) E1 and (b) E2.*

Even after attaining an equilibrium condition, a minimal strain rate variation occurs. This might be due to the viscous movement of the adsorbed water in the double layer of clayey soil. Being highly viscous, the adsorbed doesn't move under normal hydraulic conditions (Duan 2021). Several other responsible factors might be the viscous rearrangement of particles and deformation of the skeleton structure, particle sliding, and internal soil interaction. In **Figure 3.13** (c) and **Figure 3.14** (b), constant effective stress is applied for 7 continuous days. Therefore, the strain rate behaviour during loading and unloading attained an equilibrium condition in a similar pattern. In the loading pattern E_1 and E_2, it is inconsistent in the loading duration pattern; some loads are applied for 7 days, and others are applied for 24 hrs only. For those loads which applied for a short duration cannot achieve their

equilibrium. Therefore, the equilibrium condition of the remaining figures is achieved at different strain rates. Several factors significantly influence strain rate behaviour, including loading history and durations. The strain rate of 250 kPa and 1000 kPa decrease continuously to achieve equilibrium, as in **Figure 3.13** (b). The difference in the strain rate behaviour of 250 kPa and 1000 kPa is attributed to the loading pattern of E_3.

3.5. Conceptual illustration of EVPS Model in BC soil

According to the EVPS model, during creep and swelling, the soil sample attains a particular strain when the time of loading or unloading tends to infinity. This strain is called the creep strain limit and swell strain limit during loading and unloading, respectively. The line joining the creep strain limit is called Creep Equilibrium Line (CEL) and Swelling Equilibrium Line (SEL) is the line joining the swell strain limit. Beyond this CEL and SEL, there is no further change in vertical strain (Tong and Yin 2013). There exists a line called the neutral line between the CEL and SEL. It has the same slope as the reference line. In this region, the soil neither shows any

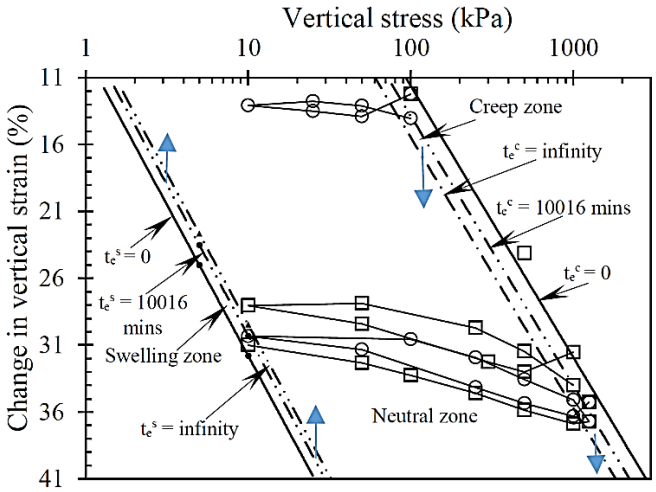

Figure 3.15: *Conceptual illustration of EVPS Model in BC soil.*

time-dependent creep nor swell. The maximum creep or swelling strain is given by the parameter ε_z^{cl} or ε_z^{sl} which is independent of pressure but a time-dependent parameter. The limit value of this parameter is $\varepsilon_z^{cl} < e_o/(1+e_o)$. The CEL and SEL are drawn parallel to the reference timelines and illustrate the creep as well as swell strain limit, the neutral zone, creep and swelling zone of BC soil in **Figure 3.15**.

The strain either in creep or swelling can be derived using their equivalent timeline. In this study, using the equivalent time (t_e =10016 min), the change in creep and swelling strain is analyzed. A comparison in the change in time-dependent axial strain in creep and swell is shown in **Figure 3.15** by considering effective stress 1250 kPa and 10 kPa, respectively. The strain at the equivalent time, t_e = 0 is 33.87% during the application of 1250 kPa. During the application of the same effective stress for an equivalent time t_e =10016 min, the delayed strain changed to 36.4%, which is observed to be increased by 2.53%. The loads are removed continuously till to reach 10 kPa. At the equivalent time, t_e = 0 the strain observed during the application of effective stress of 10 kPa is 31.79%. The delayed strain reached 30.3%, during the application of the same effective stress under equivalent time t_e =10016 min. Similarly, during the application and removal of effective stress 1250 kPa and 10 kPa, respectively, the expected strain at $t_e \rightarrow \infty$ during the creep and swelling were determined and compared with the data. It is observed that BC soil possesses significant strain during the creep stage compared to swelling. A similar observation is noticed when the time of loading as well as unloading tends to infinity. The pore water movement from microstructure (secondary structure) to macrostructure (primary structure), internal soil structure rearrangement, particle sliding, jumping of molecule bonds, and viscous adjustments of clay structure are responsible factors for creep. However, two major factors are responsible for swelling in clayey soil. Firstly, pore water entrance is

due to completing the hydration shells of the cation; this process usually occurs in dried soil. But the subsequent pore water entrance is due to osmotic processes (Nelson et al. 2015). During the swelling stage, the pre-consolidated overburden pressure restrains the free entrance of the pore water in the interconnected voids. Thus, the cation hydration between clay particles is reduced subsequently. However, such restrain is not exit in the creep stage. Therefore, the creep deformations were obvious compared to swell. The soil tends to achieve equilibrium with loading by breaking its structural arrangement. During the unloading period, the soil cannot fully recover the initial volume as the internal structure changes.

3.6. Secondary compressibility behaviour

The conventionally used secondary compression index signifies the time-dependent behaviour of geomaterials after EOP. Hypothesis A and B can describe the difference between the creep coefficients and conventionally used secondary compression index. The secondary compression index $C_{\alpha e}$ signifies the change of void ratio over the change of one log cycle of time. According to the EVPS model, the creep coefficient and secondary compression index are related as follows (Feng et al. 2017a),

$$\frac{\psi_0^c}{V} = \ln(10)\frac{C_{\alpha e}}{V} = 2.3\frac{C_{\alpha e}}{V} \qquad 3\text{-}14$$

where V signifies the total volume occupied, $V = 1 + e_0$. The secondary consolidation $C_{\alpha e}$ is calculated for each reloading cycle using the **Eqn. 3-14.** The variation of calculated $C_{\alpha e}$ against the effective stress is illustrated in **Figure 3.16 (a)**. The stresses below the pre-consolidated stress exhibit negligible change in void ratio. Therefore, the applied stress ranges from 5 kPa to 100 kPa are neglected. During the application of effective stress 50 kPa-100 kPa-250kPa-500 kPa-750kPa-1000 kPa in loading pattern E_1, the observed corresponding time-dependent parameter $C_{\alpha e}$ are 0.00030, 0.00065, 0.00410, 0.00680, 0.00729 and 0.00634 respectively. During the

second reloading cycle, the effective stress 50 kPa-250 kPa-500 kPa-1000 kPa are considered, and the corresponding time-dependent parameter $C_{\alpha e}$ 0.00015, 0.00216, 0.00271 and 0.00204 are observed, respectively. Similarly, during the third reloading cycle, the sequence of applied effective stress is 100 kPa-250 kPa-500 kPa-1000 kPa-1250 kPa, and corresponding time-dependent parameters $C_{\alpha e}$ 0.00041, 0.00155, 0.00215, 0.00190 and 0.00159 are observed, respectively.

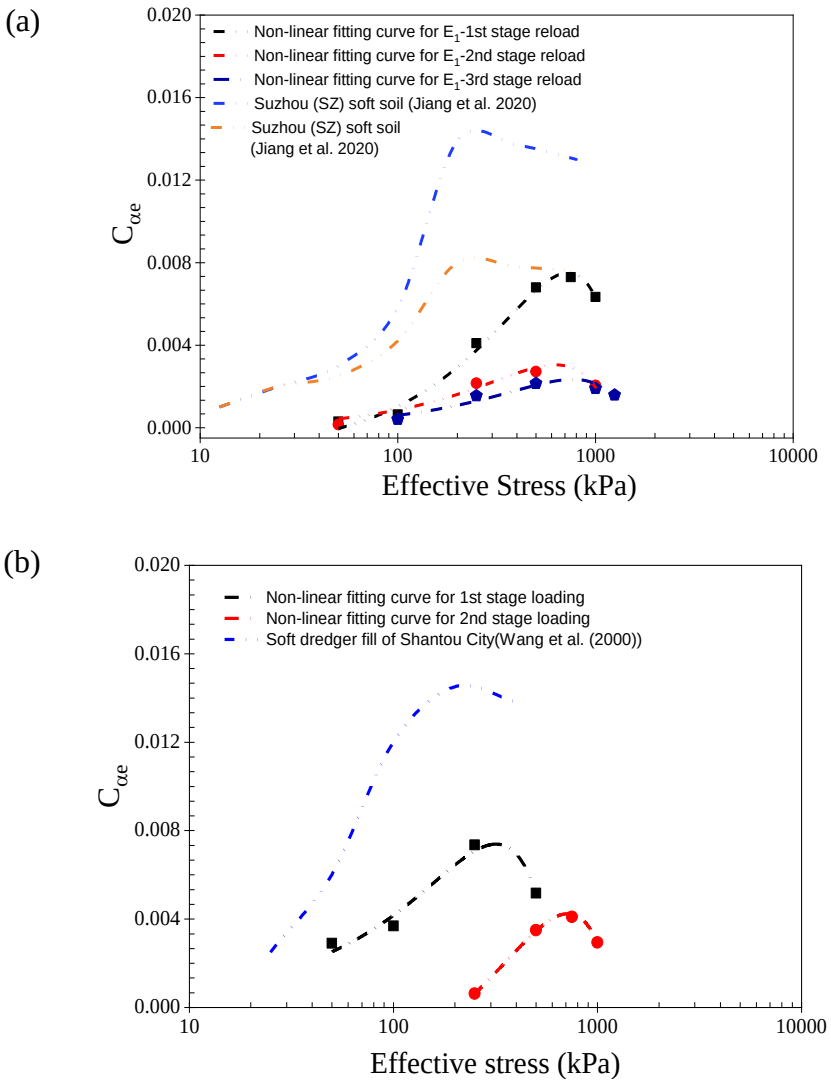

Figure 3.16: *Relationship between $C_{\alpha e}$ and applied effective stress for each reloading cycle (a) E_1 and (b) E_3.*

The fitting curve for the variation of $C_{\alpha e}$ against the effective stress is plotted for 1st, 2nd and 3rd reloading cycles. It is observed that the $C_{\alpha e}$ increase continuously with the increase of effective stress. After attaining a maximum value of $C_{\alpha e}$, the curves decrease with a further increase of effective stress. The variation of the secondary compression index is observed to be similar as obtained from other soil-like Suzhou (SZ) soft soil, Tianjin (TJ) soil, and Shanghai (SH) soft soil as studied by Jiang et al. (2020). The possible reason might be the applied effective stress leads to the movement of pore water from the microstructure (secondary structure) to the macrostructure (primary structures) after the completion of primary consolidation. The movement of pore water enhances the sliding ability of the soil particles. Once the pore inside the interaggregate and intra-aggregate particles vanishes, the soil particle attains an equilibrium. After reaching an equilibrium condition, the interparticle bonding and resistance to slipping and reorientation between the soil particles increase considerably. Therefore, the particles are approaching an oriented structure with further increased effective stress. This also enhances the contact area and the density of solids. Beyond this stage of equilibrium, several other factors as mentioned above like adsorbing water around clay particles (Yin 2013), internal soil interaction, viscous arrangement and distortion of the clay particle arrangement and their skeleton structures (Mitchell and Soga 1993b), particle sliding, delayed water that transfers and aggregates soil macro-pores are responsible which are minimal. Therefore, the creep coefficient shows decrement after attaining the maximum value. During the loading and reloading cycle, the movement of soil particles to a closer extent increases the reorientation of random particles. The particle arrangement was destroyed continuously by interacting with water incursion and expulsion. Thus, in the same applied stress, creep coefficient shows a decrement against the loading and reloading cycles.

The BC soil possesses a maximized secondary compression index during the effective application stress in the range of 633.12 kPa-757.97

kPa, no matter the number of loading-reloading cycles. It is observed that a non-linear relationship exists between the creep coefficient and the applied effective stress.

Similarly, in the loading pattern E_3 the stress below pre-consolidation pressure was neglected, as there is a negligible void ratio. Therefore, the effective stress 5 kPa-10 kPa 25 kPa are not considered. The secondary consolidation $C_{\alpha e}$ is calculated for each reloading cycle using the **Eqn. 3-14.** The variation of calculated $C_{\alpha e}$ against the effective stress is illustrated in **Figure 3.16 (b)**. During the normally consolidated effective stress, the sequence of effective stress applied consists of 50 kPa-100 kPa-250 kPa 500 kPa, and corresponding parameter $C_{\alpha e}$ 0.00290, 0.00368, 0.00736 and 0.00518 are observed, respectively. During the 1st reloading cycle, the sequence of applied effective stress consists of 250 kPa-500 kPa-750 kPa-1000 kPa, and their respective $C_{\alpha e}$ are 0.00063, 0.00350, 0.00411 and 0.00294. A similar variation of $C_{\alpha e}$ can be observed from the soft dredger soil of Shantou City (Wang et al. 2020). The maximum value of $C_{\alpha e}$ observed during the normally consolidated and 2nd reloading cycle are respectively 0.00740 and 0.00420. It is observed that the value of $C_{\alpha e}$ in the first reloading cycle is found to be reduced by 43.24%. The value of $C_{\alpha e}$ is observed to be varied in both the test E_1 and E_3 here $C_{\alpha e}$ in E_1 is higher than E_3 (in expressed in percentage by 59.33%>43.24%). In E_3, all the effective stress are applied for 7 continuous days; however, in E_1 all stress is applied for 1 day except limiting load. This shows the duration of loading is an important factor influencing the time-dependent behaviour of soft soil. The application of effective stress for a longer duration allows the soil to achieve an equilibrium of pore pressure. The result obtained in this study is found to be consistent and found similar to those studied by other researchers (J. Suzanne Powell, W. Andy Take, Greg Siemens 2012). In E_3 , there is a sudden shift of stress from 314.98 kPa to 718.55 kPa for

achieving optimum time-dependent $C_{\alpha e}$. This is because the first cycle is the normal loading cycle, while the second is the reloading cycle, which influences the rearrangement of soil particles. From all these results, it is noted that the secondary compressibility behaviour is dependent on

Table 3-5: *Secondary compressibility behaviour is given by Mesri (1973).*

Sl. No.	Value ranges	The behaviour of secondary compressibility
1.	<0.002	Very low
2.	0.002-0.004	Low
3.	0.004-0.008	Medium
4.	0.008-0.016	High
5.	0.016-0.032	Very high

parameters like duration of loading, the magnitude of the applied stress, loading history, and loading paths. Based on this parameter, Mesri classified the compressibility behaviour of different types of soil, as shown in

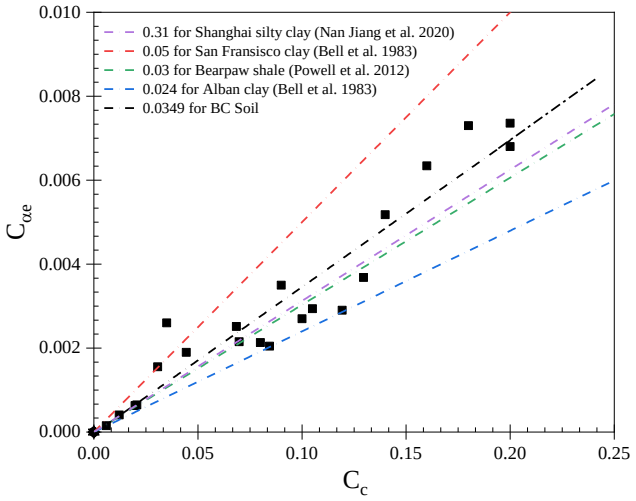

Figure 3.17: *Relationship between C_{ae} and C_c during load increments.*

Table 3-5. Here, BC soils belong to low to highly compressible soil. But in average value, the soil belongs to medium compressible soil, which is influenced by the plasticity of BC soil (Das 2019; Mesri 1973).

Mesri reports that the ratio of $C_{\alpha e}/C_c$ ranges from 0.025 for granular soil to 0.1 for peat soil, and this ratio remains consistent for a particular soil. In this study, the ratio of $C_{\alpha e}/C_c$ is calculated from the EVPS model and their relationship is compared with data derived by Mesri. The relationship of C_c with void ratio and stress is shown below;

$$\frac{C_c}{V}=\frac{\Delta\varepsilon_z}{\Delta\log\sigma'_z};\quad C_c=-\frac{\Delta e}{\Delta\log\sigma'_z} \qquad 3\text{-}15$$

where $\Delta\varepsilon_z=-\frac{e-e_0}{1+e_0}$ Similarly, for swelling behaviour,

$$\frac{C_s}{V}=\frac{\Delta\varepsilon_z}{\Delta\log\sigma'_z};\quad C_s=-\frac{\Delta e}{\Delta\log\sigma'_z} \qquad 3\text{-}16$$

where $\Delta\varepsilon_z$ denotes the change in strain, $\Delta\log\sigma'_z$ denotes the change in the effective stress over one incremental load, V denotes the volume, $V=1+e_0$, where e_0 is the initial void ratio. Using Eq. (7), the $C_{\alpha e}$ is derived from the non-linear function of the EVPS model was plotted against C_c for BC soil, as shown in **Figure 3.17**.

The $C_{\alpha e}/C_c$ for BC soil during the loading stage is observed to be 0.0354 with an R^2 value of 92%. The ratio of $C_{\alpha e}/C_c$ is varied for clayey soil with the difference in mineralogical content and origin and is influenced by the nature of formations; for example, the ratio is observed 0.05 for San Francisco clay (Graham et al. 1983), 0.024 for Alban clay (Graham et al. 1983), 0.031 for Shanghai silty clay (Jiang et al. 2020) and 0.03 for Bearpaw Shale (Powell et al. 2012).

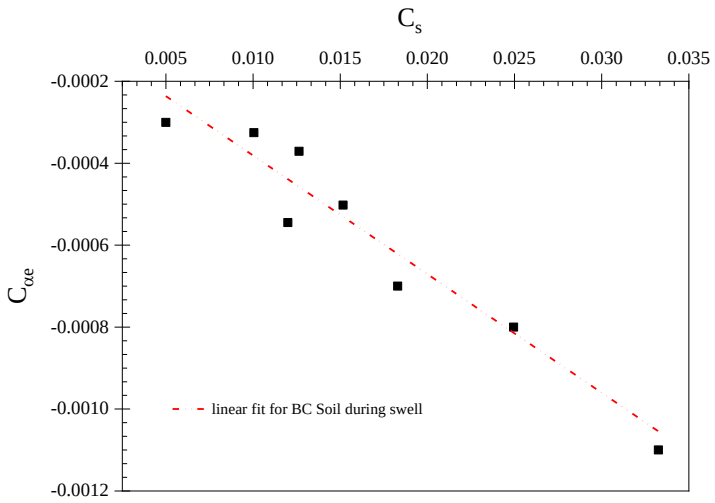

Figure 3.18: *Relationship between $C_{\alpha e}$ and C_s during unloading stages.*

Similarly, **Figure 3.18** shows the ratio of $C_{\alpha e} / C_s$ for BC soil is observed to be 0.0299 during swelling with an R^2 value of 83.76%. For BC soil, it is observed that the ratio of $C_{\alpha e} / C_s$ is reduced by 15.57% as compared to the compression ratio $C_{\alpha e} / C_c$. It is observed that the change of void ratio during creep and swelling is not identical; therefore, both ratio is observed to be different. Several factors like consolidation pressure and sustained loads during the loading and unloading stages are responsible (Mesri 1973). For example, in **Figure 3.6** (a), there is a significant strain change during the application of 500 kPa. A similar pattern can be observed in the preceding stress 250 kPa. But coming to **Figure 3.6** (b), a significant change in strain can be observed at 10 kPa, and preceding stress at 50 kPa. From this, it can be drawn that significant strain can be observed in higher stress during loading stages, whereas smaller stress in unloading stages.

3.7. Self-weight consolidation

3.7.1. Test set-up and methodology

The transparent cylindrical Perspex employed in this investigation has an interior diameter of 9.24 cm and a height of 100 cm. On the outside edge of Perspex, disposable measuring rulers of 1.5 m are fixed; the ruler has a readable resolution of 0.1 cm and a distance between two ruler ticks of 1 cm. Based on the overall volume of the cylinder, the dry weight of the soil corresponds to different concentrations (50g/L, 75g/L, 100g/L, 125g/L, 150g/L and 175g/L, are determined and were denoted by C1, C2, C3, C4, C5 and C6. Finely grinded soils (passing in 425 µm) are saturated, kept for 24 hrs, and mixed thoroughly to obtain a homogenous slurry. After 24 hrs, the slurries are transferred to the test cylinder for sedimentation,

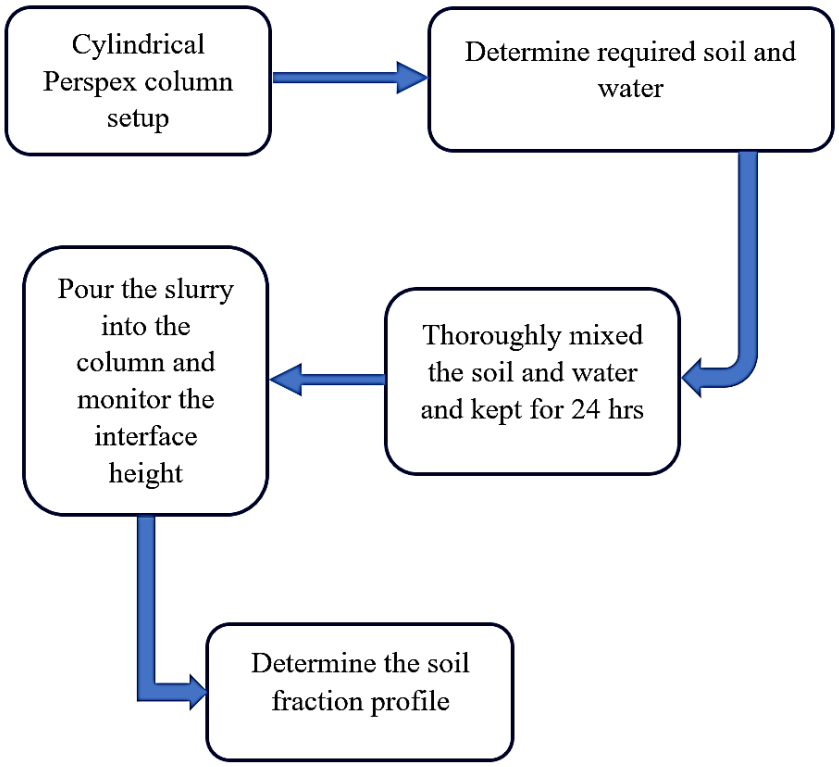

Figure 3.19: *Flowchart of the experimental procedure.*

followed by consolidation. During this whole process, the interface between the sediments and clear water is recorded manually at various time intervals, i.e., 0.25 min, 0.5 min, 1 min, 2 min, 4 min, 8 min, 16 min and so on. The overall procedure of the test set-up is illustrated in **Figure 3.19**. For a particular concentration of soil, the corresponding water content can be determined using the following equations.

$$M_w = \rho_w V_w = \rho_w \left(V_{total} - V_{solid}\right) = \rho_w \left(V_{total} - \frac{M_s}{G_s}\right) \qquad 3\text{-}17$$

where ρ_w denotes the density of water, V signifies the corresponding volume, specific gravity of the soil solid is denoted by G_s and M_s is the corresponding mass. The water content of the water content and bulk density can be determined using.

$$w = \frac{M_w}{M_s}; \quad \rho_d = \frac{M_s}{V} = \frac{\rho}{1+w} \qquad 3\text{-}18$$

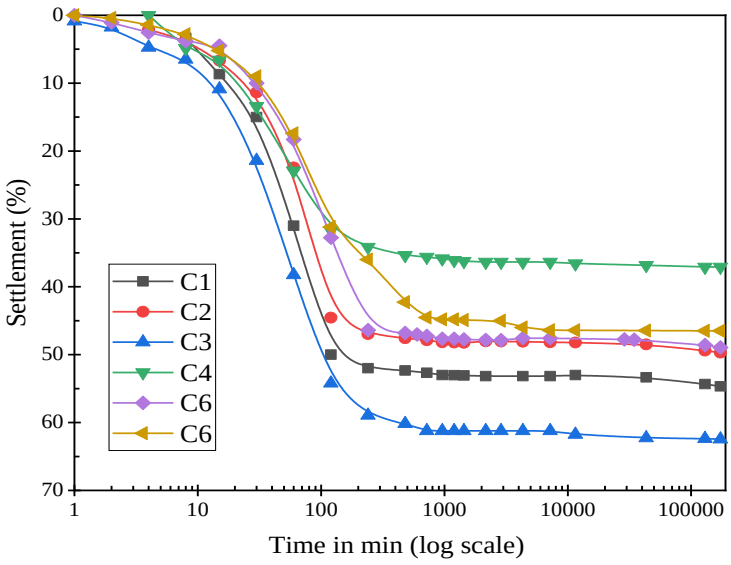

Figure 3.20: *Relationship between settlement behaviour and time for all soil concentrations.*

where, the dry density of the soil is denoted by ρ_d and ρ denotes the bulk density of the soil. Using Eqn. 3-17 and Eqn. 3-18, the required soil parameters are determined.

3.7.2. Result and discussion

The relationship between the settlement behaviour with respect to time for different concentrations of soil is illustrated in **Figure 3.20**. At any particular depth, the effective stress can be computed using the effective weight of the soil above the corresponding depth. The relationship between the void ratio profile and effective stress variation is established and illustrated in **Figure 3.21**. The data used to develop the compression curve (i.e., effective stress and void ratio) were computed from the top of the soil sediment. The results followed a similar trend for all tests with slight scatters in void ratios, in which the void ratio decreases rapidly as the effective stress increases.

In the initial stage, the void ratio reduces significantly, exhibiting a rapid downward trend. The sedimentation rate in this stage is dependent on the initial water content. Therefore, higher water content corresponds to a higher sedimentation rate. The variation of void ratio in the later stages is relatively gentle, which signifies the completion of sedimentation and initiation of self-weight consolidation. The concentration of soil also influences the settling curve. The settling curves are coincided together to develop a compression line as the void ratio reaches about 3, irrespective of the soil concentration. Even after a longer period of self-weight consolidation, the increase in density is almost 0.6%, which signifies that the physical properties (including density, vid ratio, and others) have not been improved considerably by self-weight consolidation.

The soil slurry possesses higher water content, which is significantly larger than the liquid limit, this arrangement leads to the flocculation of soil particles in water. Although there are some deformations as a result of the

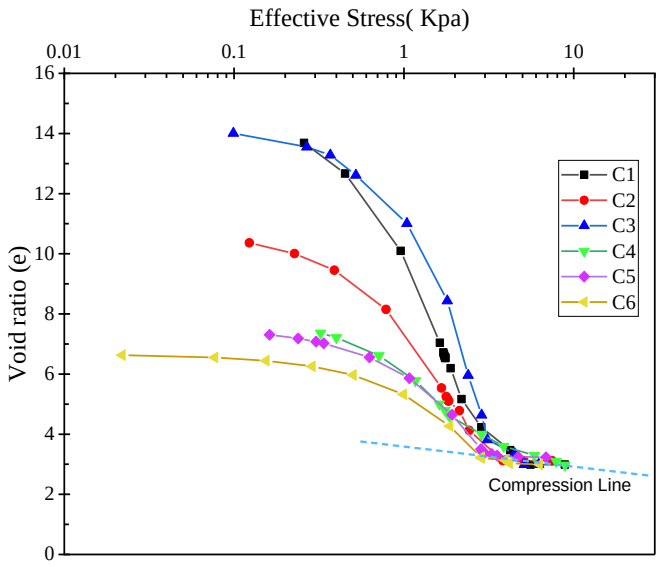

***Figure 3.21**: Void ratio profile with effective stress (kPa).*

reduced pore water during settling, the pressure does not actually release until the grains come into contact. During the initial stage of settling, the pore water pressure reduces slowly, which further speeds up in a later stage with the increase of effective stress. The variation of pore water pressure during settling is illustrated in **Figure 3.22**.

From the relationship between the settlements of soil with respect to time, it is observed that the sediment exhibits time-dependent self-weight consolidation. The nonlinear function of the EVPS Model is used to access various time-dependent behaviour. The relationship between the $\ln\left[\left(t_0^c + t_e^c\right)/t_0^c\right]$ and $\ln\left[\left(t_0^c + t_e^c\right)/t_0^c\right]/\Delta\varepsilon_z^c$ for different concentrations of the soil is illustrated in **Figure 3.23**. Here, t_e^c parameter for each concentration lies in between the 100-130 mins ranges (which is taken from the relationship between settlement and time of self-weight consolidation).

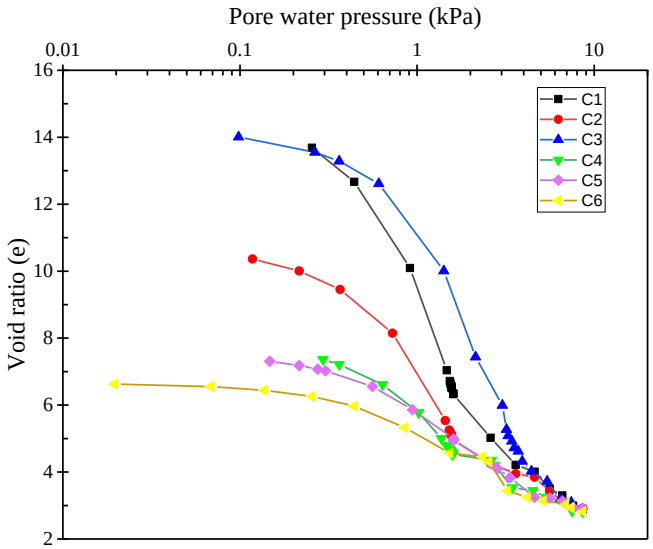

Figure 3.22: *Void ratio and pore water pressure profile.*

From the analysis, it is observed that the sediment having 100 g/L possesses the highest creep coefficient of 0.3305. The remaining sediments exhibit time-dependent behaviour; however, a particular trend of creep coefficient variation is not exhibited.

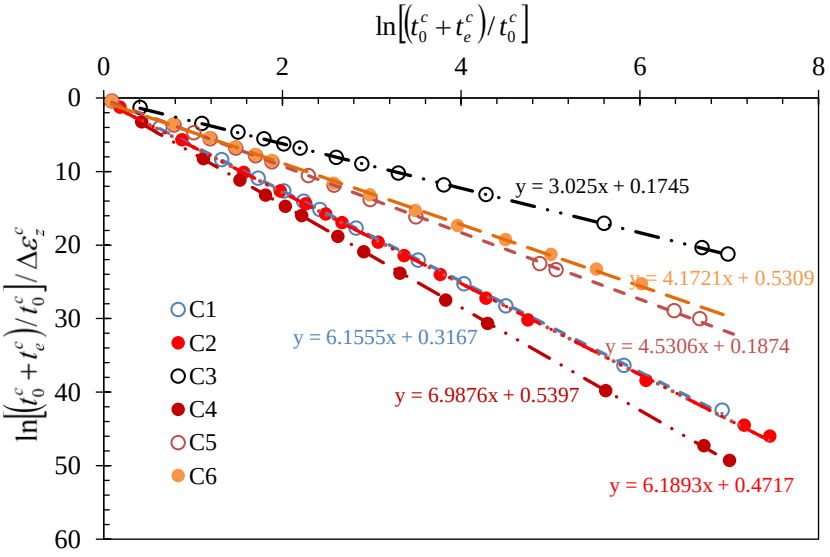

Figure 3.23: *Time-dependent parameters of self-weight consolidated soil using the EVPS Model.*

3.8. Conclusion

A series of 1-dimensional MSL oedometer tests were conducted in BC soil in varied loading patterns to investigate time-dependent parameters including $\frac{\psi_0^c}{V}$, ε_z^{cl}, $\frac{\psi_0^s}{V}$, ε_z^{sl}, $C_{\alpha e}/C_s$, $C_{\alpha e}/C_c$. Based on the experimental study, some conclusions are drawn as.

(a) The EVPS model is suitable and efficient for predicting the time-dependent behaviour of BC soil. The predicted data from the EVPS Model is consistent with the experimental data during creep and swelling.

(b) The strain observed during creep is more obvious than the time-dependent swelling strain. This might be due to the influence of overburden pressure, which resists pore-water flow in interconnected voids, thereby reducing the clay-water interaction.

(c) After the EOP, the strain rate is reduced non-linearly to achieve an equilibrium condition. The strain rate variation during the equilibrium stage is almost consistent and independent of the loading.

(d) The creep coefficient is increased with the increase of effective stress up to a particular range (between 630 kPa-760 kPa), after which it reduces continuously with the increase of effective stress.

(e) Several factors like loading duration, loading history, and loading path have also influenced secondary compressibility characteristics. The ratio of parameters $C_{\alpha e}/C_c$ for BC soil during loading is not similar to the ratio of $C_{\alpha e}/C_s$ for BC soil during swelling.

(f) The self-weight consolidated soil settling curve developed a compression line at void ratio 3, irrespective of soil concentration. Each exhibits time-dependent behaviour; however, a particular trend of creep coefficient variation is not exhibited.

Chapter 4

Long-Term Elasto-visco-plastic Behavior of reconstituted soil in Oedometer Conditions

4.1. Introduction

Globally there is enormous production of industrial waste like fly ash (FA), particularly in developing countries where coal is the primary source of energy and will remain so in future. However, continuous deposition of unutilized FA becomes alarming due to (a) limited space for disposal, (b) inhalation or ingestion triggers several diseases, (c) severe environmental and economic threats like leaching, and damage to the development of plant roots and pollution of groundwater, natural resources. From all these aspects, FA is being utilized, especially in geotechnical fields, to monitor problematic soil.

Although the previous studies provide fundamental insights into the behaviour of stabilized soil, there are specific un-researched areas, for example, the time-dependent stress-strain behaviour. The influence of admixtures on stress-strain behaviour is examined using Elasto Viscoplastic considering swelling (EVPS) Model, with special attention to creep and swelling behaviour. For this purpose, a series of consolidation tests are performed in FA-blended clayey soil in 1D oedometer conditions. After completion of the oedometer test, the microstructural behaviour of the samples is further investigated using sophisticated instruments. The correlation between the creep/swelling parameters and microstructural changes is presented, and the factors responsible for elastic, plastic and viscous behaviour are discussed. The experimental results, suitability of the prediction model along with critical observations are presented and discussed in detail.

4.2. Material and testing procedure

The BC soil used in this study is collected from Madhya Pradesh, India. The index properties and particle distribution curve of BC soil used are illustrated in **Table 3-1** and **Figure 3.1**, respectively.

Table 4-1: *Weight percentage of elements present in FA.*

Sl. No.	Elements	Weight%
1	Oxygen (O)	41.1
2	Carbon (C)	38.8
3	Silicon (Si)	9.0
4	Aluminium (Al)	6.9
5	Iron (Fe)	1.4
6	Copper (Cu)	0.9
7	Zinc (Zn)	0.9
8	Potassium (K)	0.3
9	Calcium (Ca)	0.3
10	Titanium (Ti)	0.3

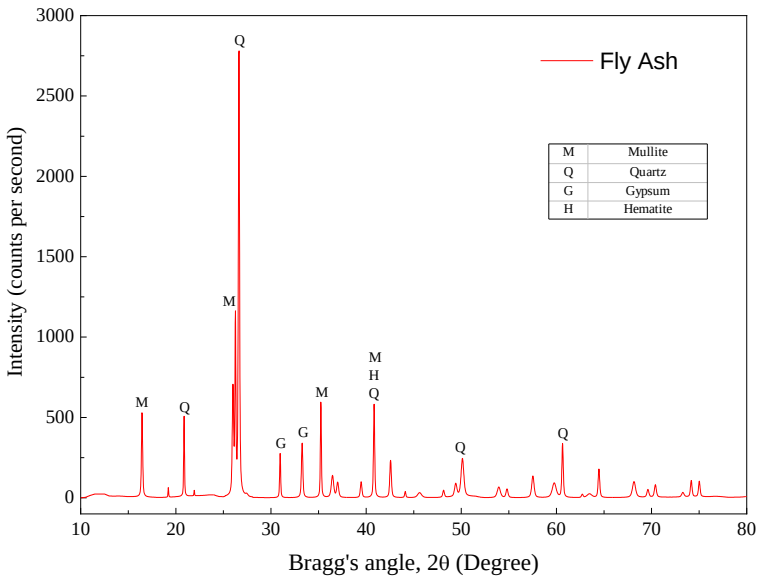

Figure 4.1: *X-Ray Diffraction Spectroscopy of FA.*

FA used in this study is also collected from the thermal power plant in Khargone, Madhya Pradesh. Energy-dispersive X-ray (EDX) analysis was conducted in JEOL JSM-7610F Plus Field Emission to examine the composition of the FA used in this study. The compositions expressed in weight percentage are illustrated in **Table 4-1**. Bruker D2 phaser XRD spectroscopy was employed to investigate the mineralogical components of FA. The XRD pattern of FA is an analysis using Panalytical X'pert Highscore Plus software, as shown in **Figure 4.1**.

Table 4-2: *Basic properties of FA blended BC soil.*

Properties	**B.C. Soil +5% fly ash**	**B.C. Soil +15% fly ash**	**B.C. Soil +25% fly ash**
Specific Gravity	2.69	2.64	2.61
Liquid limit (%)	63.13	61.46	61.11
Plastic limit (%)	32.37	32.83	34.12
Plasticity Index (%)	30.76	28.63	26.99
O.M.C. (%)	26.21	24.50	23.68
M.D.D. (g/cc)	1.43	1.44	1.41

The basic properties of the FA blended BC soil are listed in **Table 4-2**. The clay content in the sample was reduced with the addition of FA, resulting in a decrease in the double-diffused layer of soil. As a result, the plastic limit of the blended mixture was reduced with an increase in FA contents. The basic engineering properties of the blended mixture are observed to be diverted from natural soil, and its UCSC classification changes from high-plastic clays (CH) to low-plastic clays (OH).

Table 4-3: *Loading pattern for Oedometer Test.*

Loading Pattern	Sl. No.	Loading (kPa)	Period (day)	Sl. No.	Loading (kPa)	Period (day)	Sl. No.	Loading (kPa)	Period (day)	Sl. No.	Loading (kPa)	Period (day)
	1	5	1	*11*	100	1	*21*	1000	1	*31*	1000	1
	2	10	7	*12*	500	1	*22*	1250	7	*32*	1250	7
	3	25	1	*13*	1000	7	*23*	1000	1	*33*	1000	1
	4	50	1	*14*	500	1	*24*	500	1	*34*	500	1
Test-1*	*5*	100	7	*15*	250	1	*25*	250	1	*35*	250	1
	6	50	1	*16*	50	1	*26*	100	1	*36*	100	1
	7	25	1	*17*	10	7	*27*	10	7	*37*	50	1
	8	10	7	*18*	50	1	*28*	100	1	*38*	10	7
	9	25	1	*19*	250	1	*29*	250	1			
	10	50	1	*20*	500	1	*30*	500	1			
	1	5	7	*6*	250	7	*11*	10	7	*16*	1000	7
	2	10	7	*7*	500	7	*12*	50	7	*17*	1250	7
Test-2*	*3*	25	7	*8*	250	7	*13*	100	7			
	4	50	7	*9*	100	7	*14*	250	7			
	5	100	7	*10*	50	7	*15*	500	7			

* indicates the total duration of loading, for * =92 days, for **=119 days.

The BC soil passing in a 2-mm sieve and FA passing in 150 μm are oven-dried at a temperature of 110±5°C. Different quantities of FA quantity (0%, 5%, 15%, and 25%) were added by natural BC soil weight. The predetermined FA and BC samples were mixed homogenously and added to the water corresponding to the OMC of natural soil. The sample is transferred in a zip polythene bag, where the wet FA-BC mixture is matured for at least 48 h. During the whole process, care is taken to avoid the wastage of any component. The internal surface of the Oedometer ring is properly greased to reduce any possible friction between the soil particle and the steel surface. The mature FA-BC mixture is compacted in three layers in the Oedometer ring of 60 mm diameter and 20 mm height until it achieves the maximum dry density. After that, the compacted samples were weighed and transferred to the environmental chamber for curing for three days. The corresponding temperature and relative humidity of the environmental chamber are respectively 25°C and 100%. The cured sample is transferred to an oedometer and placed filter paper on both sides of the samples. The dial gauge is set to zero reading, and samples are allowed to swell freely. During this study, nominal pressure of 5 kPa is used as a seating pressure. After the free swell, the soil sample and the Oedometer ring are transferred to the oven (110±5°C) and kept for 24 h. A schematic diagram of the Oedometer is illustrated in **Figure 3.2**. Two different loading patterns (i.e., Test-1 and Test-2), as listed in **Table 4-3** were used for the Oedometer test. Test-1 is performed to investigate the effect of the unloading-reloading cycle on the swelling behaviour of the FA-BC matrix. Test-2 is performed to analyze the effect of loading duration on the swelling behaviour of the FA-BC matrix. Here stress loading and unloading are performed every 7 days, which provides an equilibrium condition and allows to study time-dependent behaviour of the FA-BC matrix (Yin 1999).

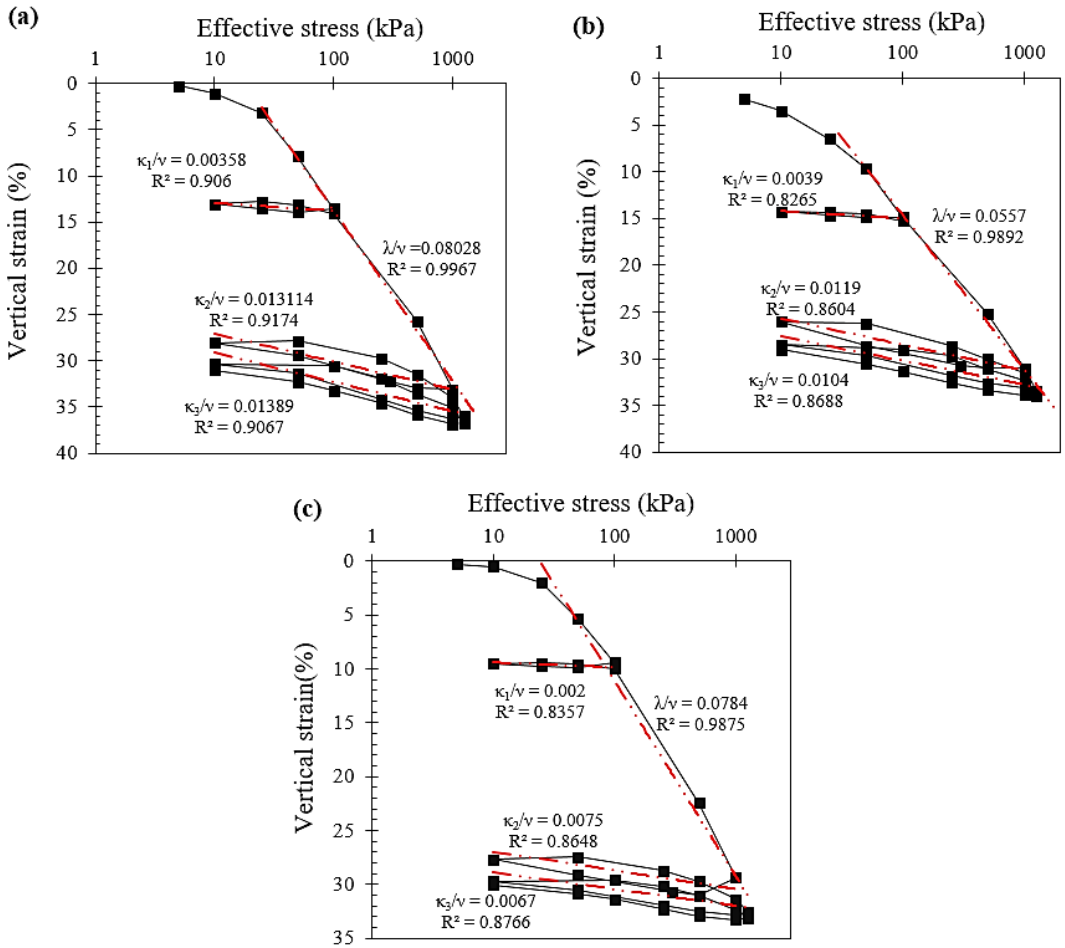

Figure 4.2: *Relationship between effective stress and vertical strain of FA-BC matrix using Test-1 loading pattern (a) BC soil, (b) 5% FA+BC soil and (c) 25% FA+BC soil.*

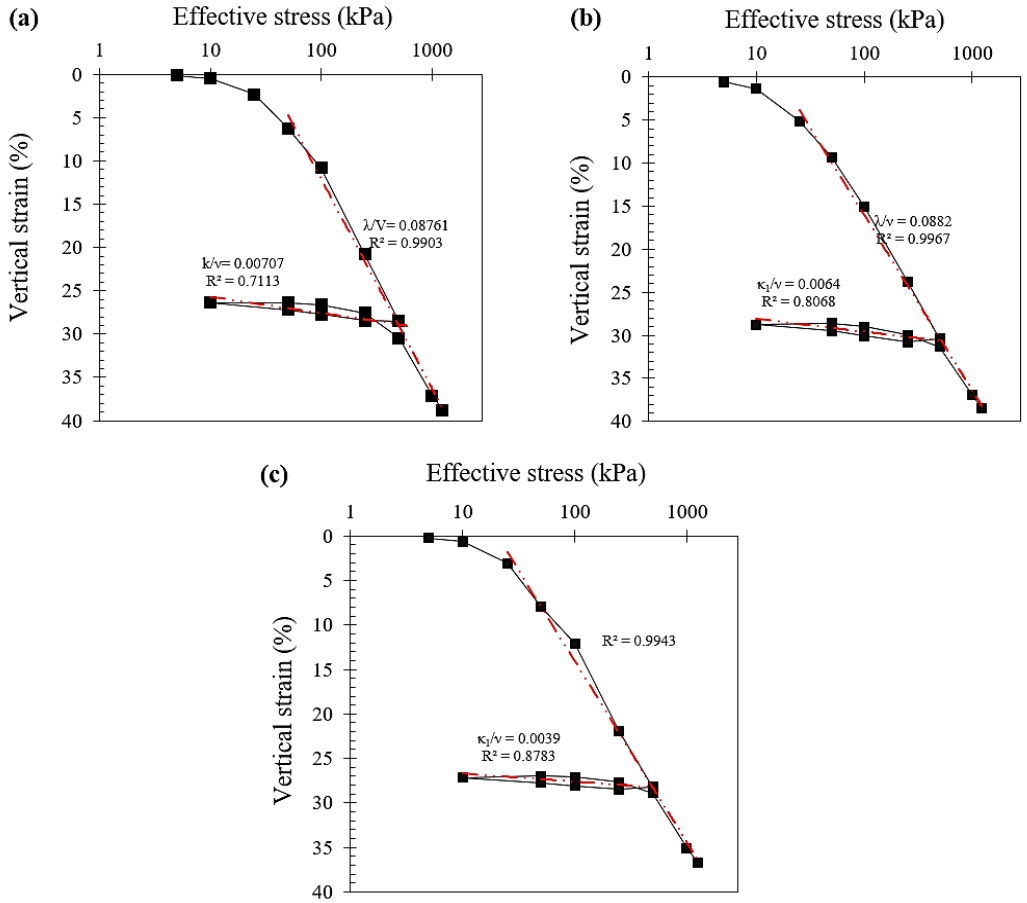

Figure 4.3: *Relationship between effective stress and vertical strain of FA-BC matrix using Test-2 loading pattern (a) BC soil, (b) 5% FA+BC soil and (c) 25% FA+BC soil.*

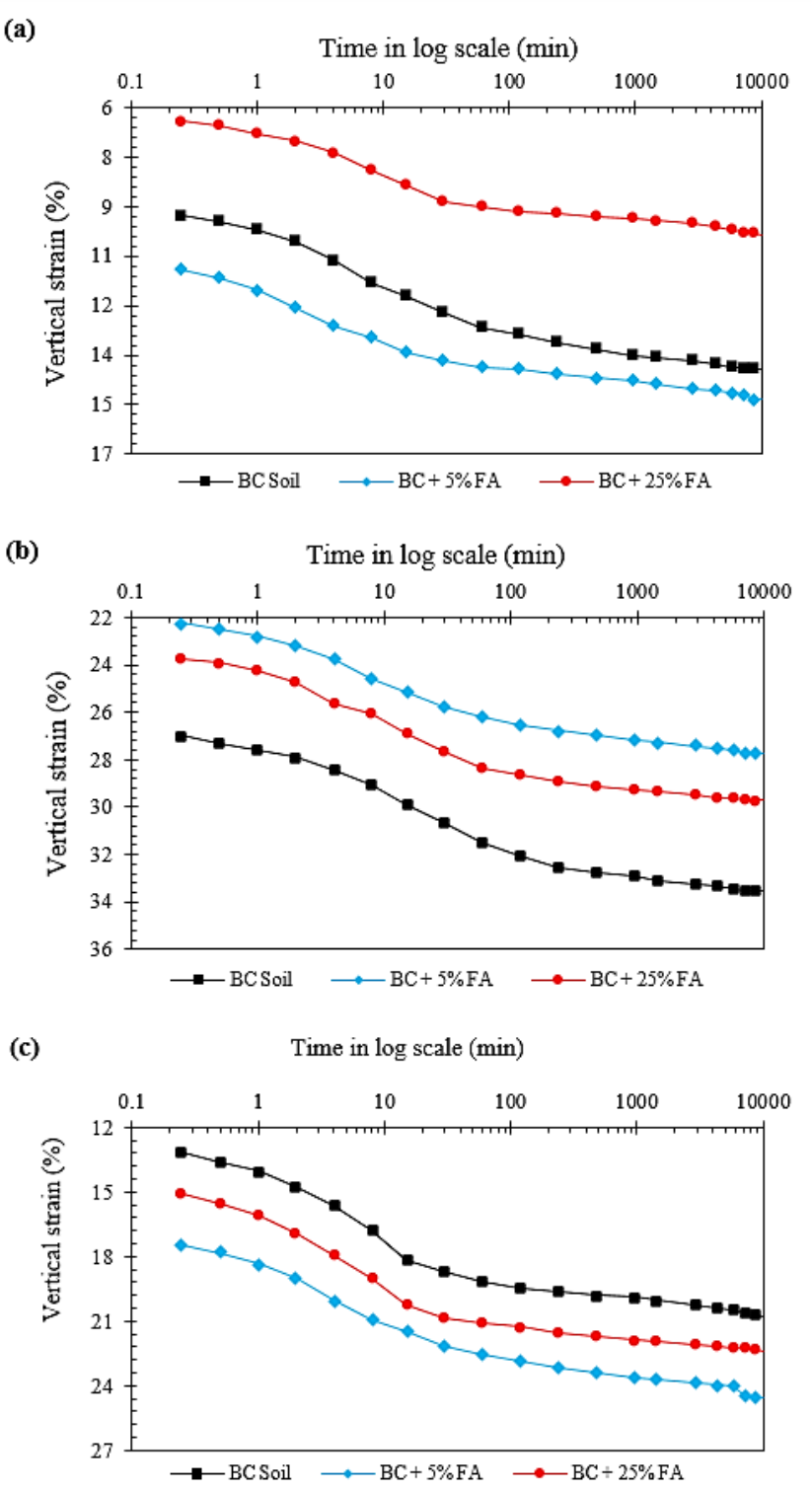

Figure 4.4: *Change in vertical strain with time during application of (a) 100 kPa for Test-1, (b) 1000 kPa for test-1 and (c) 250 kPa for Test-2.*

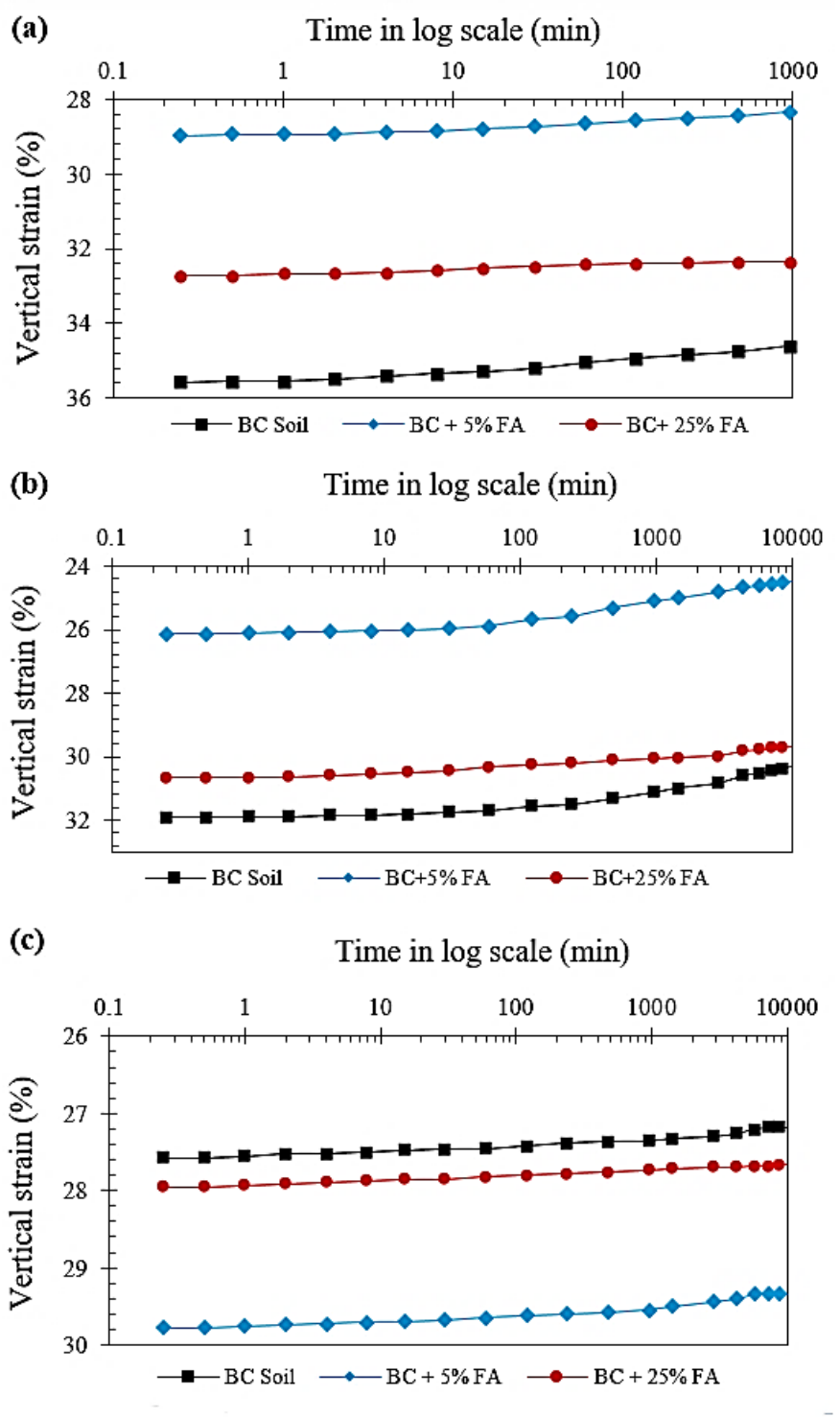

Figure 4.5: *Change in vertical strain with time (log scale) during unloading (a) 250 kPa Test-1, (b) 10 kPa Test-1 and (c) 50 kPa Test-2.*

4.3. Result and discussion

The relationship between effective stress and vertical strain of FA-BC matrix using different loading patterns are shown in **Figure 4.2** and **Figure 4.3**. The comparison between the difference in vertical strain with time (in log scale) during the loading and unloading cycle for Test-1 and Test-2 are respectively shown in **Figure 4.4** and **Figure 4.5**. The difference in colour signifies the variation in FA composition. The addition of 5% FA and 25% FA exhibits a t_{eop} ranges from 21-107 mins and 21-84 mins, respectively. The viscous effect during the primary consolidation is the major responsible factor for the non-uniqueness of the t_{eop} (Hawlader et al. 2003). It is observed that the time corresponds to the end of primary consolidation, and the beginning of secondary consolidation is reduced by adding FA. A similar observation is noted in the study made by Mir and Sridharan (Mir and Sridharan 2014). It is observed that the addition of FA reduced the overall vertical strain of the soil. The overall strain in Test-1 is found to be lesser than in Test-2 due to the difference in loading pattern, as shown in **Table 4-3**. The unloading-reloading cycle induced the structural arrangement and particle orientations.

Using the **Eqn. 3-1**, the rebounding parameters are determined for both FA-treated and untreated BC soil. It is observed that the rebounding parameters are decreased continuously with the increase of FA content, which denotes the continuous reduction of elastic strain. Using the **Eqn. 3-3**, the reference strain of both FA-treated and untreated BC soil is determined. In Test-1, the parameter λ/V is observed to be 0.08028 for BC soil; with the addition of 5% FA, it changes to 0.0557 and 0.0784 for 25% FA blended BC soil. However, in Tets-2, the parameter λ/V is observed to be 0.0876 for BC soil; with 5% FA blended, it changes to 0.0882 and 0.0885 for 25% FA blended BC soil.

It is found that the compression parameter is decreasing in FA content, especially for Test 1. However, in Test 2, it is almost constant for both the FA-treated and untreated BC soil. The continuous unloading-reloading in Test 1 will be the primary responsible factor, which brings disturbance in structural arrangement and orientations. The compressibility parameters of BC soil blended with different compositions of FA under different loading patterns are listed in **Table 4-4**. Thus, the compression parameter is observed to be dependent on the loading duration and the loading sequence.

Table 4-4: *Different compressibility parameters of BC-FA matrix under different loading patterns.*

Samples	(κ/v)	(λ/v)	(C_r/V)	(C_c/V)
BC Soil (a)	0.0036		0.0083	
	0.0131	0.0803	0.0301	0.1847
	0.0139		0.0320	
BC Soil (b)	0.0055	0.0873	0.0127	0.2008
	0.0039		0.0090	
BC+5% FA (a)	0.0119	0.0557	0.0274	0.1281
	0.0104		0.0239	
BC+5% FA (b)	0.0064	0.0882	0.0147	0.2029
	0.0020		0.0046	
BC+25% FA (a)	0.0075	0.0784	0.0173	0.1803
	0.0067		0.0154	
BC+25% FA (b)	0.0039	0.0885	0.0090	0.2036

"a" denotes Test-1, and "b" denote Test-2

4.3.1. Time-dependent parameters using linear functions

Using the linear function from **Eqn. 3-6**, the creep behaviour of FA blended soil is investigated under the application same effective stress 1000 kPa as shown in **Figure 4.6**. The creep parameter of BC soil is observed to

be 0.0033, which changes the creep parameter to 0.0028 with 5% FA blended and for BC+25% FA, it changes to 0.0024. The curve fitting parameter is more than 95%. It is found that the creep parameter of BC soil reduces continuously with the addition of FA content; it indicates a continuous reduction of creep strain with FA content.

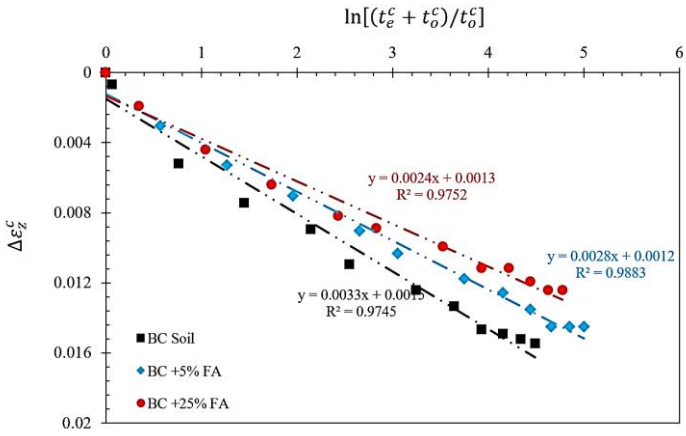

Figure 4.6: *Fitting curve for creep parameters in BC-FA matrix using linear function during application of 1000 kPa in Test-1.*

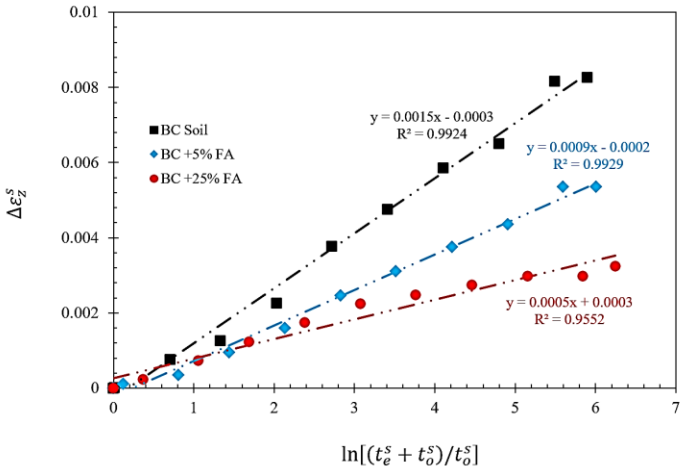

Figure 4.7: *Fitting curve for swelling parameters in BC-FA matrix using linear function during application of 250 kPa in Test-1.*

Using the linear function from **Eqn. 3-7**, the swelling behaviour of FA blended soil is investigated. During the application of 250 kPa, as shown

in **Figure 4.7**, the swelling parameter of BC soil is observed to be 0.0015, for BC+5% FA, the swelling parameter is observed to be 0.0009, and for BC+25% FA, it changes to 0.0005. The curve fitting parameter is more than 95%. It is found that the swelling parameter of BC soil reduces continuously with the addition of FA content; it indicates a continuous reduction of swelling strain with FA content.

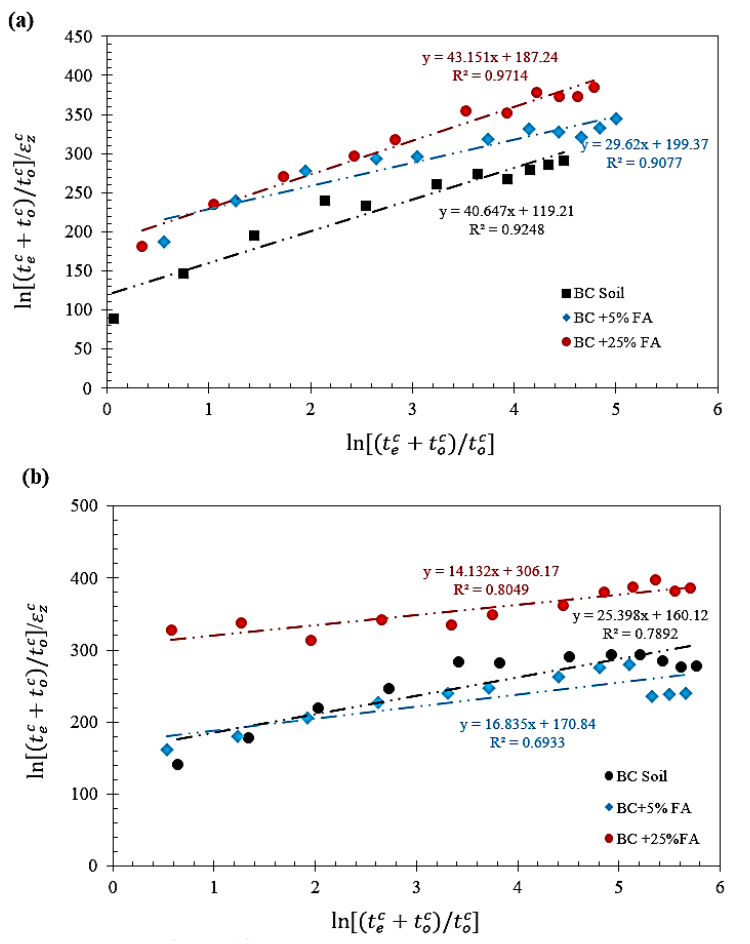

Figure 4.8: *Fitting curve of creep parameters in BC-FA matrix using the non-linear function for (a) 1000 kPa Test-1 and (b) 250 kPa for Test-2.*

4.3.2. Time-dependent parameters using non-linear functions

The creep behaviour of the FA-treated BC soil is also investigated using a non-linear function given **Eqn. 3-9** and representative data is

illustrated in **Figure 4.8**. In Test-1, during the application of 1000 kPa, the BC soil possesses a creep parameter of 0.0838; for BC+5% FA, the value is 0.00501, and for BC+25% FA, the creep parameter further changes to 0.00279. Similarly, during the application of 250 kPa, the creep parameter possessed by BC soil is observed to be 0.00624; for BC+5% FA, the value is 0.00585, and for BC+25% FA is 0.00326. Similar to the linear function, the creep parameter of both FA-treated and untreated BC soil is also decreased in the non-linear function. This particular trend is found similar in both the cases of Test-1 and Test-2. The observed data clearly denotes that creep strain is reduced with FA content. The strain rate depends on the creep coefficient ψ_0^c/V as the creep coefficient ψ_0^c/V is reduced; the corresponding strain rate will be decreased with the addition of FA.

According to the EVPS model, the creep strain attained under the application of a constant load for infinite time is given by ε_z^{cl}. There is no particular relationship between the strain limit and FA content. However, the creep strain limit is observed to decrease with the loading sequence.

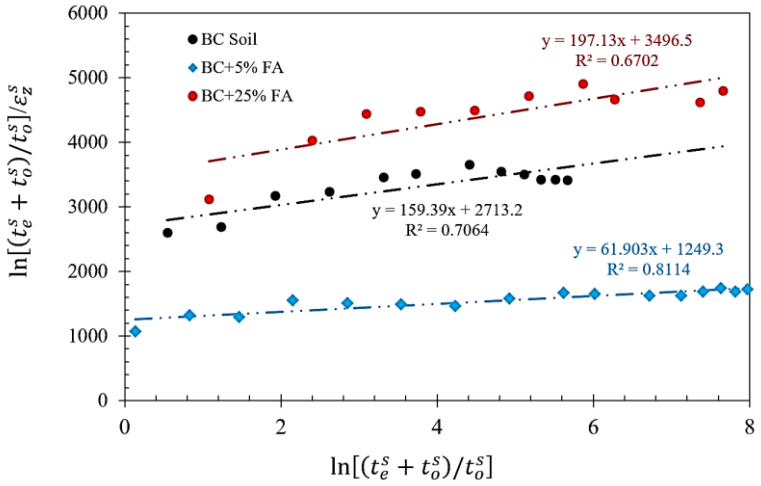

Figure 4.9: *Fitting curve of swelling parameters in BC-FA matrix using the non-linear function for 100 kPa for Test-2.*

.

Table 4-5: *Different time-dependent parameters of BC-FA matrix using EVPS Model.*

Sample	**Loading (kPa)**	**Creep coefficient** (ψ_o^c/ν)	**Creep Strain limit** (ϵ_z^{cl})	**Loading (kPa)**	**Swell Coefficient** (ψ_o^s/ν)	**Swell Strain Limit** (ϵ_z^{sl})
BC Soil (1)	1000	0.0083	0.0246	500	0.0006	-0.0050
	250	0.0013	0.0140	250	0.0012	-0.0390
	500	0.0018	0.0076	10	0.0016	-0.0140
BC Soil (2)	250	0.0062	0.0394	100	0.0008	-0.0313
	500	0.0066	0.0336	50	0.0004	-0.0090
	1000	0.0029	0.0065	10	0.0005	-0.0070
BC+5% FA (1)	1000	0.0050	0.0337	500	0.0003	-0.0021
	250	0.0012	0.0043	250	0.0006	-0.0110
	500	0.0012	0.0081	10	0.0015	-0.0150
BC+5% FA (2)	250	0.0059	0.0594	100	0.0003	-0.0162
	500	0.0060	0.0867	50	0.0004	-0.0040
	1000	0.0069	0.0301	10	0.0005	-0.0050
BC+25% FA (1)	1000	0.0028	0.0231	500	0.0004	-0.0017
	250	0.0005	0.0042	250	0.0008	-0.0107
	500	0.0010	0.0029	10	0.0014	-0.0581
BC +25% FA (2)	250	0.0032	0.0708	100	0.0003	-0.0051
	500	0.0046	0.0341	50	0.0002	-0.0004
	1000	0.0054	0.0226	10	0.0006	-0.0170

Here 1 denotes Test-1 and 2 denotes Test-2.

The swelling behaviour of the BC soil is further investigated using the non-linear function expressed in **Eqn. 3-11**. Different time-dependent parameters for the BC-FA matrix under the application of different loads from both loading patterns are listed in **Table 4-5**. It is observed that during the application of 500 kPa, the BC soil exhibits a swell coefficient of 0.0006; at 250 kPa, the parameter is found to be 0.0012, and at 10 kPa, the parameter is further changed to 0.0016. The swelling coefficient is observed to increase with the reduction of the applied stress. The swell coefficient of

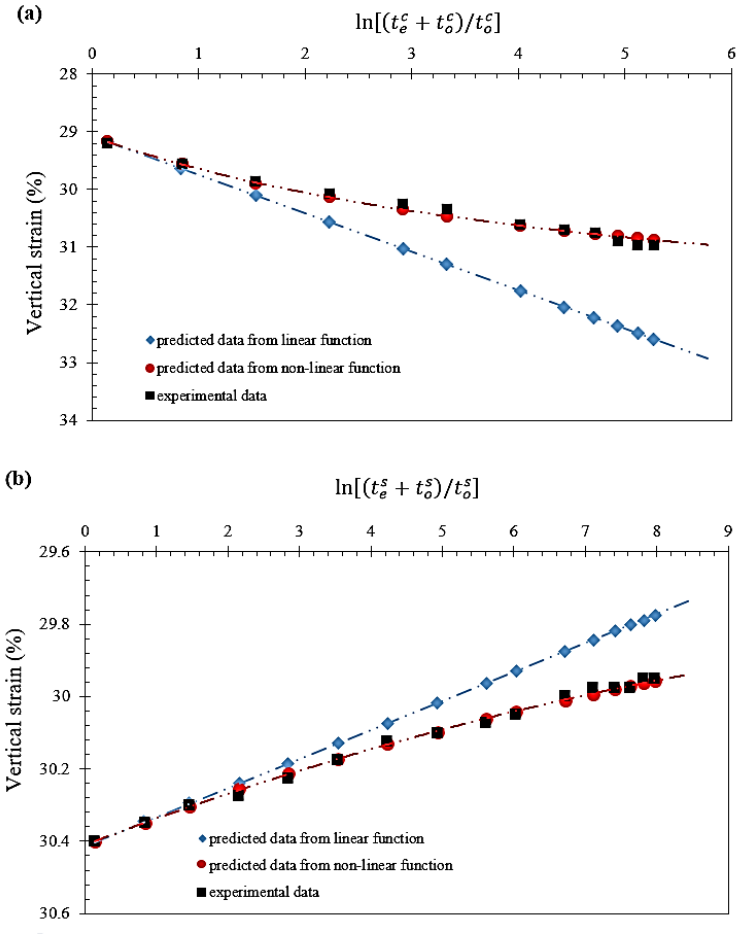

Figure 4.10: *Comparison of the vertical strain of BC-FA matrix and prediction from linear function and non-linear function (a) 500 kPa during loading and (b) 100 kPa during unloading.*

the soil is found to increase with the reduction of the vertical stress applied to it. A similar trend is followed by all the FA blended soils and BC soil of Test-1 and Test-2. This is because after consolidating, the soil tends to swell with the removal of applied loads by giving higher loads. This swelling potential is increasing with the higher removal of loads. From **Figure 4.9**, the swelling strain limit of BC soil is -0.0313, BC+5% FA is -0.0162, and BC+25% FA is -0.0051. The swelling strain limit is found to decrease with the addition of the FA contents. A comparison between the change in vertical strain obtained from experimental data and the prediction obtained from EVPS Model during loading and unloading is illustrated in **Figure 4.10** (a) and (b). In comparison, both linear and non-linear functions of the EVPS Model are also incorporated. It is observed that the linear function overestimates the strain determined by creep and swelling. However, the non-linear function's prediction is accurate and fits well with the experimental data during creep and swelling. Thus, the non-linear function can be employed for the prediction of time-dependent creep and swelling behaviour of the FA blended reconstituted soil.

4.3.3. Influence of unloading-reloading cycle on Creep Coefficient

Figure 4.11 illustrates the variation of the creep coefficient as a function of the unloading-reloading cycle in Test-1. The effective stress considered includes 1^{st}-100 kPa, 2^{nd}-1000 kPa, 3^{rd}-1250 kPa and 4^{th}-1250 kPa (bold in loading pattern).

It can be inferred that the creep coefficient derived from the non-linear function increased till 2^{nd} cycle and decreased with the further unloading-reloading cycle. After primary consolidation, the dissipation of porewater takes place from the microstructure (secondary structure) to the macrostructure (primary structure) due to the continuous restrain of effective stress (Kaczmarek and Dobak 2017). Besides the unloading-

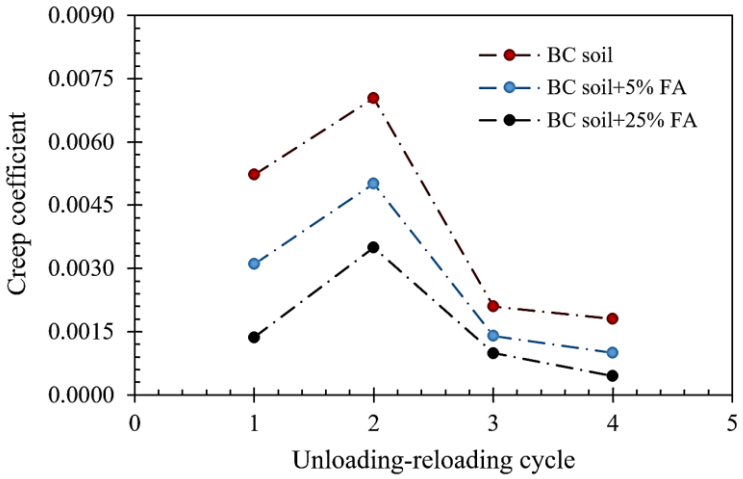

Figure 4.11: *Variation of creep coefficient with the number of unloading-reloading cycles*

reloading cycle leads to the rearrangement of soil particles, i.e. intra-aggregate pores inside and between the clay particles and interaggregate pores between the clay aggregates (Nowamooz 2014). All these factors influence the sliding ability of soil particles. Again, the creep behaviour of BC soil is more obvious than the swelling strain (as discussed in the previous Chapter), and a similar observation was reported in Hong Kong marine clay (Tong and Yin 2011). The soil cannot regain its original strain even after swelling due to its plastic and viscous behaviour. Thus, the creep coefficient decreases continuously in both natural and reconstituted soil. The further section discusses the reduction of creep coefficient with FA content through microstructural analysis.

4.3.4. Relative swelling strain behaviour

During the unloading of 50 kPa-25 kPa-10 kPa, as shown in **Figure 4.12**. The relative swelling behaviour of the FA-reconstituted soil observed a decrease continuously as the FA content increased. Aggregation occurs during the addition of fly ash, which is attributed to the time-dependent

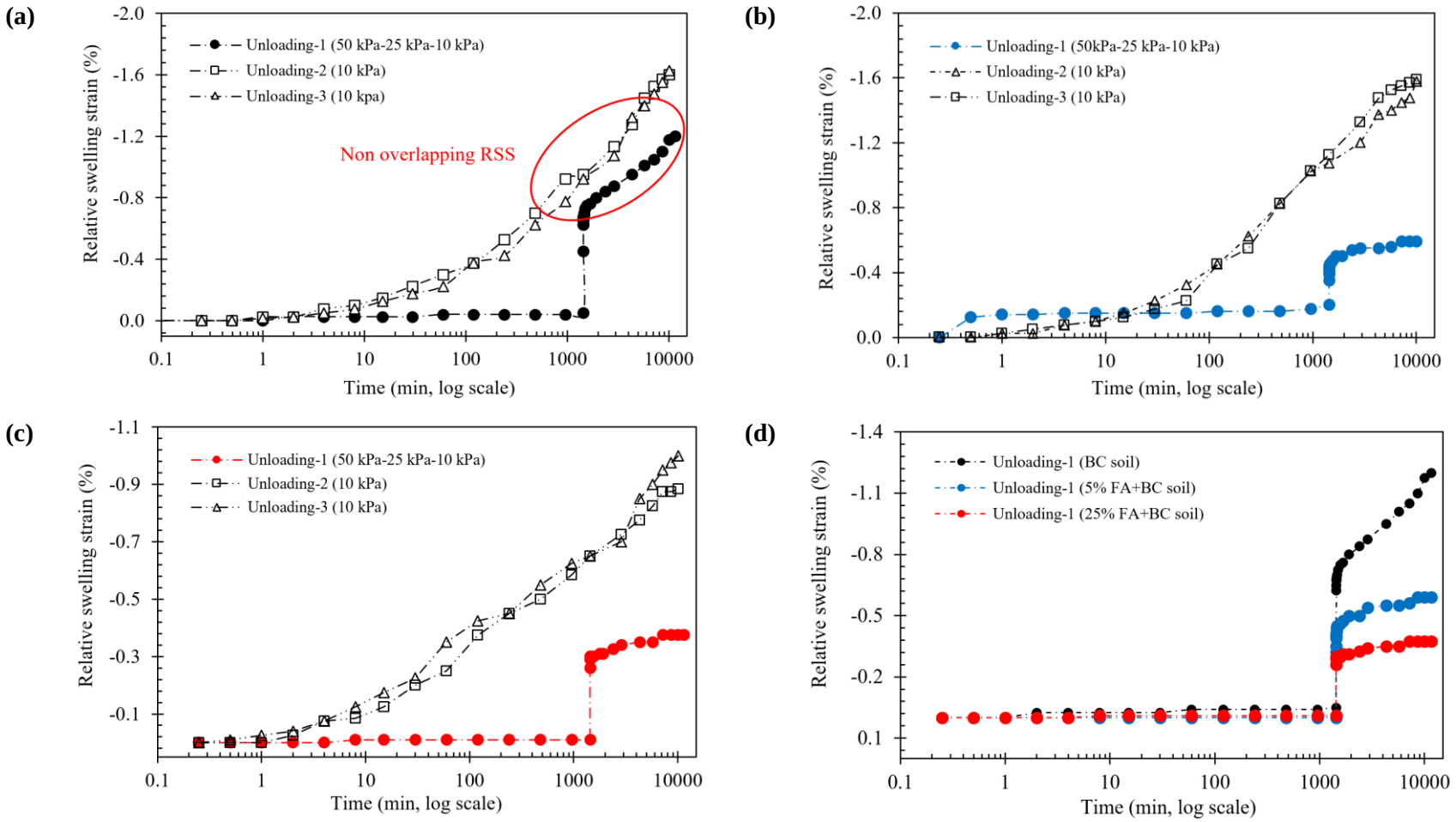

Figure 4.12: *Relative swelling strain behaviour from Test-1 for (a) BC soil, (b) 5% FA+BC soil (c) 25% FA+BC soil and (d) comparison of unloading 1 for all samples.*

pozzolanic reaction of FA thereby forming cementitious compounds. It leads to a stronger soil particle interaction and gives higher resistance to time-dependent swelling behaviour. Again, the newly formed cementitious compounds will occupy the interconnected voids of the BC-FA mixtures. Therefore, the entrance of pore water to the interconnected void is reduced as compared to the natural soil. It leads to reducing the relative swelling strain behaviour of reconstituted soil. During the removal of 10 kPa in the 2nd and 3rd unloading-reloading cycle, all soil sample, irrespective of the presence of FA or not, follows a trend of relative swelling strain behaviour. The swelling behaviour of the BC soil is attributed to the montmorillonite mineral present in it. The addition of the FA decreases the sample's clay content; this reflects the reduction of relative swelling behaviour. However, the addition of FA cannot entirely eliminate the relative swelling potential. The relative swelling strain behaviour of the soil is proportional to the interactive repulsive pressure generated during the unloading. The generated repulsive pressure is a function of the interacting specific surface at any equilibrium state. It is counterbalanced by the external pressure in its equilibrium state. Hence, the repulsive pressure depends on the stress level of rebound, that is, pre-consolidation pressure. Application of stress beyond pre-consolidation stress reduces the specific surface due to the formation of clusters and packets. During the removal of higher stress, the soil particle tends to achieve the equilibrium state by swelling. So, the soil exhibits negligible swelling strain during the 1st unloading-reloading cycle. A similar pattern can be observed in both natural and reconstituted soil, irrespective of FA content.

4.3.5. Micro-Structural Analysis

The entire testing procedure was conducted in saturated soil specimens. In the presence of water, the lime of FA undergoes a hydration reaction. As the layered silicate clay minerals possess a negative charge, it attracts the oppositely charged cations (Firat et al. 2017). Thus, dissolved

aluminate and/or silicate clay minerals are neutralized with calcium hydroxide or hydrated lime; this process is called the pozzolanic reaction. Due to the pozzolanic reaction, hydrated cementitious compounds are formed in the presence of soil water content. The reaction takes part is shown as follows (Chou 1987; Firat et al. 2017);

$$CaO + H_2O \longrightarrow Ca(OH)_2$$

$$Ca(OH)_2 \longrightarrow Ca^{++} + 2[OH]^-$$

$$Ca^{++} + 2[OH]^- + SiO_2 \longrightarrow \text{C-S-H (gel)}$$

A representative image of the BC-FA matrix in the presence of water before and after the pozzolanic reaction is illustrated in **Figure 4.13**. The by-product of the pozzolanic reaction is the cementitious material called calcium silicate hydrate (C-S-H) (Little and Nair 2009). It helps in strengthening the inter-particle contact between the soils by forming gels. Short-term hydration, long-term pozzolanic reactions and cation exchange capacity are increased with FA contents (Dayioglu et al. 2017). Thus, it influences the time-dependent behaviour of the matrix.

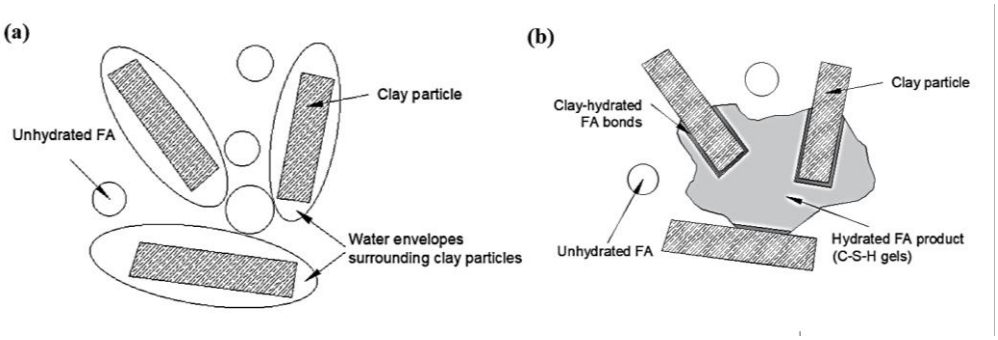

Figure 4.13: *Schematic diagram indicating (a) before cementitious gel formation and (b) after cementitious gel formation.*

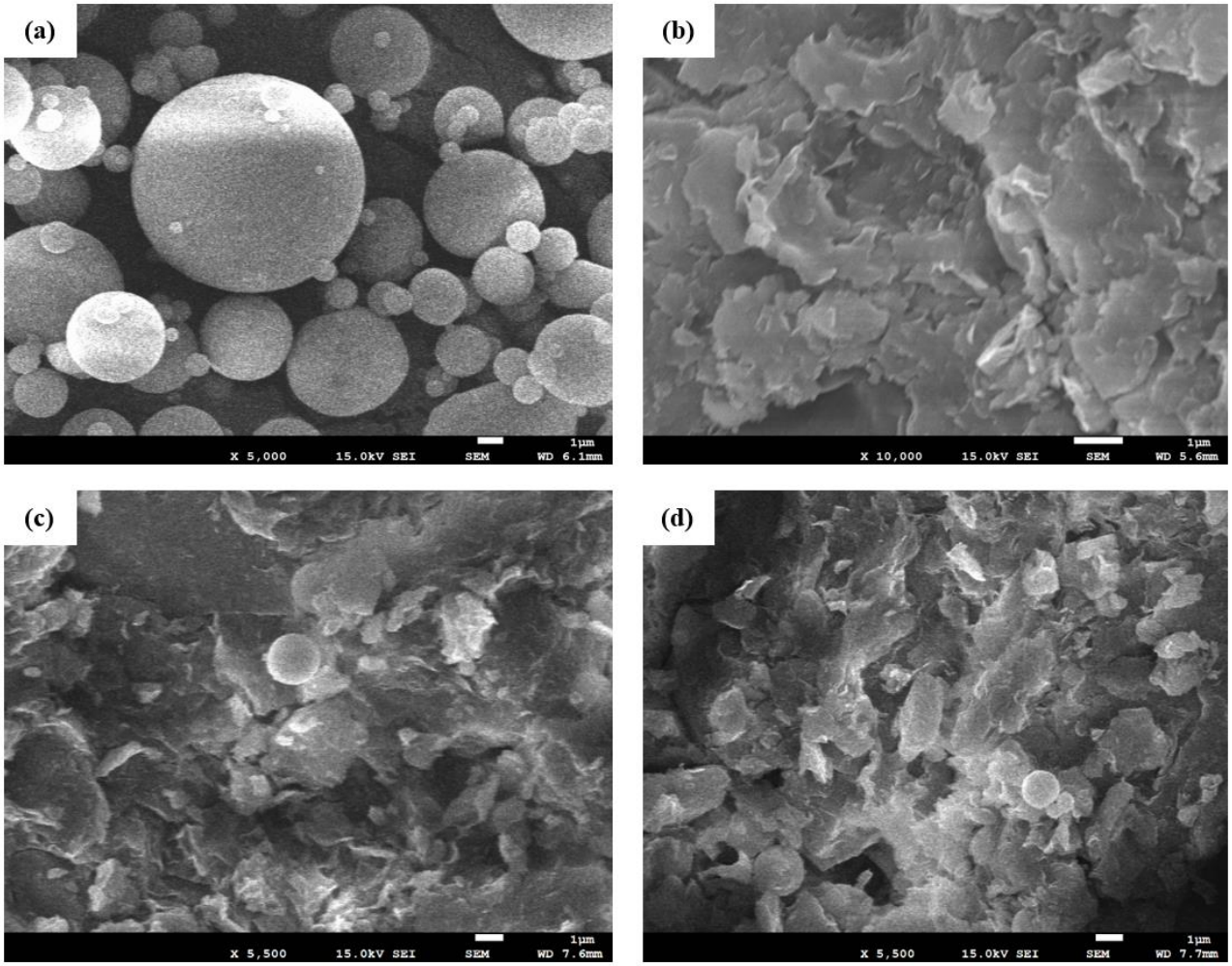

Figure 4.14: *SEM spectroscopy of (a) FA, (b) BC soil, (c) 5% FA+BC soil and (d) 25% FA+BC soil.*

4.3.5.1. Scanning Electron Microscopy (SEM)

The morphological behaviour of BC soil in the presence of FA was analyzed using the JEOL JSM-7610F Plus Field Emission SEM spectroscopy. The morphology of BC soil and FA are illustrated in **Figure 4.14** (a) and (b), respectively. It is observed that BC soil possesses a flake or fine flocculent morphological structure. This arrangement allows the BC soil to absorb significant water and exhibits significant volumetric changes. But it reduces its volume during the loading period by expelling water. This continuous process leads to exhibits of elastic behaviour of the soil. The internal arrangement of the clay particles, the interaction of particle clusters, delayed water transfer and the sliding of clay particles are responsible for the plastic and viscous nature of the soil. The FA particles are observed to be micro globular shape morphology, possibly due to their hydrophilic nature. The pozzolanic activity might be influenced by the degree of fineness of FA.

In the case of the BC-FA matrix, the pozzolanic reaction occurs in the presence of water, thereby forming cementitious material. The cementitious materials filled the pores available in the soil particles. It formed a connecting bridge between the clay particles, which enhances the overall strength behaviour by hardening the paste (as pores are reduced) and fixing the soil particles in a particular position. All these factors reduced the volumetric changes in the soil. The formation of cementitious compounds between the clay particles with the addition of FA particles is shown in **Figure 4.14** (c) and (d). From the SEM spectroscopy, higher FA blended BC soil exhibits a better interface condition between soil particles and cementitious compounds and lesser pores between the soil particles. The formation of such cementitious compounds at the microstructural level significantly influences the overall behaviour of the soil.

4.3.5.2. Fourier Transform Infrared Spectroscopy (FT-IR) Analysis

The samples collected from the consolidation test are oven-dried and prepared in powdered form to investigate the change in the functional group with FA addition. The microstructural test is conducted in Perkin Elmer FTIR System- Spectrum two Model. The wavelength used in the test ranges from 4000 cm^{-1} to 400 cm^{-1} range (Zhang et al. 2017). **Figure 4.15** illustrate the change in functional groups of the different sample with FA content. Based on the wavelength employed, there are three portions; clay and quartz mineralogical portion (3730-1750 cm^{-1}), the double bond portion signifying the presence of organic minerals (1750-1210 cm^{-1}) and other soil mineralogy (1210–4000 cm^{-1})(Le Guillou et al. 2015). From the FTIR data, significant variation can be observed in the clay and quartz mineralogy portions. The suitable reasons are explained using the XRD results in a further section. The FTIR data of FA signifies the presence of Si-O-Si bands of quartz in the 1600-1000 cm^{-1} band, and the portion from 800-500 cm^{-1} signifies the stretching of the Si-O-Si and Al-O-Si bonds of aluminosilicate

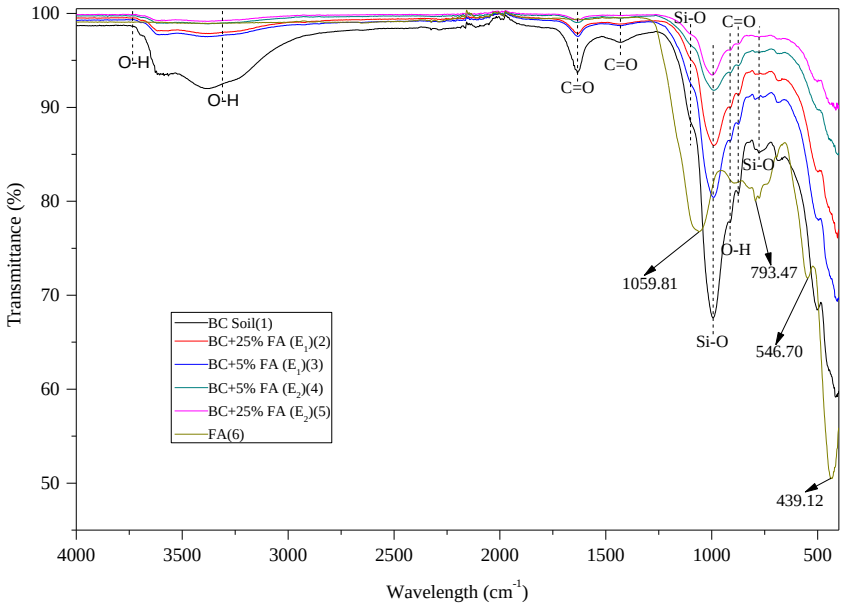

Figure 4.15: *Comparison of FTIR spectroscopy of BC soil, FA, and reconstituted soil.*

materials. Further, the Si-O-Si and O-Si-O bonds' bending vibrations are signified by an absorption pattern below 500 cm^{-1} bands (Fauzi et al. 2016).

In the case of BC soil, the absorption pattern in the wavelength range 3355-3730 cm^{-1} band signifies the stretching vibration of the hydroxyl group O-H present in the inner Al–O-H within the layer in montmorillonite minerals, whereas the band 2000 cm^{-1} denotes the presence of the quartz (Krivoshein et al. 2020). Further, the stretching vibration of O-C-O bonds in calcium carbonate lies in wavelength 873 cm^{-1} and 1432 cm^{-1} band, 777 cm^{-1} signifies the stretching vibrations of Si-O present in quartz, presence of C=O carboxylate group of organic matter is indicated by 1629 cm^{-1}, the deformation and stretch of OH in Al–O–H is denoted by 913 cm^{-1}, and vibration of Al_{VI}-O-Si and Al_{IV}-O-Si is denoted by 714 cm^{-1}. The Si-O stretching vibration is denoted by a sharp band in the range 1000-1120 cm^{-1}. Within this range, absorption at 1100 cm^{-1} signifies the in-plane stretching due to Si-O, while the peak at 1002-1012 cm^{-1} denoted the antisymmetric in-plane Si-O stretching vibrations. A small shift of the bond wavelength is observed with the addition of FA, and the transmittance of O-H bonds in clay minerals is found to increase (Criado et al. 2007; Daverey et al. 2019). The flexibility of the O-H bond is observed to be decreased with FA addition; this might be due to fixing the clay particles due to the formation of cementitious compounds. Duration of loading in the oedometer has a small influence on the bond formation behaviour; this might be due to varying in the formation of a matrix between the soil components. In a shorter duration of the loading pattern, there might be a disturbance in the equilibrium state of the BC-FA-water matrix.

4.3.5.3. X-ray diffraction spectroscopy

Further, the mineralogical characterization of FA blended reconstituted soil is performed in powdered format after completion of the consolidation test. The test is performed through Bruker D2 phaser X-ray diffraction (XRD) spectroscopy. The diffraction pattern is further studied

using Panalytical X'pert, Highscore Plus software. The diffraction pattern of BC soil presented in **Figure 4.16** (a), indicates the presence of Montmorillonite minerals in the peaks 19.7º, 23.58 º and 27.68º; while quartz is the major component observed. The presence of illite, hematite, feldspar and calcite were also observed (Choi et al. 2017; Le Guillou et al. 2015; Ma et al. 2016; Madejová et al. 2017). While minerals

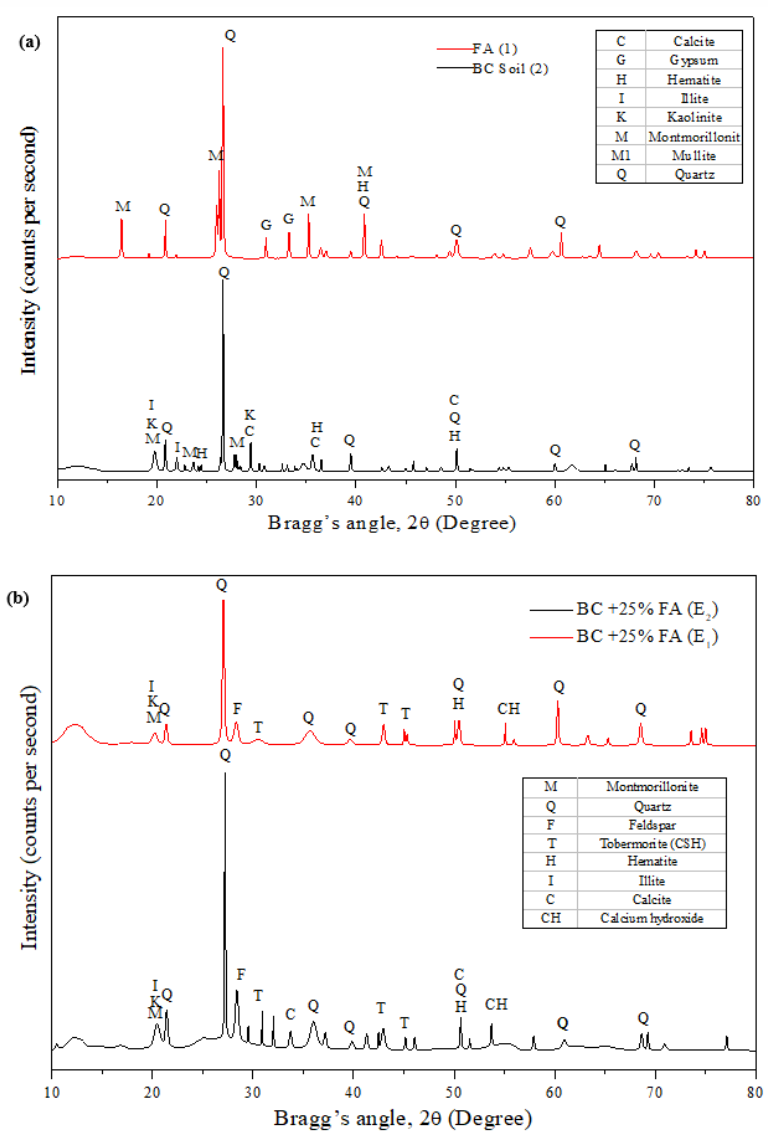

Figure 4.16: *X-ray diffraction spectroscopy of (a) BC soil, FA and (b) 25% FA+BC soil from Test-1 and Test-2.*

like hematite, gypsum, quartz and mullite are observed in the XRD result of FA (Guo et al. 2017; Liu et al. 2019).

The position of 2θ in the range of 40º-48º, and 52º-56º doesn't detect any peak in natural BC soil and FA. However, the XRD report of the BC-FA matrix in the consolidation sample exhibits the presence of peaks in these ranges as shown in **Figure 4.16** (b). These peaks signified the presence of Calcium hydroxide and Tobermorite. In 1880, Heddle reported the Tobermorite as a calcium silicate hydrate mineral (Saride and Dutta 2016; Sudhakaran et al. 2018). It is a primary nano-crystalline building block forming a cohesive-frictional material. The basic arrangement consists of an internal layered structure comprising a heterogeneous assembly with a complicated network arrangement (Palkovic et al. 2017). The samples are kept saturated in the oedometer for 92 days, and 119 days; this also influences the formation of this compound. Other minerals like hematite, feldspar, quartz and montmorillonite are also found in the FA-BC matrix.

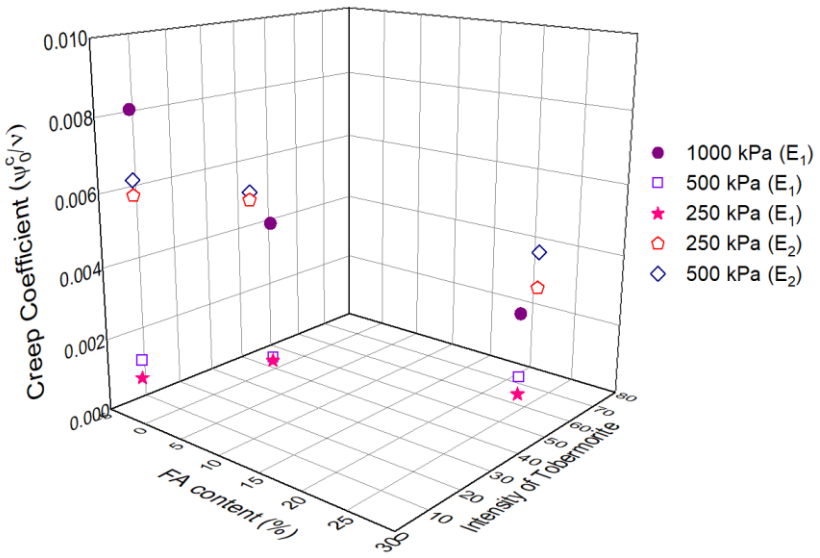

Figure 4.17: *Relationship between creep coefficient, FA content and intensity of Tobermorite formation.*

4.3.6. Time-dependent parameters with microstructure changes

As mentioned earlier, XRD spectra didn't detect the presence of any peak in the 2θ of range 42°-43°. However, as FA content increases, new peaks are observed due to the formation of Tobermorite gel. The variation of intensity of new peaks formed in this 2θ range as a function of FA content is plotted with change in the corresponding creep coefficient in both Test-1 and Test-2 in **Figure 4.17**. In Test-1, the BC soil possesses a creep coefficient value of 0.0018 during the application of 500 kPa, the parameter reduced to 0.0012 as FA content increases by 5% and the further increase of FA to 25% possess a creep coefficient of 0.0003. A similar pattern can be observed from applications 250 kPa (in Test-1) and 250 kPa (Test-2). A negligible variation in creep coefficient is observed at different FA content during the application of 250 kPa for Test-1 and Test-2. It might be due to a difference in loading and unloading pattern history (i.e. 7 days in Test-2 and 1 day in Test-1) to reach 250 kPa. During the application of 1000 kPa, BC soil possesses a creep coefficient of 0.0838, while 5% FA + BC matrix possesses 0.00501, and a further increase of FA to 25% reduces the creep coefficient to 0.00279. A sudden change in creep coefficient is observed during the application of 1000 kPa compared to other effective stress. The preceding stress of 1000 kPa was applied for a shorter period i.e., 1 day. So, the overall settlement is mostly dominated by primary consolidation. This loading sequence provides a significant period for developing gels through their interconnected voids, thereby densifying the matrix. Thus, the duration of loading must be 7-14 days, particularly for determining the time-dependent parameter of the FA-BC matrix (Feng et al. 2017a; Tan et al. 2018). From this data, it is observed that with the increase of FA content, the creep coefficient reduced continuously in both loading patterns. The addition of FA produces cementitious material in the presence of water; this changes the particle-particle interaction of BC soil. The formation of cementitious material in the soil's pores might be primarily responsible for

the continuous reduction in the creep coefficient of the FA-BC matrix. It progressively densifies the soil matrix by forming a bridge.

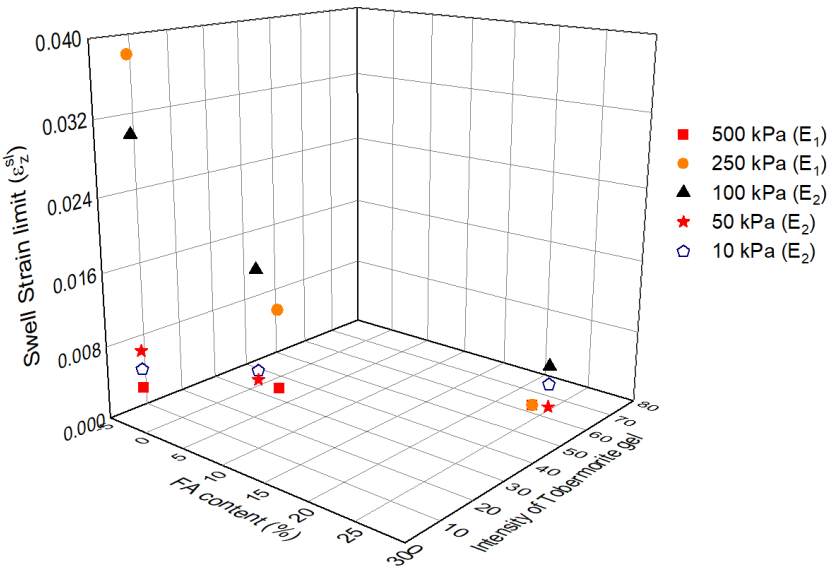

Figure 4.18: *Relationship between swell strain limit, FA content and intensity of Tobermorite.*

The intensity of Tobermorite as a function of FA composition is plotted with the variation of in swelling strain limit of the matrix in **Figure 4.18**. The swelling strain limit presented in the Z axis denotes the maximum strain the soil can achieve as the duration of unloading tends to infinity. The swelling strain limit is expressed as a positive quantity for a better interpretation of the figure. The intensity of the hydration product observed in the 2θ of range 42°-43° with the addition of FA is presented on the Y axis. In Test-1, the BC soil possesses a swelling strain limit of 0.005 under removal of 500 kPa, it reduces to 0.0021 as FA increases by 5% and further reduction of swelling strain limit to 0.0017 as FA content increases to 25%. In Test-1, the swelling strain limit obtained during the removal of 500 kPa and 250 kPa varied significantly. Here 500 kPa and 250 kPa belong to the 2nd and 3rd unloading-reloading cycle; this might be the responsible factor for the variation of swelling strain limit. Again it is inferred that the swelling

strain limit reduces continuously with the increase of effective stress; a similar observation is reported by Feng et al. (Feng et al. 2017a). A similar pattern can be observed from Test-2; during the application of 100 kPa, BC soil possesses a swelling strain limit of 0.031, it reduces to 0.0162 as FA increases by 5%, and the swelling strain limit is further reduced to 0.0051 as FA content increase to 25%. However, in Test-2, the swelling strain limit was reduced with the decrease of effective stress, i.e., 100 kPa, 50 kPa and 10 kPa. Here 10 kPa and 50 kPa are below the pre-consolidation stress, so the soil achieves an equilibrium.

From all these data, it is observed that with the increase of FA content, the swelling strain limit reduced continuously in both loading patterns. The cation exchange takes place with the addition of FA, resulting in the agglomeration of soil particles. This reduces plasticity and influences swelling behaviour. The microstructural changes can also be observed from FTIR data, in which continuous reduction of the –OH bond takes place with the addition of FA. This is because the hydrophilic nature of the fly ash (Sakthivel et al. 2013) tends to absorb water components that take part in the swelling mechanism. Besides, cementitious compounds are formed due to pozzolanic reaction in the FA-BC matrixes in the presence of water. It is distributed progressively in the pores between soil particles, reducing permeability (Chang et al. 2011). Again, the presence of remaining un-hydrated FA in the interparticle voids enhances the heterogeneity of the natural soil. All these factors enhance the interaction between the clay particles and surrounding particles. Thus, adding FA forms a more or less hard skeleton, strong material enclosing a natural soil matrix.

4.3.7. Rheological behaviour

Fly ash is also used for deep soil mixing to improve the engineering properties of soil (Mohammadinia et al. 2019), therefore, it is required to assess the microstructure behaviour of soil in a fluid condition. In this study, the microstructure behaviour of the fly ash blended soil in fluid conditions

subjected to external stresses through the Amplitude sweep test. Here, the Anton Paar-Modular Compact Rheometer (MCR) 102 with a parallel-plate sensor system is used. The configurational setup of the instruments is given in **Table 4-6**.

***Table 4-6**: The parameters used in the Rheometer.*

Parameters	Corresponding values
Plate distance	d = 2 mm
Duration of experiment	12 mins
Temperature	25ºC (controlled by Peltier unit)
Frequency (angular frequency)	05 Hz ($\omega = \pi\ s^{-1}$)
Number of measuring points	30 points
Shear deformation	γ = 0.0001% to 100%
Water content	At liquid limit (LL, 1.2 LL)

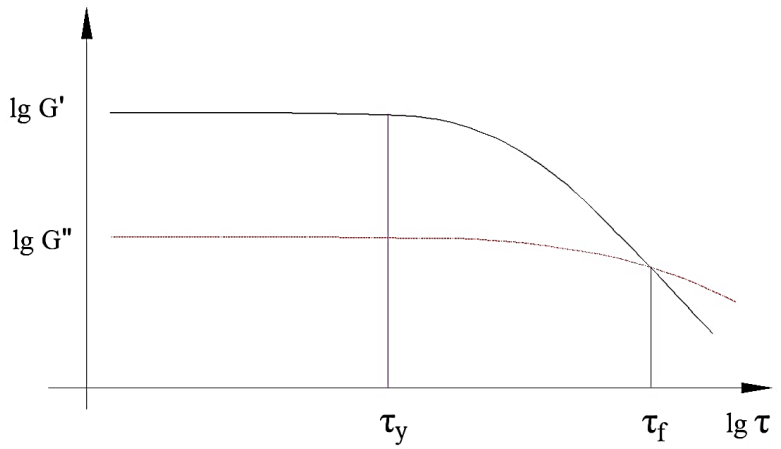

***Figure 4.19**: Relationship between the Storage modulus G', loss modulus G'', yield point τ_y and flow point τ_f.*

The prepared sample is placed between the parallel plates with proper precaution at the distance "d". The top plate is rotating in an oscillatory fashion while the bottom plate remains static throughout the whole procedure. The corresponding deflection from the top plate follows a sinusoidal function while the deflection of the bottom plate remains zero. The sensors attached to the system computerized the shear strain and average shear stress using the angular velocity and torque respectively. The frequency is maintained constant while the deflection of the measuring device is increased incrementally from one measuring point to the next. The relationship between the storage modulus G′, loss modulus G″, flow point τ_f and yield point τ_y is shown in **Figure 4.19**.

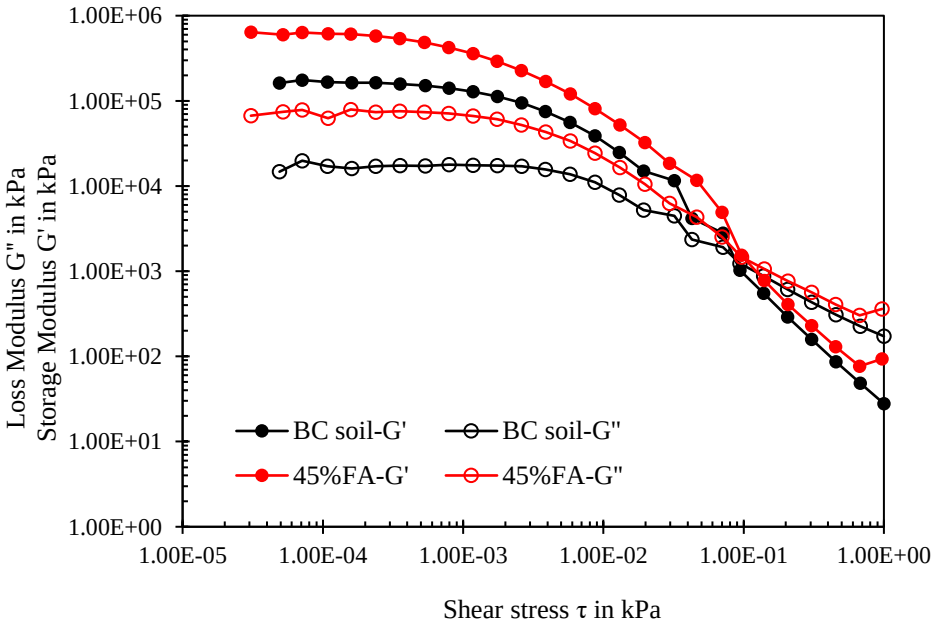

***Figure 4.20**: Amplitude sweep test data for BC soil and 45% FA blended soil.*

From **Figure 4.20**, it is observed that G' is greater than G" in the small strain which denotes that the reconstituted fluids resemble solids more. The G' is decreasing more evidently than G" as the strain increases,

which is true for most materials. The sample leaves the linear viscoelastic region (LVR) plateau at a strain below 1. As the applied strain increases, the G" overtakes the G' and the sample gradually behaves like a fluid. The cross point of G" and G' indicates the flow point which is dominated by viscous behaviour. Both the moduli G' and G" increase in presence of the fly ash content. as the fly ash content, the particle interaction enhances which leads to an increase in relative viscosity. However, a particular trend is not defined as illustrated in **Table 4-7**.

***Table 4-7**: Rheological parameters of soil blended with different compositions of fly ash in LL condition.*

	LVE range		At flow stage	
Fly ash content	γ_L	G'	γ_f	G'=G"
0%	7.93E-4	141180.51	0.086	1445.5
5%	6.67E-4	365886.24	0.057	10820.2
15%	4.49E-4	745874.11	0.103	4394.38
25%	3.89E-4	305393.53	0.091	1504.24
35%	3.12E-4	1107317.84	0.079	8999.31
45%	2.48E-4	575567.57	0.103	1384.35

As the strain increase beyond the flow strain, the disturbance of the network structure increases. The samples possessing the higher stability and gel-like character exhibits higher flow strain which is observed with the increase in fly ash content. A similar pattern is also observed in the case of samples having 1.2 times liquid limits.

4.4. Conclusion

A series of 1D Oedometer tests were conducted to investigate the time-dependent behaviour of FA-blended BC soil. The morphological and

mineralogical behaviour was analyzed after the oedometer test. Based on the experimental investigation result, the following conclusions are drawn.

(a) The addition of admixtures cannot entirely reduce the BC soil's time-dependent behaviour. The EVPS Model is suitable and can predict the time-dependent behaviour of the reconstituted soil accurately.

(b) The creep parameters are observed to be prominent in the 2^{nd} stage of the unloading-reloading cycle for both natural and reconstituted soil. Further, increasing the unloading- reloading cycle reduces the creep parameters.

(c) With the increase of applied effective stress, the creep coefficient is observed to be decreased. Creep strain limit doesn't have a relationship with effective stress and the unloading-reloading cycle. However, both parameters were reduced with the increase in FA content.

(d) The swelling strain limit and swelling coefficient increase with decreasing applied stress. Both parameters are also reduced with the increase of FA content. This might be due to the fixation of clay particles with cementitious material and reduced soil-water interaction due to decreased permeability.

(e) From FTIR spectroscopy, the flexibility of the -OH bond present in montmorillonite minerals is reduced by adding FA. This might be due to the development of cementitious materials as observed in XRD and SEM spectroscopy.

(f) The amplitude sweeps test of the BC soil containing different composition of FA is investigated and it is observed that the yield stress, viscoelastic parameters are varied significantly with the use of different FA content.

Chapter 5

Long-term swelling characteristics of BC soil under alternate Wetting–drying cycle

5.1. Introduction

Cyclic swelling-shrinkage behaviour of expansive soil leads to volumetric changes in expansive soil, crack formations and consequently tremendous losses on the infrastructure. The soil exhibits time-dependent swelling behaviour (Sivapullaiah et al. 1996b), which is too significant to be ignored, particularly for large-scale projects. However, the literature has limited information, particularly on the time-dependent swelling behaviour under alternate wetting-drying cycles.

This study uses industrially available waste materials to modify the expansive soil and investigate the time-dependent swelling behaviour. The non-linear EVPS Model is incorporated to predict the time-dependent swelling behaviour. Further, the effect of the wetting-drying cycle in time-dependent swelling parameters is analyzed and correlated with mineralogical changes using XRD and SEM spectroscopy. The crack behaviour of the oedometer samples during alternate wetting-drying cycles was also investigated.

5.2. Material and test procedure

The BC soil used in this study is collected from Indore, Madhya Pradesh, from a depth of 1.5 m below the ground. The basic properties of BC soil are illustrated in **Table 3-1**. It is observed that BC soil belongs to A2-7 A7-5 (According to AASHTO soil classification), CH (Casagrande's plasticity chart) and Skempton Activity is found to be 1.22. The class C FA used in this study is collected from the thermal power plant in Khargone, Madhya Pradesh. Using energy dispersal X-ray (EDX) analysis in JEOL

JSM-7610F Plus Field Emission, the composition of FA is examined as shown in **Table 4-1**. The mineralogical composition of FA is examined using Bruker D2 phaser X-ray diffraction (XRD) spectroscopy. Panalytical X'pert, Highscore Plus software, was used to analyze the x-ray diffraction pattern. The presence of mullite, quartz, gypsum, and hematite is observed in **Figure 4.1** (Ma et al. 2016; Madejová et al. 2017).

The time-dependent swelling behaviour of natural and reconstituted BC soil was conducted in 1D oedometer tests (conforming to ASTM D4546). The natural BC soil and FA were oven-dried for 1 day at 100±5° C. The BC soil was then crushed and passed through a 2 mm sieve; however, the FA was a sieve in 150 μm to remove unwanted lumps (Phanikumar et al. 2021). The samples are prepared in maximum dry densities (MDD) and optimum natural soil moisture content (OMC). The BC-FA mixture was prepared by adding predetermined quantities of FA to BC soil and mixed thoroughly until a homogenous mixture was achieved. The required quantities of distilled water are added to the corresponding OMC of natural soil. All mixing was done manually, and proper care was taken. The prepared samples were transferred in a polythene bag for at least 48 hrs for maturity. The internal surface of the oedometer ring (size: 60 mm diameter and 20 mm height) was appropriately greased to minimize friction. The BC-FA mixture was transferred and compacted into three layers till it reached the maximum dry unit weight of natural soil (Aldaood et al. 2014). During the whole process, special care was taken to ensure no wastage of soil particles. The compacted sample and ring were weighed, immediately transferred to the environmental chamber, and cured for 7 days.

The temperature and humidity chamber of the environmental chamber was set at 25° C and 100%, respectively. Filter papers were placed on the top and bottom of the cured sample and transferred to the oedometer cell. The dial gauge was set to zero, and a nominal surcharge of 5 kPa was applied and allowed for free swelling. After swelling, the wetted sample and

the oedometer ring were kept in the oven for 24 hrs at 100°C. The oven-dried sample was cooled for 30 minutes at room temperature (25°C ± 2°C), removed filter papers, and recorded height and weight before commencing the next cycle. The oedometer ring was greased in any wetting drying cycle stage to reduce possible friction and wastage of samples. The oedometer ring and sample were again transferred to the oedometer cell, allowing free swelling. In this test, both reconstituted and natural BC soil were subjected to four alternate wetting-drying cycles of different days (1st swell-7 days, 2nd swell-14 days, 3rd swell-7 days, and 4th swell-7 days).

5.3. Result and discussion

The change in axial deformation of the naturally available BC soil during the alternate wetting-drying cycle is illustrated in **Figure 5.1**. The BC soil exhibits a higher potential for swelling behaviour by showing an axial deformation of 30.1% and 12.60%, respectively, during the first wetting-drying cycle (for 7 days). The void ratio changes during the wetting-drying cycles are not identical; this is the primary cause of irreversible deformations (Chen et al. 2019; Shahsavani et al. 2020). Thus, BC soil

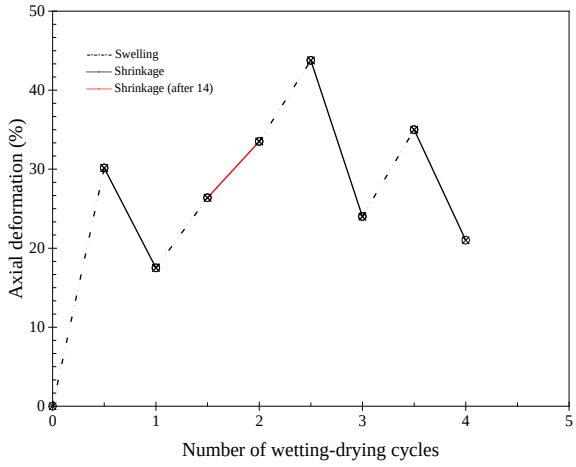

Figure 5.1: *Influence of alternate wetting-drying cycle in vertical deformation of BC soil.*

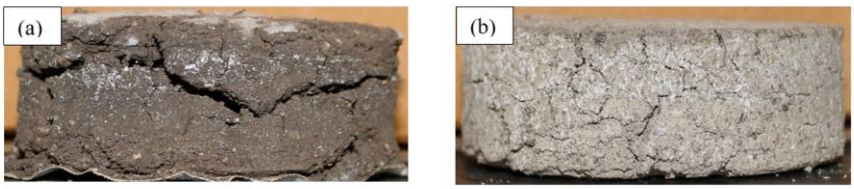

Figure 5.2: *Difference in vertical crack formation behavior (a) BC soil and (b) 35% FA+BC soil.*

exhibits an irrecoverable deformation of 17.5%. During the second stage of swelling (14 days), instead of a reduction in axial deformation, BC reveals an increase in the axial deformation during drying, which reached up to 33.5% (as marked by red lines). The possible reason might be the formation of axial cracks, as shown in **Figure 5.2**, which is also influenced by 14 days of continuous swelling. The crack development is significantly influenced by factors like water retention characteristics, fine content, and mineralogy-

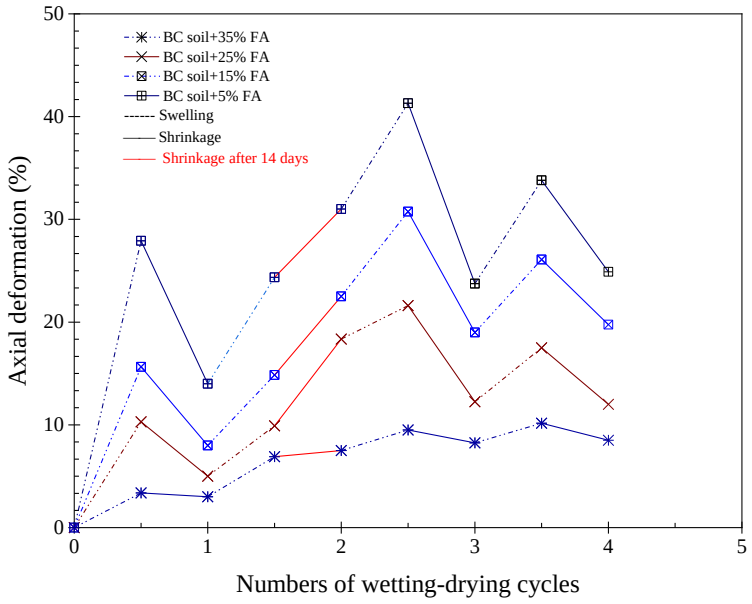

Figure 5.3*: Influence of alternate wetting-drying cycles in FA-BC matrix.*

ical composition (Stirling et al. 2017). Thus, the swelling potential of BC soil is observed to be 43.76% in the third cycle which is further reduced to 35.1% in the fourth stage of the wetting-drying cycle. Thus, irreversible deformation is found to be 5.66%. The decrease in volumetric strain with the increase in the wetting-drying cycle is observed to be in good agreement, as reported by other researchers (Yazdandoust and Yasrobi 2010).

The change in axial deformation behaviour of the FA (5%, 15%, 25% and 35%) blended reconstituted BC soil under the alternate wetting-drying cycle is exhibited in **Figure 5.3**. It shows that the addition of FA leads to a decrease in overall axial deformation during the wetting and drying stages. Similar to natural BC soil, the second wetting-drying cycle is kept for 14 days. The FA-BC soil matrix shows a continuous decrease in axial strain during the drying stage of 2nd wetting-drying cycle. In the case of 35% FA blended reconstituted BC soil, the crack and axial deformation are observed to be relatively lesser. The formation of cracks is a combined effect of both drying shrinkage and ambient temperature of the soil specimen. However, two major factors are responsible for reducing the axial crack deformations in the FA-BC matrix. Firstly, the silicate in the admixture boosts the surface hardness and resists crack development. Secondly, the homogeneity of the material reduces with the addition of the foreign admixture and thus disturbs the overall evaporation rate (George 1971). Again, the soil-specific surface area decreases and consequently lessens the water affinity (Jha and Sivapullaiah 2018). Moreover, the soil specimen attains an equilibrium state by showing a steady change of axial deformation behaviour with the increase of the wetting-drying cycles. Thus both natural BC soil and reconstituted soil exhibit a reduction in swelling potential and shrinkage behaviour with the increase in wetting-drying cycles (Shahsavani et al. 2020).

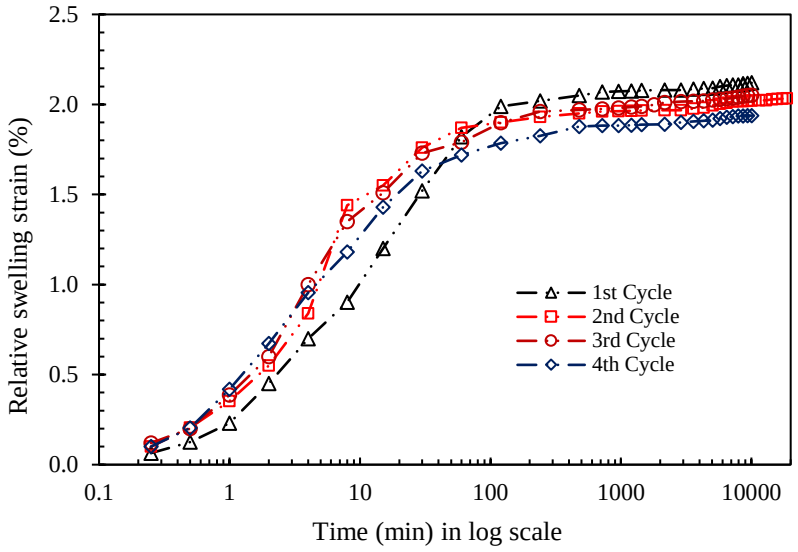

Figure 5.4: *Relative swelling strain behaviour of BC soil under alternate wetting-drying cycles.*

The relationship between the changes of vertical deformation against time can be better described using relative swelling strain (RSS). It is the amplitude of vertical strain changes during the free swell state with reference to the initial thickness of the sample expressed in terms of percentages. The RSS behaviour of BC soil during the alternate wetting-drying cycle is illustrated in **Figure 5.4**. BC soil has the ability to absorb significant water due to its flake or flocculent structural arrangement, thereby possessing a higher surface area (Singh et al. 2020; Sridharan 1991).

Thus, BC soil exhibits higher RSS than BC-FA mixture as it can regain its original structural arrangement by absorbing significant water. However, the alternate wetting-drying cycle gradually disturbs the overall structural arrangement (Zhu et al. 2017). It changes the structural elements' orientation in the micro aggregates (Chen et al. 2019). Again, the alternate wetting-drying cycle leads to particle aggregation by reducing the clay content between the initial cycle and final cycles. These are significant factors that lead to an inevitable reduction in the RSS of the BC soil with the increase of alternate wetting-drying cycles.

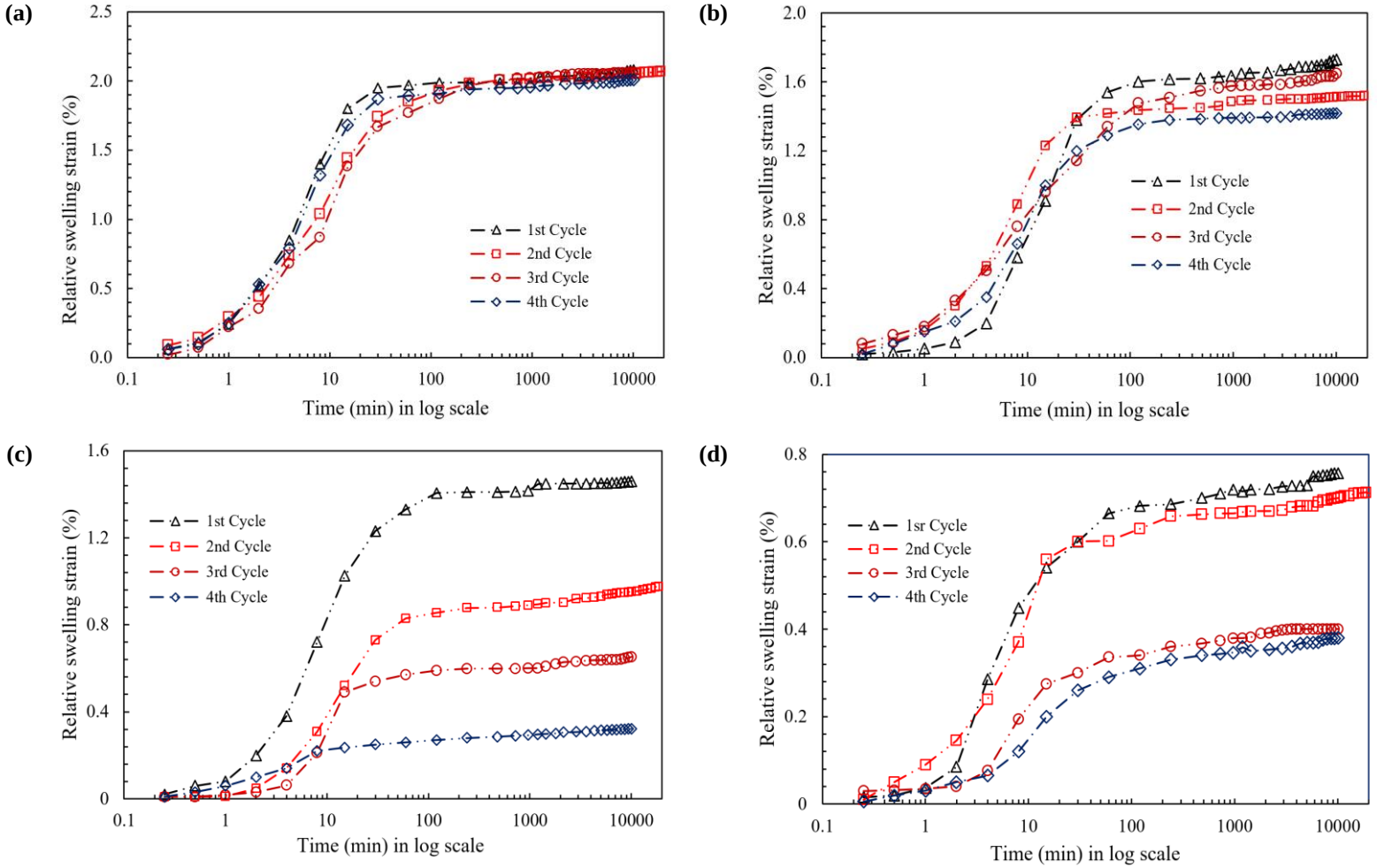

Figure 5.5: *Relative swelling strain behaviour of FA-BC matrix under alternate wetting-drying cycles.*

The variation of RSS behaviour of FA blended BC soil is illustrated in **Figure 5.5**. It shows that 5%, 15%, 25%, and 35% FA-treated specimen exhibits a lesser RSS compared to natural BC soil during the first wetting-drying cycle. As the FA content increases, the overall RSS behaviour also decreases. Similar to BC soil, the RSS behaviour of FA blended reconstituted soil is found to decrease continuously with the increase of the wetting-drying cycle. Several factors like changes in mineralogical composition by forming hydration by-products, reducing the clay content as a proportion of FA content increases, fixing the position of clay particles, and filling the void space among soil particles are responsible for decreasing the RSS behaviour of FA blended mixture (Atahu et al. 2019). As hydration by-products fill the internal voids, the BC-FA mixture is found to be denser and more heterogeneous than natural BC soil. It is also observed that the reduction of RSS behaviour of FA blended mixture under alternate wetting-frying cycle depends on the quantity of the additive used.

5.3.1. Time-dependent swelling behaviour

Time-dependent swelling is the continuous expansion of the soil volume due to the percolation of pore water through their interconnected voids. It is governed by the extrinsic and intrinsic properties of the soil (Elsharief and Sufian 2018). The overall swelling behaviour of the soil exhibits an "S" shape pattern, as illustrated in **Figure 5.6**. It can be subdivided into three phases: initial stage, primary stage, and secondary stage (Sivapullaiah et al. 1996b). The hydration of the clay particle surface is responsible for the initial stage of swelling. However, the primary stage takes place due to the development of the double-layer effect in the clay particles with the percolation of pore water (Ladd 1960). The secondary swelling stage is regarded as a time-dependent continuous increment in soil volume. Several researchers give different opinions about the origin of the secondary swelling stage. The primary causes of secondary swelling or delayed deformation are clay permeability, chemical changes, diagenetic

bond breakdown, structural adjustment, and particle rearrangement (Feng et al. 2017a; Mesri 1973). The time-dependent swelling strain ε_z^s of expansive soil is too significant to ignore.

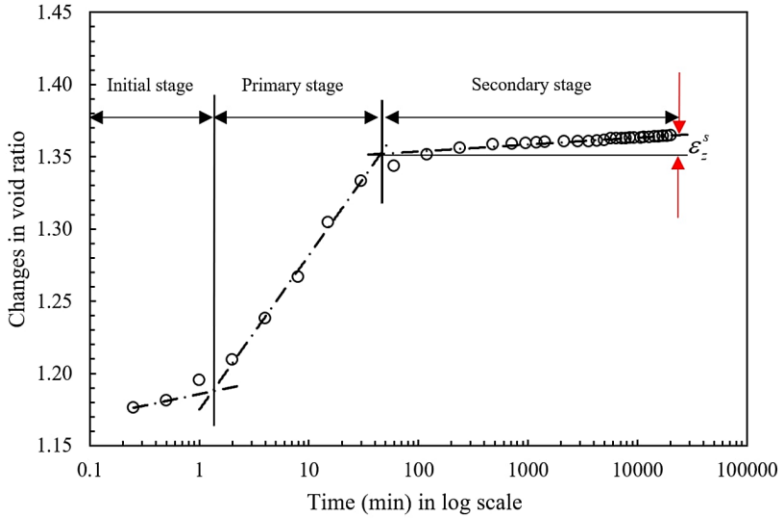

Figure 5.6: *Different stages during swelling in BC soil.*

5.3.2. Application of non-linear function of EVPS Model

It is a prediction model that can access the axial deformation behaviour in elastic, plastic, and time-dependent states based on the equivalent timeline concept. It can consider both the creep and swelling characteristics in 1D conditions (Feng et al. 2017a). The final state of strain during creep and swelling equilibrium when the time tends to infinity can be accessed using a conceptual model describing the creep equilibrium limit (CEL) and swell equilibrium limit (SEL) (Yin 1990a). The variation of axial strain comprises two major components, i.e., recoverable strain and non-recoverable strain. The change of strain is assumed to begin with respect to the reference timeline, and the time taken in strain change is considered an equivalent timeline (Yin and Tong 2011b). The reference timeline has zero equivalent time. The time-dependent swelling can be described as reverse creep behaviour, and a non-linear function of the EVPS Model is used to

investigate this behaviour. According to the EVPS model, the time-dependent strain can be expressed as follows (Feng et al. 2017a; Yin 1999),

$$\varepsilon_z^s = -\frac{\frac{\psi_0^s}{V}\ln\left(\frac{t_0^s + t_e^s}{t_0^s}\right)}{1+\frac{\psi_0^s}{V\varepsilon_z^{sl}}\ln\left(\frac{t_0^s + t_e^s}{t_0^s}\right)} \qquad 5\text{-}1$$

where $\frac{\psi_0^s}{V}$, ε_z^{sl} and t_0^s are the constant parameters (Yin 1999). $\frac{\psi_0^s}{V}$ is defined as the swell coefficient and denotes the rate of the vertical strain changes with respect to time (Feng et al. 2017a), ε_z^{sl} signifies the swell strain limit, and denotes the final strain soil can be achieved when the duration of unloading tends to zero, i.e. when the time tends to infinity, $\varepsilon_z^s = \varepsilon_z^{sl}$ (Tong and Yin 2013). In this study, t_o^s is assumed as the time corresponding to the beginning of time-dependent swelling and is taken as the time corresponding to the end of the primary swelling stage $\left(t_{EOP}\right)$(Tan et al. 2018; Zhou et al. 2018). If $\ln\left[\left(t_0^s + t_e^s\right)/t_0^s\right]$ is treated as a function *x*, the creep coefficient $\frac{\psi_0^s}{V} = a$ and the reciprocal of creep strain limit $1/\varepsilon_z^{sl} = b$, then the Eqn. 1 can be expressed as

$$\frac{1}{\varepsilon_z^s}\ln\left(\frac{t_0^s + t_e^s}{t_0^s}\right) = -\frac{1}{\varepsilon_z^{sl}}\ln\left(\frac{t_0^s + t_e^s}{t_0^s}\right) + \frac{V}{\psi_0^s} \qquad 5\text{-}2$$

The above equation is in the form of a straight line *"y=–bx+a"* putting $\frac{1}{\varepsilon_z^s}\ln\left(\frac{t_0^s + t_e^s}{t_0^s}\right) = y$. The oedometer data were used to fit a straight line between the $\ln\left[\left(t_0^s + t_e^s\right)/t_0^s\right]$ against the $\ln\left[\left(t_0^s + t_e^s\right)/t_0^s\right]/\Delta\varepsilon_z^s$. The slope and intercept observed from this straight line were employed to determine the swell strain limit and swell coefficient, respectively.

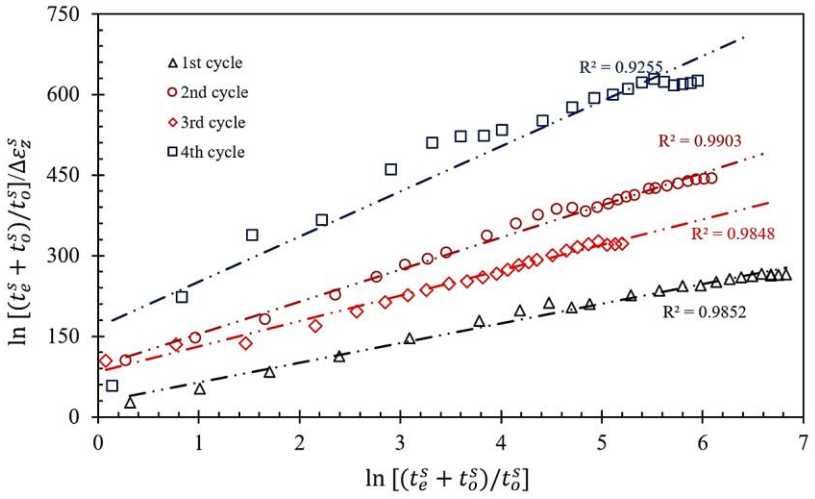

Figure 5.7: *Curve fitting for swelling parameters in 5% FA+BC soil subjected to wetting-drying cycle.*

5.3.3. Influence of wetting-drying cycle in time-dependent parameters

Figure 5.7 illustrates the variation of $\ln\left[\left(t_0^s + t_e^s\right)/t_0^s\right]/\Delta\varepsilon_z^s$ against the $\ln\left[\left(t_0^s + t_e^s\right)/t_0^s\right]$ for 5% FA blended BC soil under alternate wetting-drying cycles. During the first cycle, BC+5% FA soil possesses the value of ψ_0^s/V and ε_z^{sl} amounts to 0.0469 and 0.0247, respectively. In the 2nd cycle, the parameter ψ_0^s/V and ε_z^{sl} are found to be 0.0129 and 0.0167. Similarly, in 3rd and 4th wetting-drying cycle, the parameter ψ_0^s/V is observed to be 0.0119 and 0.0044 while the ε_z^{sl} amounts to be 0.0211 and 0.0138, respectively. The derived fitting equations for the same are also illustrated in Table 3. It is observed that the time-dependent swelling coefficient and swell strain limit are continuously decreased with the increase of wetting-drying cycles. This can be explained by two different phenomena. Firstly, the clay content and plasticity characteristics are decreased continuously with the wetting-drying cycle. The same can be explained using the concept of surface tension force arising from soil particle meniscus. During shrinkage, the minute interparticle separation

Table 5-1: *Curve fitting equations of 5% FA+BC soil.*

Nos. of cycle	Fitting equations	R^2
1st cycle	y = 36.64x + 27.449	R^2 = 0.9852
2nd cycle	y = 66.836x + 77.362	R^2 = 0.9848
3rd cycle	y = 47.264x + 83.419	R^2 = 0.9903
4th cycle	y = 83.975x + 167.51	R^2 = 0.9255

generates capillary stress that draws particles intimately and permits the development of Vander Waals bonds. This leads to a decrease in the specific surface area available for water retention, and thus the swelling potential decrease with the increase of wetting-drying cycles (Al-Homoud et al. 1995). Secondly, the particles undergo a continuous rearrangement during the alternate wetting-drying cycle. It lowers the structural orientation

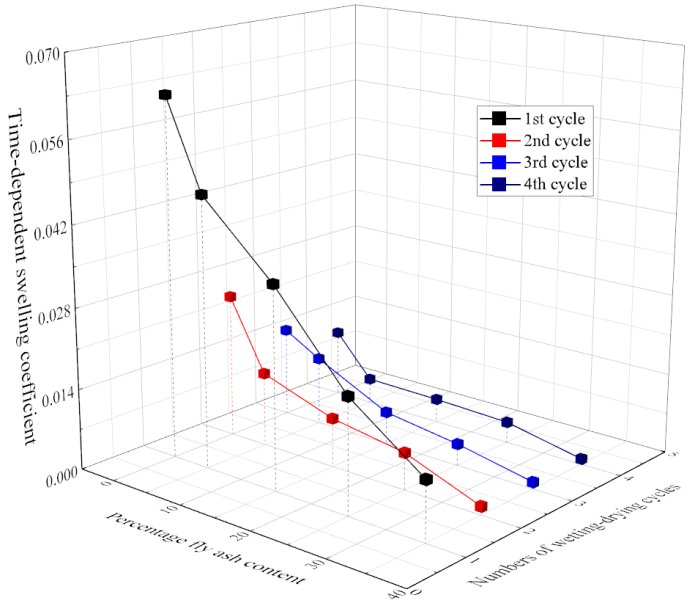

Figure 5.8*: Relationship between numbers of wetting-drying cycles, percentage FA content and time-dependent swelling coefficient.*

increase the compactness and denseness of the particles, which correspondingly decreases the water absorption capacity and thus reduces the time-dependent swelling coefficient as the wetting-drying cycle increases (Zeng and Kong 2019).

5.3.4. Effect of FA in time-dependent swelling behaviour

Figure 5.8 illustrates the variation of the time-dependent swell coefficient of both natural BC soil and FA (5%, 15%, 25% and 35%) blended soil subjected to different wetting-drying cycles. During the first cycle, the swell coefficient of BC soil is observed to be 0.0622, which is reduced to 0.0469 as the 5% FA is added. Similarly, the swell coefficient of 15%, 25% and 35% FA blended soil is observed to be 0.0350, 0.0200 and 0.0104, respectively. It is observed that the time-dependent swell coefficient decreases with the increase of FA content. In the second wetting-drying cycle, 0%, 5%, 15%, 25% and 35% FA blended mixtures possess a swell coefficient of 0.0251, 0.0129, 0.0085, 0.0065 and 0.0014. During the third wetting-drying cycle, the swell coefficient of BC soil, 5%, 25%, 25%, and 35% FA blended reconstituted soils, is observed to be 0.0156, 0.0119, 0.0057, 0.0038 and 0.0017, respectively.

In the last wetting-drying cycle, the swell coefficient of BC soil, 5%, 15%, 25%, and 35% FA blended soil, are respectively 0.0117, 0.0044, 0.0042, 0.0036 and 0.0009. It is observed that the time-dependent swell coefficient is found to decrease with the increase of FA composition and wetting-drying cycle and exhibits a non-linearly trend of reduction. The major factor responsible for reducing the time-dependent swell coefficient with the addition of FA might be cation exchange capacity. The FA provides multivalent cations like Ca2+, Al3+, Fe3+, etc. There is an exchange of cations between FA and soil (Mitchell and Soga 1993a). The cation exchange

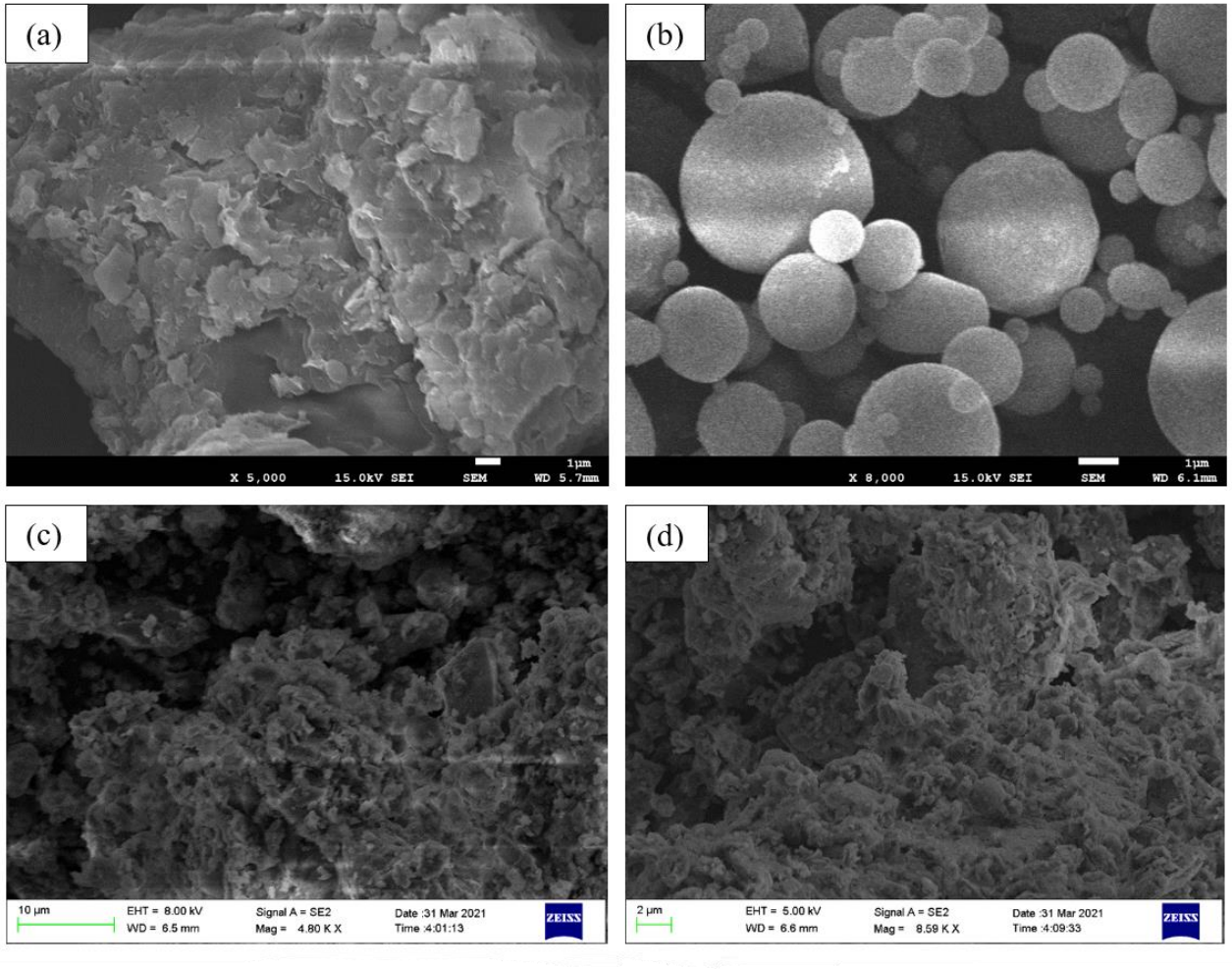

Figure 5.9: *SEM spectroscopy of (a) BC soil, (b) FA, (c) 25% FA+BC soil and (d) 35% FA+BC soil.*

allows the flocculation of clay particles, thereby forming flocculated fabrics (Erdal Cokca 2001). The addition of foreign admixture reduces the surface area and water affinity due to the heterogeneity of the blended mixture increasing continuously (Shi et al. 2018).

The mineralogical and morphological behaviour of BC soil, FA and FA-BC mixtures are also investigated using the JEOL JSM-7610F Plus Field Emission SEM and Bruker D2 phaser XRD spectroscopy. The BC soil exhibits a flake structure arrangement, as shown in **Figure 5.9** (a). It enhances the ability for water interaction and thus absorbs significant water. This arrangement influences to possess significant swelling behaviour under alternate wetting–drying cycles. The FA exhibits micro globular shape morphology as in **Figure 5.9** (b). The surface area of BC soil is reduced with the addition of FA and exhibits the formation of hydration products in 25%, and 35% FA blended BC soil, as illustrated in **Figure 5.9** (c), and (d).

Again, the XRD result clarified the formation of new mineralogy as new peaks are detected in the FA-BC mixture. XRD spectroscopy is analyzed using Panalytical X'pert Highscore Plus software. The major minerals present in the BC soil are montmorillonite, illite, calcite, quartz, hematite, and feldspar. It doesn't detect any peak in the position of 2θ ranging from 40°–48° and 52°–56°; however, new peaks can be detected in FA blended reconstituted soil as in **Figure 5.10**. These denote the presence of minerals called Tobermorite and calcium hydroxide. Tobermorite is a Calcium-Silicate-Hydrate (CSH) mineral, which Heddle reported in 1880 (Saride and Dutta 2016; Sudhakaran et al. 2018). Several researchers also proposed the relevant mechanisms. It binds the soil particles by filing all possible voids, and this process helps in fixing clay particles in a particular position (Mráz et al. 2015; Zhang and Li 2018). This influences the densification and formation of a bridge between the adjacent BC particles. Thus, the swell coefficient decrease as the FA content increases.

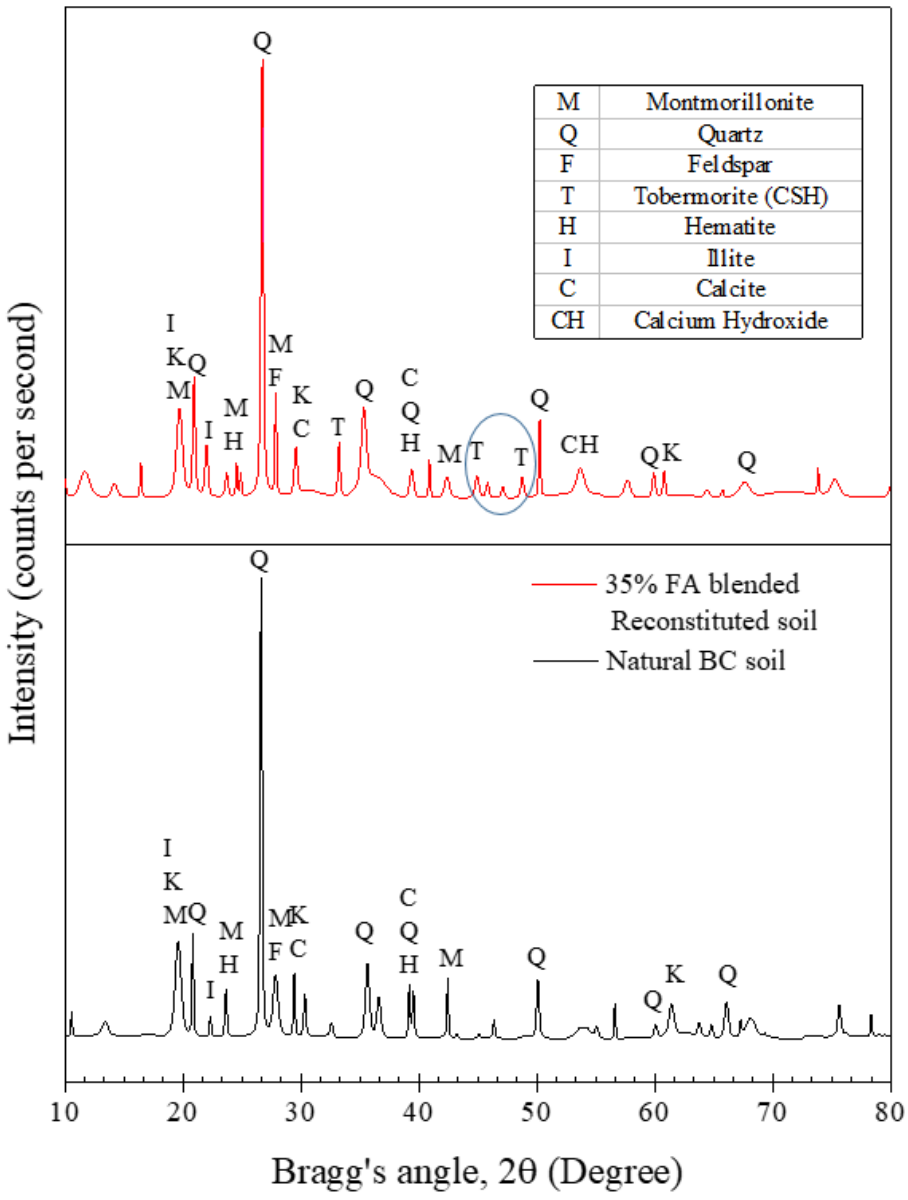

Figure 5.10: *XRD spectroscopy of FA+BC matrix (with 35% FA) and naturally available BC soil.*

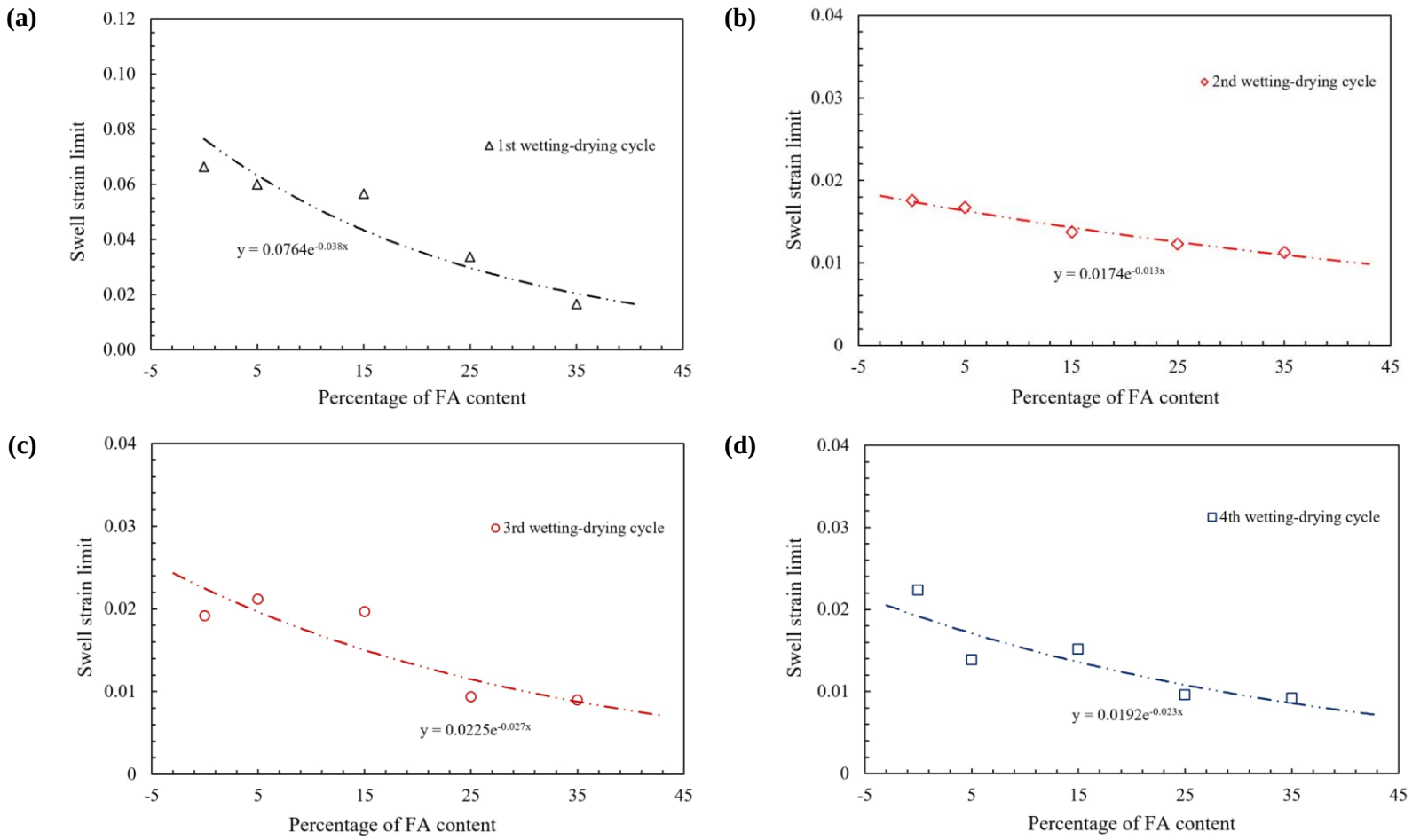

Figure 5.11: *Swelling strain behaviour of FA+BC matrix subjected to (a) first cycle, (b) second cycle, (c) third cycle and (d) fourth wetting-drying cycles.*

Figure 5.11 illustrates the variation of the swell strain limit under different wetting-drying cycles as a function of FA content. The exponential trend line is found to be the best-fitting curve to predict the change of swell strain limit with the increase of FA content. It is observed that during the first wetting-drying cycle, the swell strain limit shows a significant change with the increase of FA content, as in **Figure 5.11** (a). However, in the later stages, the changes in strain limit are observed to be consistent, as illustrated in **Figure 5.11** (b), (c) and (d). The sudden variation of swell strain limit in the first cycle compared to the remaining cycle might be due to the attaining equilibrium of the soil particle arrangement by reducing pore space and particle surface area (Estabragh et al. 2015).

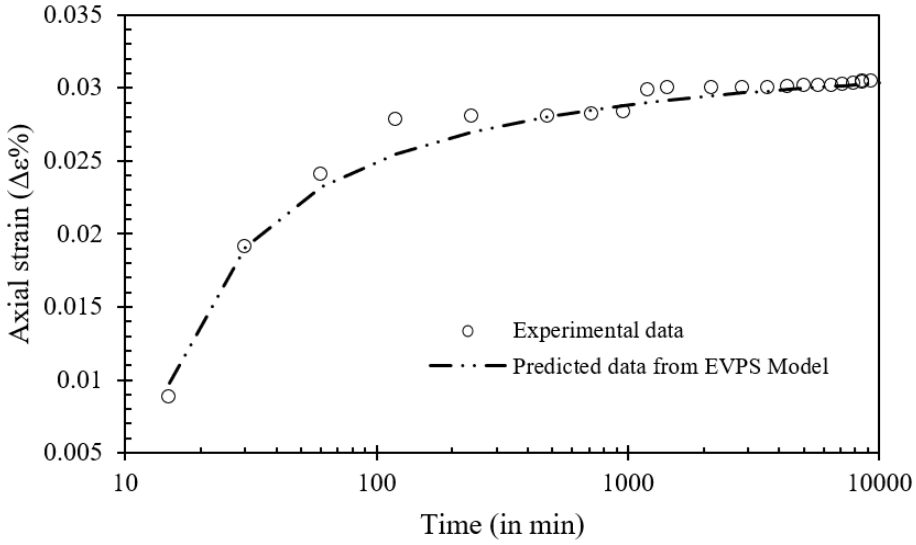

Figure 5.12: *Prediction of vertical strain behaviour of 25% FA+BC matrix subjected to wetting-drying cycle using EVPS Model.*

5.3.5. Prediction of time-dependent swelling behaviour under the wetting-drying cycle

Using the concept of swell coefficient and swell strain limit, the time-dependent swelling behaviour of 25% FA blended BC soil is predicted

using the Eqns. 1. Here the constant parameter taking t_0^s is taken as 11 mins. Other time-dependent parameters $\frac{\psi_0^s}{V}$, ε_z^{sl} are respectively 0.0434, and 0.0337. The predicted swell behaviour is compared with actual experimental data conducted in the laboratory. In both cases, it is observed that the swelling strain changes non-linearly with the increase of time. From **Figure 5.12**, it can be stated that the non-linear EVPS Model can be used to accurately predict the time-dependent swelling behaviour of Indian Black cotton soil with a wide range of admixtures in different wetting-drying cycles.

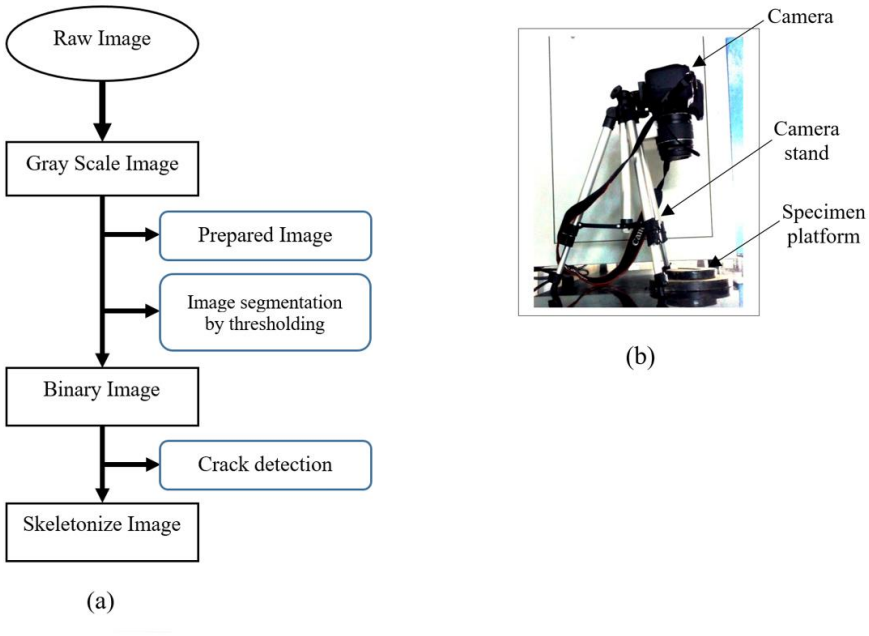

Figure 5.13: *(a) Flowchart of image processing; (b) raw Image capturing setup.*

5.3.6. Crack behaviour under alternate wetting-drying cycle

After completing every wetting-drying cycle, the RBG (Red Blue Green) image is taken using a DSLR camera from a height of 300 mm. The flowchart and instrumentation set up for image processing are shown in **Figure 5.13**. Using ImageJ software, the image is cropped circularly so that

the outer area is converted to white background and the central image as an RBG image. Further, the image is converted to an 8-bit grey-scale image. The Un-Sharpen mask is employed to sharpen and enhance the edges of the image by removing the blurred version. The crack portion of the image is separated from the intact soil in the image segmentation. It is performed by applying a threshold value in the grey-scale image. The best threshold is selected after the trial. All the pixels of the image are converted to either 0 (a black pixel) or 255 (a white pixel) based on the threshold value. The pixel whose value is smaller than the threshold pixel will become black, and the remaining will be white. The error remains after the image segmentation is corrected by binary operations. The Close function is employed in this study, which has Despeckle median filter operation. It can replace each pixel with the median value in its 3*3 neighbourhood.

The crack behaviour of natural BC and reconstituted soil is investigated, particularly after the first stage of the wetting-drying cycle. The sample compacted during the sample preparation, which leads to a densified structure arrangement, might be the possible reason for negligible crack formations during the first stage of the wetting-drying cycle. However, significant crack formation is being noticed from the subsequent cycles. The formation of cracks is a combined effect of both drying shrinkage and ambient temperature in the sample. During the exposure of the sample to a higher temperature, internal tensile stress develops in the sample; once the internal tensile stress exceeds the tensile strength of the soil, crack formation initiates (Trabelsi et al. 2012). **Figure 5.14** shows the crack behaviour of natural and reconstituted soil under different wetting-drying cycles. These cracks are divided into two main groups; primary cracks and secondary cracks. Primary cracks are formed initially and possess significant width than secondary cracks. It divides the sample into many cells; within this cell, secondary cracks developed from the evolved

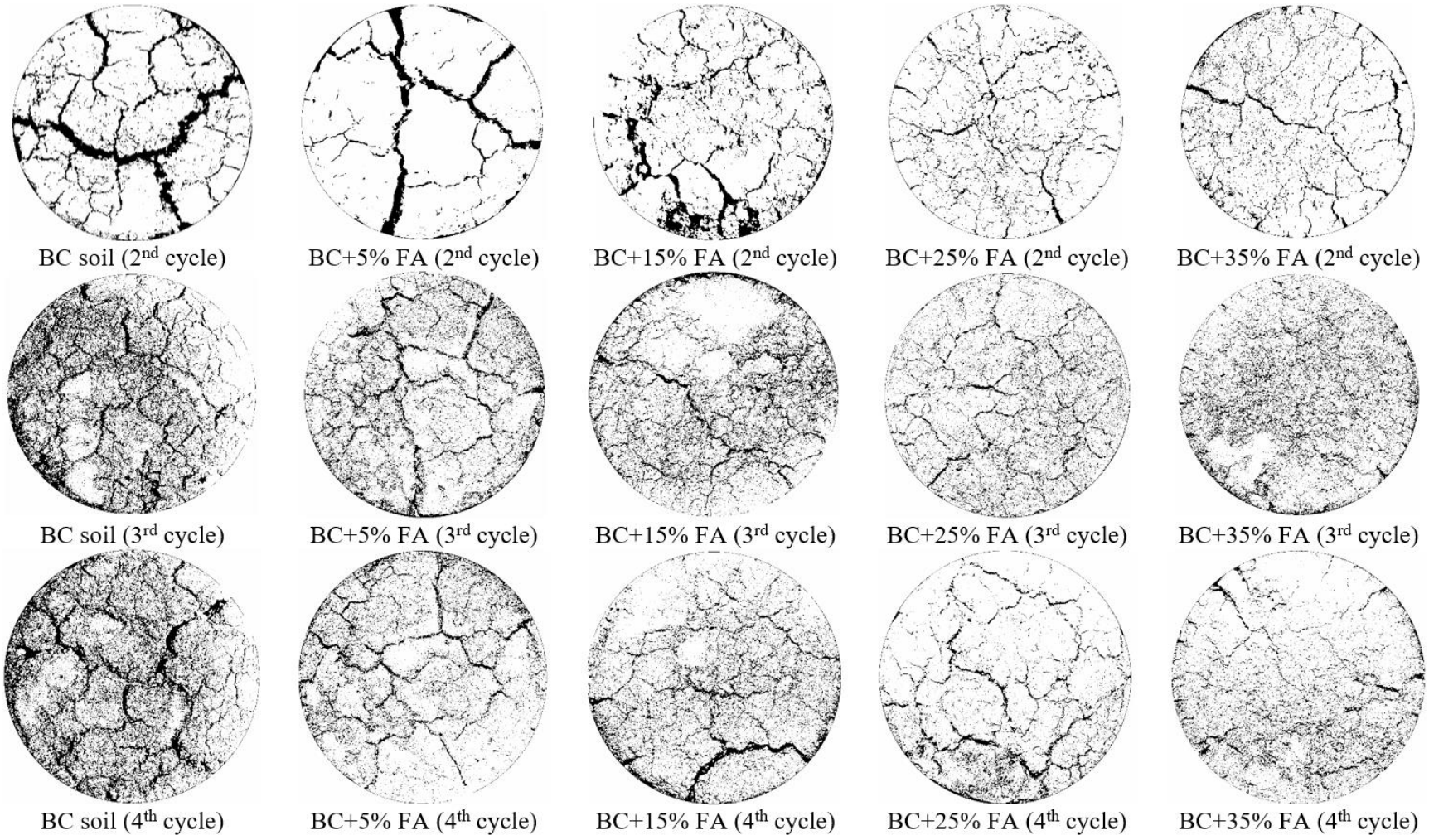

Figure 5.14: *Crack behaviour of both natural and reconstituted soil samples under different wetting drying cycles.*

stress field (Peron et al. 2013). However, the formation of both primary and secondary cracks is random in nature. From the second wetting drying cycle, the soil exhibits significant development of cracks. This might be due to being subjected to 14 continuous days for free swelling as crack development is influenced by the water retention characteristics and fine content (Stirling et al. 2017). The primary cracks in natural BC soil and lower FA content (i.e., 5% and 15%) are found significant and more or less similar even after being subjected to different wetting-drying cycles, as shown in **Figure 5.15**. The primary cracks are insignificant in higher FA-content soil and randomly develop primary and secondary cracks.

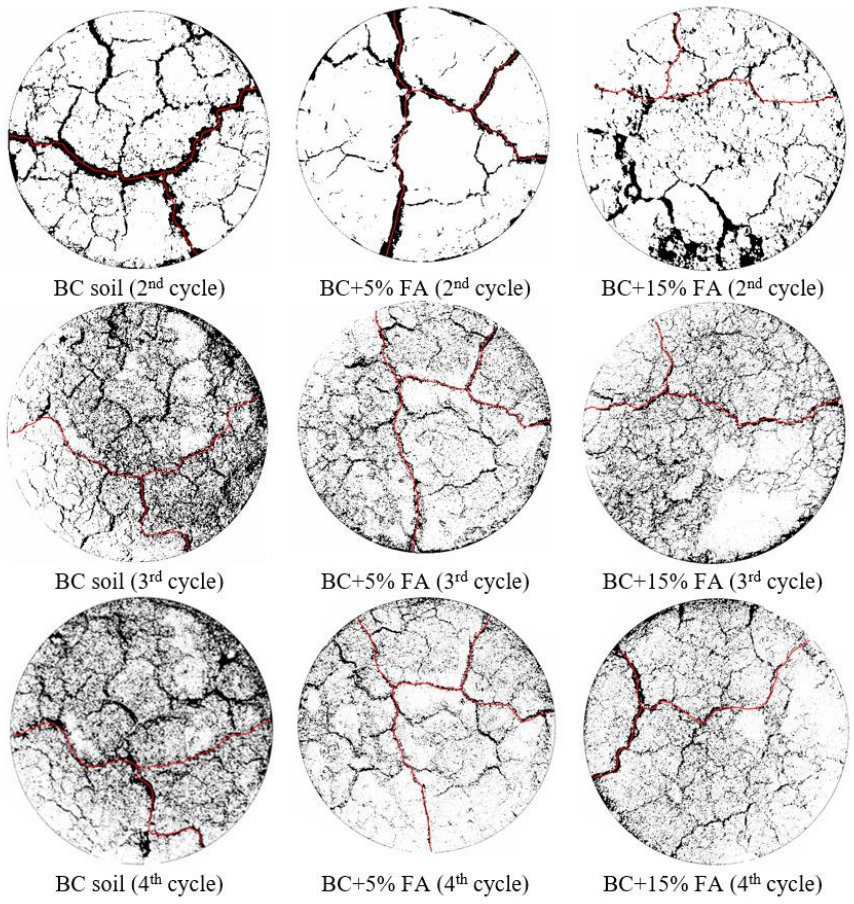

Figure 5.15: *Repetitive Primary crack behaviour under different wetting-drying cycles.*

Overall, significant numbers of secondary cracks are developed with the increase in wetting-drying cycles. The initial wetting-drying cycle leads to irreversible fabric changes, and interparticle bonds are damaged during cracking. These damage bonds and change fabrics become the weakest location and remain preferential zones for cracking in alternate wetting-drying cycles (Tang et al. 2016; Yong and Warkentin 1975). It leads to the existence of primary cracks in subsequent wetting-drying cycles. Again, the alternate wetting-drying cycles lead to soil particle rearrangement and modification of the pore system; therefore, secondary and new cracks are developed. As the FA content increase, the formation of cracks is observed to be decreasing continuously irrespective of the wetting-drying cycle. The development of preferential zones for cracking in alternate wetting-drying cycles is significantly reduced with the addition of FA. Thus, the primary cracks are significant and consistent with up to 15% FA blended soil even after being subjected to different wetting-drying cycles.

The reduction of crack formation is attributed to two significant factors. The minute particles with surface area, greater adsorption capacity, and evident chemical activity of FA initiate the agglomeration and fine particles present in the soil. Several chemicals influence the agglomeration process. Chemicals like Al and Si are beneficial for the agglomeration process as they can be combined with adsorbents through chemical bonds (Skousen et al. 2013). This agglomeration process improves the interparticle bonds and thus improves the soil structures. The cementitious compounds formed during the hydration process enhance the intermolecular interaction between soil particles (Lu et al. 2014). Secondly, the addition of FA lessens the overall homogeneity, reduces the evaporation rate, and minimizes the clay content of the soil, which helps inhibit crack growth (Yang et al. 2021).

5.4. Recommendations for FA utilization

The addition of FA in different proportions can influence several geotechnical parameters, including the creep behaviour, time-dependent swelling, swelling-shrinkage behaviour and even the crack formation of the BC soil. So, FA can be employed to improve the performance of problematic soil. From a different perspective, the leaching behaviour of the heavy metals present in the FA blended soil will contaminate soil and groundwater (Benito et al. 2001). However, utilization of FA as an admixture in the construction site is safe up to some reasonable percentages like 20% (Cetin et al. 2012). This study also observed that the addition of FA diminishes several time-dependent properties of reconstituted soil as FA increases. The percentages of FA should be chosen carefully during the design of FA blended embankment construction from the environmental aspect and time-dependent aspects.

5.5. Conclusion

In this study, a series of free swell tests were performed in natural BC and reconstituted soils (5 %, 15 %, 25 %, and 35 % FA-blended) to investigate the wetting–drying impact cycle on the time-dependent swelling behaviour. An analytical model that considers the influence of swelling and elasto-viscoplastic behaviour of soil was considered to examine the long-term time-dependent swelling behaviour of the reconstituted FA-BC matrix. Further crack behaviour of the samples was investigated through image processing. From this study, the following conclusions are drawn:

- The study predicts the time-dependent swelling behaviour of natural and reconstituted BC soil and presents the accuracy and suitability of the EVPS Model.

- The shrinkage behaviour is significantly influenced by water retention and clay content. The time-dependent swelling coefficient decreases with the increase of FA composition. The number of wetting-drying cycles and composition of FA significantly influence the overall swelling behaviour of the reconstituted soil.

- The swell strain limit decreases exponentially with the increase in FA content and reduces with wetting-drying cycles. The sudden variation of swell strain limit in the first cycle compared to the remaining cycle might be due to the attaining equilibrium of the soil particle arrangement by reducing pore space and particle surface area.

- The alternate wetting-drying cycles lead to soil particle rearrangement and modification of the pore system; therefore, secondary and new cracks are developed. The addition of FA lessens the overall homogeneity of the sample and reduces the evaporation rate, and minimizes the clay content of the soil, which helps inhibit crack growth. However, primary cracks are significant and consistent with up to 15% FA blended soil even after being subjected to different wetting-drying cycles.

- Altogether, this study presents that the utilization of industrial waste as a stabilizing additive can effectively enhance several engineering properties of problematic soil while addressing the environmental impact of waste disposal.

Chapter 6

Machine Learning in the prediction of geotechnical parameters

6.1. Introduction

Accurate prediction of long-term settlement and compressibility characteristics of problematic soil is a concern during the design of geotechnical foundations. Therefore, assessing the time-dependent behaviour and parameters like the coefficient of consolidation need to be computed beforehand. Although it can be measured from laboratories or field conditions, it is time-consuming, costly, and requires skilled technicians. In this study, Machine Learning (ML) concepts are employed to develop suitable and accurate models to predict coefficients of consolidation and time-dependent parameters (creep). This study considered several input parameters, among which data irrelevant to creep and coefficient of consolidation are discarded using Feature Selection algorithms. The selected data are used in ML algorithms and developed several models. The performance of each model is evaluated using different evaluation matrices and proposed two models that predict creep and coefficient of consolidations for globally distributed soil. This study considers several input parameters that are limited or not easy to do using the empirical correlation equation. Also, future aspects of ML in predicting creep behaviour are present in this study. In addition, the strength and limitations of models developed from ML algorithms and Abaqus simulation are also discussed by comparing their predicted data.

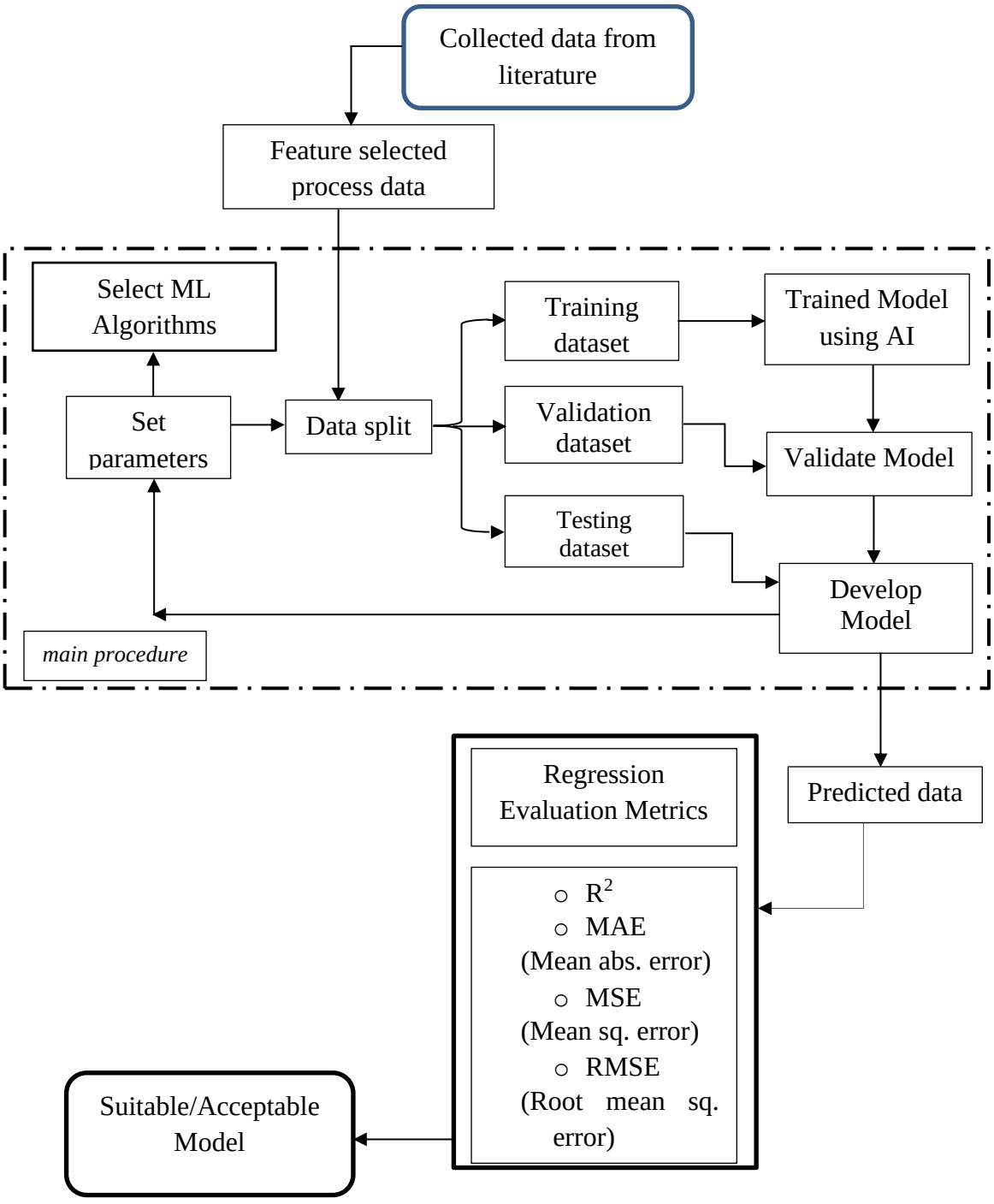

Figure 6.1: *Flowchart of proposed ML algorithm.*

6.2. Methodology and different algorithms

This study attempts to develop models which are applicable in globally distributed soil. Therefore, the data are collected from well-known, reputable, globally accepted academic databases. The numbers of input parameters for the creep model and coefficient of consolidation model are respectively 9 and 11. However, the higher number of input features is not cost-effective and creates other experimental limitations. In this study, the irrelevant/least important features are discarded using Feature Selection algorithms. The features of greater importance are further divided into testing and training datasets in each algorithm. Prediction models are developed using algorithms based on the input dataset and the complexity of the problem. Using the training dataset, several models are developed and used for prediction by testing with unseen data, i.e., testing datasets. Model Evaluation is an integral part of the development of the model. Among the various developed models, the best model that can give the best prediction and accuracy of the chosen model is determined by the Model Evaluation. **Figure 6.1** illustrates the flowchart of the proposed methodology. Different algorithms employed in this study are presented as follows.

6.2.1. Feature Elimination (FE)

Based on several pre-defined criteria, such as class classification performance, the feature selection method choose a relevant subset of the features from overall input features (Chen and Jeong 2007). The independent features are categorized according to their importance provided by training on the dataset. Depending on the importance of independent features, the least significant features are discarded and further re-fitting the model. The refitting process continue and least features is removed simultaneously until a specified number of features remains. This process of feature selection is an iterative approach because, depending on the

chosen subset of original features, the importance of a feature may change considerably (Granitto et al. 2006; Guyon et al. 2002).

This study employs the UFS technique as a pre-processor before applying an estimator model to the dataset. The independent features are categorized based on their importance, and the least important soil parameters are discarded (Gupta 2019). Among the available feature selection methods, UFS is an advanced feature selection method which is suitable for small classification-related problems (Guyon et al. 2002). The scikit-learn library of Python provides the SelectKBest class for UFS, which is the suite for selecting a specific number of features. It can be suitably applied for numerical inputs and categorical data via the f_classif() function. This feature selection enhances the relationship between the target variable and significant features. Other insignificant features are removed from the current feature space. The chosen significant features are further used to train, test, and validate the aforementioned ML algorithms.

6.2.2. Artificial Neural Networks (ANNs)

ANN is a computational algorithm consisting of many simple interconnected processors (Jain et al. 1996). The processing elements of ANNs are non-linear circuits having an n^{th} degree called nodes, having numerous input connections. ANNs are divided into subsets called layers. It consists of a hidden and output layer. The hidden layer is connected with inputs that connect ANN to the external world. The incoming information provided by the input features is processed in the hidden layer and further forwarded to the output layer. Based on the suitability of the problem, the number of hidden layers can be varied (Sheela and Deepa 2013). The complexity and calculation time is depended on the number of neurons in the hidden layer. The architecture of the ANN is illustrated in **Figure 6.2**. Suppose x is the input and the corresponding output from the model is y, then the underlying mechanism of the neural network for hidden layers one and two are respectively;

$$y = f_2\left[w_2 \sum_{i=1}^{n} f_1\left(w_1 x_i + b_1\right) + b_2 \right] \qquad 6\text{-}1$$

$$y = f_3\left[w_3 \sum f_2\left(\sum_{i=1}^{n} f_1\left(w_1 x_i + b_1\right) + b_2 \right) + b_3 \right] \qquad 6\text{-}2$$

where b_1 and b_2 are biased in hidden and output layers, w_1, w_2 are weights connecting hidden and output layers, respectively. The transfer function is denoted by f_1 and f_2.

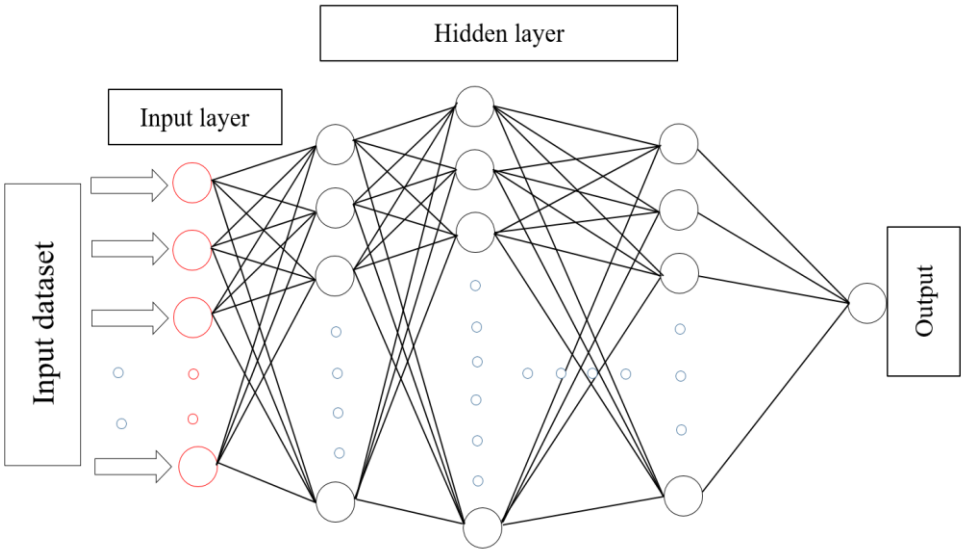

Figure 6.2: *Structure of ANN algorithm with different layers.*

Nevertheless, this structure enables to solve complex problems. The algorithm is quite robust to noise in training data. Therefore, training data containing errors doesn't influence the final output. It has the ability to detect all possible interactions between variables and gives a robust model. However, the algorithm is prone to overfitting and requires more computational resources (Tu 1996).

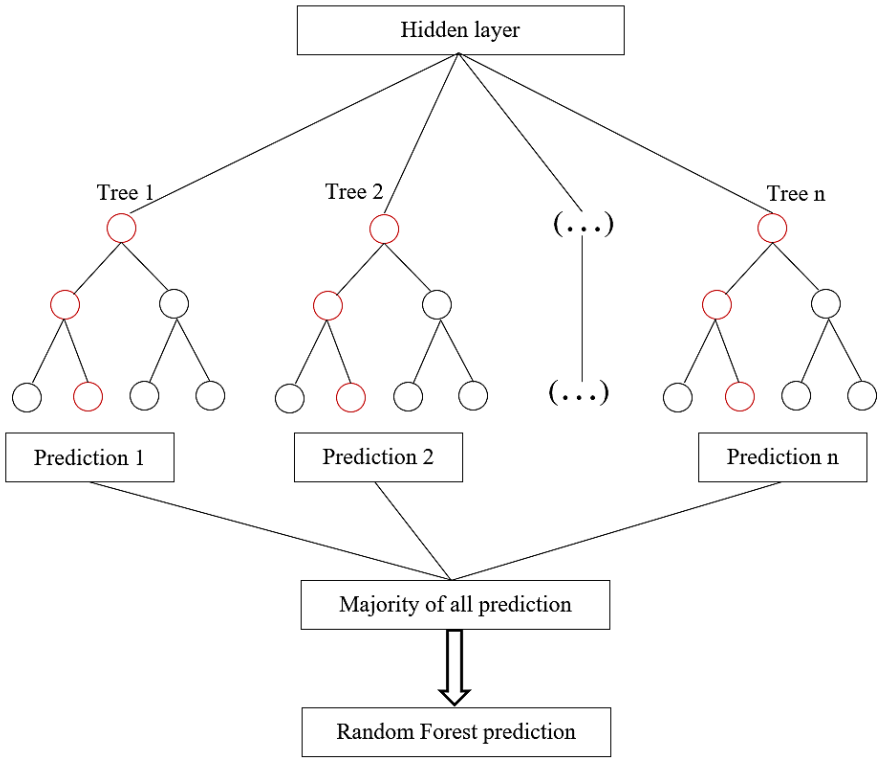

Figure 6.3: *Structure of Random Forest algorithm.*

6.2.3. Random Forest (RF)

RF is a powerful algorithm proposed by Breiman for solving regression, classification problems, and unsupervised learning (Breiman 2001). It has been applied in solving various problems related to geotechnical engineering. The basic principle of random forest is that "a group of weak learners can come together to form a strong learner" (Li and Chen 2020). Random Forest is an excellent tool used for accurate predictions by introducing the right kind of randomness. The speciality of this algorithm is that it does not overfit because of the law of large numbers. In this algorithm, many trees with identical distributions are employed to set up a forest to train the model and used to predict the sample data. It

works on the concept that multiple decision trees with varying depths aggregate to predict the output. Every decision tree is trained on a subset of the dataset called the bootstrapped dataset. The final prediction is made by taking the average of the majority of the predictions made by each individual decision tree. The bagging technique is employed to arbitrarily choose the variable candidates from the entire dataset for calibrating models (Pham et al. 2020a). The algorithm has the ability to predict accurately because of default hyper parameters. Overfitting is the major issue observed in various machine learning algorithms. However, the issue of overfitting is relatively lesser in Random Forest. The algorithm faces a computational burden with a higher number of trees (Sarica et al. 2017). A schematic diagram of RF is illustrated in **Figure 6.3**.

6.2.4. Support vector machine (SVM) algorithm

The SVM is a popularly known algorithm based on the statistical learning theory pioneered by Vapnik and his co-workers. It consists of two underlying ideas. The first one is the optimum margin classifier, which can develop a hyperplane to divide sample data. The second main idea is the use of kernel functions. The SVM has the capability to solve non-linear partitions due to the introduction of kernel function (Panakkat and Adeli 2007). For solving various problems like matter classification, problem recognition and filter issues in geotechnical engineering, the partition function of SVM is being used widely. Apart from it, SVM is also used for solving the regression problem. In the regression problem, a regression model is established to describe the relationship of given sample data, as shown in

$$L = \{(x_1, y_1), (x_2, y_2), ...\} \qquad 6\text{-}3$$

where, L is regression model, (i=1,2,3….n) is the x value of sample, (i=1,2,3….n) is the y value of the sample. To obtain a regression model between input and output, the principle and method of SVM is adopted to

solve the regression problem as that of the classification issue (Ambrožič and Turk 2003). SVM can utilize sample data to build a regression model based on the structural risk minimization principle. The algorithm has a lesser risk of overfitting. The kernel implicitly contains non-linear transformation; therefore, it doesn't require any assumption about the functional form of transformation. Lack of transparency in results and model capability reduces when the dataset has noise. Therefore, training data containing noise influence the final output (Karamizadeh et al. 2014).

6.2.5. Evaluation metrics

The coefficient of determination (R^2) evaluates the proportion of variation in the dependent variable explained by the predictors included in the model (Zhang 2017). The performance of a model is determined statistically by comparing the measured values and predicted values. Mathematically derived parameters like the correlation coefficient (R^2), the Mean Square Error (MSE), the Mean Absolute error (MAE), and Root Mean Square Error (RMSE) are used for comparison. For a given dataset, (Y_i, y_i), here $i \in 1,2,....n$ where Y denotes the actual target dataset and predicted y denotes the predicted data and $\bar{y}$ denotes the mean value of y, the evaluation matrices can be defined as follows;

$$R^2 = 1 - \frac{\sum_{i=1}^{n}(Y_i - y_i)^2}{\sum_{i=1}^{n}\left(Y_i - \bar{y}\right)^2} \qquad 6\text{-}4$$

$$MSE = \frac{\sum_{i=1}^{n}(Y_i - y_i)^2}{n} \qquad 6\text{-}5$$

$$RMSE = \sqrt{\frac{\sum_{i=1}^{n}(Y_i - y_i)^2}{n}} \quad \text{6-6}$$

$$MAE = \frac{\sum_{i=1}^{n}|Y_i - y_i|}{n} \quad \text{6-7}$$

6.3. Coefficient of consolidation parameters

6.3.1. Data collected

Different soil properties of 200 samples are collected from the literature of a well-known academic database. These are globally distributed samples which are composed of eleven independent variables. The independent variables include basic soil properties like depth of the sample availability, water content, bulk unit weight of soil, dry unit weight of soil, specific gravity, void ratio, porosity, degree of saturation, liquid limit, plastic limit, and plasticity index. These features are symbolically denoted by V_1, V_2, V_3, V_4, V_5, V_6, V_7, V_8, V_9, V_{10}, and V_{11}, respectively. These features are employed as input parameters to develop a relationship with dependent parameters using ML algorithms. The coefficient of soil consolidation (Y) is the dependent parameter, and it is measured in square centimeters per mins.

Table 6-1: *Standard statistical information of the features in the dataset.*

	V_1	V_2	V_3	V_4	V_5	V_6	V_7	V_8	V_9	V_{10}	V_{11}	Y
Min	0.15	14.500	1.440	0.689	2.315	0.442	0.307	63.893	31.500	11.630	9.590	0.003
max	41.40	112.000	2.113	1.840	3.126	2.808	0.737	100	156.000	122.000	85.000	0.600
Mean	9.77	40.045	1.822	1.345	2.683	1.096	0.494	98.049	65.786	27.408	38.716	0.065
Standard deviation	10.53	20.766	0.204	0.301	0.096	0.556	0.122	15.819	20.158	10.548	17.699	0.089

Table 6-2: *Representative input dataset after UFS feature selection along with the references.*

Sl. No.	X_1	X_2	X_3	X_4	X_5	Y	Clay types
1	2.7	0.53	99.21	38	21.5	0.115	Quaternary clay (Cai et al. 2012)
2	2.76	0.46	88.54	59.00	18.00	0.192	Indian BC soil (Pant 2007)
3	2.73	0.43	98.14	85.00	28.00	0.005	London Clay (Skempton and Henkel 1957)
4	2.68	0.68	100	105.00	30.00	0.003	London Clay (Skempton 1953)
5	2.68	0.68	86.73	87.30	34.30	0.009	Malaysia clay (Taha et al. 2000)
6	2.57	0.33	100	44.45	17.10	0.230	Nigeria clay (Yunusa et al. 2013)
7	2.70	0.56	100	48.00	23.20	0.080	Remolded soil (Sridharan and Nagaraj 2004)
8	2.70	0.60	93.91	76.20	25.55	0.038	Indian BC soil (Devi et al. 2015)
9	2.66	0.31	86.48	46.30	24.00	0.266	Iraq clay (Al-Juboori and Al-Ameri 2019)
10	2.35	0.46	96.76	74.50	26.90	0.600	Marine clay (Rao et al. 2011)
11	2.68	47.01	93.44	31.56	19.93	0.029	Vietnam Clay (Mittal et al. 2021)

In this study, the depth of remoulded soil samples is assumed as 1 m. **Table 6-1** depicts some standard statistical information of all the features employed in the dataset.

The least important features other than preselected input-independent features are removed from the current feature space. These remaining features are further used for training and testing to capture the dependent parameter Y. In this study, five significant features are selected from total input of 80 samples. The significant number of features selected in this study is chosen based on the data available in the literature. The selected independent variables are specific gravity, porosity, degree of saturation, liquid limit, and plastic limit. The selected variables are renamed as X_1, X_2, X_3, X_4 and X_5. Further significant features of 120 more samples are collected from the literature. The representative data of important features selected from UFS is illustrated in **Table 6-2**.

Table 6-3: *Evaluation matrices calculated from ANN algorithm.*

Number of neurons	R	MAE	MSE	RMSE
5 neurons	0.55857	0.039082	0.004668	0.06832
10 neurons	0.768115	0.022771	0.002915	0.053995
15 neurons	0.783582	0.030416	0.002623	0.051218
20 neurons	0.829036	0.023511	0.002119	0.046031
25 neurons	0.824621	0.025519	0.002190	0.046793
30 neurons	0.811172	0.031368	0.002265	0.047595
35 neurons	0.80000	0.027612	0.002452	0.049521

6.3.2. Result and discussion

6.3.2.1. ML-based models.

In this study, the ANN algorithms are developed in Matlab 2015. The samples with selected features are randomly split; 70% of the data (140

randomly chosen samples) is used during training, 15% of the data (30 randomly chosen samples) for validation and the remaining 15% (30 data) is employed to assess the suitability/testing of the developed model. Randomly splitting of data for training, validation, and testing reduces possible selection bias and ensures all variables receive equal attention during the training process (Crisci et al. 2012). The sigmoid function is used as a transfer function to add non-linearity to the developed model. It is a proper mathematical function with monotonicity, continuity, and differentiability, essential when training a neural network with gradient descent (Priddy and Keller 2005). A non-linear optimization Levenberg–Marquardt (LM) algorithm is used for training the selected dataset (Levenberg 1944). Several factors significantly influence the efficiency of the neutral network model. Some of the factors are the number of neurons, the number of hidden layers, the training algorithm and the cost function (Sheela and Deepa 2013). For example, if the number of neurons is higher, it leads to noise and spurious relationship between the dependent and independent variables. However, if the number of the neurons is lesser, the developed model might not captured necessary dependencies between dependent and independent variables, resulting in poor modelling (Pham et al. 2020b). The selection of a suitable number of neurons is necessary; therefore, the optimum number of neurons is chosen by performing a trial-and-error series with the number of neurons ranging from 5 to 35. During this, the number of the hidden layer is kept constant throughout. This study uses two hidden layers and one output layer to train the model. The number of the iteration and epochs given is 100 (Kurnaz et al. 2016). Several evaluation matrices for each neuron are also calculated for the overall dataset and are listed in **Table 6-3**. The variation of some evaluation matrices are also plotted in **Figure 6.4**. It is observed that the evaluation matrices R is observed to be increase with the increase of number of neurons and almost stable from 20 numbers of neurons as in **Figure 6.4** (a). Conversely, the evaluation matrices RMSE is decrease continuously with

number of neurons and remain stable from 20 neurons in **Figure 6.4** (b). Similarly, the most efficient/optimum number of neurons is found to be 20 and the ANN model developed using optimum number of neurons is used for further evaluations.

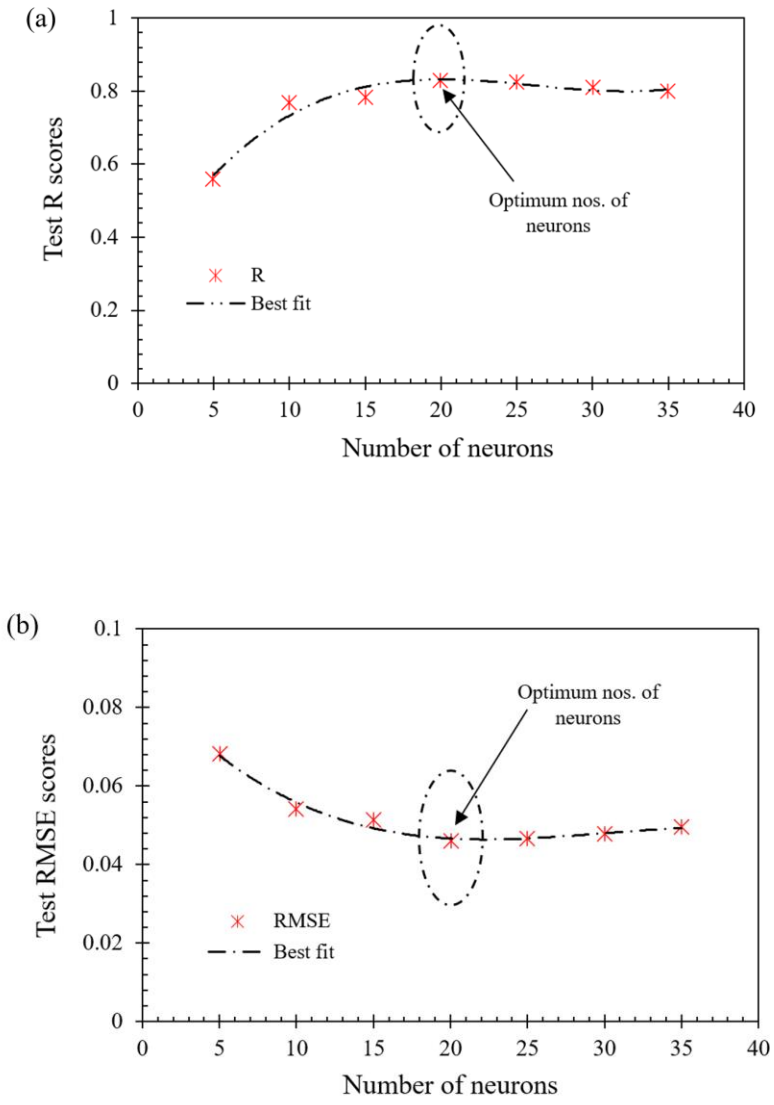

Figure 6.4: *Selection of the optimum number of neurons through (a) R scores and (b) RMSE scores.*

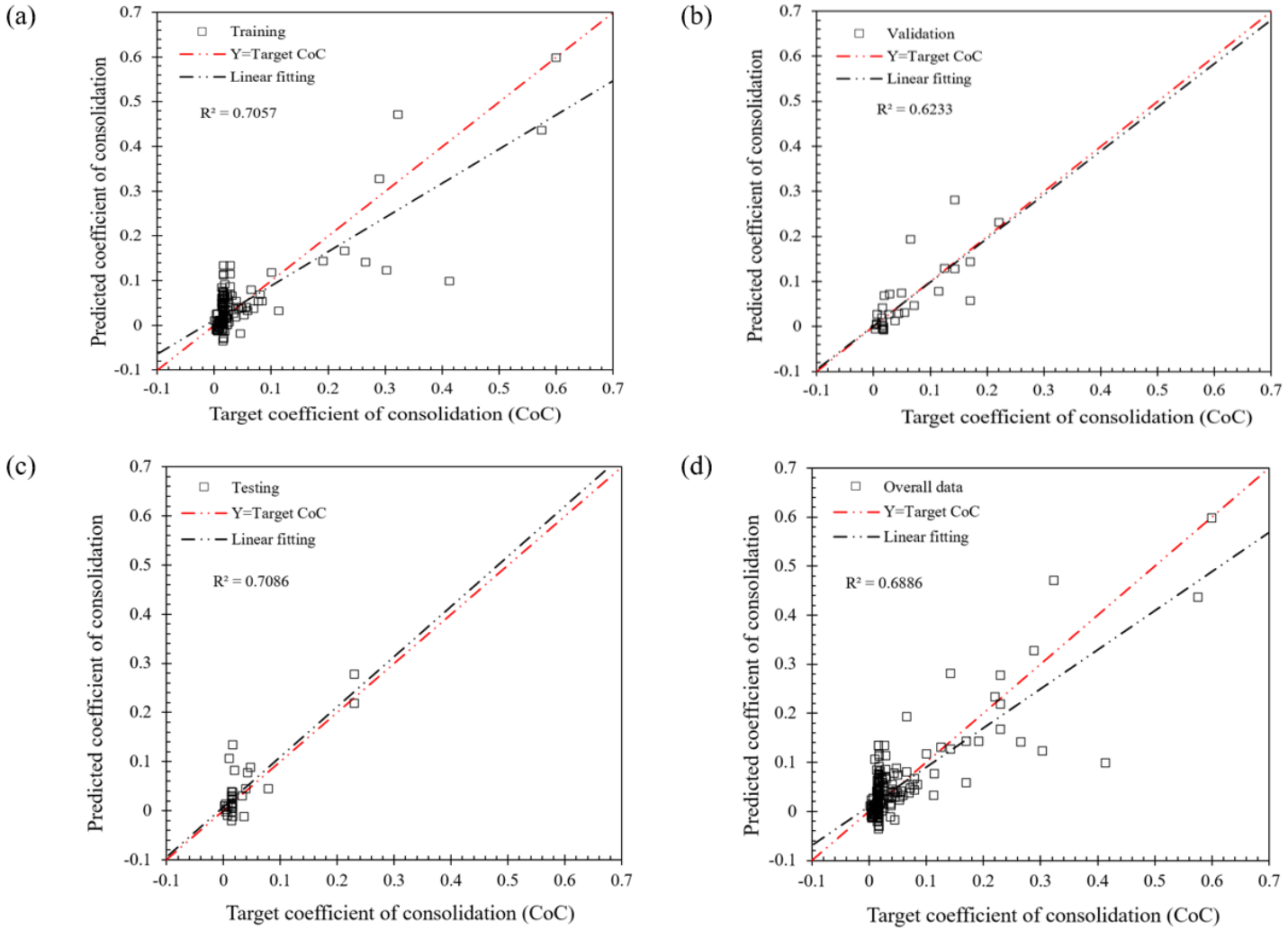

Figure 6.5: *The performance of the ANN model for the (a) training, (b) validation, (c) testing and (d) overall dataset.*

The performance of the ANN model (having 20 neurons) is illustrated in **Figure 6.5** (a), (b), (c) and (d) during training, testing, validation, and overall datasets, respectively. The black dash-dot-dash line in each plot represents the best-fit linear regression line between predicted outputs and targets (Beale et al. 1992). In contrast, the red dash-dot-dash line in each plot represents the perfect result, i.e., Output =Target/Actual measured data. The coefficient of determinations (R2) during training, validation and testing are 0.7057, 0.6233, and 0.7086, respectively. In this study, widely distributed soil samples are employed with a lesser number of samples (200 data). It reflects the less accuracy of the developed model with lesser R^2 during the training, validation and prediction stages. Again, widely distributed naturally available soil and reconstituted soil are also employed in this study.

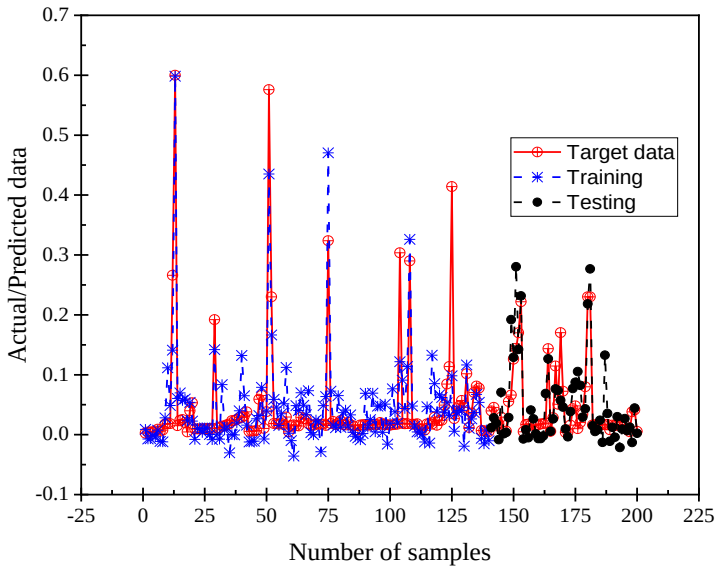

Figure 6.6: *Target and predicted dataset from ANN model during training, validation and testing.*

The collected soil possesses different quantities of clay content, permeability, and different experimentation, including the nature of loading and loading duration; therefore, the coefficient of permeability varied significantly. Thus, some of the data were collected from Nigeria clay (Yunusa et al. 2013), remoulded soil samples (Sridharan and Nagaraj 2004), and some portions of Indian Black Cotton soil (Pant 2007) possess a higher coefficient of consolidations. **Figure 6.6** illustrates the relationship between the target/measured and predicted output of the overall 200 samples. However, the model can effectively predict the consolidation coefficient in a small variation range.

Further, the pre-processed data obtained from the feature selection procedure is employed to develop a Random Forest model in RStudio software. Here a continuous non-linear regression is performed using a filter in the package "randomForest" in RStudio software. For each iteration, a corresponding model is developed. In this study, a total of 10000 models are developed. Similar to the ANN algorithm, the data are randomly split into training and testing; it reduces possible bias selection and ensures all variables receive equal attention during selection. During training, 70% of the total sample (140 data) is employed, and the remaining 30% is used to test the developed model's accuracy. However, the number of trees significantly influences the efficiency and accuracy of the developed models. Selection of a suitable number of trees is necessary; therefore, the optimum number of trees is selected by performing a series of trail-and-error with the number of trees ranging from 5 to 50. The number of iterations is kept constant throughout each tree and developed 10000 models. Among the developed models, the one with the maximum NSE (Nash-Sutcliffe Efficiency) value of training and testing was selected. NSE is a normalized statistic that determines the relative magnitude of the residual variance ("noise") compared to the measured data variance ("information") (Nash and Sutcliffe 1970). A perfect model with an error

Table 6-4: *Evaluation matrices calculated from Random Forest algorithm.*

Tree	Model No.	NSE train	NSE test	R	MAE	MSE	RMSE
5	model_4240	0.71	0.56	0.822314	0.023375	0.002249	0.047426
10	model_5974	0.82	0.54	0.866718	0.023834	0.001849	0.043004
15	model_4647	0.83	0.61	0.886905	0.023388	0.001681	0.040997
20	model_2967	0.82	0.62	0.878237	0.02549	0.001965	0.044325
25	model_2320	0.82	0.68	0.889213	0.022721	0.001995	0.044671
30	model_5618	0.84	0.64	0.91011	0.024986	0.001703	0.041265
35	model_1876	0.88	0.64	0.914932	0.022511	0.001678	0.040968
40	model_6906	0.87	0.58	0.903383	0.023835	0.002028	0.044501
45	model_4780	0.83	0.64	0.893812	0.024561	0.001885	0.043419
50	model_12	0.84	0.68	0.900611	0.023286	0.001823	0.042699

variance equal to zero has an NSE value of 1; however, a model with error variance equal to measured data variance has an NSE value of zero. The suitability and efficiency of these models are further evaluated with the testing dataset (i.e., 30% of the overall input dataset (60 data)) that are not part of the training dataset.

The predicted data of the overall dataset is used to determine the optimum number of trees through various evaluation matrices. **Table 6-4** lists the values corresponding to various evaluation matrices in the varied number of trees. **Figure 6.7** (a) illustrates the relationship between the evaluation matric R and the number of trees. It is observed that the R-value increases with the increase of the number of trees and is found stable from 30 trees. Similarly, **Figure 6.7** (b) illustrates that the evaluation matric RMSE decreases with the number of trees and is almost stable from 30 trees. Other evaluation matrices also possess the best value in 30 trees. Therefore, in this study 30 number of trees are considered the optimum value for the random forest model.

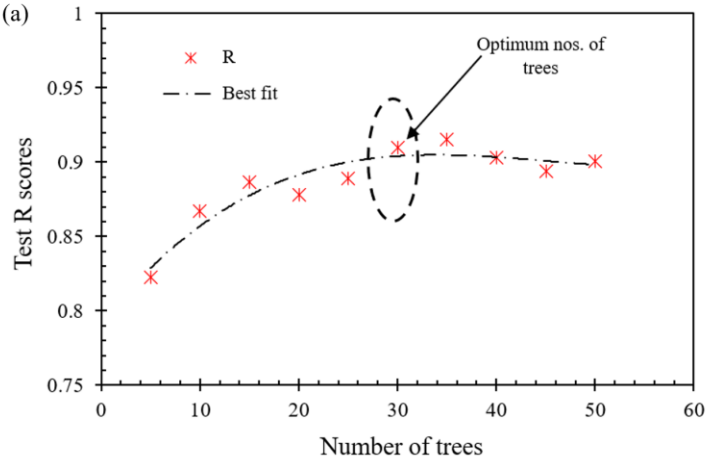

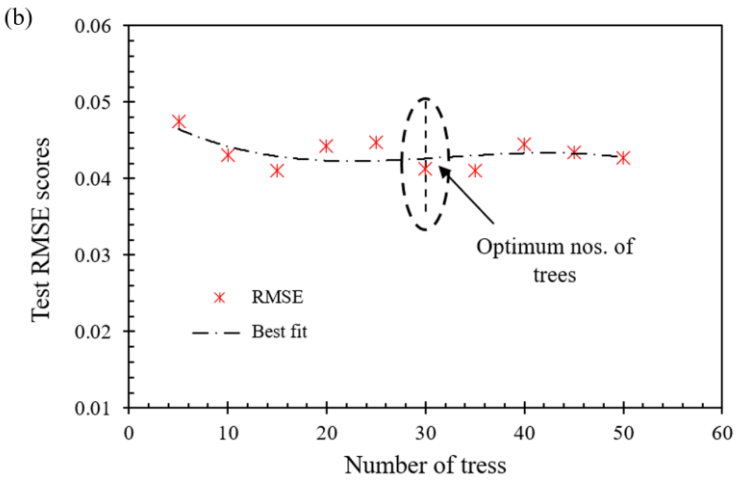

Figure 6.7: *Selection of an effective number of a tree for the Random Forest algorithm through (a) R scores and (b) RMSE scores.*

In this study, 10000 models having 30 number of trees were developed; among these, the model possessing a higher NSE value is chosen. The model_5618 possesses the highest NSE value of 0.84 and 0.64 during training and testing. All five independent variables were given as input to the selected model (model_5618) and predicted the independent output variable Y. The performance of the model during training and testing is illustrated in **Figure 6.8**. The black dash-dot-dash in the plot represents the best-fit linear regression line between the target and predicted output from model_5618. The red dash-dot-dash line in the plot represents the perfect result, i.e., Output =Target/Actual measured data. During testing, the model possesses a higher R-value greater than 0.921. The input data given in the RF algorithm is similar to the ANN algorithm. However, this study observed that the developed RF model could predict better than the ANN models. The relationship between the predicted and target output with the number of samples is illustrated in **Figure 6.9**. It is observed that the model_5618 predicted accurately even in a small input training dataset.

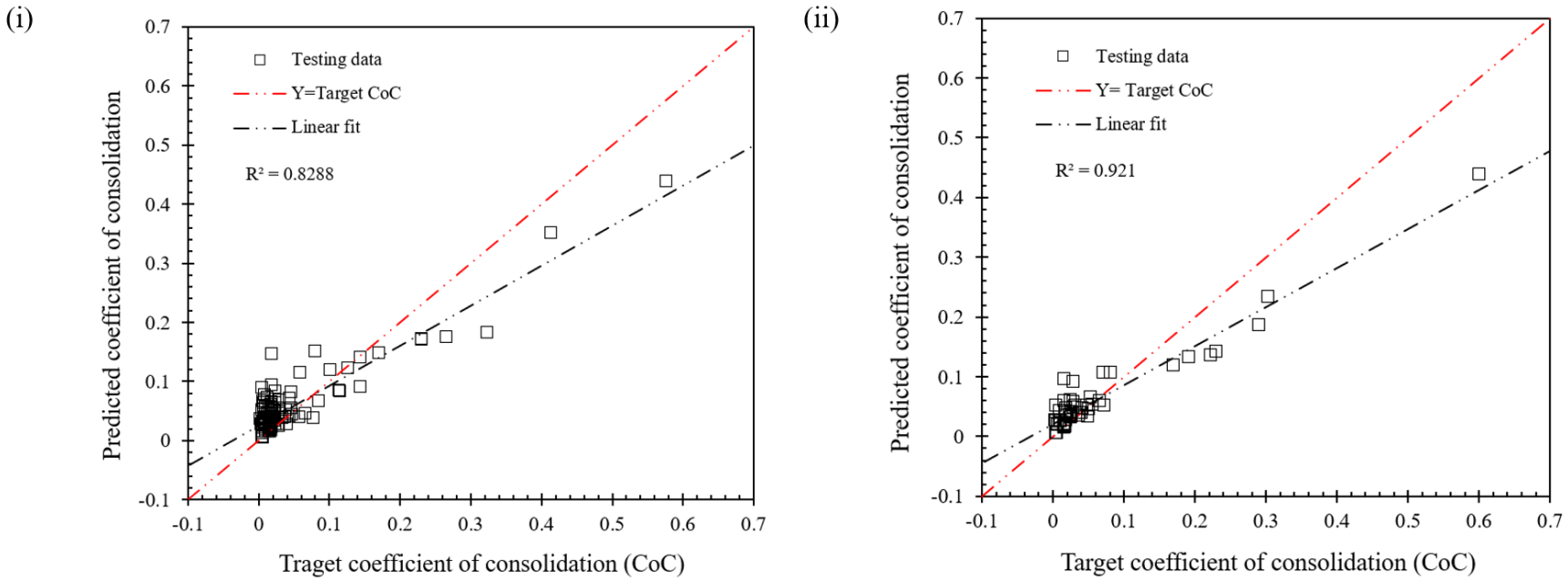

Figure 6.8: *Performance of Random Forest during (i) training and (ii) testing the algorithm.*

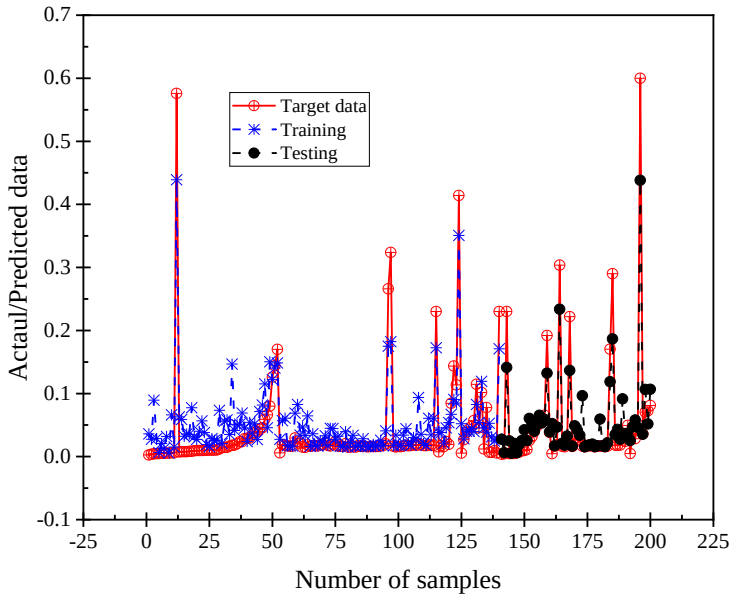

Figure 6.9: *Target and predicted dataset from Random Forest during testing.*

Further, the pre-process dataset obtained after feature selection is employed to predict the coefficient of consolidation using the SVM algorithm in RStudio software. Similar to the above algorithms, the dataset is split randomly to reduce bias and given an equal chance of selection. 140 samples (70% of overall data) are employed for training the model. In this study, the radial basis function has been used for the SVM training dataset. Like RF, 10000 iterations were performed, and a model was developed for each. The efficiency and suitability of the developed model are assessed through testing of the remaining 30% dataset (60 samples). The best model is selected using the concept of NSE value during training and testing. In contrast to the above algorithms, developed 10000 models possess significantly lesser NSE values during training and testing. Among these models, model_4067 was chosen due to an NSE value of 0.3 and 0.23 during training and testing.

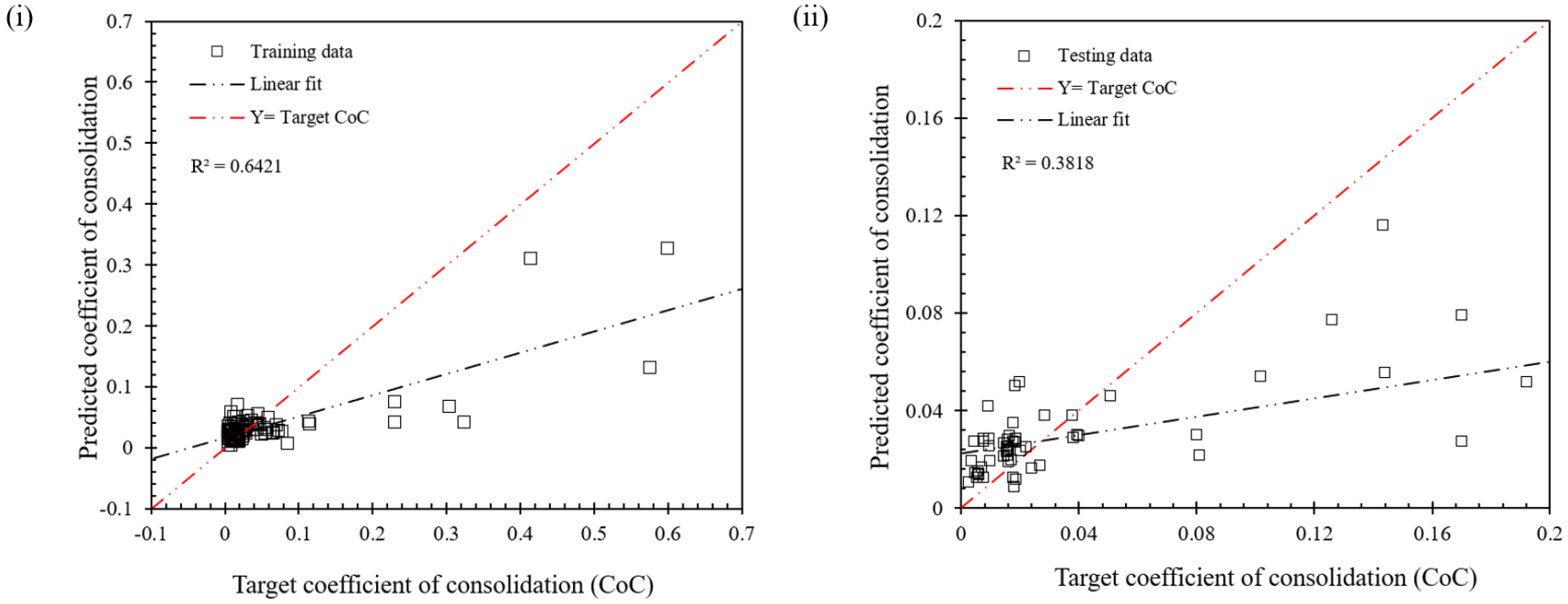

Figure 6.10: *Performance of SVM during (i) training and (ii) testing.*

Figure 6.10 illustrates the performance of the model_4067 during training and testing. The black dot-dash-dot lines in the figures represent the best linear fitting line between the predicted output and actual input data. In contrast, the red dash-dot-dash line signifies output creep coefficient = input creep coefficient. The corresponding coefficient of determination (R^2) during testing is observed to be 0.38. The relationship between the dependent output variable and predicted output from model_4067 with sample number is illustrated in **Figure 6.11**. The model applies to the dataset with a small range of target data. It is observed that the prediction obtained from model_4067 of the SVM algorithm exhibits a significant variation between actual and predicted data.

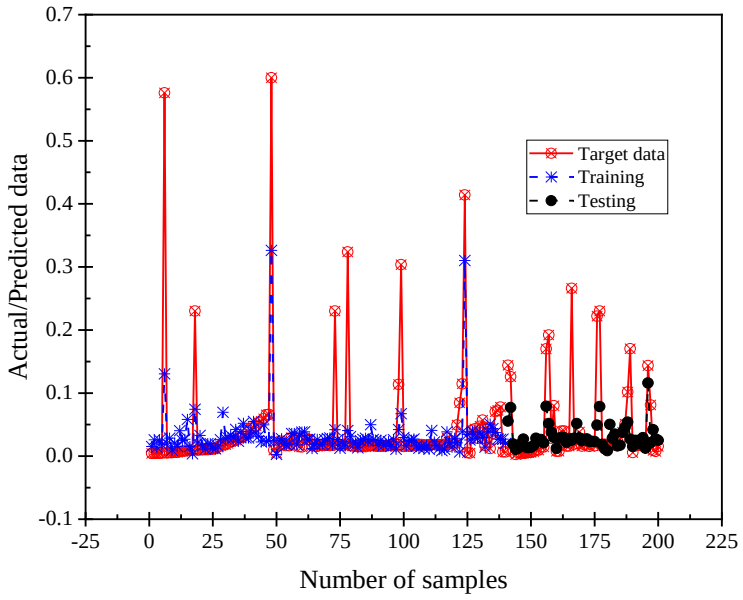

Figure 6.11: *Target and predicted dataset from SVM during testing.*

The suitability/efficiency of each and every ML algorithm is further studied using the square error diagram during testing, as illustrated in **Figure 6.12**. Actually, the data used in this study is widely varied due to

several factors such as the origin of soil, gradation, shape, percentages of clay content, sample preparation, loading sequence and initial stage of the sample, including void ratio, density, water content and gradations influence the soil properties. Therefore, there is a significant variation in their coefficient of consolidation. Again, in this study, a small dataset is collected for this study. All these significantly influence the prediction of the models. Further, the suitability of the ML model is also dependent on the input dataset. The ANN model exhibits a maximum square error of 0.0185 during testing and evaluation, as in **Figure 6.12** (a). Besides maximum square error, several other predicted samples exhibit a significant square error. However, the maximum square error observed in the RF model during testing is 0.026, as shown in **Figure 6.12** (b). The remaining samples predicted from the RF model exhibit a negligible square error of 0.008. The SVM model exhibits a maximum square error of 0.058, and many other samples also exhibit significant square errors, as shown in **Figure 6.12** (c). Even though all three algorithms can predict the coefficient of consolidation, the RF model can predict the coefficient of consolidation accurately even in a small dataset. The embedded feature selection during the model generation process in RF is the responsible factor (Pal 2017).

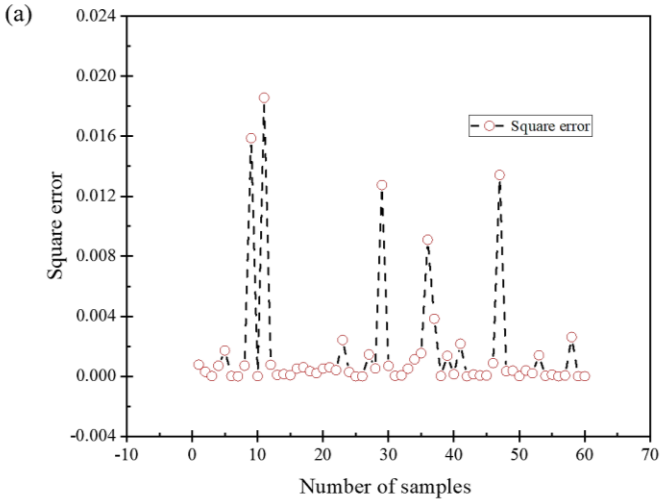

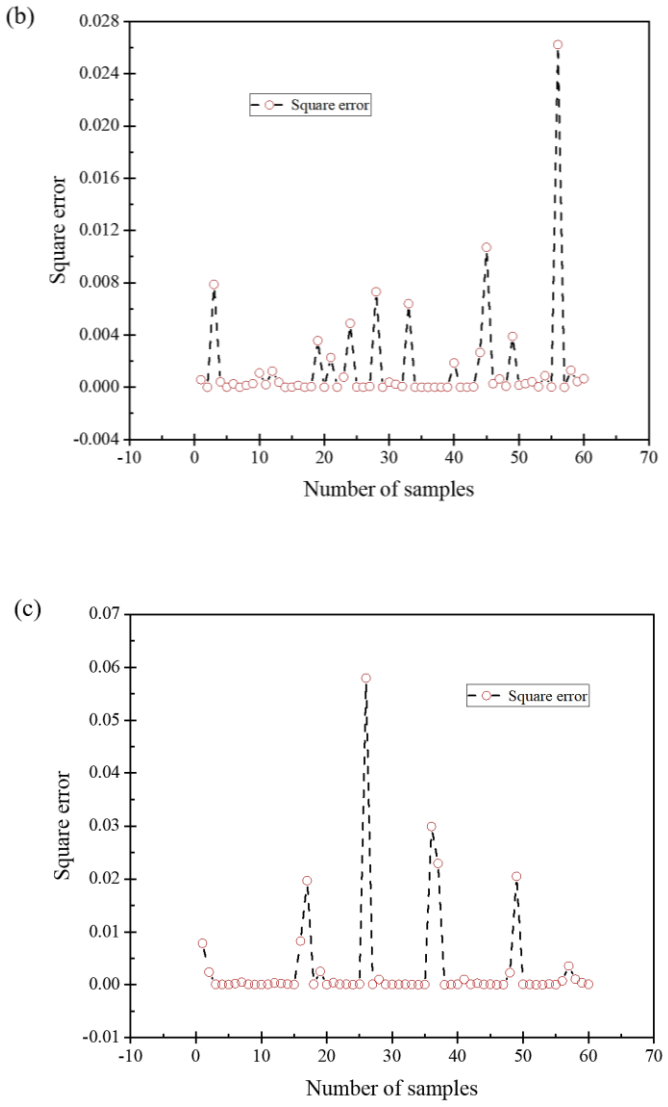

Figure 6.12: *Square errors of testing dataset (a) ANN algorithm, (b) Random Forest algorithm and (c) SVM algorithm.*

Further, the performance of the best model of each algorithm is evaluated statistically by comparing the actual output and predicted output. **Table 6-5** listed the evaluated data from different evaluation matrices like the correlation coefficient (R), MSE, and RMSE during testing only. The RF model exhibits the largest R^2 and minimum value of MSE. However, the SVM model exhibits the smallest R^2 and maximum MSE.

Table 6-5: *Performance of model through Evaluation matrices.*

Algorithm	R^2	MAE	MSE	RMSE
ANN	0.70	0.02713	0.00169	0.04107
Random Forest	0.92	0.02321	0.00148	0.03854
SVM	0.38	0.02971	0.00311	0.05579

6.3.2.2. Numerical simulation

The consolidation behaviour of Black Cotton (BC) soil, Malaysia clay and London clay is simulated using Abaqus to determine the coefficient of consolidation. A cylindrical model having 0.2 m height and 0.1 m height is developed and allowed to be permeable on top and bottom surfaces. The soil is assumed as isotropic, elastoplastic, homogeneous and obeys the extended Cam clay model. The required Cam Clay model parameters are collected from the literature and are illustrated in **Table 6-6**.

Table 6-6: *Parameters used in Abaqus simulation (from literature).*

Soil	Density, γ (kg/m^3)	void ratio, e_o	κ	λ	Permeability, K (m^2/s)
BC soil 1	1910.00	0.987	0.035	0.093	$3*10^{-10}$
BC soil 2	1990.00	0.954	0.040	0.096	$3*10^{-10}$
Malaysia soil	1548.52	1.560	0.045	0.200	$5.128*10^{-11}$
London clay 1	1906.20	0.910	0.036	0.302	$3.205*10^{-11}$
London clay 2	2098.42	0.645	0.033	0.280	$9.720*10^{-12}$
London clay 3	1906.20	0.955	0.038	0.315	$2.570*10^{-11}$
London clay 4	1970.30	0.790	0.037	0.310	$9.970*10^{-12}$

A two-dimensional axisymmetric mesh is employed in the developed model, with 12 in the z-direction (0.1 m height) and only one element in the x-direction (0.1 m wide). The horizontal and vertical

displacement components are fixed on the bottom side; however, the horizontal displacement is assumed to be fixed on the right-hand side. There is a symmetrical line on the left-hand side of the mesh (no horizontal displacement). The models were applied with different loads of 20 kPa and 50 kPa with a seating pressure of 5 kPa.

During instant load application, the top and bottom surfaces of the model are assumed to be impervious; after that, both surfaces are assumed to be fully previous so that the developed excess pore pressure is reduced to zero. **Figure 6.13** (a) illustrates the boundary condition of the developed model. In this study, three different steps are employed to run the model. In the first step, a seating pressure of 5 kPa is applied to the top of the model. In the subsequent step, a uniform pressure of (20 kPa and 50 kPa) is applied to the top surface of the model. During the last step, actual consolidation is executed by applying automatic time stepping. Durations assigned in the first, second and third steps are respectively 1, 10, and 1E+8. The representative consolidation behaviour of BC soil is illustrated in **Figure 6.13** (b). During the application of 20 kPa, the BC soil exhibits a settlement of 6.956e-3 magnitude after three-stage of loading.

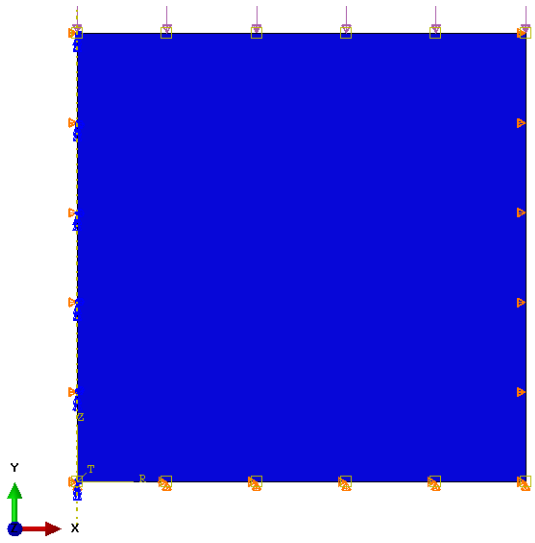

(a) Boundary conditions.

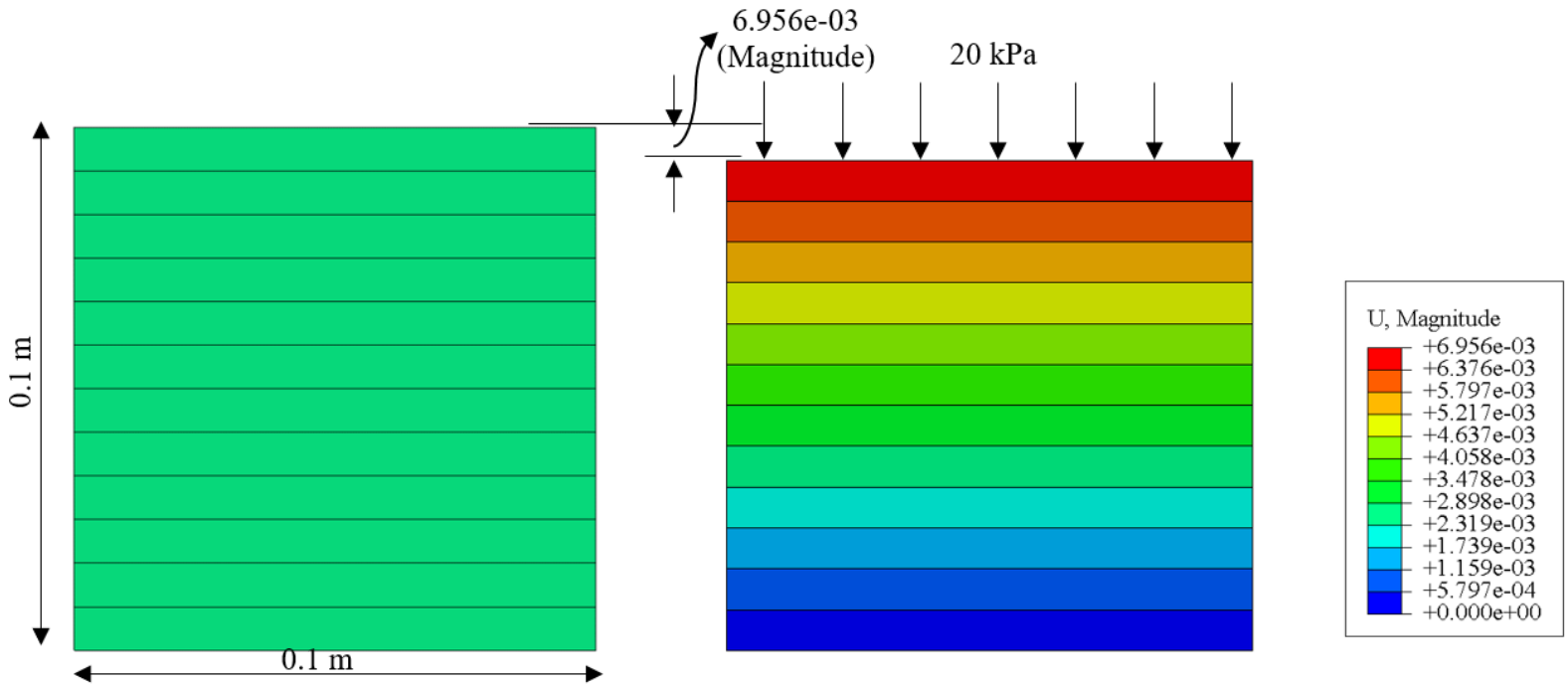

(b) BC soil settlement under application of 20 kPa.

Figure 6.13: *The boundary condition and soil settlement result from Abaqus analysis*

For a better presentation of the consolidation settlement of various soils, the settlement obtained is expressed in terms of a dimensionless parameter, the average degree of consolidation U using the following expression:

$$U = \frac{S(t)}{S_u} \qquad 6\text{-}8$$

where S(t) is defined as settlement achieved in time period t; whereas S_u is defined as ultimate consolidation settlement of the soil achieved during the application of a certain pressure. **Figure 6.14** illustrates the relationship between the variation of U and the duration of loading (in log scale) under the application of 20 kPa and 50 kPa.

Compared to other soils, London clay acquired a larger time to achieve a similar degree of consolidation. It might be due to the lower permeability of the soil. BC soil and Malaysia soil achieve higher vertical strain during the application of 50 kPa as compared with vertical strain obtained during 20 kPa. The degree of consolidation-log time curves is moving down with the increase in load. It is influenced by the higher dissipation and greater compressibility rate with the increase of applied load (Hsu and Tsai 2016; Olek 2020). In Casagrande's log time method, a relationship between the degree of consolidation and log of time is plotted, and the time required for 50% consolidation (t_{50}) is determined. The vertical coefficient of consolidation was obtained (Mir 2010)

$$C_v = \left\{T_v \times H_{av}^2\right\} / t_{50} \qquad 6\text{-}9$$

where, T_v denotes the time factor and is equal to 0.196 for 50 % consolidation and H_{av} is the average drainage path length.

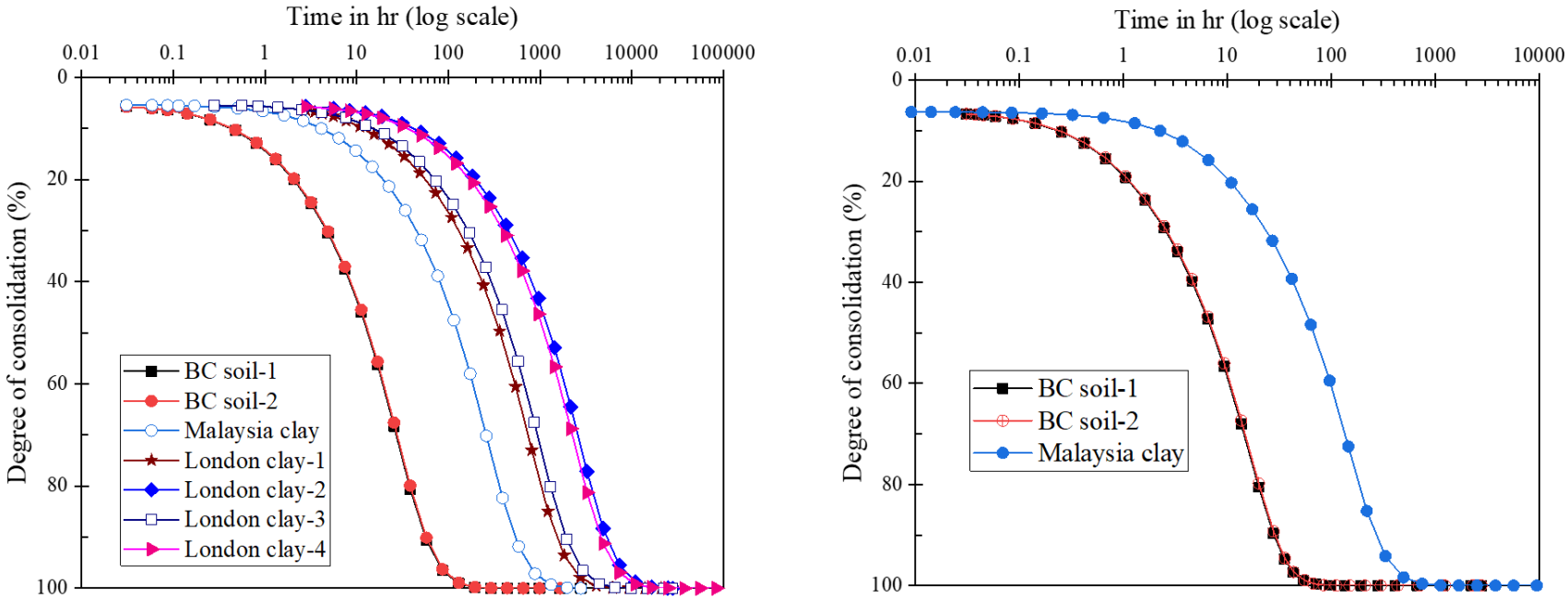

Figure 6.14: *Comparison of the computed degree of consolidation for different soils.*

Table 6-7 illustrates the comparison of the coefficient of consolidation obtained from Abaqus simulation, actual data and data obtained from ML algorithms like ANN, RF and SVM. It illustrated that the coefficient of consolidation determined from the numerical simulation is highly deviated from actual data compared to data derived from ML models, notably RF Model.

Table 6-7: *Coefficient of consolidation from several approaches.*

Clay types	Abaqus Model		Literature	Machine Learning		
	20 kPa	50 kPa	data	ANN	RF	SVM
BC soil 1	0.0626	0.0114	0.0084	0.0065	0.0588	0.0582
BC soil 2	0.0062	0.0113	0.1260	0.1290	0.1219	0.0770
Malaysia clay	0.0007	0.0012	0.0661	0.1920	0.0458	0.0244
London clay 1	0.0002	-	0.0078	0.0262	0.0589	0.0250
London clay 2	0.00006	-	0.0118	-0.0075	0.0734	0.0115
London clay 3	0.0002	-	0.0071	0.0265	0.0190	0.0165
London clay 4	0.00007	-	0.0051	-0.0101	0.0208	0.0204

Various problems are associated with geotechnical engineering, which is complex and not easily understandable. In order to solve these problems, there came the necessity of either simplifying the problem or incorporating several assumptions. Sometimes, the complex problems encountered in geotechnical engineering cannot be simulated using the available mathematical problems. In such a case, the ML approach will be significantly advantaged over the traditionally available modelling techniques. It is a data-driven approach which develops a trained model based on the input-output variables. This approach doesn't require either simplifying the problem or incorporating any assumption. All these advantages make ML a suitable and powerful modelling technique. Despite the success, there are some inherent shortcomings of ML techniques. ML does not explain how and why the different inputs relate to outputs. The practical applicability of the ML approach requires some level of expertise

as it cannot develop tractable mathematical equations (Lawal and Kwon 2020). Sometimes the predicted data acquires an opposite sign of the target data as in **Table 6-7**. It may lead to overestimation or underestimation of the geotechnical parameters, which is a major concern in engineering works. Again, the performance of the trained model depends on several factors, including the algorithm chosen, the number of iterations, learning complexity, networks, and complexity of the problems. The main advantage of random forest is its versatility which can be employed for both the regression and classification tasks. It has less possibility of overfitting than Decision Tree and any other algorithms. However, a trained forest requires significant memory for storage, as it retains information from several hundred individual trees (Chaturvedi 2008).

Being a data-driven approach, the accuracy of the models developed from ML relies on the input dataset. In this study, a small dataset (only 200 samples) is employed due to data shortage, and important parameter like percentages of clay is not considered. In this study, the author uses only three algorithms; the accuracy and applicability of other algorithms further need to be investigated. A robust model can be developed and applicable to all soil by considering the percentages of clay content, wide ranges of the dataset, other newly developed algorithms and several other inherent shortcomings like transparency and knowledge extraction.

6.4. Creep parameter

6.4.1. Data collection

A total of 150 datasets are collected from reputed and globally accepted academic databases. Each data possesses 9 independent variables, including; plastic limit, liquid limit, specific gravity, density, water content,

Table 6-8: *Representative input dataset collected from the literature.*

X_1	X_2	X_3	X_4	X_5	X_6	X_7	X_8	X_9	Y	Reference
26.1	57.3	2.69	16.28	62.9	100	50	50	31.2	0.01	(Wu et al. 2019)
34	88	2.66	14.19	87.7	99.6	100	35	54	0.0142	(Karstunen and Yin 2010)
32.37	63.13	2.69	14.3	26.21	80.11	1000	29.2	30.76	0.0012	(Johnson et al., 2022)
34.12	73.405	2.72	14.06	27.02	52.12	250	31.8	39.285	0.00155	(MJ Singh et al., 2022)
36.4	76	2.66	14.8	97	100	1000	25	39.6	0.003998	(Feng et al. 2017a)
18	30.8	2.66	19.44	28.5	92.5	400	14.6	12.8	0.0079	(Jiang et al. 2020)
19.95	35.5	2.635	17.55	48	97.7	100	30	15.55	0.00879	(Wang et al. 2020)
22	48	2.69	17.6	20	41.67	1600	75	26	0.00429	(Hameedi et al. 2020)

Table 6-9: *Standard statistical information of the features in the dataset.*

statistical information	X_1	X_2	X_3	X_4	X_5	X_6	X_7	X_8	X_9	Y
Mean	26.25	54.549	2.679	16.4	46.196	85.803	494.416	37.499	28.298	0.0077
Min	18	30.8	2.61	14.06	20	41.67	12.5	14.6	12.8	0.0002
Max	37.7	88	2.73	19.44	99	100	4000	79	54	0.1023
Mean Standard deviation	0.437	1.112	0.002	0.123	1.358	1.359	37.173	1.188	0.731	0.0004

degree of saturation, stress, clay content, and plasticity index. These are assigned as X_1, X_2, X_3, X_4, X_5, X_6, X_7, X_8, and X_9, respectively. The output target data is a creep, denoted by the symbol "Y". The data are collected from the papers mentioned herewith in **Table 6-8**. Standard statistical information on the features is mentioned in **Table 6-9**.

6.4.2. Feature selection using Extreme Gradient Boosting (XGBoost)

In this study, XGBoost is employed as a pre-processor for feature selection. It is an advanced implementation of a gradient-boosting algorithm. It enables handling both categorical and numerical variables having imbalanced data or high-dimensional features (Hsieh et al. 2019). The algorithm prevents overfitting due to the inclusion of Ridge Regression and Lasso Regression regularization. Furthermore, it provides several hyperparameter tuning options and optimizes different loss functions (Wang and Ni 2019). For any instance i^{th} at the k^{th} boost, the prediction $(\hat{y}_i)$ obtained during the implementation of XGBoost can be described as follows;

$$\hat{y}_i = \sum_{k=1}^{K} f_k(x_i), \quad f_k \in F \tag{6-10}$$

The total number of predictors is denoted by K, f_k for k^{th} predictor represents the function of the tree structure in functional space F. The input features in the i^{th} instance are denoted by x_i. Implementing the regularization term in the gradient boosting algorithm, the loss function corresponding to XGBoost is optimized for each iteration and is defined as follows.

$$L(\theta) = \sum_i l(\hat{y}_i, y_i) + \sum_k \Omega(f_k) \tag{6-11}$$

where $l(\hat{y}_i, y_i)$ determines the difference between the real target data (y_i) and corresponding prediction $(\hat{y}_i)$. Ω is the regularization term incorporated to avoid overfitting of the model (Hsieh et al. 2019).

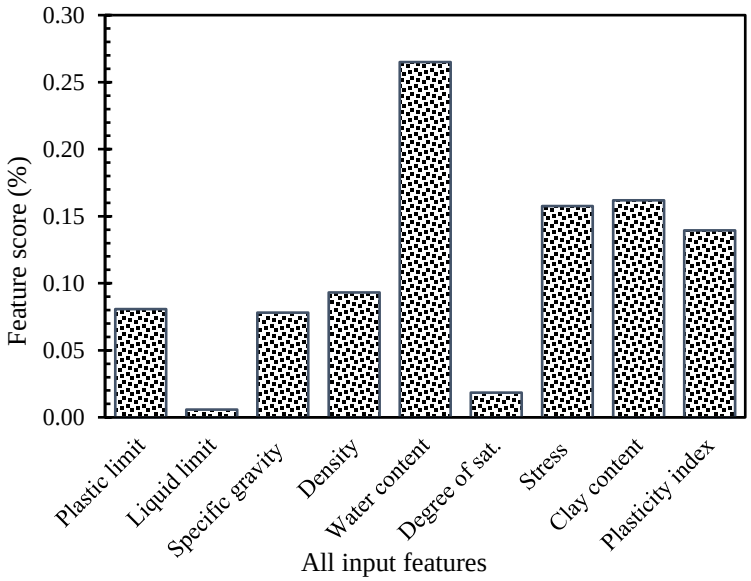

Figure 6.15: *Feature score for each input feature.*

The relationship between the input features and the target output variable is strengthened by removing the least important features. This study employed the XGBoost algorithm to determine the importance of the feature. This process is an iterative approach which depends on the chosen subset of original features (Granitto et al. 2006; Guyon et al. 2002). The feature score of all input parameters is illustrated in **Figure 6.15**. Among these nine input features, four features having comparatively higher feature scores, i.e., water content, stress, clay content and plasticity index, are chosen to develop an ANN model.

6.4.3. Result and discussion

6.4.3.1. ML approach

The input features are rescaled to a new range of values. This scaling of data gives more flexibility in designing neural networks. This normalization has the advantage of preserving exactly all relationships in the data, and it does not introduce any bias (Priddy and Keller 2005). The input features are

rescaled to lie within a range of 0 to 1. The performance of the ANN model is influenced by the number of neurons, hidden layers, activation function, and learning rate. These parameters are optimized using an open-source software library of Python interface called Keras. Three layers are employed; the first input layer was given four neurons, the second was given neurons ranging from four to twelve, and the output layer was given only one neuron. The learning rate 1e-2, 1e-3, and 1e-4 were given. The sigmoid activation function and Adam optimizer were employed. The optimizer function modifies the attributes of parameters like learning rate and weights. In this study, the Adam optimizer is employed to improve the accuracy and reduce the overall loss. The architecture of the ANN is illustrated in **Figure 6.16**. The number of the epoch was given to 100. Using the KerasTuner optimization technique, different models were developed possessing different hyper parameters. Among these models, the best five models are presented in **Table 6-10**.

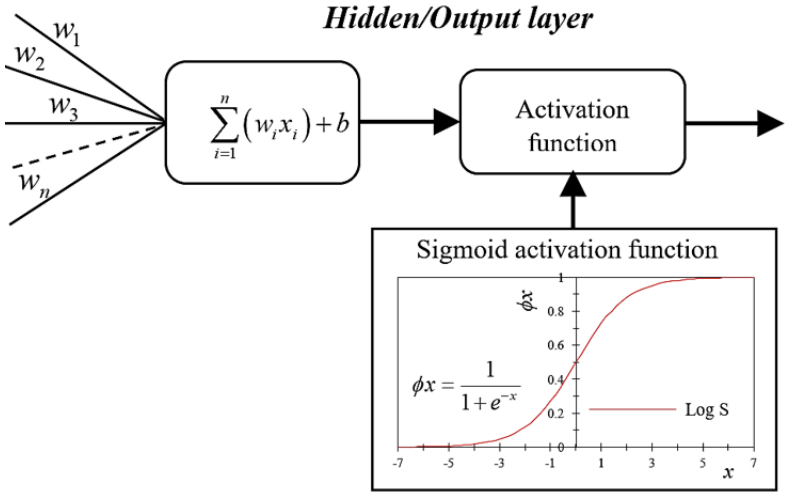

Figure 6.16: *Structure of ANN algorithm for incorporation of the activation function.*

Table 6-10: *The best models developed using the ANN algorithm.*

Model number	Number of neurons	Learning rate	Mean absolute error
Model_1	Input=4, hidden=10, output=1	0.01	0.00400
Model_2	Input=4, hidden=8, output=1	0.01	0.00427
Model_3	Input=4, hidden=8, output=1	0.001	0.00465
Model_4	Input=4, hidden=6, output=1	0.001	0.00468
Model_5	Input=4, hidden=6, output=1	0.0001	0.28340

From the five best models, the best hyperparameter with a 0.01 learning rate, and ten hidden neurons are selected, and the ANN model is trained with 100 epochs. Once the model is trained, the remaining 20% dataset is used for testing the accuracy of the model. **Figure 6.17** (a) and (b) compared the actual and predicted data during training and testing, respectively. It is observed that the mean absolute error (MAE) and root mean square error (RMSE) during model testing are 0.0040 and 0.00496. It can be stated the proposed model can predict the creep parameters accurately. In this study, a smaller dataset is used; therefore, the accuracy of the model can be enhanced by using a huge dataset. The developed five models predicted with different accuracy, as illustrated in Table 6. This might be influenced by the data used during training and testing, as the study employed the RandomSearch approach. The creep coefficient of soil depends on several factors, including the geological formation of soil, shape and gradation, methods of sample preparation, the stress history and the stress level in the ground, soil anisotropy, and the initial soil conditions like the presence of admixtures, void ratio, and the types of clay soil (Hsi and Martin 2015).

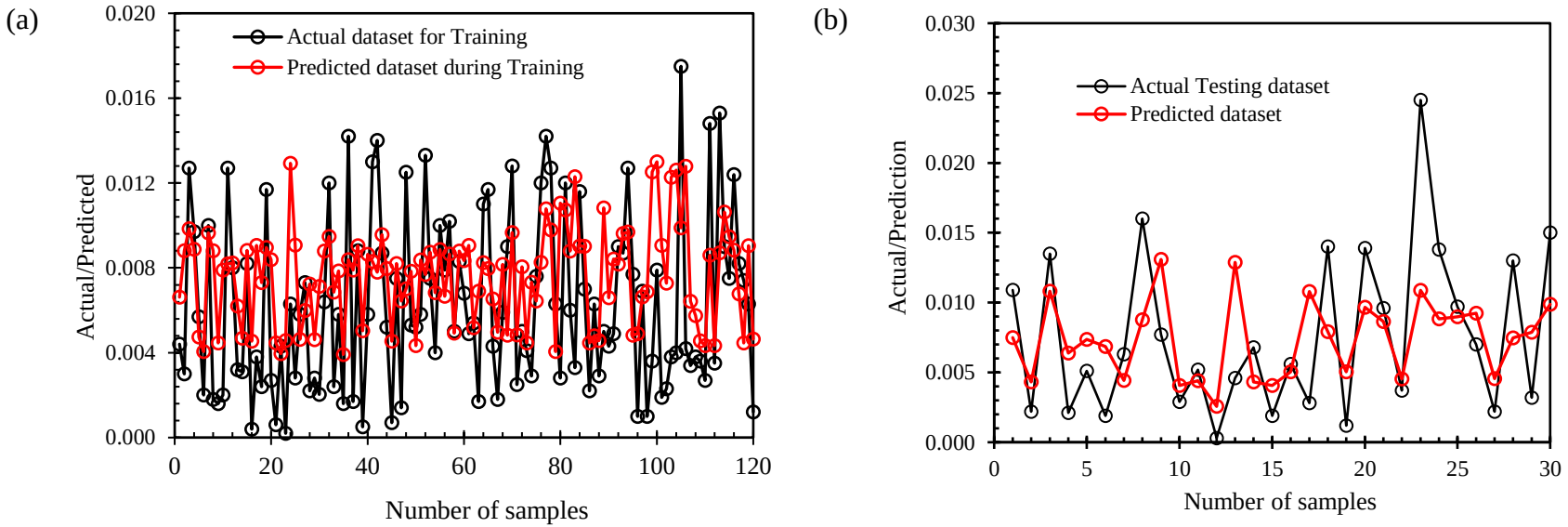

Figure 6.17: *The performance of the ANN algorithm during (a) training and (b) validation + testing.*

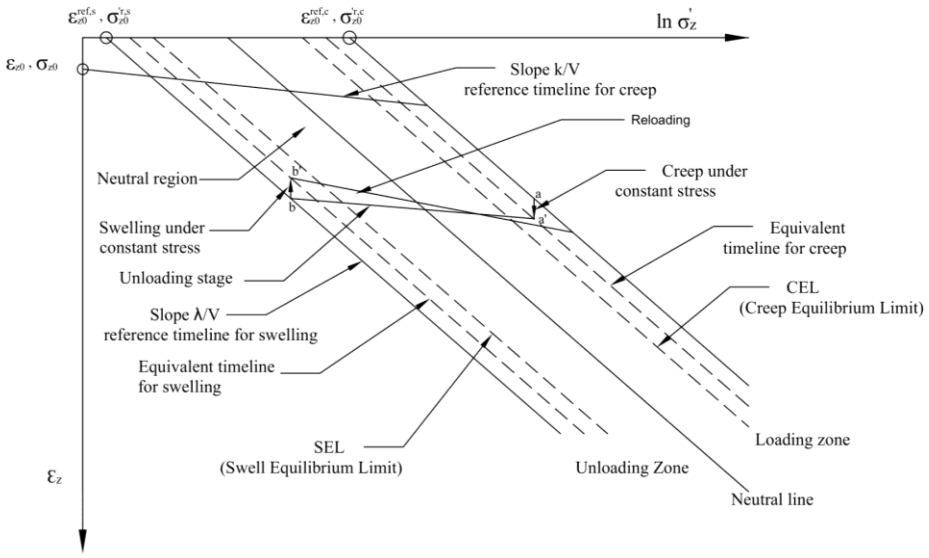

Figure 6.18: *Conceptual illustration of EVPS Model.*

6.4.3.2. Future aspects of ML in creep parameter.

The ML approach is a shortcut data-driven approach which can predict a particular parameter based on the independent input features. However, these parameters can also be achieved through experimentation or numerical simulation techniques. The experimentation procedure needs to set up a particular concept to derive the parameter. For example, the EVPS Model employs the equivalent timeline concept to derive the creep parameters or time-dependent swelling parameters. The conceptual visualization of the EVPS Model is illustrated in **Figure 6.18**. Instant recoverable vertical strain changes due to instant loading followed the particular path whose slope is given by *k/V*. However, the non-recoverable vertical strain due to instant loading followed the slope of the compression λ/V (Jian-Hua Yin and J. Graham 1994). However, during the application

of constant stress, the time-dependent strain changes are given using the equivalent timeline. In a particular equivalent timeline, the time-dependent strain corresponding to *"a"* will change to *"a'"*. Further, if the stress is applied for infinite time, the corresponding equivalent timeline is given by CEL. Similarly, the time-dependent strain corresponding to "b" during unloading will shift to *"b'"*. Further, if the stress is removed for an infinite time, the corresponding equivalent timeline is given by SEL (Tong and Yin 2013). The portion between the SEL and CEL is called the Neutral area; within this area, the strain changes are time-independent (Graham et al. 1986). The time-dependent settlement or expansion can be computed using the corresponding **Eqn. 3-8** and **Eqn. 3-10**, respectively. However, ML Model doesn't have any equations to determine time-dependent expansion or settlement. It is the significant drawback of the ML approach in predicting the creep or swelling behaviour. As the time-dependent settlement or expansion is accurately predicted using the concept of an equivalent timeline, the data derived from EVPS Model can be employed to develop an ML Model. The required independent parameters can be the applied stresses, the sample thickness, the reference timeline and corresponding strain, CEL/SEL and the initial condition of the prepared samples. The robust model based on equivalent time-line model need to consider newly developed ML algorithms and other inherent shortcomings of ML, including transparency and knowledge extraction.

6.5. Conclusion

In various geotechnical engineering projects, it is prudent to obtain an accurate, direct, and quick prediction of several engineering parameters. Among these parameters, the creep coefficient and coefficient of consolidation play a vital role in settlement prediction. This paper employs various ML algorithms like RF, ANN, and SVM to predict these parameters using globally distributed soil. Peer-review journals are inferred to collect the dataset; based on the presented work following conclusions are drawn.

(a) Among the three ML algorithms, Random Forest accurately depicts the coefficient of consolidation than the ANN and SVM algorithms. Each ML algorithm possesses its own characteristics, along with merits and demerits for applicability in a particular problem. Therefore, a similar problem has to be analyzed using different algorithms to figure out the best and most accurate one.

(b) The RF model, which accurately predicts the coefficient of consolidation, possesses 20 number of trees and is applicable in globally distributed soil. The accuracy and efficiency of the best RF model are accessed through evaluation matrices like R^2, MSE, and RMSE; corresponding data are respectively 0.92, 0.00148, and 0.03854.

(c) The coefficient of consolidation derived from numerical simulations required different assumptions, unlike ML algorithms, which are data-driven. A comparison of the coefficient of consolidation from numerical simulation and ML algorithms shows that the ML models work well in predicting the same parameter and overcoming assumptions.

(d) It is noted that the EVPS model is suitable and accurate for accessing the time-dependent behaviour of the clayey soil; however, it consumes experimental time and meticulous analysis to derive the fitting parameters. Therefore, an ANN model with three layers (with four neurons in the input layer, ten neurons in the hidden layer and one neuron in the output layer with a learning rate of 0.001) is developed to predict the creep parameters. The developed model is suitable and accurate, with corresponding values of MAE and RMSE being 0.0040 and 0.00496.

(e) The future aspect of ML in developing a robust model based on the concept of the equivalent timeline is presented. Training and testing of the robust model need to consider a vast dataset, newly developed algorithms, and other inherent shortcomings like transparency and knowledge extraction.

Chapter 7

Conclusions and Recommendations

7.1. Conclusions

The time-dependent stress-strain behaviour of clay soil is a concern for long-term sustainability and the designing of different infrastructural projects. Therefore, understanding the characteristics of expansive /problematic soil is of paramount importance for academicians and practicing engineers. A detailed investigation of time-dependent stress-strain behaviour using the EVPS Model is presented. Further, the ML approach is employed to study several parameters. Based on the presented work, the following conclusions were made.

The time-dependent compressibility behaviour of BC soil is explored using different loading patterns in 1D Oedometer. The study observed that the creep strain is more obvious than the swelling strain in BC soil. The strain rate is reduced non-linearly to achieve an equilibrium condition, and it is found to be independent of the loading. The relationship between creep coefficients and applied stresses is found to be non-linear. The creep coefficient increases significantly up to 630 kPa-760 kPa, and beyond it, the creep coefficient decreases continuously. The EVPS Model is accurate and suitable for predicting the time-dependent behaviour during creep and swelling.

Various mechanical and microstructural tests, including XRD, SEM and FTIR spectroscopy, were conducted to explore the effect of FA on the time-dependent compressibility behaviour of BC soil. It is observed that the stiffness of the reconstituted soil increases with the addition of FA. The inclusion of FA lowered the rebounding index and decreased time-dependent characteristics such as creep coefficient, creep strain limit, swell

coefficient, swell strain limit and relative swelling strain behaviour of reconstituted soil. However, these parameters cannot be completely reduced to zero. The creep parameters are found to be maximum in the 2nd unloading-reloading cycles of both natural and reconstituted soil; however, the parameter decreases in subsequent cycles. The formation of CSH gel/Tobermorite with the addition of FA reduces the flexibility of the O-H bond present in montmorillonite minerals. The EVPS Model is suitable and can effectively anticipate the time-dependent behaviour of the reconstituted soil accurately.

Further, a series of the wetting-drying cycle is performed in a 1D oedometer to investigate the durability and time-dependent swelling behaviour of BC soil blended with BC. The crack formation behaviour and microstructural changes were explored. From the experimental investigation, it is observed that the swelling-shrinkage behaviour is influenced by water retention, clay content, and the number of wetting-drying cycles. The time-dependent swelling coefficient diminished with the wetting-drying cycle and increased FA composition. The swelling strain limit is observed to be related exponentially to FA content. Further, the time-dependent swelling behaviour of BC soil and reconstituted soil is predicted using EVPS Model and presents the accuracy and suitability of the model. The addition of FA lessens the development of preferential zones for cracking in alternate wetting-drying cycles. However, primary cracks are significant and consistent with up to 15% FA blended soil even after being subjected to different wetting-drying cycles.

Several parameters related to primary consolidation behaviour need to be estimated accurately, economically and/or in the shortest path to ascertain the performance and stability of the superstructure. There are many limitations in performing the experiments; therefore, the ML approach can be employed in predicting several geotechnical parameters. In this study, several algorithms like ANN, RF and SVM are employed to

predict geotechnical parameters like the coefficient of consolidation and creep parameters. However, each ML algorithm possesses its own characteristics, along with merits and demerits for applicability in a particular problem. Therefore, a similar problem must be analyzed using different algorithms to determine the best and most accurate one. RF algorithm having 20 numbers of neurons can be employed for accurate prediction of the coefficient of consolidation. ANN model is proposed to predict the creep parameter of clay soil. Algorithms like Extreme Gradient Boosting, sigmoid function and Adam optimizers are employed to develop a model that can predict the creep parameters. It is observed that a model with three layers (with four neurons in the input layer, ten neurons in the hidden layer and one neuron in the output layer with a learning rate of 0.001) can suitably predict the creep parameters with corresponding values of MAE and RMSE being 0.0040 and 0.00496. ML approach can be incorporated in the prediction of the settlement behaviour of the soil based on the equivalent timeline. However, developing a robust model needs to consider a vast dataset, newly developed algorithms, and other inherent shortcomings like transparency and knowledge extraction.

7.2. Recommendation and future works

The EVPS Model can be employed to predict time-dependent parameters of both natural and reconstituted BC soil precisely and accurately. BC soil exhibits a maximum value of creep parameters in the stress ranges from 630 kPa-760 kPa. Therefore, embankment can be compacted beyond this stress level to encounter time-dependent behaviour up to an extent. FA can be utilized to improve the time-dependent compressibility behaviour especially creep and swelling parameters; however, special consideration for the duration of curing is recommended. FA can be utilized to reduce the possible crack formation in alternate wetting-drying cycles. It is recommended to choose suitable percentages of

FA carefully during the design of FA blended embankment construction from the environmental aspect and time-dependent aspects.

The nonlinear function of the EVPS model can be employed to determine related time-dependent parameters in wetting-drying cycles. RF models accurately predict the coefficient of consolidation, while the ANN can be employed for the prediction of creep parameters. However, it is recommended to choose the relevant parameters like the activation function, optimizer, epoch and number of layers/trees.

The present study is devoted to investigating the time-dependent behaviour of BC soil with /without FA. Therefore, the following would be possible future works.

- As discussed earlier, all experimental investigations are conducted at room temperature, and adding FA can improve the time-dependent behaviour of problematic soil. However, further investigations are required to consider actual field conditions like the temperature variation effect and biological effects.
- In the wetting-drying cycle, several microstructural tests were not covered in this study, including the change in pH, cation exchange capacity in each wetting-drying cycle and their relationship with time-dependent parameters.
- FA can be used to improve the time-dependent compressibility behaviour of soil; subsequently, it causes a leaching effect which is not considered in this study. Therefore, a combined study to determine optimum FA content is necessary.
- A robust ML model to predict the coefficient of consolidation can be developed in the future and applicable in global soil by considering huge datasets and other models. Further, a robust ML model can be developed based on the equivalent timeline concept to predict the time-dependent settlement of clayey soil.

References

Abdullah, H. H., Shahin, M. A., and Walske, M. L. (2019). "Geo-mechanical behavior of clay soils stabilized at ambient temperature with fly-ash geopolymer-incorporated granulated slag." Soils and Foundations, Elsevier, 59(6), 1906–1920.

Al-Homoud, A. S., Basma, A. A., Husein Malkawi, A. I., and Al Bashabsheh, M. A. (1995). "Cyclic swelling behavior of clays." Journal of geotechnical engineering, American Society of Civil Engineers, 121(7), 562–565.

Al-Juboori, W. A., and Al-Ameri, A. F. (2019). "Observation of Consolidation and Permeability Parameters of Soil Stabilized By Cutback Asphalt." Journal of University of Babylon for Engineering Sciences, 27(3), 182–195.

Aldaood, A., Bouasker, M., and Al-Mukhtar, M. (2014). "Free swell potential of lime-treated gypseous soil." Applied Clay Science, Elsevier, 102, 93–103.

Alzaidy, M. N. J. (2019). "Stabilization of Soils Using Chemical Admixtures: A Review." Journal of University of Babylon for Engineering Sciences, 27(1), 51–62.

Ambrožič, T., and Turk, G. (2003). "Prediction of subsidence due to underground mining by artificial neural networks." Computers & Geosciences, Elsevier, 29(5), 627–637.

Atahu, M. K., Saathoff, F., and Gebissa, A. (2019). "Strength and compressibility behaviors of expansive soil treated with coffee husk ash." Journal of Rock Mechanics and Geotechnical Engineering, Elsevier, 11(2), 337–348.

Augustesen, A., Liingaard, M., and Lade, P. V. (2004). "Evaluation of time-dependent behavior of soils." International Journal of Geomechanics, American Society of Civil Engineers, 4(3), 137–156.

Bachus, R. C., Terzariol, M., Pasten, C., Chong, S. H., Dai, S., Cha, M. S., Kim, S., Jang, J., Papadopoulos, E., and Roshankhah, S. (2019). "Characterization and engineering properties of dry and ponded class-F fly ash." Journal of Geotechnical and Geoenvironmental Engineering, American Society of Civil Engineers, 145(3), 4019003.

Barden, L. (1965). "Consolidation of clay with non-linear viscosity." Geotechnique, Thomas Telford Ltd, 15(4), 345–362.

Bardhan, A., GuhaRay, A., Gupta, S., Pradhan, B., and Gokceoglu, C. (2022). “A novel integrated approach of ELM and modified equilibrium optimizer for predicting soil compression index of subgrade layer of Dedicated Freight Corridor.” Transportation Geotechnics, Elsevier, 32, 100678.

Basma, A. A., Al-Homoud, A. S., Malkawi, A. I. H., and Al-Bashabsheh, M. A. (1996). “Swelling-shrinkage behavior of natural expansive clays.” Applied Clay Science, Elsevier, 11(2–4), 211–227.

Beale, M. H., Hagan, M. T., and Demuth, H. B. (1992). “Neural network toolbox user’s guide.” The MathWorks Inc, 103.

Benito, Y., Ruiz, M., Cosmen, P., and Merino, J. L. (2001). “Study of leaches obtained from the disposal of fly ash from PFBC and AFBC processes.” Chemical Engineering Journal, Elsevier, 84(2), 167–171.

Bin-Shafique, S., Rahman, K., Yaykiran, M., and Azfar, I. (2010). “The long-term performance of two fly ash stabilized fine-grained soil subbases.” Resources, Conservation and Recycling, Elsevier, 54(10), 666–672.

Bjerrum, L. (1967). “Engineering geology of Norwegian normally-consolidated marine clays as related to settlements of building.” Geotechnique, 17(2), 81–118.

Boone, S. J. (2010). “A critical reappraisal of ‘preconsolidation pressure’ interpretations using the oedometer test.” Canadian Geotechnical Journal, 47(3), 281–296.

Breiman, L. (2001). “Random forests.” Machine learning, Springer, 45(1), 5–32.

Bui, D. T., Hoang, N.-D., and Nhu, V.-H. (2019). “A swarm intelligence-based machine learning approach for predicting soil shear strength for road construction: a case study at Trung Luong National Expressway Project (Vietnam).” Engineering with Computers, Springer, 35(3), 955–965.

Bui, D. T., Nhu, V.-H., and Hoang, N.-D. (2018). “Prediction of soil compression coefficient for urban housing project using novel integration machine learning approach of swarm intelligence and multi-layer perceptron neural network.” Advanced Engineering Informatics, Elsevier, 38, 593–604.

Buisman, A. S. (1936). “Results of long duration settlement tests.” Proc. 1st ICSMFE, Cambridge, 103–107.

Burland, J. B. (1967). “Deformation of soft clay.” University of Cambridge.

Butterfield, R. (1979). “A natural compression law for soils (an advance on e-log p’).” Géotechnique, 29(4).

Cai, G., Liu, S., and Puppala, A. J. (2012). “Predictions of coefficient of consolidation from CPTU dissipation tests in Quaternary clays.” Bulletin of Engineering Geology and the Environment, Springer, 71(2), 337–350.

Cetin, B., Aydilek, A. H., and Li, L. (2012). “Manganese and Chromium Leaching from High Carbon Fly Ash Amended Embankments.” GeoCongress 2012: State of the Art and Practice in Geotechnical Engineering, 3756–3764.

Chang, D. T. T., Lee, W.-C., Guo, L.-L., and Yang, K. C. (2011). “Fly ash reducing the permeability of soil-cement mixture for the application of seepage cutoff.” Condition, Reliability, and Resilience Assessment of Tunnels and Bridges, 142–150.

Chaturvedi, D. K. (2008). “Factors affecting the performance of artificial neural network models.” Soft Computing: Techniques and its Applications in Electrical Engineering, Springer, 51–85.

Chen, F. H. (1965). “The use of piers to preventing the uplifting of lightly structured founded on expansive soils.” Proceedings of the Engineering Effects of Moisture Changes in Soils, International Research and Engineering Conference on Expansive Clay Soils, College Station, Tex, 108–119.

Chen, R., and Ng, C. W. W. (2013). “Impact of wetting–drying cycles on hydro-mechanical behavior of an unsaturated compacted clay.” Applied clay science, Elsevier, 86, 38–46.

Chen, W.-B., Feng, W.-Q., and Yin, J.-H. (2020a). “Effects of water content on resilient modulus of a granular material with high fines content.” Construction and Building Materials, Elsevier, 236, 117542.

Chen, W.-B., Feng, W.-Q., Yin, J.-H., and Borana, L. (2020b). “LVDTs-based radial strain measurement system for static and cyclic behavior of geomaterials.” Measurement, Elsevier, 155, 107526.

Chen, W.-B., Feng, W.-Q., Yin, J.-H., Borana, L., and Chen, R.-P. (2019). “Characterization of permanent axial strain of granular materials subjected to cyclic loading based on shakedown theory.” Construction and Building Materials, Elsevier, 198, 751–761.

Chen, W.-B., Feng, W.-Q., Yin, J.-H., Chen, J.-M., Borana, L., and Chen, R.-P. (2020c). “New model for predicting permanent strain of granular materials in embankment subjected to low cyclic loadings.”

Journal of Geotechnical and Geoenvironmental Engineering, American Society of Civil Engineers, 146(9), 4020084.

Chen, X., and Jeong, J. C. (2007). “Enhanced recursive feature elimination.” Sixth International Conference on Machine Learning and Applications (ICMLA 2007), IEEE, 429–435.

Cheng, C.-M., and Yin, J.-H. (2005). “Strain-Rate Dependent Stress--Strain Behavior of Undisturbed Hong Kong Marine Deposits under Oedometric and Triaxial Stress States.” Marine Georesources and Geotechnology, Taylor & Francis, 23(1–2), 61–92.

Choi, Y., Naidu, G., Jeong, S., Vigneswaran, S., Lee, S., Wang, R., and Fane, A. G. (2017). “Experimental comparison of submerged membrane distillation configurations for concentrated brine treatment.” Desalination, Elsevier, 420, 54–62.

Chou, L. (1987). “Lime stabilization: Reactions, properties, design, and construction.” State of the Art Report, 5, 564–605.

Cokca, E. (2001). “Use of class c fly ashes for the stabilizationof an expansive soil.” Journal of Geotechnical and Geoenvironmental Engineering, American Society of Civil Engineers, 127(7), 568–573.

Conte, E., and Troncone, A. (2006). “One-dimensional consolidation under general time-dependent loading.” Canadian Geotechnical Journal, NRC Research Press Ottawa, Canada, 43(11), 1107–1116.

Criado, M., Fernández-Jiménez, A., and Palomo, A. (2007). “Alkali activation of fly ash: Effect of the SiO2/Na2O ratio: Part I: FTIR study.” Microporous and mesoporous materials, Elsevier, 106(1–3), 180–191.

Crisci, C., Ghattas, B., and Perera, G. (2012). “A review of supervised machine learning algorithms and their applications to ecological data.” Ecological Modelling, Elsevier, 240, 113–122.

Das, B. M. (2003). “Chemical and mechanical stabilization.” Transportation Research Board.

Das, B. M. (2019). Advanced soil mechanics. Crc Press.

Das, B. M. (2021). Principles of geotechnical engineering. Cengage learning.

Datta, S. K. G. M. (2005). Geotechnical engineering. Tata McGraw-Hill Education.

Daverey, A., Tiwari, N., and Dutta, K. (2019). “Utilization of extracts of Musa paradisica (banana) peels and Dolichos lablab (Indian bean)

seeds as low-cost natural coagulants for turbidity removal from water." Environmental Science and Pollution Research, Springer, 26(33), 34177–34183.

Davidson, S. E. (1956). Factors influencing swelling and shrinking in soils. Texas A&M University.

Davis, E. H., and Raymond, G. P. (1965). "A non-linear theory of consolidation." Geotechnique, Thomas Telford Ltd, 15(2), 161–173.

Day, R. W. (1994). "Swell-shrink behavior of compacted clay." Journal of geotechnical engineering, American Society of Civil Engineers, 120(3), 618–623.

Dayioglu, M., Cetin, B., and Nam, S. (2017). "Stabilization of expansive Belle Fourche shale clay with different chemical additives." Applied Clay Science, Elsevier, 146, 56–69.

Devi, S. P., Devi, K. R., Prasad, D. S. V, and Raju, G. (2015). "Study on consolidation and correlation with index properties of different soils in Manipur valley." Int J Eng Res Dev, 11(05), 57–63.

Duan, X. (2021). "Mechanical effects of solid water on the particle skeleton of soil: mechanism analysis." Geofluids, Hindawi, 2021.

Edil, T. B., Acosta, H. A., and Benson, C. H. (2006a). "Stabilizing soft fine-grained soils with fly ash." Journal of materials in civil engineering, American Society of Civil Engineers, 18(2), 283–294.

Edil, T. B., Acosta, H. A., and Benson, C. H. (2006b). "Stabilizing soft fine-grained soils with fly ash." Journal of Materials in Civil Engineering, 18(2), 283–294.

Elsharief, A. M., and Sufian, M. (2018). "Time rate of swelling of compacted highly plastic clay soil from Sudan." MATEC Web of Conferences, EDP Sciences, 2032.

Erdal Cokca. (2001). "Use of Class C fly Ashes for the Stabilization of an Expansive Soil." Journal of Geotechnical and Geoenvironmental Engineering, 127(7)(July), 568–573.

Erzin, Y., MolaAbasi, H., Kordnaeij, A., and Erzin, S. (2020). "Prediction of Compression Index of Saturated Clays Using Robust Optimization Model." Journal of Soft Computing in Civil Engineering, Pouyan Press, 4(3), 1–16.

Estabragh, A. R., Parsaei, B., and Javadi, A. A. (2015). "Laboratory investigation of the effect of cyclic wetting and drying on the behaviour of an expansive soil." Soils and Foundations, Elsevier, 55(2), 304–314.

Fatahi, B., Le, T. M., Le, M. Q., and Khabbaz, H. (2013). “Soil creep effects on ground lateral deformation and pore water pressure under embankments.” Geomechanics and Geoengineering, Taylor & Francis, 8(2), 107–124.

Fauzi, A., Nuruddin, M. F., Malkawi, A. B., and Abdullah, M. (2016). “Study of fly ash characterization as a cementitious material.” Procedia engineering, Elsevier, 148, 487–493.

Feng, W., Lalit, B., Yin, Z., and Yin, J. (2017a). “Long-term Non-linear creep and swelling behavior of Hong Kong marine deposits in oedometer condition.” Computers and Geotechnics, Elsevier Ltd, 84, 1–15.

Feng, W. Q., Yin, J. H., Tao, X. M., Tong, F., and Chen, W. B. (2017b). “Time and strain-rate effects on viscous stress-strain behavior of plasticine material.” International Journal of Geomechanics.

Firat, S., Khatib, J. M., Yilmaz, G., and Comert, A. T. (2017). “Effect of curing time on selected properties of soil stabilized with fly ash, marble dust and waste sand for road sub-base materials.” Waste Management & Research, SAGE Publications Sage UK: London, England, 35(7), 747–756.

Fredlund, D. G., Rahardjo, H., and Fredlund, M. D. (2012). Unsaturated Soil Mechanics in Engineering Practice. John Wiley & Sons, Inc.

Garlanger, J. E., and Šuklje. (1973). “Discussion: The consolidation of soils exhibiting creep under constant effective stress.” Géotechnique, Thomas Telford Ltd, 23(2), 283–284.

George, K. P. (1971). “Shrinkage cracking of soil-cement base: theoretical and model studies.” Highway Research Record, 351, 115–133.

Gidigasu, S. S. R., and Gawu, S. K. Y. (2013). “The Mode of Formation, Nature and Geotechnical characteristics of Black Cotton Soils-A Review.” Standard Scientific Research and Essays, 1(14), 377–390.

Göktepe, A. B., Sezer, A., Sezer, G. I., and Ramyar, K. (2008). “Classification of time-dependent unconfined strength of fly ash treated clay.” Construction and Building Materials, Elsevier, 22(4), 675–683.

Graham, J., Crooks, J. H. A., and Bell, A. L. (1983). “Time effects on the stress-strain behaviour of natural soft clays.” Géotechnique, Thomas Telford Ltd, 33(3), 327–340.

Graham, J., Sunn, B. C. C., and Gray, M. N. (1986). “Strength and volume change characteristics of a sand-bentonite buffer.” Proc., 2nd Int.

Conf. on Radioactive Waste Management, Canadian Nuclear Society and the American Nuclear Society, Washington, DC, 188–194.

Granitto, P. M., Furlanello, C., Biasioli, F., and Gasperi, F. (2006). "Recursive feature elimination with random forest for PTR-MS analysis of agroindustrial products." Chemometrics and intelligent laboratory systems, Elsevier, 83(2), 83–90.

Le Guillou, F., Wetterlind, W., Rossel, R. A. V., Hicks, W., Grundy, M., and Tuomi, S. (2015). "How does grinding affect the mid-infrared spectra of soil and their multivariate calibrations to texture and organic carbon?" Soil Research, CSIRO, 53(8), 913–921.

Guo, Y., Liu, M., He, X., Tan, H., Ma, B., and Chen, F. (2017). "Effect of wet-and dry-grind fly ash on the durability of concrete." Zkg International, Bauverlag Bv Gmbh Avenwedder Str 55, 33311 Gutersloh, Germany, 70(4), 50–55.

Gupta, C. (2019). "Feature Selection and Analysis for Standard Machine Learning Classification of Audio Beehive Samples."

Gupta, C., and Sharma, R. K. (n.d.). "Study of black cotton soil and local clay soil for sub-grade characteristic."

Guyon, I., Weston, J., Barnhill, S., and Vapnik, V. (2002). "Gene selection for cancer classification using support vector machines." Machine learning, Springer, 46(1), 389–422.

Hameedi, M. K., Al Omari, R. R., and Fattah, M. Y. (2020). "Compression and Creep Indices of Organic Clayey Soil." IOP Conference Series: Materials Science and Engineering, IOP Publishing, 12035.

Havel, F. (2004). "Creep in soft soils." Fakultet for ingeniørvitenskap og teknologi.

Hawlader, B. C., Muhunthan, B., and Imai, G. (2003). "Viscosity effects on one-dimensional consolidation of clay." International Journal of Geomechanics, American Society of Civil Engineers, 3(1), 99–110.

Holtz, R. D., Jamiolkowski, M. B., and Lancellotta, R. (1986). "Lessons from oedometer tests on high quality samples." Journal of geotechnical engineering, American Society of Civil Engineers, 112(8), 768–776.

Hoy, M., Rachan, R., Horpibulsuk, S., Arulrajah, A., and Mirzababaei, M. (2017). "Effect of wetting–drying cycles on compressive strength and microstructure of recycled asphalt pavement–Fly ash geopolymer." Construction and Building Materials, Elsevier, 144, 624–634.

Hsi, J., and Martin, J. (2015). “Soft Ground Treatment and Performance, Yelgun to Chinderah Freeway, New South Wales, Australia.” Ground Improvement Case Histories: Compaction, Grouting and Geosynthetics, Butterworth-Heinemann, 137.

Hsieh, C.-P., Chen, Y.-T., Beh, W.-K., and Wu, A.-Y. A. (2019). “Feature selection framework for XGBoost based on electrodermal activity in stress detection.” 2019 IEEE International Workshop on Signal Processing Systems (SiPS), IEEE, 330–335.

Hsu, T.-W., and Tsai, T.-H. (2016). “Combined vertical and radial consolidation under time-dependent loading.” International Journal of Geomechanics, American Society of Civil Engineers, 16(3), 4015073.

Ik, N. S. (2009). “Estimation of swell index of fine grained soils using regression equations and artificial neural networks.” Scientific Research and Essays, Academic Journals, 4(10), 1047–1056.

Imai, G. (1995). “Analytical examination of the foundations to formulate consolidation phenomena with inherent time-dependence.” Proc of Int. Symp. on Compression and Consolidation of Clayey Soils, 1995, 891–935.

Imai, G., and TANG, Y. (1992). “A constitutive equation of one-dimensional consolidation derived from inter-connected tests.” Soils and Foundations, The Japanese Geotechnical Society, 32(2), 83–96.

J. Suzanne Powell, W. Andy Take, Greg Siemens, V. H. R. (2012). “Time-dependent behaviour of the Bearpaw Shale in oedometric loading and unloading.” Canadian Geotechnical Journal, 49(12), 427–441.

Jaditager, M., and Sivakugan, N. (2018). “Consolidation behavior of fly ash-based geopolymer-stabilized dredged mud.” Journal of Waterway, Port, Coastal, and Ocean Engineering, American Society of Civil Engineers, 144(4), 6018003.

Jain, A. K., Mao, J., and Mohiuddin, K. M. (1996). “Artificial neural networks: A tutorial.” Computer, IEEE, 29(3), 31–44.

Jha, A. K., and Sivapullaiah, P. V. (2018). “Potential of fly ash to suppress the susceptible behavior of lime-treated gypseous soil.” Soils and foundations, Elsevier, 58(3), 654–665.

Jian-Hua Yin and J. Graham. (1994). “Equivalent times and one-dimensional elastic viscoplastic modelling of time-dependent stress strain behavior of clays.” Canadian Geotechnical Journal, 31, 42–52.

Jiang, N., Wang, C., Wu, Q., and Li, S. (2020). “Influence of Structure and Liquid Limit on the Secondary Compressibility of Soft Soils.” Journal

of Marine Science and Engineering, Multidisciplinary Digital Publishing Institute, 8(9), 627.

Johnson Singh, M., Feng, W., Xu, D., Dubey, M., and Borana, L. (2022). "Long-Term Elastoviscoplastic Behavior of Fly Ash–Blended Indian Montmorillonite Clay in Oedometer Conditions." International Journal of Geomechanics, American Society of Civil Engineers, 22(3), 4021306.

Jones Jr, D. E., and Holtz, W. G. (1973). "Expansive soils-the hidden disaster." Civil Engineering, 43(8).

Kabbaj, M., Oka, F., Leroueil, S., and Tavenas, F. (1986). "Consolidation of natural clays and laboratory testing." Consolidation of soils: Testing and evaluation, ASTM International.

Kaczmarek, Ł., and Dobak, P. (2017). "Contemporary overview of soil creep phenomenon." Contemporary Trends in Geoscience, 6(1), 28–40.

Kalkan, E. (2011). "Impact of wetting–drying cycles on swelling behavior of clayey soils modified by silica fume." Applied Clay Science, Elsevier, 52(4), 345–352.

Kaniraj, S. R., and Gayathri, V. (2004). "Permeability and consolidation characteristics of compacted fly ash." Journal of energy engineering, American Society of Civil Engineers, 130(1), 18–43.

Karamizadeh, S., Abdullah, S. M., Halimi, M., Shayan, J., and javad Rajabi, M. (2014). "Advantage and drawback of support vector machine functionality." 2014 international conference on computer, communications, and control technology (I4CT), IEEE, 63–65.

Karstunen, M., and Yin, Z.-Y. (2010). "Modelling time-dependent behaviour of Murro test embankment." Géotechnique, Thomas Telford Ltd, 60(10), 735–749.

Katti, R. K. (1978). Search for solutions to problems in black cotton soils. Indian Institute of Technology.

Kim, B., Prezzi, M., and Salgado, R. (2005). "Geotechnical properties of fly and bottom ash mixtures for use in highway embankments." Journal of Geotechnical and Geoenvironmental Engineering, American Society of Civil Engineers, 131(7), 914–924.

Kleppe, J. H., and Olson, R. E. (1985). "Desiccation cracking of soil barriers." Hydraulic barriers in soil and rock, ASTM International.

Kocataskin, F. (1957). "A Literature Survey on Soil Stabilization Lime-Flyash Admixtures: Informational Report." Purdue University.

Kordnaeij, A., Kalantary, F., Kordtabar, B., and Mola-Abasi, H. (2015). "Prediction of recompression index using GMDH-type neural network based on geotechnical soil properties." Soils and Foundations, Elsevier, 55(6), 1335–1345.

Krivoshein, P. K., Volkov, D. S., Rogova, O. B., and Proskurnin, M. A. (2020). "FTIR photoacoustic spectroscopy for identification and assessment of soil components: chernozems and their size fractions." Photoacoustics, Elsevier, 18, 100162.

Kumar, P., Chandra, S., and Vishal, R. (2006). "Comparative study of different subbase materials." Journal of Materials in Civil Engineering, American Society of Civil Engineers, 18(4), 576–580.

Kurnaz, T. F., Dagdeviren, U., Yildiz, M., and Ozkan, O. (2016). "Prediction of compressibility parameters of the soils using artificial neural network." SpringerPlus, Springer, 5(1), 1–11.

Ladd, C. C. (1960). "Mechanisms of swelling by compacted clay." Highway Research Board Bulletin, (245).

Lawal, A. I., and Kwon, S. (2020). "Application of artificial intelligence to rock mechanics: An overview." Journal of Rock Mechanics and Geotechnical Engineering, Elsevier.

Leroueil, S. (1988). "Tenth Canadian Geotechnical Colloquium: Recent developments in consolidation of natural clays." Canadian Geotechnical Journal, NRC Research Press Ottawa, Canada, 25(1), 85–107.

Leroueil, S., Kabbaj, M., Tavenas, F., and Bouchard, R. (1985). "Stress–strain–strain rate relation for the compressibility of sensitive natural clays." Géotechnique, Thomas Telford Ltd, 35(2), 159–180.

Leroueil, S., Tavenas, F., Samson, L., and Morin, P. (1983). "Preconsolidation pressure of Champlain clays. Part II. Laboratory determination." Canadian Geotechnical Journal, NRC Research Press Ottawa, Canada, 20(4), 803–816.

Levenberg, K. (1944). "A method for the solution of certain non-linear problems in least squares." Quarterly of applied mathematics, 2(2), 164–168.

Li, Y., and Chen, W. (2020). "A Comparative Performance Assessment of Ensemble Learning for Credit Scoring." Mathematics, Multidisciplinary Digital Publishing Institute, 8(10), 1756.

Little, D. N., and Nair, S. (2009). "Recommended practice for stabilization of subgrade soils and base materials." NCHRP, Texas A&M

University, Texas, Transportation Research Board of the National Academies, National Cooperative Highway Research Program, Transportation Research Board.

Liu, Y., Zeng, F., Sun, B., Jia, P., and Graham, I. T. (2019). "Structural Characterizations of Aluminosilicates in Two Types of Fly Ash Samples from Shanxi Province, North China." Minerals, Multidisciplinary Digital Publishing Institute, 9(6), 358.

Lu, S.-G., Sun, F.-F., and Zong, Y.-T. (2014). "Effect of rice husk biochar and coal fly ash on some physical properties of expansive clayey soil (Vertisol)." Catena, Elsevier, 114, 37–44.

Ma, C., Chen, L., and Chen, B. (2016). "Experimental study of effect of fly ash on self-compacting rammed earth construction stabilized with cement-based composites." Journal of Materials in Civil Engineering, 28(7), 1–10.

Madejová, J., Gates, W. P., and Petit, S. (2017). "IR spectra of clay minerals." Developments in Clay Science, Elsevier, 107–149.

Mesri, G. (1973). "Coefficient of secondary compression." ASCE J Soil Mech Found Div-v 99, American Society of Civil Engineers (ASCE), (SM1), 123–137.

Mesri, G., and Castro, A. (1987). "C α/C c concept and K 0 during secondary compression." Journal of Geotechnical Engineering, American Society of Civil Engineers, 113(3), 230–247.

Mesri, G., and Choi, Y. K. (1985). "Settlement analysis of embankments on soft clays." Journal of Geotechnical Engineering, American Society of Civil Engineers, 111(4), 441–464.

Mir, B. A. (2010). "Study of the influence of smear zone around sand compaction pile on properties of composite ground." Ph. D. Thesis, IIT Bombay.

Mir, B. A., and Sridharan, A. (2014). "Volume change behavior of clayey soil–fly ash mixtures." International Journal of Geotechnical Engineering, Taylor & Francis, 8(1), 72–83.

Mitchell, J. K., and Soga, K. (1993a). "Fundamentals of Soil Behavior, John Wiley&Sons." Inc., New York, 422.

Mitchell, J. K., and Soga, K. (1993b). Fundamentals of Soil Behavior. Wiley, New York.

Mittal, M., Satapathy, S. C., Pal, V., Agarwal, B., Goyal, L. M., and Parwekar, P. (2021). "Prediction of Coefficient of Consolidation in

Soil using Machine Learning Techniques." Microprocessors and Microsystems, Elsevier, 103830.

Mohammadinia, Alireza, Mahdi M Disfani, David Conomy, Arul Arulrajah, Suksun Horpibulsuk, and Stephen Darmawan. (2019). "Utilization of Alkali-Activated Fly Ash for Construction of Deep Mixed Columns in Loose Sands." Journal of Materials in Civil Engineering 31 (10). American Society of Civil Engineers: 4019233.

Mohammadzadeh S, D., Kazemi, S.-F., Mosavi, A., Nasseralshariati, E., and Tah, J. H. M. (2019). "Prediction of compression index of fine-grained soils using a gene expression programming model." Infrastructures, Multidisciplinary Digital Publishing Institute, 4(2), 26.

Mráz, V., Valentin, J., Suda, J., and Kopecký, L. (2015). "Experimental assessment of fly-ash stabilized and recycled mixes." Journal of Testing and Evaluation, ASTM International, 43(2), 1–15.

Nabil, M., Mustapha, A., and Rios, S. (2020). "Impact of wetting—drying cycles on the mechanical properties of lime-stabilized soils." International Journal of Pavement Research and Technology, Springer, 13(1), 83–92.

Nash, J. E., and Sutcliffe, J. V. (1970). "River flow forecasting through conceptual models part I—A discussion of principles." Journal of hydrology, Elsevier, 10(3), 282–290.

Navarro, A. (2001). "Secondary compression of clays as a local dehydration process." Géotechnique, 51(10), 859–869.

Nelson, J. D., Chao, K. C., Overton, D. D., and Nelson, E. J. (2015). Foundation engineering for expansive soils. John Wiley & Sons.

Nguyen, M. D., Pham, B. T., Ho, L. S., Ly, H.-B., Le, T.-T., Qi, C., Le, V. M., Le, L. M., Prakash, I., and Bui, D. T. (2020). "Soft-computing techniques for prediction of soils consolidation coefficient." Catena, Elsevier, 195, 104802.

Nguyen, M. D., Pham, B. T., Tuyen, T. T., Hai Yen, H. P., Prakash, I., Vu, T. T., Chapi, K., Shirzadi, A., Shahabi, H., and Dou, J. (2019). "Development of an artificial intelligence approach for prediction of consolidation coefficient of soft soil: A sensitivity analysis." The Open Construction and Building Technology Journal, 13(1).

Nowamooz, H. (2014). "Effective stress concept on multi-scale swelling soils." Applied clay science, Elsevier, 101, 205–214.

Olek, B. S. (2020). “Experimental insights into consolidation rates during one-dimensional loading with special reference to excess pore water pressure.” Acta Geotechnica, Springer, 15(12), 3571–3591.

Omidi, G. H., Thomas, J. C., and Brown, K. W. (1996). “Effect of desiccation cracking on the hydraulic conductivity of a compacted clay liner.” Water, Air, and Soil Pollution, Springer, 89(1), 91–103.

Pal, R. (2017). “Overview of predictive modeling based on genomic characterizations.” Predictive modeling of drug sensitivity, Elsevier, 121–148.

Palkovic, S. D., Yip, S., and Büyüköztürk, O. (2017). “A cohesive-frictional force field (CFFF) for colloidal calcium-silicate-hydrates.” Journal of the Mechanics and Physics of Solids, Elsevier, 109, 160–177.

Panakkat, A., and Adeli, H. (2007). “Neural network models for earthquake magnitude prediction using multiple seismicity indicators.” International journal of neural systems, World Scientific, 17(01), 13–33.

Pant, R. R. (2007). “Evaluation of consolidation parameters of cohesive soils using PCPT method.”

Park, H. Il, and Lee, S. R. (2011). “Evaluation of the compression index of soils using an artificial neural network.” Computers and Geotechnics, Elsevier, 38(4), 472–481.

Paul, S. C., Panda, B., Zhu, H.-H., and Garg, A. (2019). “An artificial intelligence model for computing optimum fly ash content for structural-grade concrete.” Advances in Civil Engineering Materials, ASTM International, 8(1), 56–70.

Peron, H., Laloui, L., Hu, L.-B., and Hueckel, T. (2013). “Formation of drying crack patterns in soils: a deterministic approach.” Acta Geotechnica, Springer, 8(2), 215–221.

Perzyna, P. (1966). “Fundamental problems in viscoplasticity.” Advances in applied mechanics, Elsevier, 243–377.

Pham, B. T., Nguyen, M. D., Van Dao, D., Prakash, I., Ly, H.-B., Le, T.-T., Ho, L. S., Nguyen, K. T., Ngo, T. Q., and Hoang, V. (2019). “Development of artificial intelligence models for the prediction of Compression Coefficient of soil: An application of Monte Carlo sensitivity analysis.” Science of The Total Environment, Elsevier, 679, 172–184.

Pham, B. T., Qi, C., Ho, L. S., Nguyen-Thoi, T., Al-Ansari, N., Nguyen, M. D., Nguyen, H. D., Ly, H.-B., Le, H. Van, and Prakash, I. (2020a). “A

novel hybrid soft computing model using random forest and particle swarm optimization for estimation of undrained shear strength of soil." Sustainability, Multidisciplinary Digital Publishing Institute, 12(6), 2218.

Pham, B. T., Singho, S. K., and Ly, H.-B. (2020b). "Using Artificial Neural Network (ANN) for prediction of soil." Vietnam Journal of Earth Sciences, 42(4), 311–319.

Phanikumar, B. R. (2009). "Effect of lime and fly ash on swell, consolidation and shear strength characteristics of expansive clays: a comparative study." Geomechanics and Geoengineering: An international journal, Taylor & Francis, 4(2), 175–181.

Phanikumar, B. R., Dembla, S., and Yatindra, A. (2021). "Swelling Behaviour of an Expansive Clay Blended With Fine Sand and Fly Ash." Geotechnical and Geological Engineering, Springer, 39(1), 583–591.

Phanikumar, B. R., and Sharma, R. S. (2007). "Volume change behavior of fly ash-stabilized clays." Journal of materials in Civil Engineering, American Society of Civil Engineers, 19(1), 67–74.

Powell, J. S., Take, W. A., Siemens, G., and Remenda, V. H. (2012). "Time-dependent behaviour of the Bearpaw Shale in oedometric loading and unloading." Canadian Geotechnical Journal, NRC Research Press, 49(4), 427–441.

Prasad, B., and Mondal, K. K. (2009). "Environmental impact of manganese due to its leaching from coal fly ash." Journal of environmental science & engineering, 51(1), 27–32.

Priddy, K. L., and Keller, P. E. (2005). Artificial neural networks: an introduction. SPIE press.

Ramesh, S., and Thyagaraj, T. (2020). "Effect of Sand Content on Cyclic Swell-Shrink Behavior of Compacted Expansive Soil." Geo-Congress 2020: Geo-Systems, Sustainability, Geoenvironmental Engineering, and Unsaturated Soil Mechanics, American Society of Civil Engineers Reston, VA, 141–150.

Rao, D. K., Raju, G. V. R. P., and Kumar, K. A. (2011). "Consolidation Characteristics Of Treated Marine Clay For Foundation Soil Beds." Engg Journals Publication.

Rao, K. S. S., and Tripathy, S. (2003). "Effect of aging on swelling and swell-shrink behavior of a compacted expansive soil." Geotechnical Testing Journal, ASTM International, 26(1), 36–46.

Rao, S. M., Reddy, B. V. V, and Muttharam, M. (2001). “The impact of cyclic wetting and drying on the swelling behaviour of stabilized expansive soils.” Engineering geology, Elsevier, 60(1–4), 223–233.

Rosenbalm, D., and Zapata, C. E. (2017). “Effect of wetting and drying cycles on the behavior of compacted expansive soils.” Journal of Materials in Civil Engineering, American Society of Civil Engineers, 29(1), 4016191.

Rowe, P. W. (1959). “Measurement of the coefficient of consolidation of lacustrine clay.” Geotechnique, Thomas Telford Ltd, 9(3), 107–118.

Sakthivel, T., Reid, D. L., Goldstein, I., Hench, L., and Seal, S. (2013). “Hydrophobic high surface area zeolites derived from fly ash for oil spill remediation.” Environmental science & technology, ACS Publications, 47(11), 5843–5850.

Sarica, A., Cerasa, A., and Quattrone, A. (2017). “Random forest algorithm for the classification of neuroimaging data in Alzheimer’s disease: a systematic review.” Frontiers in aging neuroscience, Frontiers, 9, 329.

Saride, S., and Dutta, T. T. (2016). “Effect of fly-ash stabilization on stiffness modulus degradation of expansive clays.” Journal of Materials in Civil Engineering, 28(12), 1–12.

Sebastian Bryson, L., Mahmoodabadi, M., and Adu-Gyamfi, K. (2017). “Prediction of Consolidation and Shear Behavior of Fly Ash–Soil Mixtures Using Mixture Theory.” Journal of Materials in Civil Engineering, American Society of Civil Engineers, 29(11), 4017222.

Seed, H. B., Woodward, R. J., and Lundgren, R. (1963). “Prediction of swelling potential for compacted clays.” Transactions of the American Society of Civil Engineers, American Society of Civil Engineers, 128(1), 1443–1477.

Shahsavani, S., Vakili, A. H., and Mokhberi, M. (2020). “The effect of wetting and drying cycles on the swelling-shrinkage behavior of the expansive soils improved by nanosilica and industrial waste.” Bulletin of Engineering Geology and the Environment, Springer, 79, 4765–4781.

Sharma, A. K., and Sivapullaiah, P. V. (2017). “Swelling behaviour of expansive soil treated with fly ash–GGBS based binder.” Geomechanics and Geoengineering, Taylor & Francis, 12(3), 191–200.

Sheela, K. G., and Deepa, S. N. (2013). “Review on methods to fix number of hidden neurons in neural networks.” Mathematical Problems in Engineering, Hindawi, 2013.

Shi, X. S., Yin, J., Feng, W., and Chen, W. (2018). “Creep coefficient of binary sand–bentonite mixtures in oedometer testing using mixture theory.” International Journal of Geomechanics, American Society of Civil Engineers, 18(12), 4018159.

Shukla, S., Sivakugan, N., and Das, B. (2009). “Methods for determination of the coefficient of consolidation and field observations of time rate of settlement—an overview.” International Journal of Geotechnical Engineering, Taylor & Francis, 3(1), 89–108.

Singh, A., and Mitchell, J. K. (1968). “General stress-strain-time function for soils.” Journal of the Soil Mechanics and Foundations Division, American Society of Civil Engineers, 94(1), 21–46.

Singh, G. (2013). “Environmental aspects of coal combustion residues from thermal power plants.” Thermal Power Plants-Advanced Applications, InTech, Rijeka, Croatia, 153–177.

Singh, M. J., Borana, L., Weiqiang, F., and Xu, D.-S. (2021). “Long-Term Swelling Characteristics of Montmorillonite Clay with and without Fly Ash: Wetting–Drying Cycle Influence in 1D Oedometer Condition.” Journal of Testing and Evaluation, ASTM International, 51(1).

Singh, M. J., Feng, W. Q., Xu, D. S., and Borana, L. (2022). “Time-dependent compressibility characteristics of Montmorillonite Clay using EVPS Model.” Geomechanics and Engineering, 28(2), 171–180.

Singh, M. J., Weiqiang, F., Dong-Sheng, X., and Borana, L. (2020). “Experimental Study of Compression Behavior of Indian Black Cotton Soil in Oedometer Condition.” International Journal of Geosynthetics and Ground Engineering, 6(2), 30.

Sivapullaiah, P. V, Prashanth, J. P., and Sridharan, A. (1996a). “Effect of fly ash on the index properties of black cotton soil.” Soils and Foundations, The Japanese Geotechnical Society, 36(1), 97–103.

Sivapullaiah, P. V, Sridharan, A., and Stalin, V. K. (1996b). “Swelling behaviour of soil bentonite mixtures.” Canadian Geotechnical Journal, NRC Research Press Ottawa, Canada, 33(5), 808–814.

Skempton, A. W. (1953). “The post-glacial clays of Thames estuary at Tilbury and Shell-haven.” Proc., 3rd ICSMFE, 302–308.

Skempton, A. W., and Henkel, D. J. (1957). “Tests on London Clay from deep borings at Paddington, Victoria and the South Bank.” Proc. 4th Int. Conf. Soil Mech. Found. Engng, London, 100–106.

Skousen, J., Yang, J. E., Lee, J.-S., and Ziemkiewicz, P. (2013). “Review of fly ash as a soil amendment.” Geosystem Engineering, Taylor & Francis, 16(3), 249–256.

Sobhan, K., and Mashnad, M. (2003). “Mechanical stabilization of cemented soil–fly ash mixtures with recycled plastic strips.” Journal of environmental engineering, American Society of Civil Engineers, 129(10), 943–947.

Solanki, P., Khoury, N., and Zaman, M. M. (2009). “Engineering properties and moisture susceptibility of silty clay stabilized with lime, class C fly ash, and cement kiln dust.” Journal of Materials in Civil Engineering, American Society of Civil Engineers, 21(12), 749–757.

Soltani, A., Raeesi, R., and O’Kelly, B. C. (2020). “Cyclic swell–shrink behaviour of an expansive soil treated with a sulfonated oil.” Proceedings of the Institution of Civil Engineers-Ground Improvement, Thomas Telford Ltd, 1–14.

Sridharan, A. (1991). “Engineering Behaviour of Fine Grained Soils A Fundamental Approach.” Indian Geotechnical Journal, 21(2), 133–144.

Sridharan, A., and Nagaraj, H. B. (2004). “Coefficient of consolidation and its correlation with index properties of remolded soils.” Geotechnical testing journal, ASTM International, 27(5), 469–474.

Sridharan, A., Pandian, N. S., and Srinivas, S. (2001). “Compaction behaviour of Indian coal ashes.” Proceedings of the Institution of Civil Engineers-Ground Improvement, Thomas Telford Ltd, 5(1), 13–22.

Stirling, R. A., Glendinning, S., and Davie, C. T. (2017). “Modelling the deterioration of the near surface caused by drying induced cracking.” Applied Clay Science, Elsevier, 146, 176–185.

Sudhakaran, S. P., Sharma, A. K., and Kolathayar, S. (2018). “Soil stabilization using bottom ash and areca fiber: Experimental investigations and reliability analysis.” Journal of Materials in Civil Engineering, American Society of Civil Engineers, 30(8), 4018169.

Suklje, L. (1957). “The analysis of the consolidation process by the isotaches method.” Proc. 4th ICSMFE, 200–206.

Taha, M. R., Ahmed, J., and Asmirza, S. (2000). “One-dimensional consolidation of Kelang clay.” Pertanika Journal of Science & Technology, 8(1), 19–29.

Tan, F., Zhou, W., and Yuen, K. (2018). “Effect of loading duration on uncertainty in creep analysis of clay.” International Journal for

Numerical and Analytical Methods in Geomechanics, Wiley Online Library, 42(11), 1235–1254.

Tang, C.-S., Cui, Y.-J., Shi, B., Tang, A.-M., and An, N. (2016). "Effect of wetting-drying cycles on soil desiccation cracking behaviour." E3S Web of conferences, EDP Sciences, 12003.

Tang, C.-S., Cui, Y.-J., Shi, B., Tang, A.-M., and Liu, C. (2011). "Desiccation and cracking behaviour of clay layer from slurry state under wetting–drying cycles." Geoderma, Elsevier, 166(1), 111–118.

Tavenas, F., Leroueil, S., Rochelle, P. La, and Roy, M. (1978). "Creep behaviour of an undisturbed lightly overconsolidated clay." Canadian Geotechnical Journal, NRC Research Press Ottawa, Canada, 15(3), 402–423.

Taylor, D. W. (1942). Research on consolidation of clays. Massachusetts Institute of Technology.

Thermal Civil Design Division, C. E. A. N. D. (2020). Report on Fly Ash Generation At Coal / Lignite Based Thermal Power Stations and its Utilization in the Country for 1st half of the year 2019-2020.

Tong, F., and Yin, J.-H. (2011). "Nonlinear creep and swelling behavior of bentonite mixed with different sand contents under oedometric condition." Marine Georesources & Geotechnology, Taylor & Francis, 29(4), 346–363.

Tong, F., and Yin, J.-H. (2013). "Experimental and constitutive modeling of relaxation behaviors of three clayey soils." Journal of geotechnical and geoenvironmental engineering, American Society of Civil Engineers, 139(11), 1973–1981.

Trabelsi, H., Jamei, M., Zenzri, H., and Olivella, S. (2012). "Crack patterns in clayey soils: Experiments and modeling." International Journal for Numerical and Analytical methods in geomechanics, Wiley Online Library, 36(11), 1410–1433.

Tripathy, S., and Rao, K. S. S. (2009). "Cyclic swell–shrink behaviour of a compacted expansive soil." Geotechnical and Geological Engineering, Springer, 27(1), 89–103.

Tu, J. V. (1996). "Advantages and disadvantages of using artificial neural networks versus logistic regression for predicting medical outcomes." Journal of clinical epidemiology, Elsevier, 49(11), 1225–1231.

Vaid, Y. P., and Campanella, R. G. (1977). "Time-dependent behavior of undisturbed clay." Journal of the Geotechnical Engineering Division, American Society of Civil Engineers, 103(7), 693–709.

Vorwerk, S., Cameron, D., and Keppel, G. (2015). “Clay Soil in Suburban Environments: Movement and Stabilization through Vegetation.” Ground Improvement Case Histories, Elsevier, 655–682.

Wang, G., and Wei, X. (2015). “Modeling swelling–shrinkage behavior of compacted expansive soils during wetting–drying cycles.” Canadian Geotechnical Journal, NRC Research Press, 52(6), 783–794.

Wang, W., Luo, Q., Yuan, B., and Chen, X. (2020). “An Investigation of Time-Dependent Deformation Characteristics of Soft Dredger Fill.” Advances in Civil Engineering, Hindawi, 2020.

Wang, Y., and Ni, X. S. (2019). “A XGBoost risk model via feature selection and Bayesian hyper-parameter optimization.” arXiv preprint arXiv:1901.08433.

Wu, Z., Deng, Y., Cui, Y., Zhou, A., Feng, Q., and Xue, H. (2019). “Experimental study on creep behavior in oedometer tests of reconstituted soft clays.” International Journal of Geomechanics, American Society of Civil Engineers, 19(3), 4018198.

Xue, K., Wang, S., Hu, Y., and Li, M. (2020). “Creep behavior of red-clay under triaxial compression condition.” Frontiers in Earth Science, Frontiers, 345.

Yang, B., Liu, J., Zhao, X., and Zheng, S. (2021). “Evaporation and cracked soda soil improved by fly ash from recycled materials.” Land Degradation & Development, Wiley Online Library.

Yazdandoust, F., and Yasrobi, S. S. (2010). “Effect of cyclic wetting and drying on swelling behavior of polymer-stabilized expansive clays.” Applied Clay Science, Elsevier, 50(4), 461–468.

Yesiller, N., Miller, C. J., Inci, G., and Yaldo, K. (2000). “Desiccation and cracking behavior of three compacted landfill liner soils.” Engineering Geology, Elsevier, 57(1–2), 105–121.

Yilmaz, Y., Coban, H. S., Cetin, B., and Edil, T. B. (2019). “Use of standard and off-spec fly ashes for soil stabilization.” Journal of Materials in Civil Engineering, 31(2), 1–11.

Yin, J.-H. (1990a). “Constitutive modelling of time-dependent stress-strain behaviour of soils.”

Yin, J.-H. (1999). “Non-linear creep of soils in oedometer tests.” Geotechnique, 49(5), 699–707.

Yin, J.-H. (2015a). “Fundamental issues of elastic viscoplastic modeling of the time-dependent stress–strain behavior of geomaterials.”

International Journal of Geomechanics, American Society of Civil Engineers, 15(5), A4015002.

Yin, J.-H., and Graham, J. (1994). “Equivalent times and one-dimensional elastic viscoplastic modelling of time-dependent stress–strain behaviour of clays.” Canadian Geotechnical Journal, NRC Research Press, 31(1), 42–52.

Yin, J.-H., and Tong, F. (2011a). “Constitutive modeling of time-dependent stress–strain behaviour of saturated soils exhibiting both creep and swelling.” Canadian Geotechnical Journal, NRC Research Press, 48(12), 1870–1885.

Yin, J.-H., Zhu, J.-G., and Graham, J. (2002). “A new elastic viscoplastic model for time-dependent behaviour of normally and overconsolidated clays: theory and verification.” Canadian Geotechnical Journal, NRC Research Press, 39(1), 157–173.

Yin, J. (2013). “Review of Elastic Visco-Plastic Modeling of the Time-Dependent Stress-Strain Behavior of soils and its extension and applications.” Springer-Verlag Berlin Heidelberg, (3), 149–157.

Yin, J. (2015b). “Fundamental Issues of Elastic Viscoplastic Modeling of the Time-Dependent Stress – Strain Behavior of Geomaterials.” ASCE, (1), 1–9.

Yin, J., and Feng, W. Q. (2018). “Validation of a new simplified hypothesis B method for calculating consolidation settlement of clayey soils exhibiting creep.” Geotechnical Engineering, Southeast Asian Geotechnical Society, 49(2), 12–21.

Yin, J. H. (1990b). “Constitutive Modelling of time dependent stress strain behavior of soils.” Phd Thesis, The University Of Manitoba.

Yin, J., and Tong, F. (2011b). “Constitutive modeling of time-dependent stress – strain behaviour of saturated soils exhibiting both creep and swelling.” Canadian Geotechnical Journal, 48, 1870–1885.

Yong, R. N., and Warkentin, B. P. (1975). “Soil Properties and Soil Behavior.” Elsevier, Amsterdam. Appendices Appendix A: Liquid and plastic limit test Nafferton Clay, 14, 10–16.

Yuan, Y. (2016). “A new elasto-viscoplastic model for rate-dependent behavior of clays.” Massachusetts Institute of Technology.

Yunusa, G. H., Hamza, U., Abdulfatah, A. Y., and Suleiman, A. (2013). “Geotechnical investigation into the causes of cracks in building: A case study.” Electronic Journal of Geotechnical Engineering, 18, 2823–2833.

Zeng, Z., and Kong, L. (2019). “Effect of wetting–drying–freezing–thawing cycles on the swelling behaviour of the Yanji mudstone.” Environmental Earth Sciences, Springer, 78(15), 1–14.

Zhang, C.-C., Zhu, H.-H., Shi, B., and Fatahi, B. (2018). “A long term evaluation of circular mat foundations on clay deposits using fractional derivatives.” Computers and Geotechnics, Elsevier, 94, 72–82.

Zhang, D. (2017). “A coefficient of determination for generalized linear models.” The American Statistician, Taylor & Francis, 71(4), 310–316.

Zhang, J., and Li, C. (2018). “Experimental study on lime and fly ash–stabilized sintered red mud in road base.” Journal of Testing and Evaluation, ASTM International, 46(4), 1539–1547.

Zhang, J., Xiao, J., Li, S., and Ran, W. (2017). “Manure amendment increases the content of nanomineral allophane in an acid arable soil.” Scientific reports, Nature Publishing Group, 7(1), 1–8.

Zhou, W.-H., Tan, F., and Yuen, K.-V. (2018). “Model updating and uncertainty analysis for creep behavior of soft soil.” Computers and Geotechnics, Elsevier, 100, 135–143.

Zhu, H.-H., Liu, L.-C., Pei, H.-F., and Shi, B. (2012). “Settlement analysis of viscoelastic foundation under vertical line load using a fractional Kelvin-Voigt model.” Geomechanics and Engineering, Techno-Press, P. O. Box 33 Yusong Taejon 305-600 Korea, Republic of, 4(1), 67–78.

Zhu, H.-H., Zhang, C.-C., Mei, G.-X., Shi, B., and Gao, L. (2017). “Prediction of one-dimensional compression behavior of Nansha clay using fractional derivatives.” Marine Georesources & Geotechnology, Taylor & Francis, 35(5), 688–697.

Zia, N., and Fox, P. J. (2000). “Engineering properties of loess-fly ash mixtures for roadbase construction.” Transportation Research Record, SAGE Publications Sage CA: Los Angeles, CA, 1714(1), 49–56.